UNIVERSITY OF CALIFORNIA
RIVERSIDE

The Microbial Ecology of the Salton Sea: How an Extreme Environment Selects for Microbial Metabolism & Survival

A Dissertation submitted in partial satisfaction
of the requirements for the degree of

Doctor of Philosophy

in

Genetics, Genomics, and Bioinformatics

by

Linton Freund

September 2024

Dissertation Committee:
Dr. Emma Aronson, Chairperson
Dr. Jason Stajich
Dr. Will Porter

The Dissertation of Linton Freund is approved:

_____

_____

_____

Committee Chairperson

University of California, Riverside

Acknowledgements

To Dr. Emma Aronson, thank you for giving me the opportunity of a lifetime to earn my PhD in your lab. You introduced me to the Salton Sea and its fascinating microbial ecology, and provided me the resources I needed to flourish and explore my passions for metagenomics. I have grown to be an independent scientist, and greatly appreciate your guidance for helping me reach this point. I am so deeply grateful for your ongoing support, encouragement, and wisdom.

To my committee, Dr. Jason Stajich and Dr. Will Porter, thank you both for your valuable mentorship and support throughout this journey. Dr. Stajich, I am grateful for all our intense conversations discussing bioinformatics approaches to metagenomics. I also deeply appreciate your support as a mentor when I was feeling stuck in my research. Dr. Porter, I cannot thank you enough for all your help and expertise throughout our work together. You always treated me as a colleague, and even though I was not in your lab, you always made time to meet with me and read my frantic weekend, late-night emails. I cherish your mentorship and your endless encouragement, and would not have reached this point in my project without you!

To Dr. Marko Spasojevich, thank you for being a source of knowledge when it came to statistics and ecology. Your words “it depends on the question” will forever ring in my head and bring me back to Earth when I dive too deep into the statistics, thank you so much. To Dr. Mike Lee, I would not have developed the knowledge I have about metagenomics if not for your guidance and care. You always responded to my inquiries

and delved into the mechanics behind certain methods, and I have learned so much from you – thank you.

To my lab mate Talyssa Topacio, there are not enough words to express how truly thankful I am for you! There is no way I would have survived this program without you. You taught me how to not only do so many wet lab procedures, but you reminded me that making mistakes is part of the learning process and builds confidence in one's self. Your expertise and hard work keep our lab afloat, and joining the Aronson lab around the same time as you was truly the greatest gift. There are not enough thanks in this world for you, thank you so much!

To my incredible collaborators Caroline Hung, Dr. Charlie Diamond, Dr. Tim Lyons, and Dr. Yaning Miao. Caroline and Charlie, thank you so much for your effort to collect samples from the Salton Sea. More importantly, thank you both so much for indulging in hours-long discussions about the Salton Sea's geochemistry and microbial ecology. I have learned so much from you both and greatly appreciate your insight and expertise regarding the Salton Sea's geochemistry and the importance of public policy in remediating neglected ecosystems. Caroline, I am especially grateful for our everlasting text threads about the Salton Sea sulfur cycle. Your passion for your research and the importance of public policy is powerful and inspiring. Dr. Tim Lyons, thank you so much for your ongoing support, wealth of knowledge, and passion for understanding the Salton Sea system. I am so grateful for the enthralling discussions we've had about the Salton Sea's sulfur cycle and what this means for the Salton Sea's microbial diversity. Dr. Yaning Miao, thank you so much for your knowledge and expertise regarding the wind

back trajectories and surface type frequency data that you generated for this work. I am indebted to you for your hard work!

To my current and previous lab mates Dr. Mia Maltz, Talyssa Topacio, Dr. Yang Yang, Jorge Pastrana, Robin Bond, Marina Zaza, Jordan Dagan, and Abbey Lyew, thank you for all your ongoing support, expertise, and kindness. Mia, thank you so much for your expertise and passion for teaching and science. I have learned so much from you and am truly grateful for your guidance and encouragement. Yang, it was such a pleasure to get to know you in lab and hear your wisdom about how to survive the PhD program. Thank you for your endless support! Talyssa, you deserve all the "thank you"s so I am taking this opportunity to thank you again for being such an incredible colleague, lab mate, and friend throughout this process. Marina, I am so glad you joined our lab! It's been such a joy to get to know you and work with you, and I am so thankful for your determination. Robin and Jordan, thank you both for your hard work and support. Robin, I really enjoyed our field trips and always had a blast collecting samples with you, no matter the temperature! Jorge, it's been a joy to work with you and geek out about microbial ecology and soils. I am so grateful for your friendship and cannot wait to see what unfolds for you in this lab. Abbey, I am so grateful for your hard work and interest in microbiology. You helped me process so many samples for my projects and it's a joy to see you grow as a scientist.

To incredible undergrads that worked in the Aronson lab during my PhD, I am so deeply grateful for your hard work and fun conversations in the lab. Krystal Truong, Allie Keen, Annu Valliyanal, Iknoor Sandhu, Amanda Ly, Ryan Lee, Isaac Jun, Abbey Lyew,

Mason Mangan, Diana Le, Nicole Wolman, Joseph Valdez, Erasmo Lopez, Astrid Elliott, Pauline Crecencia, Evie Alerbico, Jahlen Pinelo, and Olivia Dinh – you have all helped me so much with processing dust collectors, performing DNA extractions, acid washing endlessly, and bringing so much joy into the lab. I enjoyed working with you all and am indebted to your hard work on this project.

I would not have survived this program without the incredible support system I built while at UC Riverside. Dr. Femila Manoj, thank you for the constant chats, the venting, the videos of Pong, and most importantly the laughs and deep conversations. I am so glad we met during our very first quarter. Dr. Fabi Pulido, thank you for your wisdom, kindness, and joy. I love that we can discuss true crime, metagenomics, politics, and laugh about silly videos together. To Catherine Wells and Dr. Christian Wells, thank you both for becoming my family. Catherine, you're a sister to me and I wouldn't be here without your support, kindness, and understanding. Christian, thank you for your friendship and your thoughtfulness. To Dr. John Burnett and Aaron Goodwin, thank you both for being two of the best friends and roommates I could ever ask for. John, I deeply cherish our friendship in all its levels. We can truly talk about anything, and I would not have made it through this year without you. Aaron, you are an utter joy to be around and such an inspiration to me. You inspire me to stand in my convictions always and remain open, thank you. I love my 1404 Le Conte family!

To the incredible friends I made during the strike and to the members of the Grads for a Free Palestine – I am beholden to you for radicalizing me and showing me what justice and community look like. You have taught me what it means to unapologetically

stand for what is just, and that when we invest in building our community, we keep us safe. There are not enough “thank you”s to express my gratitude and appreciation.

To Sara Olson and Justine Rodriguez, thank you for being the best friends anyone could ask for. You have always been there for me throughout my educational journey, and you both inspire me to work hard and love harder. I love you both so much, thank you. I cannot wait to see us continue to follow our dreams together.

To Dr. Erik Sease, my partner in crime. There are not enough words to thank you for your support, your partnership, your humor, your passion, your brilliance, your kindness. I could not ask for a better partner, and I am so lucky to have endured this journey with you. I cannot wait to see what our future together holds. I could write an entire dissertation on how grateful I am for you, thank you.

To my mom, my dad, my brother, and my sister-in-law – thank you all for your endless support and encouragement. Mom, you have always been my biggest cheerleader and I could never have achieved this without you believing in me. I love you so much! Dad, thank you for support and guidance, and for pushing me to be the best version of myself. Your work ethic has always inspired me to work hard for my ambitions, and I am so grateful for you – I love you. Adam, you and I started this journey to graduate school together and I am so lucky that I got to follow this path alongside you. We are doing it and I so proud of us for following our dreams together, love you bro. Juliet, thank you for becoming the sister I never had. I love you so much, thank you for tolerating all of us when you don’t have to!

To last but certainly not least, Deetsi, my child. I would not have made it this far without you by my side every step of the way. From college to a masters to a PhD and next a postdoc, you have always been my other half. Your unconditional love, emotional intuition, intelligence, and sweetness has been the greatest gift. Our bond is a treasure that has sustained me throughout my graduate school education and I would not be here without you. I love you!

Dedication

Zayde, all that I do, I do to honor you and your legacy. I would give anything for you to be here and celebrate this achievement with me. In your life and in your death, I continue to learn what it means to stand for justice and equity. With every step in my journey, I hold you, your story, your joy, and your compassion with me. I will always be your "sveetheart", and I promise that I will continue to proudly, unapologetically stand for what is right. I learned and continue to learn that from you.

Though this dissertation contains the scientific research I've done, please know that the entirety of my PhD journey is a dedication to you. I have found myself, I have found community, and I know what it means to say "never again" and mean it with every fiber of my being. I am learning what it means to be unafraid in standing for the most marginalized as you did. Your resilience and your constant choice to not only survive but to love and to find joy is a choice I never lose sight of.

As we watch colonization and white supremacy commit genocide and ecocide against those in Palestine, Sudan, Congo, Haiti, all around the world to the communities living amidst Salton Sea, I will continue to uphold your legacy and stand for what is right. I will continue to embody tikkun olam. I will not let my rage eat my joy. There is so much more I could say Zayde but please know that all this is for you. To our hero, our Maccabee, our Zayde, thank you.

ABSTRACT OF THE DISSERTATION

The Microbial Ecology of the Salton Sea: How an Extreme Environment Selects for Microbial Metabolism & Survival

by

Linton Freund

Doctor of Philosophy, Graduate Program in Genetics, Genomics, and Bioinformatics
University of California, Riverside, September 2024
Dr. Emma Aronson, Chairperson

Microorganisms are ubiquitous in their distributions and are integral to global nutrient cycling. Yet, microbial metabolic strategies are niche-specific, as environmental conditions including nutrient and moisture availability, oxygen concentration, and salinity select for certain microbial adaptations. The Salton Sea, a hypersaline and eutrophic lake in Southern California, presents a unique opportunity to investigate how the environment selects for microbial survival and dispersal, which has urgent implications for both ecosystem stability and public health impacts.

In Chapter 1, we explored the geochemistry of the Salton Sea sub-ecosystems (i.e., the playa, seawater, and aeolian) and how they structure their respective microbiomes. We also detail the paucity of research into these communities and describe modern methods like metagenomics and wind modeling that could be used to characterize the Salton Sea microbiomes. In Chapter 2, we examined the Salton Seawater microbiome within a water column during periods of lake stratification and turnover in 2020 and 2021. We characterized the taxonomic composition of the lake's microbiome

across seasons by sequencing the bacterial 16S rRNA gene (V3-V4) and used metagenomic sequencing to assess the community's capacity for sulfur cycling. While microbiome composition significantly varied between seasons, halophilic, mixotrophic bacteria consistently dominated the water column. Additionally, sulfur oxidation genes were shared across depths and their relative coverage fluctuated with seasonal shifts in oxygen, sulfide, and sulfate concentrations. In Chapter 3, we used amplicon sequencing of the 16S rRNA gene (V3-V4), metagenomic sequencing, and wind geospatial data to characterize the aeolian dust microbiome and their adaptations that permit atmospheric survival and dispersal. We identified a core aeolian microbiome including bacterial genera such as *Massilia*, *Sphingomonas*, and 11 other stress-tolerant taxa. We also observed that the dust microbiome contains the necessary adaptations for persisting in dust, including UV radiation resistance genes and osmotic resistance genes, and that the distribution of these traits was driven by wind conditions. Together, these findings demonstrate that harsh environments select for microbial survival strategies, which in turn, regulate the ecosystems' geochemistry and stability. Furthermore, this relationship structures both microbial colonization and dispersal, which may pose a danger to the public upon exposure.

Table of Contents

List of Figures

List of Tables

Introduction

The Salton Sea is a hypersaline, polluted lake within Southern California that is rapidly shrinking, directly leading to heightened dust emissions in the region that are inhaled by the local population. Exposure to this dust has led to a high incidence of respiratory distress within the nearby community, where access to healthcare and employment opportunities are lacking. The chemical composition of this dust has been investigated to determine its toxic components, however, the culprit(s) responsible have yet to be identified. While microorganisms have been hypothesized as contributors to the toxicity of this dust, the dust microbiome from the Salton Sea has not been explored. Additionally, though microorganisms within the Salton Seawater have been classified, these studies did not examine the microbial community within the larger context of the Salton Sea's unique geochemistry. Thus, understanding the microbiomes and their functional traits would clarify their role in the decline of this ecosystem as well as and how this relationship is a detriment to public health.

This dissertation aims to understand how substrate-specific microbiomes within the Salton Sea, specifically the seawater and aeolian dust microbiomes, survive in these extreme environments. Clarifying these survival strategies allows us to understand how environmental microbiomes influence the habitability of these ecosystems via dispersal and nutrient cycling. Furthermore, analyzing the abiotic factors that select for the diversity in microbial survival strategies provides insight into the conditions that encourage the survival of potentially pathogenic microorganisms, and how these microorganisms conserve and share metabolic and pathogenic traits.

The first chapter of this work offers a detailed history of how the Salton Sea formed, what is currently known about its unique geochemistry, and expands on the putative microbial ecology of the sub-ecosystem microbiomes (i.e., the playa, seawater, and dust microbiomes) as well as how we can study these communities. The second chapter examines the microbial ecology within a water column in the Salton Sea by classifying the taxonomic composition of the seawater microbiome as well as the sulfur cycling pathways utilized by this community across seasons. The third chapter explores the aeolian (i.e., wind-blown) dust microbiome from the Salton Sea and identifies a core set of bacterial genera that can colonize atmospheric dust. Additionally, this chapter investigates the distribution of certain survival strategies used by the aeolian dust microbiome and how these adaptations promote its pathogenicity upon inhalation. Collectively, this work establishes that environmental microbiomes and their adaptations serve as the interface between ecosystem function and public health.

CHAPTER I

Title: Microbiome Interactions and their Ecological Implications at the Salton Sea

Authors: Freund, H.L.[1], Maltz, Mia R.[2], Swenson, Mark P.[2], Topacio, Talyssa M.[2], Montellano, Vanessa M.[2], Porter, William[3], and Aronson, Emma L.[2]

1. Genetics, Genomics, and Bioinformatics Program, University of California, Riverside, CA
2. Department of Microbiology and Plant Pathology, University of California, Riverside, CA
3. Department of Environmental Sciences, University of California, Riverside, CA

Abstract

Although the Salton Sea was once a thriving destination for humans and wildlife, it has now degraded to the point of ecosystem collapse. Increases in local dust emissions have introduced aeolian (wind-blown) microorganisms that travel, along with contaminants and minerals, into the atmosphere, detrimentally impacting inhabitants of the region. Proliferation of certain microbial groups in regions of the Sea may have a disproportionate impact on local ecological systems. Yet, little is known about how the biogeochemical processes of this drying lakebed influence microbial community composition and dispersal. To elucidate how these microorganisms contribute, and adapt, to the Sea's volatile conditions, we synthesize research on three niche-specific microbiomes — the Sea, exposed lakebed (playa) and aeolian —and highlight modern molecular techniques, such as metagenomics, coupled with physical science methodologies, including transport modeling, to predict how the drying lakebed will affect microbial processes. We argue that an explicit consideration of microbial groups within this system is needed to provide vital information about the distribution and functional roles of ecologically pertinent microbial groups. Such knowledge could help inform regulatory measures aimed at restoring the health of the Sea's human and ecological systems

Introduction

As impacts of climate change and policy-driven pollution worsen in the Salton Sea region, there is an urgent need to predict the Sea's ecosystem health and stability in response to water influx changes. Although there is increasing evidence about the

harmful effects of environmental degradation on wildlife within the Salton Sea, less is known about how microorganisms respond to mounting degradation throughout the region (California Natural Resources Agency 2020; Jones and Fleck 2020; Kjelland and Swannack 2018; Marti-Cardona et al. 2008; Moreau et al. 2007). Microorganisms and their respective communities (i.e., microbiomes) are ubiquitous, and the foundation of nutrient cycling within ecosystems (Falkowski et al. 2008). While the effects of long-term environmental stress on microbial communities are less understood, research indicates that microorganisms are sensitive to natural and anthropogenic perturbations, and thus may serve as useful indicators of ecosystem productivity (Karimi et al. 2017; Maltz et al. 2017).

Without an explicit consideration of environmental microorganisms and their stress-response tactics, we may undermine our ability to respond to changing environmental and regulatory measures. For instance, policy decisions, plummeting water quality, and reduced Sea levels may have varying effects on microorganisms within this novel and vulnerable ecosystem. Moreover, understanding how the degraded environment surrounding the Salton Sea influences microbial processes, interactions and biogeochemical cycling is particularly important for assessing microbial contributions to overall ecosystem functionality, as well as for illuminating connections between policy- and climate-driven environmental changes and the health of nearby human and ecological systems.

Agricultural Runoff, Dust Emissions

The implementation of the Quantification Settlement Agreement in 2003 diverted water from the Colorado River to other areas, which massively reduced inflows to the Salton Sea (California Natural Resources Agency 2020). The New, Alamo and Whitewater rivers feed the Salton Sea with agricultural runoff containing pesticides, metals, salts and other elements (Vogl and Henry 2002). Specifically, copper, arsenic, manganese and selenium have been detected at levels above the U.S. Environmental Protection Agency threshold in water and sediment samples (Moreau et al. 2007; Xu et al. 2016). Selenium is of particular concern due to its consistently high concentrations in local fish (i.e., tilapia), at levels surpassing Aquatic Life Criteria standards (Xu et al. 2016). Federally banned pesticides including polychlorinated biphenyls (PCBs), dichlorodiphenyltrichloroethane (DDT) and dichlorodiphenylethane (DDE) have also been detected in in the muscle tissue of local fish species (Moreau et al. 2007; Riedel et al. 2002; Sapozhnikova et al. 2004; Xu et al. 2016) and in water, exposed lakebed (playa), and submerged playa samples (Sapozhnikova et al. 2004; Wang et al. 2012; Xu et al. 2016). Selenium, DDT and other pollutants accumulate in detritus, and are introduced into the Salton Sea's trophic network when consumed by algae, invertebrates and fish (Saiki et al. 2012). While the accumulation of these contaminants are detrimental to animal biodiversity (Canton and Van Derveer 1997; Köhler and Triebskorn 2013; Riedel et al. 2002), the extent to which pollution alters the Sea's trophic structure warrants further study.

In addition to pollutants, agricultural effluent delivers excess nutrients to the Salton Sea, leading to eutrophication and subsequent die-offs of aerobic organisms (Beman et al. 2005; Chaffin and Bridgeman 2014; Heisler et al. 2008). Nutrient enrichment leads to harmful algal blooms as these algae consume a majority of the Sea's dissolved oxygen. Eventually, these algae die off in the absence of sufficient oxygen, as other microorganisms decompose detritus and deplete the remaining dissolved oxygen (Qin et al. 2013). Additionally, strong winds during spring and summer seasons create upwellings of anoxic water and sulfide from the lake bottom to the surface (Marti-Cardona et al. 2008; Reese et al. 2008).

Toxic plumes coupled with persisting anoxic conditions contribute to ongoing loss of wildlife, with particularly high mortality in local and migratory birds such as eared grebes (*Podiceps nigricollis*), fish such as Mozambique tilapia (*Oreochromis mossambicus*) and invertebrates such as pileworms (*Neanthes succinea*; Anderson et al. 2007; Carmichael and Li 2006; Marti-Cardona et al. 2008). Microbial pathogens, including *Pasteurella multocida*, cyanotoxins and botulinum toxin, have all been associated with mass die-off events (Carmichael and Li 2006; Meteyer et al. 2004; Nol et al. 2004); however, not all die-off events have been linked to heightened concentrations of these particular pathogens or toxins. Understanding how the region's fauna and their trophic structures respond to eutrophication, upwellings and other natural processes will differentiate between vulnerable and resilient aspects of the Salton Sea ecosystem.

As playa exposure increases due to reduced inflow and hypersalinity, pollution and eutrophication exacerbate stressful conditions within the Salton Sea ecosystem. Over the next decade, the volume of inflow will be reduced by 40% and the volume of the Sea itself will be reduced by more than 60% (Cohen 2014). Ongoing shrinkage of the Salton Sea not only increases salinity in the Sea and the playa (California Natural Resources Agency 2020), but also exposes additional lakebed sediment, leading to heightened dust emissions in the area (Frie et al. 2017). These emissions are expected to contribute to already high levels of background particulate matter (Frie et al. 2017; Frie et al. 2019; US Fish and Wildlife 2014). Wet playas like the Salton Sea are vulnerable to erosion as capillary action in the sediment brings groundwater to the playa surface (Buck et al. 2011), softening sediment and stimulating groundwater evaporation (Reynolds et al. 2007). Playa emissions and aerosolized Sea spray contribute to the composition of the dust, which consists of minerals (e.g., selenium, sodium and sulfate), metals (e.g., cadmium and chromium; Buck et al. 2011; Frie et al. 2017; Frie et al. 2019) and dust-associated microorganisms, along with their respective microbial metabolites. These contributed materials, particulate matter size, and strong winds collectively influence dust composition, reduce local air quality and threaten downwind niches upon deposition.

Dust emissions disperse microbial components from dust to surrounding locations (Frie et al. 2017; Griffin 2007), and the harsh, arid climate of the Salton Sea provides habitat for microorganisms acclimated to these inhospitable conditions (Paul and Mormile 2017). Salinity, nutrient availability, pH, oxygen concentration and

temperature collectively affect microbial composition and functional trait diversity. Most microorganisms are able to regenerate rapidly and transfer genes horizontally, which permits uptake of DNA from the environment as well as the sharing of DNA with other microbial species or viruses (Johnston et al. 2014). Altogether, these abilities allow microorganisms to easily adapt to the unique selective pressures of their environment.

Microbial metabolic functions may be more dependent on environmental pressures than on evolutionary or phylogenetic relationships (Allison and Martiny 2008; Louca et al. 2017; Shade et al. 2012). Likewise, pollutants, excess nutrients and geophysical processes may alter the collection of microorganisms found within the Salton Sea's sub-ecosystems (Figure 1). The sub-ecosystem microbiomes include the playa, seawater and the wind-driven microorganisms that travel along with dust throughout the atmosphere (i.e., the aeolian microbiome). Interactions between environmental microbiomes and the ecosystem regulate the availability and accumulation of certain minerals. For example, anaerobic microorganisms in extreme environments akin to the Salton Sea can use selenate (SeO_4^{2-}) or selenite (SeO_3^{2-}) as electron acceptors; this reduces it to elemental selenium (Nancharaiah and Lens 2015), which accumulates in sediment. Other anaerobes can reduce sulfate to hydrogen sulfide, which consumes dissolved oxygen and yields harmful "gypsum" blooms, which are somewhat analogous to algal blooms (Ma et al. 2020). Clarifying how these microbiomes contribute to the trophic structures and chemical cycling

within the Salton Sea is crucial to promoting the long-term sustainability and functionality of this ecosystem.

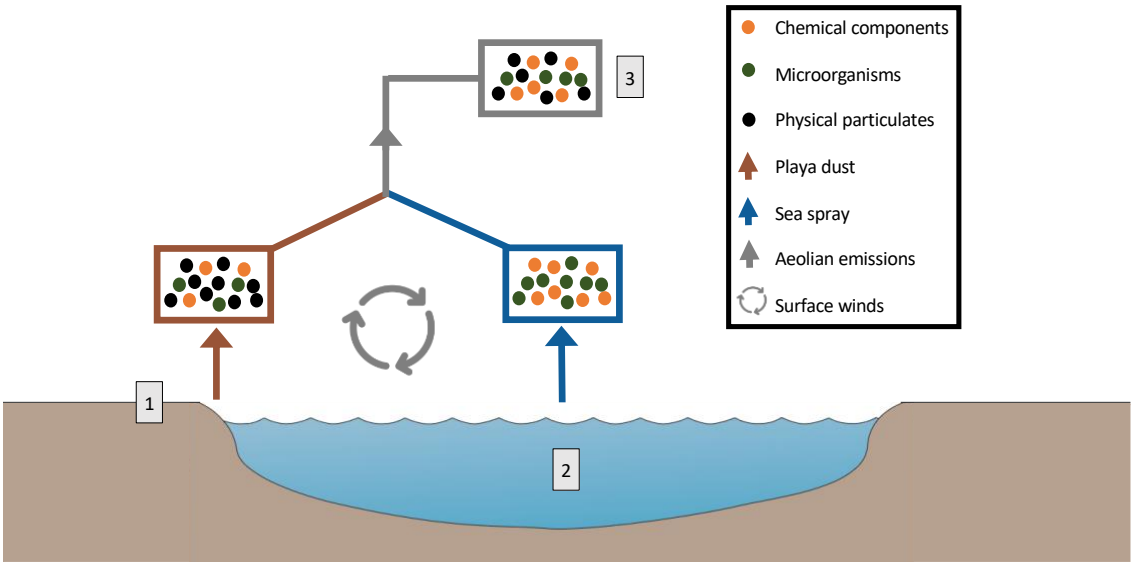

Figure 1. Interactions among Salton Sea's Dynamic Sub-Ecosystems. There are three environmental microbiomes: (1) playa, (2) seawater and (3) aeolian; sea spray and playa dust contribute to the aeolian microbiome. As the Salton Sea recedes, lakebed sediment is exposed and concurrently transforms into playa. Playa emits loose particulates that entrain microorganisms, chemicals and sediment into the atmosphere, which travel throughout the region via surface winds.

Sea Microbiome

For decades, studies on the microbial composition of the Salton Sea have focused heavily on cyanobacteria. Cyanotoxins — specifically microcystin — contribute to the high frequency of avian mortality events occurring at the Sea (Carmichael and Li 2006; Meteyer et al. 2004). Additionally, cyanobacteria and other phytoplankton taxa form microbial mats that sit above the water surface (Wood et al. 2002) and thus are easy to investigate. Nevertheless, these studies have failed to capture the microbial diversity that persists below the Sea surface.

The Salton Sea is characterized by hypersaline, alkaline and anoxic conditions where anaerobes and extremophiles (i.e., microorganisms that inhabit extreme environments) prevail (González et al. 1998; Reese et al. 2008). These extremophiles include halophiles, or salt-loving microorganisms, and alkaliphiles, which thrive in conditions with a pH of 8 or greater (Andrei et al. 2012; Mesbah and Wiegel 2008).

To date, only two studies have examined microbial phylogenetic diversity in Salton Sea water (Dillon et al. 2009; Hawley et al. 2014; online technical Appendix Table 1). In contrast to previous work, these studies showed that Cyanobacteria compose less than 5% of the total taxa found in Sea water samples (Dillon et al. 2009; Hawley et al. 2014); instead, they detected high abundances of microorganisms from both Proteobacteria and Bacteroidetes phyla. Beyond Cyanobacteria, Dillon et al. (2009) observed seasonal shifts in the relative abundance of Gammaproteobacteria and Alphaproteobacteria classes, and the Bacteroidetes phylum.

Proteobacteria are likely the most abundant phylum detected in Salton Sea water (Hawley et al. 2014). Rhodobacterales, an order within Alphaproteobacteria, was highly abundant within the summer months (Dillon et al. 2009). Rhodobacterales is composed primarily of photoautotrophs, which are capable of anaerobic photosynthesis, and haloalkaliphiles, which have been identified globally in saline, alkaline lakes (Kopejtka et al. 2017). Further determining which taxa within the Proteobacteria are most common and abundant would be a promising area for future research, as finer taxonomic resolution from this abundant phylum has rarely been reported. Given that a majority of these analyses about Salton Sea water capture

microbial diversity only at the Sea surface, and neglect to characterize the microbial diversity of the water column, future work assessing microbiome structure below the water surface would be particularly valuable. For example, exploring the taxonomic diversity of microorganisms within the Sea's water column, particularly during seasonal upwellings and eutrophication events, would identify microorganisms responsible for depleting dissolved oxygen supplies via detritus consumption or sulfate reduction (Reese et al. 2008); classifying these microorganisms could improve predictions of anoxic periods within the Salton Sea and similar ecosystems.

Playa Microbiome

Because of their intimate associations within the Salton Sea, the biogeochemical interactions of the playa and the sediment beneath the lake are challenging to differentiate. Similar to microorganisms in Salton Sea water, anaerobes and extremophiles have a selective advantage in this niche due to the extremely high concentration of sulfate and salt in the sediments, which is compounded by the lack of oxygen and phosphorus resources (Swan et al. 2007).

Sediment depth gradients have been shown to differentially structure microbial communities. Most Archaea have been observed with equal abundance across lakebed sediment depths (Swan et al. 2010). However, Crenarchaeaota (i.e., Archaea phylum) and bacterial communities consistently exhibit similar abundances with depth. Likewise, the relative abundance of certain bacterial classes, including Betaproteobacteria, Gammaproteobacteria and Clostridia, correspond with both increased depth and salinity in the Salton Sea.

Several taxa found in Salton Sea playa have also been identified in marine sediments (Dillon et al. 2009; Swan et al. 2010) as well as haloalkaline lake sediments and salt flats (McGonigle et al. 2019; Rojas et al. 2018; Yang et al. 2016). Saline concentration has been identified as one of the most important factors in structuring microbial communities across ecosystem types (Lozupone and Knight 2007). These findings indicate that salinity and oxygen availability are crucial environmental drivers of microbial assembly in the Salton Sea playa.

Although the microbial composition beneath playa crusts has been studied to some extent (Dillon et al. 2009; Swan et al. 2010), the microorganisms of the superficial playa have largely been neglected. Increased playa exposure directly corresponds to greater dust fluxes in the region (Buck et al. 2011; Frie et al. 2019; Parajuli and Zender 2018), entraining both chemical and microbial components into dispersing dust (Figure 1). Heightened playa emissions correspond to salt precipitation on the playa surface (Buck et al. 2011), driving the microbial community structure at this playa–dust interface. Considering that playa surfaces are global dust contributors (Abuduwaili et al. 2010; Kandakji et al. 2020; Reheis et al. 2002; Reynolds et al. 2007; Ziyaee et al. 2018), characterizing and quantifying the impact of dispersing playa microorganisms on surrounding ecosystems and inhabitants of the region may be particularly important. Moreover, integrating these putative impacts into our understanding of wind-driven playa erosion may greatly advance our assessment of the vulnerability and toxicity of playa particulate matter. To understand the influence of both sediment and playa on dust composition — as

well as associated exposure and deposition risks for downstream niches — the phylogenetic structure, functional diversity and seasonal variation of the playa microbiome must be investigated.

Aeolian Microbiome

In addition to minerals and trace metals, microorganisms can become entrained in both playa dust and Sea spray, along with their microbial toxins, which may be capable of withstanding turbulent conditions and long-distance transport (Figure 1; Tang et al. 2017). Microorganisms persisting among and on dust compose the aeolian microbiome, which includes all bacteria, archaea, fungi and viruses that circulate in the atmosphere. Some fungal spores and bacteria are capable of surviving within — or atop — dust as single cells or filaments, moving freely or attaching to individual particles (Samake et al. 2017).

Dust microorganisms have adapted to a unique set of environmental stressors including wind stress, ultraviolet radiation, humidity, temperature and nutrient availability. These microorganisms are equipped with a particular combination of traits, such as melanin production (Grishkan 2011) or biofilm formation (Aalismail et al. 2019), which enables their survival within this inhospitable airborne environment (Grishkan 2011). Several studies have reported higher microbial abundance on large dust particles at higher temperatures or low relative humidity (Lighthart and Shaffer 1997; Polymenakou et al. 2008; Yamaguchi et al. 2012), which are common features of the Salton Basin. Increased microbial burden also often correlates with enriched organic matter and minerals in dust (Tang et al. 2017). Collectively, these results

suggest that larger dust particles shelter, sustain and protect microorganisms to ensure their dispersion and survival.

Numerous microorganisms isolated from dust remain viable for long durations of time. Bacterial and fungal isolates from dust not only can be successfully grown in the laboratory environment (Maki et al. 2019; Yamaguchi et al. 2012), but also have been shown to be metabolically active while in transit (Tang et al. 2017). Additionally, airborne microorganisms can facilitate ice nucleation, promoting cloud formation and precipitation (Amato et al. 2015; Bowers et al. 2009; Failor et al. 2017; Gaston et al. 2017). Therefore, aeolian microorganisms may threaten downwind ecosystems by altering precipitation and temperature, or disturbing stable microbiomes upon deposition. Moreover, exposure risks from airborne pathogenic microorganisms originating in the Salton Sea, and associated playa, may yield deleterious consequences for plants and animals, as well as human populations. Construction and farm workers may be particularly vulnerable to increased inhalation risks and exposure to dust-associated microorganisms, based on their occupational hazards (Gorris et al. 2018).

Although the microorganisms inhabiting the seawater and sediment of the Salton Sea have been examined, the dust microbiome has yet to be characterized. Given their remarkable ability to withstand environmental stress in the airborne environment, the aeolian microbiome could be dominated by either dormant or stress-resistant microorganisms. This resistant aeolian microbiome within Salton Sea dust could contribute to the health impacts of air quality in the region, especially if microbial

groups break dormancy or actively interact with plant, animal or human hosts upon deposition. Some microbial adaptations likely permit their survival in dust. For example, bacteria from the genus Bacillus, which have been identified in dust samples from across the globe (Tignat-Perrier et al. 2019), have the ability to form endospores, allowing them to survive harsh environments via dormancy (Nicholson et al. 2000). Upon deposition, these dormant and resistant microorganisms may perform vital ecosystem functions, or they may pose formidable threats to inhabitants of the region. Motile microorganisms exhibiting chemotaxis may also be uniquely suited to explore porous environments and establish in favorable niches upon deposition (Scheidweiler et al. 2020). Therefore, exploring the functional attributes and microbiome structure within dust surrounding the Salton Sea would clarify the contribution of the aeolian microbiome to either promoting ecosystem stability or exacerbating regional public health crises.

Methods for Further Study

Future examination of the Salton Sea must comprehensively explore the playa, seawater and aeolian microbiomes to characterize their structural similarities, as well as any differences among these communities. Temporal and compositional differences may influence the interactions between these microbiomes and their surrounding environment, as well as overall nutrient availability within the Salton Sea ecosystem. Common methodologies used in human and environmental microbiome research could be tailored to explore both the taxonomic and functional diversity of Salton Sea microbiomes.

Sampling and Analysis Strategies

Multiple sample types (e.g., dust, water, playa) should be collected, at a variety of time points, from a replicated set of diverse locations within and around the Sea. As sample collection procedures will differ between media types (soil cores, dust collection, water samples), technological advances, such as the use of drones, water skimmers or seawater samplers (Xing et al. 2017), could be advantageous. Other valuable approaches may use semi-permanent passive samplers (Aciego et al. 2017; Frie et al. 2019), portable sampling platforms (Docherty et al. 2018) or active samplers, which collect all airborne cells and spores using filters from a known air volume (Frie et al. 2017).

Sample processing procedures may include filtering dust suspensions and seawater, using sterile 0.2- μm filters to capture bacteria and other microorganisms on the filter, while allowing passage of water and other aqueous substances. From unfiltered suspensions, microbial biomass can be determined using flow cytometry (Schmidt et al. 2020) or phospholipid fatty acids (PLFA; Buyer and Sasser 2012).

Amplicon marker genes, such as the 16S rRNA gene in bacteria or the internal transcribed spacer (ITS) region of fungal rRNA (Knight et al. 2018; Nilsson et al. 2019), are selected for amplification or quantitative polymerase chain reactions (qPCR; Manter and Vivanco 2007) to determine the taxonomic diversity and the relative abundance of important microbial groups across samples. Amplicon marker gene sequencing is currently the most cost-effective, high-throughput next-generation

sequencing (NGS) method for studying microbiome composition across ecosystems (Liu et al. 2020).

Microbiome composition may be altered by both seasonal and agricultural geochemical fluxes within the Salton Sea, which also may select for metabolic strategies employed by these microbiomes. Sampling campaigns across time points at the same locations will capture temporal and seasonal variation, as upwelling events in the summer are known to change surface water chemistry by increasing sulfide levels and reducing dissolved oxygen content (Reese et al. 2008; Watts et al. 2001). Organo-chloride pesticides (OCPs) accumulate within previously underwater sediments, and may subsequently volatilize or evaporate as polluted sediments are increasingly exposed. As these pesticide-laden sediments become entrained in dust, OCPs are likely transported throughout the region via increased wind speeds and storms (LeBlanc et al. 2002), exacerbating dust inhalation risks. Although microorganisms from the playa or aeolian microbiomes may be capable of metabolizing recalcitrant or labile components from polluted dust, ecophysiological assays and metabolic models would be required to quantify the extent to which these toxins can be transformed or biodegraded by extant microorganisms. Future work incorporating and altering model parameters would facilitate our ability to predict future fate and transport of toxic dust based on future water influx and climate change scenarios (D'Amato et al. 2008).

Changes in geochemistry, such as total organic carbon concentrations, pH and nutrient levels, have pointed to detectable shifts in playa microbiomes in similar

hypersaline water bodies (Hollister et al. 2010). Collecting soil core samples from the playa over a distance transect would help to elaborate how geochemical variation impacts Salton Sea terrestrial microbiomes. Furthermore, as reductions in sea volume expand the exposed playa, these sampling strategies and subsequent analyses could clarify how microbiomes transition with their environments from moist to dry conditions.

The impact of dust composition and evaporite minerals (e.g., magnesium, calcium, sulfate) on aeolian microbial metabolism and assembly could be studied via deploying dust collectors (Aarons et al. 2019; Frie et al. 2019). Dust samples can be analyzed using stable isotope ratios, such as 87Sr/86Sr and 143Nd/144Nd, to detail the provenance of the dust and its corresponding microbial community (Figure 1; Aciego et al. 2017; Dastrup et al. 2018; Xie et al. 2020; Yan et al. 2020). Furthermore, Sr-Nd isotopic analyses of Salton Sea dust may reveal geochemical features of the dust's provenance (i.e., the geography and climate) that may select for microbial migration from the Sea and the playa to the aeolian microbiome. Coupled with NGS technologies, this comprehensive analytical approach will explicate the dynamics within the playa, seawater and aeolian microbiomes, as well as their associated implications for microbial dispersal throughout the Salton Sea Basin.

Meta-Omics Analyses

Exploring diversity in Salton Sea microbiomes could leverage sophisticated molecular techniques (i.e., -omics), such as high-throughput NGS methods, shotgun metagenomics, metatranscriptomics or metaproteomics. Briefly, a shotgun

metagenome describes the collection of genomic material from a particular ecosystem, including both eukaryotic and prokaryotic genomes (Quince et al. 2017). Metagenomics can be used to characterize taxon-level microbial diversity and categorize putative functions performed by the microbial community. Although metagenomics can identify the functional traits within a microbiome, metatranscriptomics confirms which traits are actively expressed by the microbiome at a given time. A metatranscriptome includes the totality of gene (i.e., RNA) transcripts found within an environment (Shakya et al. 2019). Recently, metaproteomics has been used to complement NGS methods, via classifying and quantifying proteins produced by microbiomes (Hettich et al. 2013). Metagenomics has been used to study Salton Sea leaf litter (Chase et al. 2018; Chase et al. 2019; online technical Appendix Table 1) and seawater (Hawley et al. 2014), but these studies did not detail the functional diversity of their samples. Salton Sea playa and aeolian metagenomes have not been thoroughly described, nor have metatranscriptomic or metaproteomic approaches been employed yet for characterizing the activity of Salton Sea microbiomes. Because of the dearth of information on microbiome structure within the region, the Salton Sea presents a unique opportunity to utilize -omics techniques to study both microbial taxonomic and functional diversity across sub-ecosystems, which compose the larger ecosystem (Figure 1).

Metagenomic, metatranscriptomic and metaproteomic analyses have been performed on a wide variety of sample types, including the human gut (Long et al.

2020), soil (Romero-Olivares et al. 2019), deep-sea sediments (Mason et al. 2014), cloud water (Amato et al. 2019) and airborne dust particulates (Aalismail et al. 2019). These techniques allow for the comparative analyses of microbial genomes, transcriptomes and proteomes from different systems and ultimately identifies both shared taxa and genes among microbiomes. Functional annotation of metagenomes and metatranscriptomes, using comprehensive databases such as the Kyoto Encyclopedia of Genes and Genomes (KEGG) database (Kanehisa et al. 2016; Kanehisa et al. 2017; Kanehisa et al. 2019) and analytical tools like KoFamScan (Aramaki et al. 2020), detail the functional traits that are differentially expressed under specific environmental conditions (Amato et al. 2019; Chung et al. 2020; Shakya et al. 2019). For instance, soil metatranscriptomes may indicate whether microbial communities are actively allocating resources to stress response or proliferation (Romero-Olivares et al. 2019). Functional annotations can then guide the classification of proteins, such as microbial exudates, identified in metaproteomes (Hettich et al. 2013). Collectively, these analyses may further reveal metabolic strategies that enable microbial persistence in harsh conditions (Brewer et al. 2019). Furthermore, understanding these associated metabolic processes may reveal mechanisms that drive microbiome-resource interactions throughout this dynamic ecosystem.

Modeling Dust Emissions

Mineral dust advection, or dust transference by fluid flow, has been shown to be an important vector for the long-range transport of microbial organisms, especially in

and around desert environments such as the Salton Basin. While smaller particulates have longer atmospheric lifetimes due to their slower deposition velocities, larger aerosols (> 5 μm) typical of desert surfaces are especially efficient vectors of microbial dispersal (Yamaguchi et al. 2012). Dust transport patterns and ranges are thus dependent on both particle size and meteorology, with strong wind systems capable of relocating larger particles — along with any attached microorganisms — across continental distances (Perry et al. 1997). The Salton Sea region is one of the dustiest in the United States, with both the Coachella Valley and Imperial Valley regions consistently exceeding daily EPA standards for particulate matter (PM10). Moreover, these regions exhibit strong seasonality and frequent wind storm–driven dust events (Evan 2019; US Environmental Protection Agency 2020). This makes the patterns of dust emissions and transport, as driven by seasonal meteorology and sporadic dust storms, important for understanding regional sources and biogeographic patterns of local microorganisms.

Available tools for identifying sources of advected dust include trajectory or dispersion models such as the Hybrid Single Particle Lagrangian Integrated Trajectory Model (HYSPLIT; Stein et al. 2015). By combining local wind fields with physical dust deposition parameters, these models can run forwards (to estimate patterns of dust transportation and deposition from a given source) or generate backwards trajectories (to assess likely emission sources for particles collected at a given receptor site). These methods have been used previously to examine long range transport patterns of source-specific microbial populations (Cáliz et al. 2018; Rosselli

et al. 2015; Stres et al. 2013; Yamaguchi et al. 2012) and impacts of dust storms on downwind microbial communities (Hagh Doust et al. 2017; Mazar et al. 2016).

Our group has generated backward trajectories to evaluate the wind patterns blowing from the Salton Sea and estimate relative contributions of particulates reaching our passive dust collectors over a finite time period. Furthermore, we have explored the distribution and elemental composition in the Salton Sea region (Frie et al. 2019), which provides valuable context for explaining how seasonally shifting dust patterns — along with chemicals, physical particulates and associated microbial transport — may influence local microbiomes.

Conservation and Public Health in the Sea

Characterizing the unique microbial communities of the Salton Sea will complement ongoing investigations of the impacts of pollution on local residents and wildlife. Yet, many questions remain. For instance, how does the aeolian microbiome influence the lung microbiome? The aeolian microbiome may exacerbate respiratory symptoms via incidentally inhaled aeroallergens and particulate matter, resulting in the disproportionately higher rates of asthma and chronic respiratory disease detected in nearby communities (California Department of Public Health n.d.; Farzan et al. 2019). Can we explain long-term exposure effects of Salton Sea dust on the health of wildlife and local residents by comparing the Salton Sea microbial communities with unpolluted microbial communities, collected in analogous systems? The microorganisms themselves, in addition to their extracellular exudates (Chae et al. 2017; Rolph et al. 2018), may serve as bioindicators of either eutrophication or

pollution in soil, water or dust (Bouchez et al. 2016; Karimi et al. 2017; Schloter et al. 2018). Furthermore, historical exposure to pollutants may select for microorganisms that are uniquely suited for tolerating — or even ameliorating — toxicity within these particular systems.

In the interest of augmenting restoration efforts, how can we best deploy particular microbial taxa from the Salton Sea sub-ecosystems to remediate polluted systems via biodegradation or metal transformation (i.e., bioremediation; Kumar et al. 2019; Sher and Rehman 2019; Voica et al. 2016)? Novel opportunities for restoration may arise as human activities, such as mining and food production, increase apace with the shrinking of the Salton Sea. To illustrate one example, lithium mining of geothermal brines in the Salton Sea (Vikström et al. 2013), coupled with evaporation, may provide opportunities to leverage endemic microorganisms for bioremediation. Yet, microbial bioremediation may not be sufficient to mitigate the environmental impacts and deleterious human health outcomes for inhabitants of the region exposed to air pollution; this pollution may be exacerbated by evaporating novel brines, replete with toxic metals such as arsenic and manganese, which may cause neurological issues in children (Dion et al. 2018). To promote community health and ecosystem stability, we must investigate the dynamic interactions among the playa, seawater and aeolian microbiomes throughout the region. Furthermore, a thorough characterization of the functional attributes of dust microbiomes is needed to inform holistic approaches for addressing regional public health crises throughout the Salton Sea Basin.

Conclusions

The Salton Sea crisis necessitates immediate action as conditions rapidly worsen. Reduced precipitation and increasing temperatures are drivers of drought throughout California (Luo et al. 2017), advancing the diminution of the Salton Sea. Playa erosion and resulting dust emissions are predicted to rise (Parajuli and Zender 2018), which could interfere with incoming radiation and induce subsequent changes to local climate (Von Schneidemesser et al. 2015). Fluctuations in nutrient availability as a result of climate shifts will select for specific microbial functions (Louca et al. 2017; Louca et al. 2018), altering the overall trophic structure in the Sea. To better understand ecosystem resilience in this unpredictable landscape, more research is needed on the functional potential of these interacting environmental microbiomes and their contributions to nutrient cycling.

Any actions taken to increase the stability or conservation of this ecosystem may have public health implications, and vice versa, and we must anticipate the consequences of inaction to humans and wildlife. Careful consideration of the impacts of restoration or mitigation attempts must be holistically examined, as approaches addressing one area of concern may inadvertently yield adverse consequences for other areas. With greater knowledge, resources can be allocated towards strategic measures that aim to ameliorate the health of local human populations and promote the restoration of diverse wildlife and microbial communities that support resilient ecosystems.

References

Aalismail NA, Ngugi DK, Díaz-Rúa R, et al. 2019. Functional metagenomicanalysis of dust-associated microbiomes above the Red Sea. Sci Rep 9:13741. https://doi.org/10.1038/s41598-019-50194-0

Aarons SM, Arvin LJ, Aciego SM, et al. 2019. Competing droughts affect dust delivery to Sierra Nevada. Aeolian Res 41:100545. https://doi.org/10.1016/j.aeolia.2019.100545

Abuduwaili J, Liu DW, Wu GY. 2010. Saline dust storms and their ecological impacts in arid regions. J Arid Land 2:144–50. http://jal.xjegi.com/10.3724/SP.J.1227.2010.00144

Aciego SM, Riebe CS, Hart SC, et al. 2017. Dust outpaces bedrock in nutrient supply to montane forest ecosystems. Nat Commun 8:148200. https://doi.org/10.1038/ncomms14800

Allison SD, Martiny JBH. 2008. Resistance, resilience, and redundancy in microbial communities. P Natl Acad Sci USA 105(Supplement 1):11512–9. https://doi.org/10.1073/pnas.0801925105

Amato P, Besaury L, Joly M, et al. 2019. Metatranscriptomic exploration of microbial functioning in clouds. Sci Rep 9:4383. https://doi.org/10.1038/s41598-019-41032-4

Amato P, Joly M, Schaupp C, et al. 2015. Survival and ice nucleation activity of bacteria as aerosols in a cloud simulation chamber. Atmos Chem Phys 15:6455–65. https://doi.org/10.5194/acp-15-6455-2015

Anderson TW, Tiffany MA, Hurlbert SH. 2007. Stratification, sulfide, worms, and decline of the Eared Grebe (Podiceps nigricollis) at the Salton Sea, California. Lake Reserv Manage 23:500–17. https://doi.org/10.1080/07438140709354034

Andrei AŞ,. Banciu HL, Oren A. 2012. Living with salt: Metabolic and phylogenetic diversity of archaea inhabiting saline ecosystems. FEMS Microbiol Lett 330:1–9. https://doi.org/10.1111/j.1574-6968.2012.02526.x

Aramaki T, Blanc-Mathieu R, Endo H, et al. 2020. KofamKOALA: KEGG Ortholog assignment based on profile HMM and adaptive score threshold. Bioinformatics 36:2251–2. https://doi.org/10.1093/bioinformatics/btz859

Arnal RE. 1958. Rhizopoda
from the Salton Sea, California. Contrib Cushman Found Foram Res 9:36–45. https://cushman- foundation.org/PersonifyEbusi- ness/Portals/0/pdf/pubarchive/ccffr/09ccffr2.pdf

Arnal RE. 1961. Limnology, sedi- mentation, and microorganisms of the Salton Sea, California. Geol Soc Am Bull 72:427–78. https://doi.org/10.1130/0016-7606(1961)72[427:LSAMOT]2 .0.CO;2

Beman JM, Arrigo KR, Matson PA. 2005. Agricultural runoff fuels large phytoplankton blooms in vulnerable areas of the ocean. Nature 434:211–14. https://doi.org/10.1038/nature03370

Bouchez T, Blieux AL, Dequiedt S, et al. 2016. Molecular microbiology methods for environmental diagnosis. Environ Chem Lett 14:423–41. https://doi.org/10.1007/s10311-016-0581-3

Bowers RM, Lauber CL, Wiedinmyer C, M et al. 2009. Characterization of airborne microbial communities at a high-elevation site and their potential to act as atmospheric ice nuclei. Appl Environ Microb 75:5121–30. https://doi.org/10.1128/AEM.00447-09

Brewer TE, Aronson EL, Arogyaswamy K, et al. 2019. Ecological and genomic attributes of novel bacterial taxa that thrive in subsurface soil horizons. mBio 10:1–14. https://doi.org/10.1128/mBio.01318-19

Buck BJ, King J, Etyemezian V. 2011. Effects of salt mineralogy on dust emissions, Salton Sea, California. Soil Sci Soc Am J 75:1971–85. https://doi.org/10.2136/sssaj2011.0049

Buyer JS, Sasser M. 2012. High throughput phospholipid fatty acid analysis of soils. Appl Soil Ecol 61:127–30. https://doi.org/10.1016/j.apsoil.2012.06.005

California Department of Public Health. (n.d.). California Breathing County Asthma Data Tool. Environmental Health Investigations Branch. www.cdph.ca.gov/Programs/CCDPHP/DEODC/EHIB/CPE/Pages/CaliforniaBreathingData.aspx

California Natural Resources Agency. 2020. 2020 Annual Report on the Salton Sea Management Program. 48 p. https://saltonsea.ca.gov/wp-content/uploads/2020/02/2020-Annual-Report_2-21-20-v3.pdf

Cáliz J, Triadó-Margarit X, Camarero L, Casamayor EO. 2018. A long-term survey unveils strong seasonal patterns in the airborne microbiome coupled to general and regional atmospheric circulations. P Natl Acad SciUSA 115:12229–34. https://doi.org/10.1073/pnas.1812826115

Canton SP, Van Derveer WD. 1997. Selenium toxicity to aquatic life: An argument for sediment-based water quality criteria. Environ Toxicol Chem 16:1255–9. https://doi.org/10.1002/etc.5620160622

Carmichael WW, Li RH. 2006. Cyanobacteria toxins in the Salton Sea. Saline Syst 2:1–13. https://doi.org/10.1186/1746-1448-2-5.

Chae Y, Cui R, Woong Kim S, et al. 2017. Exoenzyme activity in contaminated soils before and after soil washing: ß-glucosidase activity as a biological indicator of soil health. Ecotox Environ Safe 135:368–74. https://doi.org/10.1016/j.ecoenv.2016.10.007

Chaffin JD, Bridgeman TB. 2014. Organic and inorganic nitrogen utilization by nitrogen-stressed cyanobacteria during bloom conditions. J Appl Phycol 26:299–309. https://doi.org/10.1007/s10811-013-0118-0

Chase AB, Arevalo P, Brodie EL, et al. 2019. Maintenance of sympatric and allopatric populations in free-living terrestrial bacteria. mBio 10:1–11. https://doi.org/10.1128/mBio.02361-19

Chase AB, Gomez-Lunar Z, Lopez AE, et al. 2018. Emergence of soil bacterial ecotypes along a climate gradient. Environ Microbiol 20:4112–26. https://doi.org/10.1111/1462-2920.14405

Chung YW, Gwak HJ, Moon S, et al. 2020. Functional dynamics of bacterial species in the mouse gut microbiome revealed by metagenomic and metatranscriptomic analyses. PLoS ONE 15:1–19. https://doi.org/10.1371/journal.pone.0227886

Cohen MJ. 2014. Hazard's toll: The costs of inaction at the Salton Sea. Oakland, Calif.: Pacific Institute. 50 p. https://pacinst.org/publication/hazards-toll/

Dastrup DB, Carling GT, Collins SA, et al. 2018. Aeolian dust chemistry and bacterial communities in snow are unique to airshed locations across northern Utah, USA. Atmos Environ 193:251–61. https://doi.org/10.1016/j.atmosenv.2018.09.016

Dillon JG, McMath LM, Trout AL. 2009. Seasonal changes in bacterial diversity in the Salton Sea. Hydrobiologia 632:49–64. https://doi.org/10.1007/s10750-009-9827-4

Dion LA, Saint-Amour D, Sauvé S, et al. 2018. Changes in water manganese levels and longitudinal assessment of intellectual function in children exposed through drinking water. NeuroToxicology 64:118–25. https://doi.org/10.1016/j.neuro.2017.08.015

Docherty KM, Pearce DS, Lemmer KM, Hale RL. 2018. Distributing regionally, distinguishing locally: Examining the underlying effects of local land use on airborne bacterial biodiversity. Environ Microbiol 20:3529–42. https://doi.org/10.1111/1462-2920.14307

Evan AT. 2019. Downslope winds and dust storms in the salton basin. Mon Weather Rev 147:2387–2402. https://doi.org/10.1175/MWR-D-18-0357.1

Failor KC, Schmale DG, Vinatzer BA, Monteil CL. 2017. Ice nucleation active bacteria in precipitation are genetically diverse and nucleate ice by employing different mechanisms. ISME J 11:2740–53. https://doi.org/10.1038/ismej.2017.124

Falkowski PG, Fenchel T, Delong EF. 2008. The microbial engines that drive earth's biogeochemical cycles. Science 320:1034–39. https://doi.org/10.1126/science.1153213

Farzan SF, Razafy M, Eckel SP, et al. 2019. Assessment of respiratory health symptoms and asthma in children near a drying saline lake. Int J Environ Res Public Health 16:3828. https://doi.org/10.3390/ijerph16203828

Frie AL, Dingle JH, Ying SC, Bahreini R. 2017. The effect of a receding saline lake (The Salton Sea) on airborne particulate matter composition. Environ Sci Technol 51:8283–92. https://doi.org/10.1021/acs.est.7b01773

Frie AL, Garrison AC, Schaefer MV, et al. 2019. Dust sources in the Salton Sea Basin: A clear case of an anthropogenically impacted dust budget. Environ Sci Technol 53:9378–88. https://doi.org/10.1021/acs.est.9b02137

Gaston CJ, Pratt KA, Suski KJ, et al. 2017. Laboratory studies of the cloud droplet activation properties and corresponding chemistry of saline playa dust. Environ Sci Technol 51:1348–56. https://doi.org/10.1021/acs.est.6b04487

González MR, Hart CM, Verfaillie JR, Hurlbert SH. 1998. Salinity and fish effects on Salton Sea microecosystems: Water chemistry and nutrient cycling. Hydrobiologia 381:105–28. https://doi.org/10.1023/A:1003227624686

Gorris ME, Cat LA, Zender CS, et al. 2018. Coccidioidomycosis dynamics in relation to climate in the southwestern United States. GeoHealth 2:6–24. https://doi.org/10.1002/2017GH000095

Griffin DW. 2007. Atmospheric movement of microorganisms in clouds of desert dust and implications for human health. Clin Microbiol Rev 20:459–77. https://doi.org/10.1128/cmr.00039-06

Grishkan I. 2011. Ecological stress: Melanization as a response in fungi to radiation. In Horikoshi K, ed. Extremophiles Handbook. p 1135–45. Tokyo: Springer Japan.

Hagh Doust N, Akbarinia M, Safaie N, et al. 2017. Community analysis of Persian oak fungal microbiome under dust storm conditions. Fungal Ecol 29:1–9. https://doi.org/10.1016/j.funeco.2017.05.002

Hawley ER, Schackwitz W, Hess M. 2014. Metagenomic sequencing of two Salton Sea microbiomes. Genome Announc 2:2010–1. https://doi.org/10.1128/genomeA.01208-13

Heisler J, Glibert PM, Burkholder JM, et al. 2008. Eutrophication and harmful algal blooms: A scientific consensus. Harmful Algae 8:3–13. https://doi.org/10.1016/j.hal.2008.08.006

Hettich RL., Pan C, Chourey K, Giannone RJ. 2013. Metaproteomics: Harnessing the power of high performance mass spectrometry to identify the suite of proteins that control metabolic activities in microbial communities. Anal Chem 85:4203–14. https://doi.org/10.1021/ac303053e

Hollister EB, Engledow AS, Hammett AJM, et al. 2010. Shifts in microbial community structure along an ecological gradient of hypersaline soils and sediments. ISME J 4:829–38. https://doi.org/10.1038/ismej.2010.3

Johnston C, Martin B, Fichant G, et al. 2014. Bacterial transformation: Distribution, shared mechanisms and divergent control. Nat Rev Microbiol 12:181–96. https://doi.org/10.1038/nrmicro3199

Jones BA, Fleck J. 2020. Shrinking lakes, air pollution, and human health: Evidence from California's Salton Sea. Sci Total Environ 7127:136490. https://doi.org/10.1016/j.scitotenv.2019.136490

Kandakji T, Gill TE, Lee JA. 2020. Identifying and characterizing dust point sources in the southwestern United States using remote sensing and GIS. Geomorphology 353:107019. https://doi.org/10.1016/j.geomorph.2019.107019

Kanehisa M, Furumichi M, Tanabe M, et al. 2017. KEGG: New perspectives on genomes, pathways, diseases and drugs. Nucleic Acid Res 45:D353–61. https://doi.org/10.1093/nar/gkw1092

Kanehisa M, Sato Y, Furumichi M, et al. 2019. New approach for understanding genome variations in KEGG. Nucleic Acid Res 47:D590–5. https://doi.org/10.1093/nar/gky962

Kanehisa M, Sato Y, Morishima K. 2016. BlastKOALA and GhostKOALA: KEGG tools for functional characterization of genome and metagenome sequences. J Mol Biol 428:726–31. https://doi.org/10.1016/j.jmb.2015.11.006

Karimi B, Maron PA, Chemidlin-Prevost Boure N, et al. 2017. Microbial diversity and ecological networks as indicators of environmental quality. Environ Chem Lett 15:265–81. https://doi.org/10.1007/s10311-017-0614-6

Kjelland ME, Swannack TM. 2018. Salton Sea days of future past: Modeling impacts of alternative water transfer scenarios on fish and bird population dynamics. Ecol Inform 43:124–45. https://doi.org/10.1016/j.ecoinf.2017.06.001

Knight R, Vrbanac A, Taylor BC, et al. 2018. Best practices for analysing microbiomes. Nat Rev Microbiol 16:410–22. https://doi.org/10.1038/s41579-018-0029-9

Köhler HR, Triebskorn R. 2013. Wildlife ecotoxicology of pesticides: Can we track effects to the population level and beyond? Science 341:759–65. https://doi.org/10.1126/science.1237591

Kopejtka K, Tomasch J, Zeng Y, et al. 2017. Genomic analysis of the evolution of phototrophy among haloalkaliphilic rhodobacterales. Genome Biol Evol 9:1950–62. https://doi.org/10.1093/gbe/evx141

Kumar G, Prasad JS, Suman A, Pandey G. 2019. Bioremediation of petroleum hydrocarbon-polluted soil using microbial enzymes. In Bhatt P, ed. Smart Bioremediation Technologies. Academic Press. p 307–17. https://doi.org/10.1016/B978-0-12-818307-6.00016-0.

Lighthart B, Shaffer BT. 1997. Increased airborne bacterial survival as a function of particle content and size. Aerosol Sci Tech 27:439–46. https://doi.org/10.1080/02786829708965483

Liu YX, Qin Y, Chen T, et al. 2020. A practical guide to amplicon and metagenomic analysis of microbiome data. Protein Cell 12:315–30. https://doi.org/10.1007/s13238-020-00724-8

Long S, Yang Y, Shen C, et al. 2020. Metaproteomics characterizes human gut microbiome function in colorectal cancer. NPJ Biofilms and Microbiomes 6. https://doi.org/10.1038/s41522-020-0123-4

Louca S, Jacques SMS, Pires APF, et al. 2017. High taxonomic variability despite stable functional structure across microbial communities. Nat Ecol Evol 1:0015. https://doi.org/10.1038/s41559-016-0015

Louca S, Polz MF, Mazel F, et al. 2018. Function and functional redundancy in microbial systems. Nat Ecol Evol 2:936–43. https://doi.org/10.1038/s41559-018-0519-1

Lozupone CA, Knight R. 2007. Global patterns in bacterial diversity. P Natl Acad Sci USA 104:11436–40. https://doi.org/10.1073/pnas.0611525104

Luo L, Apps D, Arcand S, et al. 2017. Contribution of temperature and precipitation anomalies to the California drought during 2012–2015. Geophys Res Lett 44:3184–92. https://doi.org/10.1002/2016GL072027

Ma J, Duan H, He L, et al. 2020. Spatiotemporal pattern of gypsum blooms in the Salton Sea, California, during 2000-2018. Int J Appl Earth Obs 89:102090. https://doi.org/10.1016/j.jag.2020.102090

Maki T, Bin C, Kai K, et al. 2019. Vertical distributions of airborne microorganisms over Asian dust source region of Taklimakan and Gobi Desert. Atmos Environ 214:116848. https://doi.org/10.1016/j.atmosenv.2019.116848

Maltz MR, Treseder KK, McGuire KL. 2017. Links between plant and fungal diversity in habitat fragments of coastal shrubland. PLoS ONE 12: e0184991. https://doi.org/10.1371/journal.pone.0184991

Manter DK, Vivanco JM. 2007. Use of the ITS primers, ITS1F and ITS4, to characterize fungal abundance and diversity in mixed-template samples by qPCR and length heterogeneity analysis. J Microbiol Meth 71:7–14. https://doi.org/10.1016/j.mimet.2007.06.016

Marti-Cardona B, Steissberg TE, Schladow SG, Hook SJ. 2008. Relating fish kills to upwellings and wind patterns in the Salton Sea. Hydrobiologia 604:85–95. https://doi.org/10.1007/978-1-4020-8806-3_7

Mason OU, Scott NM, Gonzalez A, et al. 2014. Metagenomics reveals sediment microbial community response to Deepwater Horizon oil spill. ISME J 8:1464–75. https://doi.org/10.1038/ismej.2013.254

Mazar Y, Cytryn E, Erel Y, Rudich Y. 2016. Effect of dust storms on the atmospheric microbiome in the eastern Mediterranean. Environ SciTechnol 50:4194–4202. https://doi.org/10.1021/acs.est.5b06348

McGonigle JM, Bernau JA, Bowen BB, Brazelton WJ. 2019. Robust archaeal and bacterial communities inhabit shallow subsurface sediments of the Bonneville Salt Flats. mSphere 4:1–12. https://doi.org/10.1128/mSphere.00378-19

Mesbah NM, Wiegel J. 2008. Life at extreme limits: The anaerobic halophilic alkalithermophiles. Ann NY Acad Sci 1125:44–57. https://doi.org/10.1196/annals.1419.028

Meteyer CU, Audet DJ, Rocke TE, et al. 2004. Investigation of a large-scale eared grebe (Podiceps nigricollis) die-off at the Salton Sea, California, in 1992. Stud Avian Biol:141–51.

Moreau MF, Surico-Bennett J, Vicario-Fisher M, et al. 2007. Selenium, arsenic, DDT and other contaminants in four fish species in the Salton Sea, California, their temporal

trends, and their potential impact on human consumers and wildlife. Lake Reserv Manage 23:536–9. https://doi.org/10.1080/07438140709354037

Nancharaiah YV, Lens PNL. 2015. Ecology and biotechnology of selenium-respiring bacteria. Microbiol Mol Biol Rev 79:61–80. https://doi.org/10.1128/MMBR.00037-14

Nicholson WL, Munakata N, Horneck G, et al. 2000. Resistance of Bacillus endospores to extreme terrestrial and extraterrestrial environments. Microbiol Mol Biol Rev 64:548–72. https://doi.org/10.1128/MMBR.64.3.548-572.2000

Nilsson RH, Anslan S, Bahram M, et al. 2019. Mycobiome diversity: high-throughput sequencing and identification of fungi. Nat Rev Microbiol 17:95–109. https://doi.org/10.1038/s41579-018-0116-y

Nol P, Rocke TE, Gross K, Yuill TM. 2004. Prevalence of neurotoxic of Clostridium botulinum type C in the gastrointestinal tracts of tilapia (Oreochromis mossambicus in the Salton Sea. J Wildlife Dis 40:414–9. https://doi.org/10.7589/0090-3558-40.3.414

Parajuli SP, Zender CS. 2018. Projected changes in dust emissions and regional air quality due to the shrinking Salton Sea. Aeolian Res 33:82–92. https://doi.org/10.1016/j.aeolia.2018.05.004

Paul VG, Mormile MR. 2017. A case for the protection of saline and hypersaline environments: A microbiological perspective. FEMS Microbiol Ecol 93:fix091. https://doi.org/10.1093/femsec/fix091

Perry KD, Cahill TA, Eldred RA, et al. 1997. Long-range transport of North African dust to the eastern United States. J Geophys Res-Atmos 102:11225–38. https://doi.org/10.1029/97JD00260

Polymenakou PN, Mandalakis M, Stephanou EG, Tselepides A. 2008. Particle size distribution of airborne microorganisms and pathogens during an intense African dust event in the eastern Mediterranean. Environ Health Persp 116:292–6. https://doi.org/10.1289/ehp.10684

Qin BQ, Gao G, Zhu GW, et al. 2013. Lake eutrophication and its ecosystem response. Chinese Sci Bull 58:961–70. https://doi.org/10.1007/s11434-012-5560-x

Quince C, Walker AW, Simpson JT, et al. 2017. Shotgun metagenomics, from sampling to analysis. Nat Biotechnol 35:833–44. https://doi.org/10.1038/nbt.3935

Reese BK, Anderson MA, Amrhein C. 2008. Hydrogen sulfide production and volatilization in a polymictic eutrophic saline lake, Salton Sea, California. Sci Total Environ 406:205–18. https://doi.org/10.1016/j.scitotenv.2008.07.021

Reheis MC, Budahn JR, Lamothe PJ. 2002. Geochemical evidence for diversity of dust sources in the southwestern United States. Geochim Cosmochim Ac 66:1569–87. https://doi.org/10.1016/S0016-7037(01)00864-X

Reynolds RL, Yount JC, Reheis M, et al. 2007. Dust emission from wet and dry playas in the Mojave Desert, USA. Earth Surf Proc Land 32:1811–27. https://doi.org/10.1002/esp.1515

Riedel R, Schlenk D, Frank D, Costa-Pierce B. 2002. Analyses of organic and inorganic contaminants in Salton Sea fish. Mar Pollut Bull 44:403–11. https://doi.org/10.1016/s0025-326x(01)00254-5

Rojas P, Rodriguez N, de la Fuenta V, Sanchez-Mata D, et al. 2018. Microbial diversity associated to the anaerobic sediments of a soda lake (Mono Lake, CA). Can J Microbiol 64:385–92. https://doi.org/10.1139/cjm-2017-0657

Rolph CA, Gwyther CL, Tyrrel SF, et al. 2018. Sources of airborne endotoxins in ambient air and exposure of nearby communities—A review. Atmosphere 9:75. https://doi.org/10.3390/atmos9100375

Romero-Olivares AL, Meléndrez-Carballo G, Lago-Lestón A, Treseder KK. 2019. Soil metatranscriptomes under long-term experimental warming and drying: Fungi allocate resources to cell metabolic maintenance rather than decay. Front Microbiol 10:1914. https://doi.org/10.3389/fmicb.2019.01914

Rosselli R, Fiamma M, Deligios M, et al. 2015. Microbial immigration across the Mediterranean via airborne dust. Sci Rep 5:16306. https://doi.org/10.1038/srep16306

Saiki MK, Martin BA, May TW. 2012. Selenium in aquatic biota inhabiting agricultural drains in the Salton Sea Basin, California. Environ Monit Assess 184:5623–40. https://doi.org/10.1007/s10661-011-2367-1

Samake A, Uzu G, Martins JMF, et al. 2017. The unexpected role of bioaerosols in the Oxidative Potential of PM. Sci Rep 7:10978. https://doi.org/10.1038/s41598-017-11178-0

Sapozhnikova Y, Bawardi O, Schlenk D. 2004. Pesticides and PCBs in sediments and fish from the Salton Sea, California, USA. Chemosphere 55:797–809. https://doi.org/10.1016/j.chemosphere.2003.12.009

Scheidweiler D, Miele F, Peter H, et al. 2020. Trait-specific dispersal of bacteria in heterogeneous porous environments: From pore to porous medium scale. J R Soc Interface 17:2020.0046. Https://doi.org/10.1098/rsif.2020.0046

Schloter M, Nannipieri P, Sørensen SJ, van Elsas JD. 2018. Microbial indicators for soil quality. Biol Fert Soils 54:1–10. https://doi.org/10.1007/s00374-017-1248-3

Schmidt KT, Maltz M, Ta P, B et al. 2020. Identifying mechanisms for successful ecological restoration with salvaged topsoil in coastal sage scrub communities. Diversity 12:150. https://doi.org/10.3390/d12040150

Von Schneidemesser E, Monks PS, Allan JD, et al. 2015. Chemistry and the linkages between air quality and climate change. Chem Rev 115:3856–97. https://doi.org/10.1021/acs.chemrev.5b00089

Shade A, Peter H, Allison SD, et al. 2012. Fundamentals of microbial community resistance and resilience. Front Microbiol 3:1–19. https://doi.org/10.3389/fmicb.2012.00417

Shakya M, Lo CC, Chain PSG. 2019. Advances and challenges in metatranscriptomic analysis. Front Genet 10:1–10. https://doi.org/10.3389/fgene.2019.00904

Sher S, Rehman A. 2019. Use of heavy metals resistant bacteria—a strategy for arsenic bioremediation. Appl Microbiol Biot 103:6007–21. https://doi.org/10.1007/s00253-019-09933-6

Stein AF, Draxler RR, Rolph GD, et al. 2015. NOAA's hysplit atmospheric transport and dispersion modeling system. B Am Meteorol Soc 96:2059–77. https://doi.org/10.1175/BAMS-D-14-00110.1

Stres B, Sul WJ, Murovec B, Tiedje JM. 2013. Recently deglaciated high-altitude soils of the Himalaya: Diverse environments, heterogenous bacterial communities and long-range dust inputs from the upper troposphere. PLoS ONE 8:e76440. https://doi.org/10.1371/journal.pone.0076440.

Swan BK, Ehrhardt CJ, Reifel KM, et al. 2010. Archaeal and bacterial communities respond differently to environmental gradients in anoxic sediments of a California hypersaline lake, the Salton Sea. Appl Environ Microbiol 76:757–68. https://doi.org/10.1128/aem.02409-09

Swan BK, Watts JM, Reifel KM, Hurlbert SH. 2007. Role of the polychaete Neanthes succinea in phosphorus regeneration from sediments in the Salton Sea, California. Hydrobiologia 576:111–25. http://doi.org/10.1007/s10750-006-0298-6

Tang K, Huang Z, Huang J, et al. 2017. Characterization of atmospheric bioaerosols along the transport pathway of Asian dust during the Dust-Bioaerosol 2016 Campaign. Atmos Chem Phys 18:7131–48. https://doi.org/10.5194/acp-18-7131-2018

Tignat-Perrier R, Dommergue A, Thollot A, et al. 2019. Global airborne microbial communities controlled by surrounding landscapes and wind conditions. Sci Rep 9:14441. https://doi.org/10.1038/s41598-019-51073-4

US Environmental Protection Agency. (n.d.). Air Quality System Data Mart. www.epa.gov/airdata

US Fish and Wildlife. 2014. DRECP Chapter III. 7. Biological Resources Chapter III.

Vikström H, Davidsson S, Höök M. 2013. Lithium availability and future production outlooks. Appl Energ 110:252–66. https://doi.org/10.1016/j.apenergy.2013.04.005

Vogl RA, Henry RN. 2002. Characteristics and contaminants of the Salton Sea sediments. Hydrobiologia 473:47–54. http://doi.org/10.1023/A:1016509113214

Voica DM, Bartha L, Banciu HL, Oren A. 2016. Heavy metal resistance in halophilic Bacteria and Archaea. FEMS Microbiol Lett 363:fnw146. https://doi.org/10.1093/femsle/fnw146

Wang W, Delgado-Moreno L, Conkle JL, et al. 2012. Characterization of sediment contamination patterns by hydrophobic pesticides to preserve ecosystem functions of drainage lakes. J Soil Sediment 12:1407–18. https://doi.org/10.1007/s11368-012-0560-7

Watts JM, Swan BK, Tiffany MA, Hurlbert SH. 2001. Thermal, mixing, and oxygen regimes of the Salton Sea, California, 1997-1999. Hydrobiologia 466:159–76. https://doi.org/10.1023/A:1014599719989

Wood AM, Miller SR, Li WKW, Castenholz RW. 2002. Preliminary studies of cyanobacteria, picoplankton, and virioplankton in the Salton Sea with special attention to phylogenetic diversity among eight strains of filamentous cyanobacteria. Hydrobiologia 473:77–92. https://doi.org/10.1023/A:1016573400010

Xie Y, Liu L, Kang C, Chi Y. 2020. Sr-Nd isotopic characteristics of the Northeast Sandy Land, China and their implications for tracing sources of regional dust. Catena 184:104303. https://doi.org/10.1016/j.catena.2019.104303

Xing S, Hou X, Aldahan A, et al. 2017. Water circulation and marine environment in the antarctic traced by speciation of 129I and 127I. Sci Rep 7:7726. https://doi.org/10.1038/s41598-017-07765-w

Xu EG, Bui C, Lamerdin C, Schlenk D. 2016. Spatial and temporal assessment of environmental contaminants in water, sediments and fish of the Salton Sea and its two primary tributaries, California, USA, from 2002 to 2012. Sci Total Environ 559:130–40. https://doi.org/10.1016/j.scitotenv.2016.03.144

Yamaguchi N, Ichijo T, Sakotani A, et al. 2012. Global dispersion of bacterial cells on Asian dust. Sci Rep 2:25. https://doi.org/10.1038/srep00525

Yan Y, Zheng Q, Yu RL, et al. 2020. Characteristics and provenance implications of rare earth elements and Sr–Nd isotopes in PM2.5 aerosols and PM2.5 fugitive dusts from an inland city of southeastern China. Atmos Environ 220:117069. https://doi.org/10.1016/j.atmosenv.2019.117069

Yang J, Ma L, Jiang H, et al. 2016. Salinity shapes microbial diversity and community structure in surface sediments of the Qinghai-Tibetan Lakes. Sci Rep 6:25078. https://doi.org/10.1038/srep25078

Ziyaee A, Karimi A, Hirmas DR, et al. 2018. Spatial and temporal variations of airborne dust fallout in Khorasan Razavi Province, Northeastern Iran. Geoderma 326:42–55. Https://doi.org/10.1016/j.geoderma.2018.04.010

Appendix A: Supplemental Information for Chapter 1

Title: Microbiome Interactions and their Ecological Implications at the Salton Sea

Table A.1.1. Microbial Studies within the Salton Sea Ecosystem
Studies that focused on microorganisms within the Salton Sea, including which type of sample was collected in their study, as well as the type and taxonomic resolution of microorganisms identified in their work. Each study has been assigned numeric codes, depending on methods used within a particular study; numeric codes in ascending order correspond to: 1 = culture-based methods, 2 = chain termination sequencing (i.e., Sanger sequencing chemistry), 3 = next-generation sequencing, 4 = biochemical assays, 5 = biomass and/or microscopic assays.

Study	Sample type	Microbial group	Taxa resolution	Methods
Chase et al. 2019	leaf-litter	Bacteria	Strain	3
Chase et al. 2018	leaf-litter	Bacteria	Strain	3, 4
Schilling et al. 2018	sediment	Bacteria	NA	1, 4, 5
Zhou et al. 2017	water	Bacteria	Species	1, 4, 5
Fradet et al. 2016	sediment	Bacteria, Archaea	Species	1, 3
Hawley et al. 2014	water	Bacteria	Phylum	3
VillaRomero et al. 2013	water, sediment	Bacteria	NA	1, 4, 5
Saiki et al. 2012	water, sediment	Eukaryotes	Species	4, 5
Swan et al. 2010	sediment	Bacteria, Archaea	Class	2, 4
Van Ginkel et al. 2010	water, sediment	Bacteria	Species	1, 2, 4
Dillon et al. 2009	water, sediment	Bacteria	Genus	2, 4
Tiffany et al. 2007	water	Eukaryotes	Species	5
Carmichael & Li 2006	water, tissue	Bacteria, Eukaryotes	Genus	1, 2, 4, 5
Lange & Tiffany 2002	water	Eukaryotes	Species	5
Okeke et al. 2002	sediment	Bacteria, Archaea	Species	1, 2, 4, 5
Reifel et al. 2002	water	Eukaryotes	Species	5
Wood et al. 2002	water, sediment	Bacteria, Eukaryotes	Strain	1, 2, 5
Arnal 1961	water, sediment	Eukaryotes	Species	4, 5
Arnal 1958	sediment	Eukaryotes	Species	5

CHAPTER II

Title: Diversity of Sulfur Cycling Halophiles within the Salton Sea, California's Largest Lake

Authors: Freund, L.[1], Hung, Caroline[2], Topacio, Talyssa M.[3], Diamond, Charlie[2], Fresquez, Alyson[2], Lyons, Tim[2], and Aronson, Emma L.[3]

1. Genetics, Genomics, and Bioinformatics Program, University of California, Riverside, CA
2. Department of Earth and Planetary Sciences, University of California, Riverside, CA
3. Department of Microbiology and Plant Pathology, University of California, Riverside, CA

Abstract

Microorganisms are the biotic foundation for nutrient cycling across ecosystems, and their assembly is often based on the nutrient availability of their environment. Though previous research has explored the seasonal lake turnover and geochemical cycling within the Salton Sea, California's largest lake, the microbial community of this extreme ecosystem has been largely overlooked. We collected seawater from a single location within the Salton Sea at 0m, 3m, 4m, 5m, 7m, 9m, 10m, and 10.5m depths in August 2021, December 2021, and April 2022. We observed that the water column microbiome was influenced by seasonal shifts in geochemistry, varying significantly by time point ($R^2 = 0.59$, $P = 0.003$). Of the geochemical features measured, temperature ($R^2 = 0.27$, $P = 0.004$), dissolved organic matter ($R^2 = 0.13$, $P = 0.004$), and dissolved oxygen ($R^2 = 0.089$, $P = 0.004$) were significant drivers of microbial composition. In addition, several halophilic chemoorganotrophs, phototrophs, and mixotrophs were consistently found in samples across depths and time points, though their relative abundances fluctuated. We also observed a high relative coverage of sulfur cycling genes, particularly sulfur oxidizing genes, in the metagenomes and metagenome-assembled genomes isolated from the 0m, 5m, and 10m samples from the water column. Our work demonstrates that the microbiome within the Salton Seawater has the capacity to metabolize sulfur species and utilize multiple trophic strategies, such as alternating between chemorganotrophy and chemolithoautrophy, to survive this harsh environment. Together, these results suggest that the Salton Sea microbiome is integral in the cycling

of nutrients within this ever-changing ecosystem, most notably sulfur, and thus contributes to the seasonal geochemical dynamics of the Salton Sea.

Introduction

The Salton Sea is a terminal, hypersaline lake located in Southern California that receives agricultural runoff as its main source of inflow (Tompson 2016). Since the Quantification Settlement Agreement in 2003, Colorado River water intended for farms in Imperial County was diverted to support growing populations in Southern California, reducing freshwater input into the Sea (Taylor 2018). This reduction in inflow coupled with agricultural runoff entering the Salton Sea has contributed to its drop in volume and surface area as well as its hypersalinity. Furthermore, the agricultural runoff coming from the New, Alamo, and Whitewater Rivers introduce high concentrations of nitrogen, phosphorous, and sulfur into the Salton Sea, along with a range of agricultural chemicals and pesticides, contributing to the lake's eutrophic and polluted status (Reese et al. 2008).

Despite the shallowness of the Salton Sea, it is a holomictic lake that experiences regular stratification in the warm summer months. Temperatures in the region rise and warm the surface water of the lake, creating a thermocline that separates the surface water (i.e., epilimnion) from the bottom waters (i.e., hypolimnion). The difference in density throughout the water column prevents dissolved oxygen in the epilimnion from flowing into to the hypolimnion, leading to an oxycline (i.e., an oxygen gradient). Anoxia in the hypolimnion allows for anaerobic, sulfate reducing bacteria to decompose organic matter and reduce sulfate (SO_4) to hydrogen sulfide (H_2S), leading to H_2S accumulation in the hypolimnion (Tiffany et al. 2007, Reese et al. 2008). As temperatures in the area

cool, the water column thermocline dissipates and lake turnover ensues, oxygenating the water column and stimulating sulfide oxidation. Lake mixing continues until temperatures in the Salton Sea region rise again in late spring, initiating the lake stratification cycle again. This seasonal stratification is expected to weaken as the lake continues to shrink because the lakes' shallow depth will prevent an oxycline from forming, inhibiting sulfate reduction in an oxygenated water column and subsequently preventing the accumulation of H_2S in the hypolimnion.

Seasonal lake stratification and oxidation-reduction regulate the lake's sulfur cycle, which greatly impacts the health and stability of this ecosystem. Summer winds in the region are occasionally strong enough to overcome the shallow lake's stratification, causing upwellings that introduce H_2S from the reducing hypolimnion to the oxic epilimnion (Reese et al. 2008). Rapid sulfide oxidation consumes the available oxygen in the water and contributes to gypsum crystal formation and precipitation, covering the surface of the Salton Sea in what is known as a gypsum bloom (Tiffany et al. 2007). These conditions are not only fatal to fish and birds but also fatal to phototrophic organisms in the water column by blocking out sunlight (Anderson et al. 2007, Ma et al. 2020). Additionally, SO_4 in the form of $MgSO_4$ and $CaSO_4$ minerals have also been found in high concentrations in the Salton Sea's exposed playa and dust attributed to the playa (Buck et al. 2011, Frie et al. 2019). These SO_4 minerals can hydrate and dehydrate repeatedly depending on their surrounding conditions, disrupting the sediment surface and increasing its vulnerability to wind erosion, leading to higher dust flux in the area

(Buck et al. 2011, Frie et al. 2019). The sulfur cycle in the Salton Sea is a crucial process that contributes to this ecosystem's dynamic structure and function.

While the Salton Sea's seasonal stratification and sulfur cycle have been well studied, the involvement of microorganisms in these dynamic processes has been neglected. To date, investigations into the Salton Sea microbiome have only focused on surface water microbial communities, and the functional diversity of the seawater microbiome is unknown (Freund et al. 2022). Considering that microorganisms are integral players in biogeochemical cycling within ecosystems, there is a need to understand how microorganisms are involved in the nutrient cycling of extreme ecosystems like the Salton Sea. For example, research from other sulfidic systems has shown that biological sulfide oxidation happens at a greater rate than abioitic sulfide oxidation (Luther et al. 2011), suggesting that sulfide oxidizing microorganisms are key drivers of rapid sulfur cycling. Without investigating the microbial contributions to nutrient cycling within an ecosystem, we cannot holistically understand the geochemical dynamics that create, maintain, and degrade extreme ecosystems such as the Salton Sea. Here, we explored the taxonomic and functional diversity of the Salton Sea microbiome across the water column. We utilized amplicon, marker gene sequencing (i.e., 16S rRNA sequencing) to determine the microbial composition of the Salton Sea water columns, as well as shotgun metagenomic sequencing to assess the functional capacity of a subset of these. The goal of this work is to better understand the distribution of microorganisms and their functions within the Salton Sea, and how these microbial communities regulate the geochemistry in their extreme, dynamic environment.

Methods

Seawater Collection & Processing

Water was collected from the same GPS coordinate (33.26265, -115.739) in the within the center of the southern basin in Salton Sea in August 2021, December 2021, and April 2022 (Supplemental Table 1). 1L of seawater was collected per depth, per timepoint using an ALEXIS peristaltic pump (Proactive Environmental Products) into acid-washed 1L Nalgene bottles from the following eight depths: 0m, 3m, 4m, 5m, 7m, 9m, 10m, and 10.5m. These sampling depths were selected at the chemoclines to access the hydrogen sulfide gradient and various microbial communities throughout the water column. Upon collection, the 1L seawater samples were transported back to the lab one ice and immediately filtered through two subsequent vacuum filtrations. For the first filtration, an acid-washed, sterilized glass funnel holding an autoclaved 5 μm filter (47-mm diameter; Durapore Membrane filters, Millipore Sigma, Temecula, CA, USA) was used to filter the 1L sample into an acid-washed, 1L flask to remove large aggregates from the sample. The resulting filtrate is then immediately vacuum filtered through an acid-washed, sterilized glass funnel holding a sterile 0.2 μm filter (47-mm diameter; Pall Supor 200 Sterile Grid filters, Pall Corporation, Port Washington, NY, USA) into an acid-washed, 1L flask. This second filtration is performed to capture microbial biomass on the 0.2 μm filters for future DNA extractions. Multiple 0.2 μm filters were used to process each 1L sample. Both the 5 and 0.2 μm filters were stored in sterile Whirl-pak bags respectively at -20 °C.

Geochemical Sampling Methods

For all water monitoring and sampling, the deepest portion of the southern basin was accessed at 33.26265, -115.739. Temperature, conductivity, pH, turbidity, dissolved oxygen (DO; in mg/L and percent saturation), dissolved organic matter (DOM), salinity, and oxidation-reduction potential (ORP) was determined *in situ* with a calibrated YSI EXO2 multi-parameter sonde probe (YSI Incorporated, Yellow Springs, OH, USA; Supplemental Table 1). Water column samples were collected with a battery-powered peristaltic pump with in-situ filtering capabilities. Samples collected for sulfide and sulfate analyses were filtered at 0.4 micron and preserved immediately with powdered zinc acetate for sulfide and sulfate concentration determinations.

Water column sulfates were precipitated as $BaSO_4$ by addition of saturated $BaCl_2$ solution (250g/L) followed by brief acidification (4N HCl) to remove carbonates, rinsed to neutral pH and remove sodium chloride, and then dried. Sulfate concentrations were determined gravimetrically. Total dissolved sulfide ($\Sigma S^{2-} = H_2S + HS^- + S^{2-}$) concentration in the water column (i.e., liquid phase) were determined from 1 mL sample aliquots dispensed into 2 mL microcentrifuge tubes pre-filled with 0.5 mL of 20% zinc acetate solution. Samples were then vortexed for 5 s and stored at 4^{o}C in the dark until analysis. Sulfide concentration was determined colorimetrically using the method of Cline (Cline 1969).

DNA Extraction and Amplification

DNA extraction from the 0.2 μm filters were performed in duplicate with the Qiagen DNeasy PowerWater kit (Qiagen, Germantown, MD, USA), and the extracts

were quantified with a NanoDrop 2000 (Thermo Fisher Scientific, Wilmington, DE, USA). Half of the duplicate extracts were then purified via a bead clean-up using AMPure XP Beads and quantified with a NanoDrop 2000. Raw and clean DNA extracts were stored at −20 °C. Clean DNA extracts were amplified and indexed with 2-step PCR. Extracts from August 2021 were amplified with Nextera-adapted Klindworth primers (Klindworth et al. 2013)targeting the 16S rRNA V3-V4 region. Amplification products were cleaned in an AMPure magnetic bead clean up step then indexed with Illumina Nextera XT indices (Illumina, San Diego, CA, USA). Clean DNA Extracts from December 2021 and April 2022 were quantified using the NanoDrop 2000 and high-yield samples (>10 ng/uL) were normalized to 10 ng/uL. Clean and normalized samples were amplified with DipSeq adapted Klindworth primers (Klindworth et al. 2013) and cleaned up using an AMPure magnetic bead clean up step before being indexed using DipSeq indices. While the use of different sequencing indices may introduce potential variation, denoising and filtering of the reads via the DADA2 pipeline (please see the "Bioinformatics-Amplicon Sequence Data" section) yielded an even distribution of reads across samples before amplicon sequence variants (ASV) were assigned (Supplemental Figure 1). Furthermore, raw sequencing reads were transformed and/or normalized before downstream analyses. For the August 2021 samples prepared with the Nextera XT Index Kit, each amplification reaction contained the following: 1uL of DNA template, 5uL each of the 1uM forward and reverse index primers, 12.5 uL of PCR KAPA HiFi HotStart Ready Mix, and 1.5 uL of PCR grade water to create a 25uL reaction. For the December 2021 and April 2022 samples prepared with the DIP-seq adapted Klindworth primers,

each amplification reaction contained the following: 2uL of DNA template, 12.5 uL Phusion HSII Hi-Fidelity Ready Mix, 1uL each of the 1uM forward and reverse index primers, 0.1uL of BSA, and 8.5uL of water to yield a 25 uL reaction. Before sequencing submission, indexed products were cleaned with an AMPure magnetic bead clean up step and quantified using Qubit. Samples were then pooled relative to their DNA concentration.

DNA Sequencing

The amplified, pooled DNA extracts were sequenced via the Illumina, Inc. MiSeq platform (Illumina 2017) by the UC Riverside Genomics Core. Raw DNA extracts collected from the 0m, 5m, and 10m samples from each timepoint were sent on dry ice to the SeqCenter for shotgun metagenome sequencing. The SeqCenter prepared these libraries using the Illumina DNA Prep kit and IDT 10bp UDI indices and sequenced the libraries on an Illumina NextSeq 2000 (2 x 151bp).

Bioinformatics – Amplicon Sequence Data

Amplicon sequences were demultiplexed by the UC Riverside Genomics Core, and the FASTQ sequences were assessed for sequencing quality via FastQC (Andrews n.d.). In addition to FastQC, the eestats2 program (Edgar and Flyvbjerg 2015) was used to determine the percentage of reads of specific lengths that will pass through the expect error threshold for a specific sample. The results supplied by FastQC and eestats2 were used to determine where the reads should be trimmed across the samples. Before trimming, there was a total of 4,237,100 reads across all 24 samples (including forward and reverse reads) that were 301 base pairs long. The reads were then trimmed and

filtered with BBDuk, a k-mer-based trimming and decontamination program from the BBTools suite created by the Joint Genome Institute (Bushnell n.d.), resulting in a total of 4,232,018 trimmed reads across the samples. After trimming, the Divisive Amplicon Denoising Algorithm 2 (DADA2) pipeline (Callahan et al. 2016) was used via the RStudio environment (version 2023.03.0+386) to assign reads to amplicon sequence variants (ASVs). Contaminant ASVs identified by the "decontam" package for R, as well as ASVs identified in the PCR positive and negative controls, were removed from the ASV count data. Singletons and ASVs that were assigned to "Chloroplast" or "Mitochondria" taxonomic classifications were also removed from the ASV count data set (Davis et al. 2018). Prior to decontamination (i.e., removing ASVs identified in library preparation or sequencing controls, as well as ASVs assigned to mitochondria or chloroplasts), there was a total of 515,899 ASVs. After decontamination, there was 313,035 ASVs that were used for taxonomic identification.

Bioinformatics – Metagenome Sequence Data

In total there were nine samples submitted for shotgun metagenome sequencing, with each metagenome collected at the 0m, 5m, or 10m depths in August 2021, December 2021, and April 2022. The sequence quality of the shotgun metagenomic data was assessed using FastQC (Andrews n.d.), and adapter and primer sequences were trimmed using BBDuk (Bushnell n.d.). There was a total of 126,416,634 read pairs before the metagenome sequences prior to trimming. After trimming, there were 120,169,462 read pairs used for contig assembly. BBNorm (BBTools suite, (Bushnell n.d.) was used to normalize the depth of trimmed read coverage in each metagenome. This

normalization step ensures that there is an equal distribution of reads across all the sequenced regions, which is a necessary consideration with shotgun metagenomes due to their unequal sequence coverage (Bushnell n.d.). The normalized reads are then error-corrected with SPades (Bankevich et al. 2012) and subsequently used for contig assembly with metaSPades (Nurk et al. 2017), a metagenome-specific assembler available within SPades. The quality of the assembled contigs was determined using MetaQuast (Mikheenko et al. 2016). Trimmed, non-normalized metagenomic reads were then aligned to the assembled contigs using BWA-MEM. After read mapping, contigs and scaffolds were binned into genomes (i.e., metagenome-assembled genomes; MAGs) with metaBAT (Kang et al. 2019), using the read mapping results from BWA-MEM to guide the binning. The quality and completeness of the MAGs was determined using CheckM (Parks et al. 2015). A custom bash script was then used to read the output from CheckM and parse out bins based on their completeness and contamination, identifying high-quality (i.e., >80% complete, <5% contamination) bins for downstream analyses (Bowers et al. 2017; Supplemental Table 2). Gene prediction was performed on the contigs and high-quality MAGs respectively using Prodigal (Hyatt et al. 2010a). KOFamScan was then used to assign functions and KEGG orthologies (i.e., KO identifiers) to the predicted genes (Hyatt et al. 2010b, Aramaki et al. 2020) in the contigs and high-quality MAGs. Genes assigned the same KO ID are functional orthologs of one another, and thus code for the same function across organisms. High-quality MAGs were also taxonomically annotated using GTDB-tk (Chaumeil et al. 2020).

The number of reads that mapped to each gene in both contigs and high-quality MAGs was determined using featureCounts (Liao et al. 2014), which compares the alignment file created by BWA-MEM and the predicted genes found by Prodigal. The number of reads mapped to each gene calculated by featureCounts was combined with the functional annotations from KOFamScan via a custom bash script. The featureCounts results were then used to calculate depth of coverage for each gene in R by dividing the number of reads mapped to a gene by the gene's length. Multiple genes were assigned the same KO identifier(s); thus, the coverage for each gene assigned the same KO were summed together to calculate coverage per KO assignment within contigs and high-quality MAGs respectively. The summed depth of coverage per KO was subsequently transformed via a center-log ratio transformation using the vegan package's "decostand" command (Oksanen et al. 2020) to normalize the gene coverages by their respective sample library size (Quinn et al. 2018, 2019, Pereira et al. 2018, Xia 2023). Non-transformed, summed KO coverages within the contigs and high-quality MAGs were used as input in a custom R script to create binary presence-absence tables for functions of interest.

Statistical Analyses and Data Visualization

The 16S rRNA amplicon data, the annotated contigs and MAGs, and the geochemistry data (i.e., dissolved oxygen (DO%), oxidative-reduction potential (ORP), dissolved organic matter (DOM), salinity, temperature, sulfate concentrations, and hydrogen sulfide concentrations) were analyzed in the RStudio environment using R software version 4.2.2. All environmental variables considered were centered and scaled

via the “scale” function from “base” package in R before statistical analyses were performed. Correlations between the environmental variables were determined using the “cor.test” function from the “stats” package and visualized using the “corrplot.mixed” function from the “corrplot” package (Wei and Simko 2021).

Raw, decontaminated 16S V3-V4 rRNA amplicon counts were rarefied to a sequencing depth of 7,381 using the “rrarefy” function from the “vegan” package (Oksanen et al. 2020). The sequencing depth used for rarefaction was the minimum number of total ASV counts observed across samples, which was identified using the “min” and “rowSums” functions from the “base” package in R. Shannon-Wiener diversity (i.e., alpha diversity) and species richness of the rarefied 16S V3-V4 rRNA amplicon count data (i.e., microbial composition data) were calculated using the “diversity” and “specnumber” functions from the “vegan” package. Alpha diversity and species richness were assessed for normality via Shapiro-Wilks tests using the “shapiro.test” function from the “stats” package. The Shapiro-Wilks test determined that alpha diversity was normally distributed ($P = 0.711$) and species richness was not normally distributed ($P = 0.009$), and thus, analyzing species richness would require non-parametric statistical tests for this work. A t-test was used to compare the means of alpha diversity between time points by using the “t.test” function from the “stats” package, and p-values were adjusted using the Bonferroni correction via the “p.adjust” function from the “stats” package. An analysis of variance (ANOVA) was also used to compare the variance of alpha diversity between time points by using the “aov” function from the “stats” package. After the ANOVA, a Tukey’s Honest Significant Difference (HSD) test

was used via the "TukeyHSD" function from the "stats" package to determine which time points' variances were significantly different from one another. Then, a Levene's test was used via the "leveneTest" function from the "car" package to compare the homogeneity of variances across timepoints (Fox and Weisberg 2019).

A Wilcoxon test was used to compare the mean of species richness between time points using the "wilcox.test" function from the "stats" package, and p-values were adjusted using the Bonferroni correction via the "p.adjust" function from the "stats" package. Additionally, a Kruskal-Wallis test was used to compare variance of species richness between time points using the "kruskal.test" function from the "stats" package. After the Kruskal-Wallis, a Dunn test was used via the "dunn_test" function from the "rstatix" package to determine which time points' variances were significantly different from one another. To then compare the homogeneity of variances across time points, a Fligner-Killeen test using the "fligner.test" function from the "stats" package was performed.

To determine if environmental variables could accurately predict the distribution of alpha diversity and species richness across samples, generalized linear models were used. Specifically, to assess the impact of environmental variables on Alpha diversity, a generalized linear model (i.e., GLM, a using a Gaussian distribution) was run via the "glm" function from the "stats". As for species richness, a GLM (using a negative binomial distribution) was run via the "glm.nb" function from the "MASS" package. Environmental variables were chosen for these GLMs based on their ecological importance and on their correlations to one another. P-values from multivariate GLMs as

well as the ANOVA and Kruskal-Wallis tests were adjusted using the Bonferroni correction via the “p.adjust” function from the “stats” package (R Core Team 2024).

Beta diversity of the microbial composition data was performed by first transforming the data via a center-log ratio (i.e., CLR) transformation using the “decostand” function from the “vegan” package. This function adds a pseudocount of 1 to all function counts, including those functions that have a count of zero, before performing the transformation. Then a Euclidean distance matrix of the CLR-transformed 16S V3-V4 amplicon count data was created using the “dist” function from the “vegan” package and used as input to create a Principal Coordinates Analysis (i.e., PCoA) with the “pcoa” function from the “vegan” package. Homogeneity of variance in the microbial composition data across time points were compared using the “betadisper” function from the “vegan” package. Permutational multivariate analyses of variance (PERMANOVA) were performed with the “adonis2” function from the “vegan” package to determine if there were significant differences in microbial composition across time points and depths. All p-values for the PERMANOVAs were adjusted using the Bonferroni correction via the “p.adjust” function from the “stats” package.

A Detrended Correspondence Analysis (i.e., DCA) was performed using the “decorana” function from the “vegan” package to determine if there was an arch effect present within the microbial composition data across sites and within sites. Due to the length of the first DCA axes, Redundancy Analysis (i.e., RDA) was chosen to determine if and how the microbial composition data are constrained by the geochemistry data. RDAs were calculated using the “rda” function from the “vegan” package. The variation

explained by the RDAs was obtained using the "RsquareAdj" function from the "vegan" package, and the significance of the RDAs was determined using the "anova" function from the "stats" package. The variance inflation factors for each predictor variable (i.e., the geochemistry data) in the RDAs was determined using the "vif.cca" function from the "vegan" package. To find the best fitting model, the "ordistep" and "ordiR2step" functions from the "vegan" package were used. The "ordistep" function builds the RDA stepwise to determine which variables lead to significant changes in variance and a lower AIC value for the model. The "ordiR2step" function builds the RDA stepwise based on which variables maximize the adjusted variation explained by each predictor variable considered (i.e., their adjusted R^2) and are statistically significant. All p-values for the multivariate RDAs with the best fit were adjusted using the Bonferroni correction via the "p.adjust" function from the "stats" package.

Results

Seasonal Environmental Differences

Environmental conditions throughout the water columns significantly varied across time, between August 2021, December 2021, and April 2022. Specifically, percent saturation of dissolved oxygen (i.e., %DO; P = 2.937e-04), dissolved organic matter (i.e., DOM; P = 3.508e-05), oxidative-reduction potential (i.e., ORP; P = 5.112e-05), sulfate concentration (P = 2.83e-06), hydrogen sulfide concentration (P = 0.005), and temperature (P = 3.524e-05) significantly varied across sampling dates. Hydrogen sulfide concentration was significantly different in August when compared to December (P =

0.03) and April (P = 0.016), whereas December and April did not significantly differ from one another (P = 0.703).

Of the three time points studied, temperature was at its peak throughout the water column in August 2021 compared to December 2021 and April 2022 (Supplemental Table 1). Hydrogen sulfide concentration and DOM were also at their highest in August relative to December and April, particularly at 7m and below. Conversely, ORP and %DO were at their lowest in August. Within August 2021, %DO had a strong, negative correlation with DOM (r = -0.889, P = 0.003) and depth (r = -0.930, P = 0.0008), and a strong positive correlation with temperature (r = 0.821, P = 0.012). DOM was also strong, negatively correlated with ORP (r = -0.804, P = 0.016) but strongly, positively correlated with hydrogen sulfide concentration (r = 0.854, P = 0.007) and depth (r = 0.977, P = 2.84e-05). Hydrogen sulfide concentration and ORP (r = -0.971, P = 6.06e-05), as well as ORP and depth (r = -0.720, P = 0.044), were also strongly, negatively correlated.

By December 2021, temperature and hydrogen sulfide concentration throughout the water column was at its lowest whereas sulfate concentration and %DO was at its highest relative to August and April. %DO was still significantly, negatively correlated with depth (r = -0.770, P = 0.025). ORP and temperature were strongly, negatively correlated (r = -0.819, P = 0.013). These were the only correlations observed in the geochemistry data in December.

In April 2022, DOM had reached its lowest concentration relative to August and December, whereas ORP was at its highest throughout the water column. %DO strongly,

positively correlated with temperature (r = 0.920, P = 0.001), but negatively correlated with DOM concentration (r = -0.942, P = 0.0004) and depth (r = -0.873, P = 0.005). DOM is strongly, negatively correlated with temperature (r = -0.996, P = 1.098e-07) but positively correlated with depth (r = 0.738, P = 0.0365).

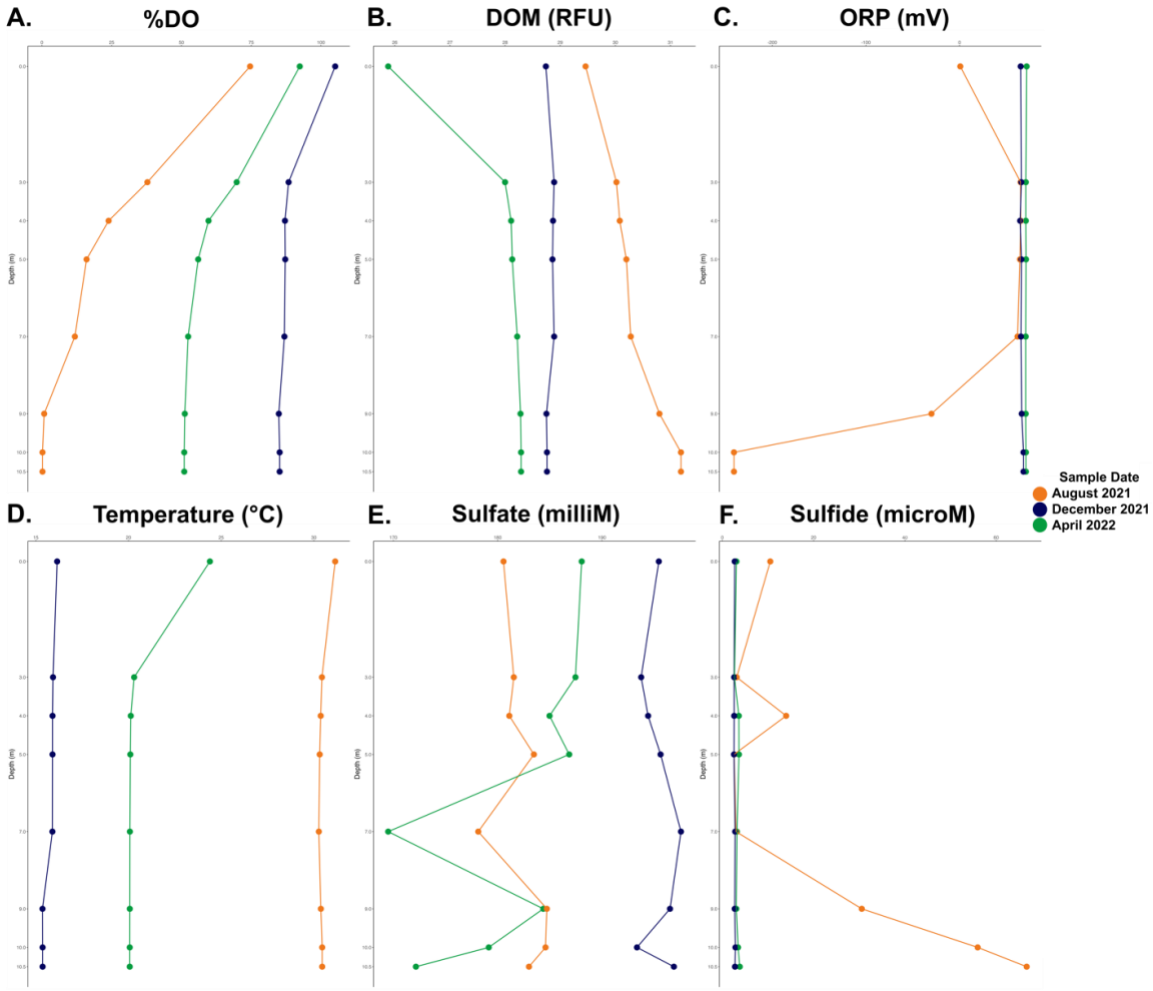

Figure 1. Vertical Profiles of (A) % Dissolved Oxygen, (B) Dissolved Organic Matter, (C) Oxidative-Reduction Potential, (D) Temperature, (E) Sulfate, and (F) Sulfide in Our Sampling Location in the Salton Sea. Measurements were taken in August 2021 (orange), December 2021 (blue), and April 2022 (green) at 8 different depths (0m, 3m, 4m, 5m, 7m, 9m, 10m, and 10.5m).

Alpha Diversity and Species Richness

Alpha diversity increased from August 2021 to December 2021 to April 2022 (Figure 2, Supplemental Table 3). Mean alpha diversity in August 2021 was significantly lower than both December 2021 ($P = 0.018$) and April 2022 ($P = 0.044$), but December and April did not significantly differ from one another ($P = 1$). Additionally, the sample from the 9m depth consistently had the lowest alpha diversity of all the samples from each time point. Alpha diversity significantly varied across time points ($P = 0.011$), yet this trend did not hold true when comparing time points in a pair-wise fashion (Supplemental Table 4). The variance in alpha diversity of August 2021 was also significantly different than December 2021 ($P = 0.017$) and April 2022 ($P = 0.01$), whereas the variance in alpha diversity did not significantly differ between December 2021 and August 2021 ($P = 0.96$). Lastly, a generalized linear model determined that temperature C ($P = 0.0004$) and SO_4 ($P = 0.036$) together were the only environmental variables that significantly predicted alpha diversity ($R^2_{adj} = 0.406$, $P = 0.0016$).

In contrast to alpha diversity, species richness appears to slightly decrease across time points (Supplemental Table 3); but richness was not significantly different between any of the time points (Figure 2). The variance of species richness also did not vary significantly overall ($P = 0.5$, Supplemental Table 4). However, as was observed with alpha diversity, the 9m sample at each time point consistently maintained the lowest species richness. Furthermore, ORP ($P = 0.627$) and SO_4 concentration ($P = 0.0085$) interacted significantly to predict species richness across time points (McFadden's Pseudo $R^2 = 0.346$, $P = 0.0057$).

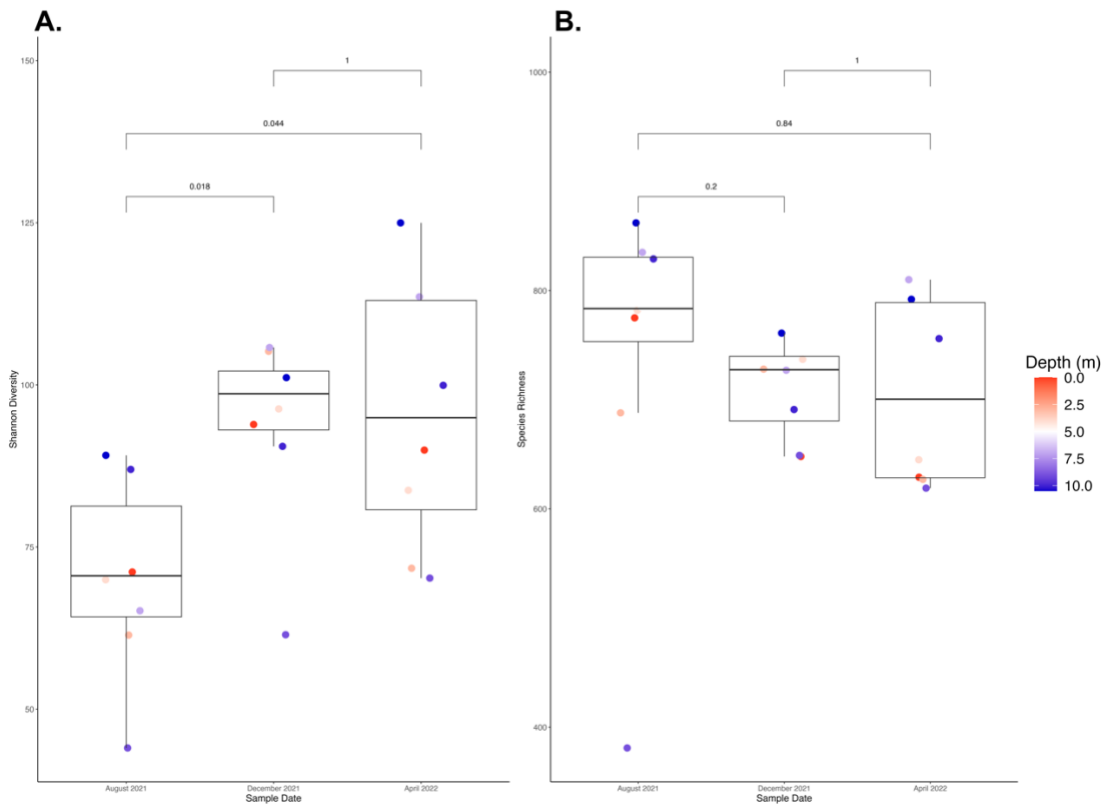

Figure 2. Alpha (Shannon) Diversity (A) and Species Richness (B) by Time Point. These box-and-whisker plots compare alpha diversity and species richness by time point. Each point represents a sample and are colorized by depth, with red being the shallow depths and blue as the deeper depths. The statistical comparisons shown are the adjusted p-values from a t-test comparing Shannon diversity by time point and a Wilcoxon test for comparing species richness by time point.

Microbial Composition and Diversity

Microbial composition significantly varied between time points ($R^2 = 0.59$, $P = 0.003$); however, it should be noted that the dispersion of microbial composition was not homogeneous between time points ($P = 0.0003$). A principal coordinates analysis (PCoA) showed that microbial composition is tightly clustered by time point, rather than the depth that each sample originated from (Figure 3). Microbial composition throughout the water column in August 2021 exhibited the greatest dispersion in microbial

composition and is significantly greater than the microbial dispersion in December 2021 (P = 0.0034) and April 2022 (P = 0.0004). A PERMANOVA confirmed that the variance in microbial composition across time points were significantly different from one another: August 2021 and December 2021 (R^2 = 0.49, P = 0.003), December 2021 and April 2022 (R^2 = 0.55, P = 0.003), and August 2021 and April 2022 (R^2 = 0.52, P = 0.006; Supplemental Table 5).

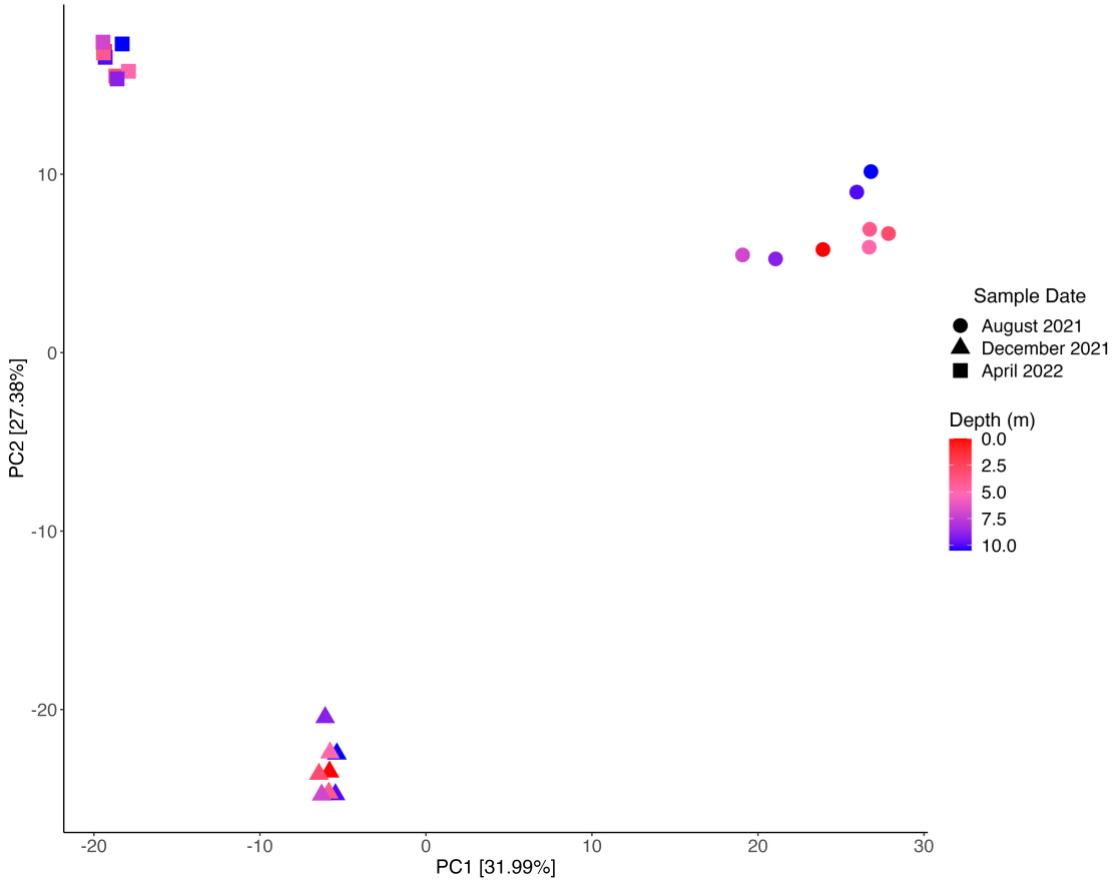

Figure 3. Principal Coordinates Analysis (PCoA) of Microbial Composition by Time Point and Depth. Each point represents a sample, with its shape corresponding to the sampling time point and the color corresponding to the sampling depth. The first axis of variation (PC1) represents 31.99% of the variation, and the second axis of variation (PC2) represents 27.38% of the variation.

Within each time point, patterns of microbial taxa remained consistent throughout the water column (Supplemental Figure 2). Thus, we describe the total relative abundance of microbial taxa throughout the water column as opposed to focusing on specific depths. Two microbial families, Microbacteriaceae and Nitriliruptoraceae, dominated the water column microbiome across depths and time points. The relative abundance of Microbacteriaceae decreased from 29.45% in August 2021 to 27.29% in December 2021 to 11.49% by April 2022. Conversely the relative abundance of Nitriliruptoraceae increased from 12.18% in August 2021 to 14.08% in December 2021 to 26.98% in April 2022. Litoricolaceae appeared as the third most abundant family in August 2021 (10.24%) and April 2022 (9.24%) but was replaced by Ilumatobacteraceae in December 2021 (9.98%).

A single genus from the Microbacteriaceae family, *DS001*, accounted for over a third of the total relative abundance of the water column microbiome in August 2021 (39.40%) and December 2021 (39.57%; Figure 4). By April 2022, the relative abundance of DS001 throughout the water column had dropped to 11.87%. *Litoricola* represented 15.22% of the relative abundance throughout the water column in August 2021, decreased to 4.51% of the total relative abundance in December 2021, then increased to 16.66% of the water column microbiome in April 2022. *Synechococcus CC9902* was the third most abundant genus in August 2021 at 7.78% of the total relative abundance, but decreased to 2.44% in December 2021, then to less than 1% in April 2022. *Truepera* increased in total relative abundance from 1.96% in August 2021 to 3.36% to 12.56% in

April 2022, becoming the second most abundant genus in the water column at that time point.

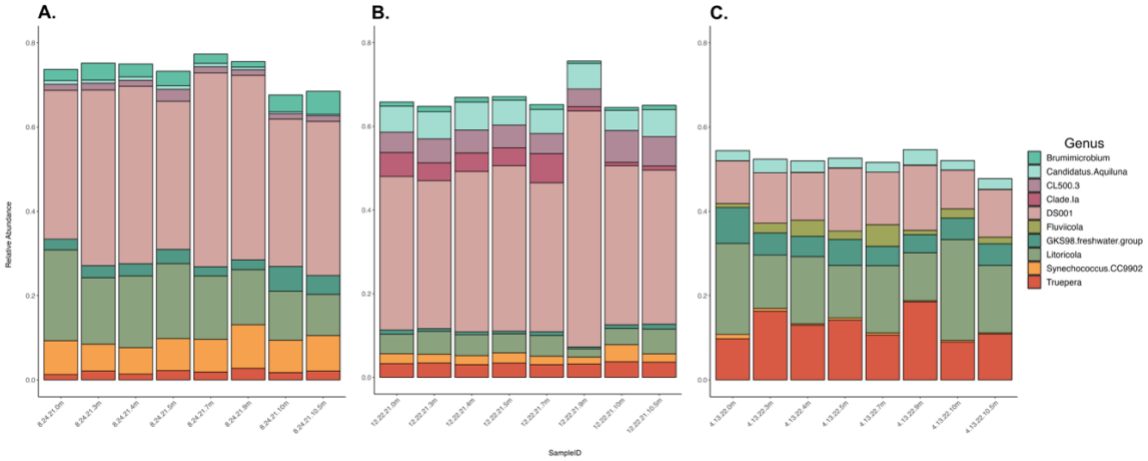

Figure 4. Relative Abundance of the Top 10 Most Abundant Bacterial Genera by Time Point. These stacked bar plots display the relative abundance of the top 10 most abundant bacterial genera (16S rRNA) in August 2021 (**A**), December 2021 (**B**), and April 2022 (**C**). The x-axis contains the Sample IDs organized in order of increasing depth, and the y-axis is the relative abundance.

Temperature, DOM, and %DO are significant environmental drivers of overall microbial composition throughout the water column (Figure 5, Supplemental Table 6). Redundancy analyses found that temperature was the environmental driver that explained the greatest variance in microbial composition across time points ($R^2 = 0.27$, $P_{adj} = 0.004$), followed by DOM ($R^2 = 0.13$, $P_{adj} = 0.004$), then %DO ($R^2 = 0.089$, $P_{adj} = 0.004$). When evaluating environmental drivers of microbial composition within August 2021, DOM appeared to be the only significant variable ($P_{adj} = 0.002$). However, DOM only explained 10.91% of the variation observed in the microbial assembly in this time point. In December 2021, ORP was the most significant environmental driver ($P_{adj} = 0.012$), but only explained 4.23% of the total variation in microbial composition. DOM

was the only near significant environmental driver in April 2022 (P_{adj} = 0.068) but constrained only 1.5% of the total variation in microbial composition.

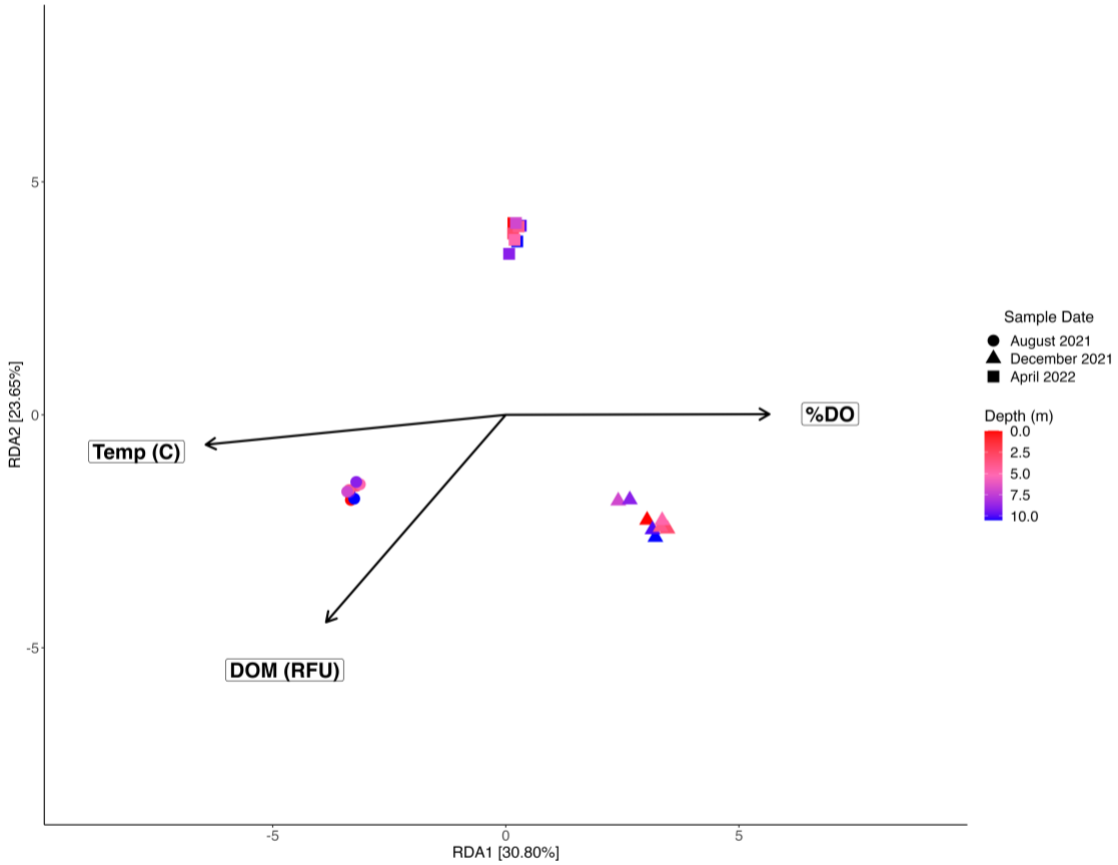

Fig 5. Redundancy Analysis of Environmental Variables and Microbial Composition. This is a redundancy analysis showing the significant environmental variables driving microbial (16S rRNA) composition. Each point represents a sample with its shape corresponding to its sampling time point, and the color corresponding to its sampling depth. Temperature (R^2 = 0.27, P = 0.004), dissolved organic matter (DOM; R^2 = 0.13, P = 0.004), and percent saturation of dissolved oxygen (%DO; R^2 = 0.089, P = 0.004) significantly drive microbial composition across sites.

Taxonomic Annotation of MAGs

A total of 1,907,889 contigs were assembled from these nine metagenomes and subsequently binned into 231 metagenome-assembled genome (MAG) bins. Bins with 80% completeness and < 5% contamination were classified as “good” bins and used for

taxonomic annotation (Anantharaman et al. 2016, Bowers et al. 2017). Out of 231 MAGs, 35 bins had a completeness of > 80% and contamination < 5% and thus were selected for functional and taxonomic annotation. All 35 MAGs were identified as *Bacteria* and were assigned to the following phyla: *Proteobacteria* (n = 14), *Bacteroidota* (n = 12), *Actinobacteriota* (n = 8), and *Cyanobacteria* (n = 1; Supplemental Table 7). All 14 *Proteobacteria* MAGs were of the *Gammaproteobacteria* class and all 12 of the *Bacteroidota* MAGs belonged to the *Bacteroidia* class. *Actinobacteriota* MAGs were split between the *Acidimicrobiia* class (n = 4) and the *Actinomycetia* class (n = 4). Of the 35 MAGs, 26 were taxonomically classified at the Genus level (Supplemental Table 7). Eight MAGs were assigned to the genus *HIMB30* of the *Litoricolaceae* family and did not reflect a pattern by season or depth; *HIMB30* was isolated in metagenomes from all depths and timepoints except for the 5m August 2021 sample. Five MAGs were assigned to the genus *UBA3478* of the *Flavobacteriaceae* family, which was found in August 2021 (i.e., 0m and 5m samples) and April 2022 (i.e., 0m, 5m, and 10m samples) but absent during December 2021 at all depths. Four MAGs were assigned to the genus *Casp-actino5* of the family *Ilumatobacteraceae* and were isolated from the 5m metagenome in August 2021 and the 0m, 5m, and 10m metagenomes in December 2021, but was absent at all depths in April 2022. MAGs assigned to the *SKUL01* genus (n = 3) were only found in the December 2021 metagenomes, with one MAG coming from each sampling depth. MAGs assigned to the genera *CSBr16-57R1* (n = 2) and *M55B157* (n = 2) were both found only in the April 2022 metagenomes, with *CSBr16-57R1* found in the 0m and 10m metagenomes and *M55B157* found in the 5m and 10m metagenomes. The singleton

MAGs belonging to the genera *Synechococcus_C* and *UBA4419* respectively were only found in the 5m metagenome from August 2021.

Functional Annotation of Metagenomes

Gene coverage as well as the presence/absence of genes of interest were used to determine how prevalent certain functions of interest are in both contigs and MAGs throughout the water column. To understand the nutritional strategies employed by microorganisms in the Salton Sea, genes involved in sulfur energy metabolisms, phototrophy, and carbon fixation pathways were examined in the contigs and MAGs respectively.

Sulfur Cycling Genes

KO identifiers of genes involved in assimilatory sulfate reduction, dissimilatory sulfate reduction, thiosulfate oxidation, hydrogen sulfide oxidation, sulfite oxidation, and sulfur disproportionation were compared within and between each sample metagenome's contigs.

The relative depth of coverage of sulfur cycling genes varied across all depths and timepoints by pathway. Genes assigned to KOs involved thiosulfate oxidation pathway (i.e., *soxABCDXYZ*; the SOX pathway) exhibited relatively higher coverages in August 2021 compared to other sulfur cycling pathways in this timepoint. The thiosulfate oxidation pathway oxidizes thiosulfate (S_2O_3) into SO_4. Depth of coverage was also relatively high for genes involved in oxidizing hydrogen sulfide to polysulfide species and/or elemental sulfur (i.e., hydrogen sulfide:quinone oxidoreductase, *sqr*; hydrogen sulfide dehydrogenase flavoprotein chain, *fccB*), as well as genes involved in sulfur

disproportionation (i.e., thiosulfate reductase/polyhydrogen sulfide reductase chain, *phsA/psrA*). Sulfur disproportionation is a process in which sulfur species act as an electron donor and an electron acceptor, yielding H_2S and SO_4. The SOX pathway, *fccB,* and *phsA/psrA* displayed the highest relative coverages in the 5m metagenome, whereas *sqr* had the highest relative coverage in the 0m metagenome. Sulfite dehydrogenase (quinone) subunit SoeA (i.e., *soeA*), which oxidizes sulfite (i.e., SO_3) to SO_4, had lower relative coverage compared to other hydrogen sulfide oxidizing genes in August 2021, and was only observed in the August 2021 metagenomes. Two genes involved in dissimlatory sulfate redox, dissimilatory sulfite reductase subunits alpha and beta, *dsrAB,* were found in the August 2021 with low relative coverage. Specifically, *dsrB* was present at all depths in August 2021, whereas *dsrA* was present at the 0m and 5m depths, but not at 10m. *dsrAB* can oxidize H_2S into SO_3. Sulfate adenylyltransferase (i.e., *sat*, *met3*), which is involved in both dissimilatory and assimilatory sulfate reduction, exhibited a lower relative coverage in August 2021 compared to other sulfate reduction genes. The assimilatory sulfate reduction pathway was almost complete in the August 2021 metagenomes, only missing sulfite reductase (NADH) flavoprotein alpha-component (i.e., *cysJ*) across all depths and sulfite reductase (NADPH) hemoprotein beta-component (i.e., *cysI*) at the 0m and 10m depths. Two genes within this pathway, bifunctional enzyme CysN/CysC (i.e., *cysNC*) and sulfate adenylyltransferase subunit 2 (i.e., *cysD*), exhibited relatively higher coverage in August 2021 compared to other assimilatory and dissimilatory sulfate redox genes. *cysD* exhibited the highest coverage in the 0m metagenome in August 2021, and *cysNC* maintained similar relative coverage in the 0m

and 5m metagenomes but decreased in the 10m metagenome. Two genes belonging to the assimilatory sulfate reduction pathway were observed only in August 2021: *cysI* in the 5m metagenome and sulfite reductase (i.e., *sir*), found in each metagenome.

The 0m, 5m, and 10m metagenomes exhibited lower relative coverage of the SOX pathway and *fccB* in December 2021 compared to August 2021. Conversely, dissimilatory sulfate redox genes adenylylsulfate reductase, subunits A and B (i.e., *aprAB*) and *dsrAB* had the highest relative coverage in December 2021 at all depths compared to other sulfur metabolic pathways at this timepoint. Specifically, *aprAB* had higher relative coverage than *dsrAB* across depths, with the highest relative coverage of *aprAB* in the 10m contigs. *aprAB* were only observed in the December 2021 metagenomes. *aprAB* can oxidize SO_3 into adenylyl sulfate (APS). Additionally, relative coverage of *dsrAB* was higher in December 2021 than August 2021 at all sampling depths. *Sqr* maintained high relative coverage across depths in December 2021, with the highest coverage also found in the 10m contigs. As was observed in August 2021, *cysNC* and *cysD* exhibited higher relative coverage across the depths in December 2021 compared to other KOs involved in the assimilatory sulfate reduction pathway. Both *cysD*, which reduces SO_4 into APS, and *cysNC*, which reduces APS to phosphoadenylyl sulfate (PAPS), were observed to have the highest relative coverage in the 10m metagenome. The only observance of sulfite reductase (NADH) flavoprotein alpha-component (i.e., *cysJ*), a member of the assimilatory sulfate reduction pathway that reduces SO_3 into H_2S, was in the 0m metagenome in December 2021.

Relative coverage of genes in the SOX pathway and hydrogen sulfide oxidation (i.e., *sqr, fccB*) increased across the metagenomes in April 2022. Relative coverage of the SOX pathway across the metagenomes was lower in April 2022 compared to August 2021. However, *sqr* exhibited the highest relative coverage in the April 2022 metagenomes, with the highest coverage found in the 5m contigs. Only one gene involved with the dissimilatory sulfate redox pathway, *sat/met3,* was found with low relative coverage in the April metagenomes from the 5m and 10m depths. High relative coverage of *cysD* and *cysNC* was maintained in April 2022. Specifically, *cysNC* exhibited the highest relative coverage in the 0m metagenome, and *cysD* exhibited the highest relative coverage in the 5m metagenome. April 2022 metagenomes contained less sulfur cycling genes (i.e., 14 of the 22 genes) than both August 2021 (i.e., 19 of the 22 genes) and December 2021 (i.e., 19 of 22 genes).

Figure 6. Relative Coverage of Sulfur Metabolic Genes in Salton Seawater Metagenomes. This is a heatmap detailing the relative coverage (i.e., centered-log ratio transformation of read coverage per gene) of sulfur cycling genes identified in the 0m, 5m, and 10m metagenomes. Each column represents a metagenome, which are sectioned by their respective sampling time points, and each row represents a different KO assignment given to genes found in the metagenomes. The darker purple the square, the higher the relative coverage of that KO is. Gray squares represent genes that were not found in the metagenomes.

Sulfur Cycling in MAGs

KO identifiers of genes involved in the sulfur metabolisms described above were also examined within the MAGs from each sample. Of the 35 high-quality MAGs identified and annotated, 15 MAGs contained sulfur metabolic genes. Within these 15

MAGs, eight of the MAGs were assigned to the bacterial genus *HIMB30*. Two of the 15 MAGs were assigned to the bacterial genus *Casp-actino5*, and 1 MAG was assigned to the genus *SKUL01*. The remaining four MAGs were not given bacterial genus assignments; however, three of these MAGs were assigned to the *GCF-002020875* bacterial family, and one MAG was assigned to the *Crocinitomicaceae* bacterial family.

Two MAGs isolated from the 0m and 10m August 2021 samples respectively (and assigned to the *HIMB30* genus) contained only sulfur oxidation genes. The MAG isolated from the 0m August 2021 sample contained all the SOX genes excluding the *soxB* gene, whereas the MAG found in the 10m depth in August 2021 contained all SOX genes (*soxABCDXYZ)* as well as the *sqr* gene involved in oxidizing hydrogen sulfide.

Ten MAGs isolated from December 2021 metagenomes across depths contained sulfur metabolic genes. Six of the ten MAGs contained only sulfur oxidation genes. One MAGs only contained the *soxB* gene, and one MAG contained all the SOX genes excluding *soxB*. Three MAGs contained only the *sqr* gene or both *sqr* and *fccB*, involved in oxidizing hydrogen sulfide. One MAG contained the *sqr* and *soxB* gene. These MAGs containing sulfur oxidation genes were assigned to the bacterial genera *HIMB30*, *Casp-actino5*, or their genus assignment was unknown. Three of the ten MAGs had genes involved in assimilatory sulfate reduction, specifically the *cysNC*, *cysH*, and *cysD* genes. One MAG containing the *cysNC*, *cysD*, and *sqr* genes was assigned to the bacterial genus *Casp-actino5*. One MAG assigned to the genus *SKUL01* contained only the *cysH* gene, and the MAG containing *cysH* and *cysD* genes was not assigned to a genus. A single

MAG (that did not receive a genus assignment) contained both *dsrAB* genes involved in dissimilatory sulfate reduction genes, as well as the *sqr* and *fccB* genes.

Three MAGs isolated in April 2022 contained only sulfur oxidation genes and exhibited the highest relative coverage of their genes compared to all the MAGs containing sulfur metabolic genes. All three MAGs were assigned to the bacterial genus *HIMB30*, and each MAG came from the 0m, 5m, and 10m samples respectively. Two MAGs, isolated from 0m and 10m metagenomes, contained only SOX genes, with one MAG having a complete SOX pathway. The other MAG contained a single gene, *sqr*. The MAG with the complete SOX pathway exhibited the highest relative coverage of all the MAGs discussed here and was isolated from the 10m metagenome.

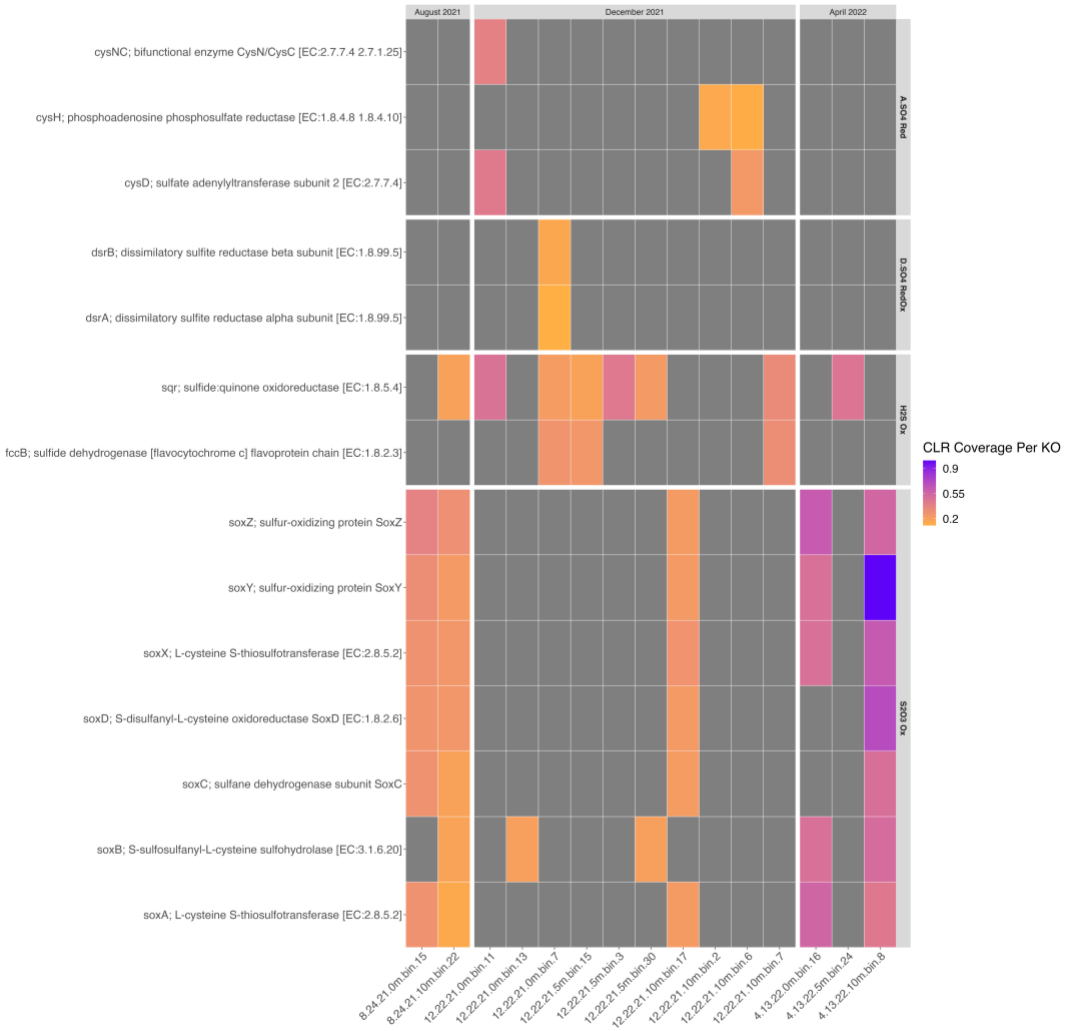

Fig 7. Relative Coverage of Sulfur Cycling Genes in Salton Seawater MAGs. This is a heatmap detailing the relative coverage (i.e., centered-log ratio transformation of read coverage per gene) of sulfur cycling genes identified in metagenome-assembled genomes (MAGs) isolated from the the 0m, 5m, and 10m metagenomes. Each column represents a bin (i.e., MAG), which are sectioned by their respective sampling time points, and each row represents a different KO assignment given to genes found in the metagenomes. The darker purple the square, the higher the relative coverage of that KO is. Gray squares represent genes that were not found in the MAGs.

Phototrophy and Carbon Fixation in Contigs

KO identifiers of genes involved in carbon fixation pathways such as the Calvin-Benson-Bessham cycle (CBB), 3-hydroxypropionate bicycle (3HP), the 3-

hydroxypropionate/4-hydroxybutyrate cycle (3HP/4HB), the reductive acetyl-CoA pathway (RAcCoa), the dicarboxylate/4-hydroxybutyrate cycle (DC/4HB), and the reductive tricarboxylic acid cycle (rTCA). Additionally, KO identifiers of genes involved in oxygenic photosynthesis, anoxygenic photosynthesis, and photoheterotrophy were compared within and between each sample metagenome's contigs.

Genes involved in the CBB, RAcCoa, rTCA, and 3HP cycles were present in the metagenomes (Supplemental Figure 3). Of these pathways, genes involved in the CBB pathway had the highest relative coverage across all depths and time points. The December 2021 metagenomes appeared to have the highest relative coverage of CBB genes compared to the other time points. However, not all CBB genes were present across depths and time points. For example, sedoheptulose-bisphosphatase was only present in the 10m metagenome from December 2021 with relatively low coverage. Additionally, Rubisco genes (i.e., ribulose-bisphosphate carboxylase small chain *rbcS* and large chain *rbcL*) phosphoribulokinase (*PRK*), known to be necessary for oxygenic photosynthesis, were found at relatively low coverage across depths and time points. The rTCA pathway exhibited the highest relative coverage in the August 2021 metagenomes, and the RAcCoa and 3HP pathways exhibited the highest relative coverage across the April 2022 metagenomes. The only pathway that was complete in any metagenome was the 3HP pathway, which appeared to be complete in the 0m and 5m metagenomes from August 2021, though the relative coverage of these genes was not equal across the pathway.

Genes involved in Photosystem I and II, anoxygenic photosynthesis, and in bacterial rhodopsin complexes (i.e., sensory rhodopsin, *sop*; beta-carotene 15,15'-dioxygenase associated with proteorhodopsin, *blh*) were found in the metagenomes across depths and time points (Supplemental Figure 4). Of all the phototrophic genes examined, bacterial rhodopsin genes exhibited the highest relative coverage. The *blh* gene had the highest relative coverage across all depths and timepoints, with the highest relative coverage in the April 2022 metagenomes. This gene is part of the retinal biosynthesis operon that is required for a functional proteorhodopsin (Martinez et al. 2007). The *sop* gene also exhibited higher relative coverage than other phototrophic genes (excluding *blh*), with the highest relative coverage across the December 2021 metagenomes. Oxygenic photosynthetic genes, particularly those involved in the Photosystem II (PS II) exhibited higher relative coverage in the December 2021 metagenomes, notably the 0m and 5m metagenomes. However, photosystem II P680 reaction center D1 protein (*psbA*), a gene within PS II, exhibited the highest relative coverage in the August 2021 metagenomes, specifically in the 5m metagenome. Additionally, most of the genes involved in Photosystem I (PS I) were absent across the April 2022 metagenomes. The anoxygenic photosynthesis genes considered here (*pufM*, *pufL*) were both present only in the August 2021 metagenomes, and exhibited lower relative coverage compared to other phototrophic genes.

Phototrophy and Carbon Fixation in MAGs

As was done with the contigs, KO identifiers of genes involved in carbon fixation pathways (i.e., CBB, 3HP, 3HP/4HB, RAcCoa, DC/4HB), and rTCA) and genes involved

in various types of phototrophy (i.e., oxygenic photosynthesis, anoxygenic photosynthesis, and photoheterotrophy) were compared within and between the MAGs from each metagenome.

Out of 35 MAGs, 27 MAGs contained carbon fixation genes. 21 MAGs contained genes involved in the CBB pathway, yet no MAG contained a complete CBB pathway (Supplemental Figure 5). Only 1 MAG (i.e., 8.2.21.10m.bin.22, assigned to the *HIMB30* genus) contained the three genes necessary for photosynthesis (i.e., *rbcS*, *rbcL*, *PRK*). This MAG also contained the 9 of the 12 CBB genes examined, the most of any MAG, and contained all the genes in the RAcCoa pathway. In total, 16 of the 35 MAGs contain genes belonging to multiple C fixation pathways. A portion of these MAGs with genes from multiple C fixation pathways were assigned to the *HIMB30*, *Casp-actino5*, and *M55B157* genera. Overall, the CBB genes exhibited the highest relative coverage of all the C fixation genes considered across the MAGs.

Only one MAG contained genes involved in phototrophy (Supplemental Figure 6); this MAG (12.22.21.0m.bin.13) was assigned to the genus *HIMB30*. This MAG contained *blh* gene at high relative coverage, and the *sop* gene at lower relative coverage. As described above, the *blh* gene contributes to the function of proteorhodopsin and the *sop* gene is involved in the sensory rhodopsin complex. Genes involved in oxygenic and anoxygenic photosynthesis were not found in the MAGs.

Discussion

The Salton Sea is a hypersaline lake in Southern California that is rapidly shrinking due to evaporation and water diversion. The only water the lake receives is

from agricultural runoff, contributing its eutrophic status (Tompson 2016). Though previous research has explored the microbial composition of the surface water, investigations into the microbial ecology of the water column across seasons have been lacking. Furthermore, the geochemical cycling resulting from stratification and turnover in the Salton Sea have been studied (Tiffany et al. 2007, Reese et al. 2008), yet the microbial contributions to these cycles have only been speculative. Here, we explore the microbial composition and functional diversity throughout the Salton Sea water column at eight depths across three different seasons. We specifically highlight microbial sulfur cycling genes because, while it is established that sulfate-reducing and sulfide-oxidizing bacteria contribute to the sulfur cycle (Tiffany et al. 2007), the metabolisms used and those performing these redox reactions were unknown. Collectively our findings suggest that halophilic chemoheterotrophs and phototrophs with the ability to oxidize hydrogen sulfide, thiosulfate, and other sulfur species dominate the Salton Sea across seasons even when hydrogen sulfide is depleted, yet their respective abundances and functional diversity fluctuates with changes in the geochemical profile of the water column.

Halophiles are Found Across Time and Depth

Across August 2021, December 2021, and April 2022, salinity in the Salton Sea water column fluctuated between 57 ppt – 61.54 ppt (Figure 1), maintaining its hypersaline status during periods of lake stratification and mixing. Hypersaline waterbodies such as the Salton Sea select for halophilic microorganisms that can withstand high osmotic stress (Aanderud et al. 2016). As hypothesized, the major bacterial genera that were present across all time points and depths in the water column

included known halophiles such as *DS001* of the Microbacteriaceae family, *Litoricola* of the Litoricolaceae family, *Synechococcus* of the Synechococcaceae family, and *Truepera* of the Trueperaceae family. These organisms have been isolated from saline and hypersaline waterbodies from around the globe, however, only the Cyanobacteria *Synechococcus* has been previously identified in Salton Seawater samples (Wood et al. 2002, Carmichael and Li 2006). *DS001* was of particular interest because this genus found with a relative abundance of at least 5% in every sample and had a relative abundance of at least 20% in all samples collected in August 2021 and December 2021. *DS001* has been found in hypersaline lakes including the La Brava-La Punta Lake system in the Atacama Desert, Lake Chiprana in the Menegros Desert, and Florida Bay within the Florida Everglades (Casamayor et al. 2013, Salazar et al. 2020, Laas et al. 2022). *Litoricola*, another dominating genus throughout the time points, has been found in the Florida Bay as well as other marine sources like the mariculture ponds in the Shandong province of China, the Xiamen Sea in the Fuijan province of China, and in the East Sea near the Gangwon province of South Korea (Kim et al. 2007, Huang et al. 2018, Laas et al. 2022). *Truepera* was also isolated from the mariculture ponds in the Shandong province and is known to be facultatively halophilic (Albuquerque et al. 2005, Huang et al. 2018). Collectively these results demonstrate that halotolerance is the most basic requirement for microbial survival within the Salton Sea water column.

Lake Stratification Cycle Structures Microbial Communities

Despite the resilience of these halophilic taxa across time and depths, the water column microbiome was affected by seasonal differences in geochemistry. Redundancy

analysis and a principal coordinates analysis revealed that not only do microbial communities throughout the water column cluster together by time point, but their compositional differences are driven by temperature, DOM, and %DO. Furthermore, alpha diversity across the water column significantly differed between August 2021 (i.e., as lake stratification subsides) verses December 2021 and April 2022 (i.e., as the water column is mixing and oxygenated), whereas species richness did not exhibit this pattern. These findings suggest that the overall microbial community is fluctuating with the seasonal geochemical transitions associated with fluctuating thermo- and chemo-clines. Though many dominant microbial genera found in the water column, such as *DS001* and *Litoricola*, were observed across seasons and depths, their respective relative abundances were variable over time, further suggesting that the seasonal geochemistry is structuring the water column microbiome.

Seasonal Lake Stratification and Sulfur Availability Select for Sulfur Oxidation and Intermediate Sulfur Cycling

Thermoclines control the diffusivity of oxygen and other nutrients throughout the water column, thus selecting for the electron acceptors and electron donors of the geochemical constituents that are present in accordance to oxidation-reduction at a given depth. In turn, the distribution of these molecules selects for the metabolic strategies used by aerobes and anaerobes within an ecosystem. This is true for bacterial sulfur cycling pathways in the Salton Sea; the fluctuating prevalence of genes in the metagenomes that code for sulfur cycling enzymes paralleled the seasonal variations in the oxycline and sulfur chemoclines that form and dissipate across the water column. Many genes

involved in thiosulfate, sulfur, and hydrogen sulfide oxidation pathways were present across the metagenomes and the MAGs, yet the relative coverage of these genes varied by pathway in each season. The functional plasticity and redundancy observed in the Salton Seawater metagenomes and MAGs show that the water column is selecting for functional diversity over taxonomic diversity in the water column microbiome.

Genes coding for proteins involved in hydrogen sulfide oxidation (i.e., oxidize sulfide to polysulfide or sulfur respectively; *sqr, fccB*) and thiosulfate oxidation pathway (i.e., oxidizes thiosulfate [$S_2O_3^{2-}$] to sulfate [SO_4^{2-}]; *soxABCDXYZ* or SOX pathway) exhibited the highest relative coverage compared to other sulfur cycling genes in August 2021 (Figure 6), when the oxycline was still present and hydrogen sulfide was at its highest concentration in the hypolimnion, with an average concentration of 23.30μM. Additionally, two of the nine MAGs isolated from August 2021 metagenomes contained most of the genes coding for enzymes in the SOX pathway and were assigned to the genus *HIMB30*, a bacterium that is a known halophile capable of sulfide oxidation (Huggett and Rappé 2012, Savoie et al. 2021). These findings suggesting that various hydrogen sulfide oxidation strategies are conserved in the microbiome while the lake was still stratified in August 2021 and hydrogen sulfide was available to oxidize. Furthermore, it appears that sulfide oxidation was most prominent in the 5m metagenome in August 2021, which corresponds to the depths where the oxic and anoxic waters interface. The relative coverage of genes assigned to *phsA/psrA*, which performs elemental sulfur/thiosulfate disproportionation (i.e., sulfur compound acts as an electron donor and acceptor), was also found at a relatively higher coverage in the 5m and 10m

metagenomes in August 2021. This result indicates that microorganisms in the lowest depths of the stratified Salton Sea are aerotolerant and capable of sulfur disproportionation.

As water temperatures cooled by nearly 15ºC in December 2021, sulfate and %DO were at their highest concentrations, and hydrogen sulfide was depleted due to microbial sulfide oxidation. The relative coverages of genes involved in the reverse dissimilatory sulfate reduction pathway (i.e., *rDSR* pathway), notably *aprAB*, were higher than the relative coverages of the SOX genes at this time. *rDSR* genes code for dissimilatory sulfate reduction proteins that work in reverse (i.e., not sulfate reduction) to oxidize sulfite into adenylyl sulfate (i.e., APS) and subsequently sulfate. Thus, the December 2021 metagenomes reflect that incomplete sulfate oxidation and intermediate sulfur cycling are ongoing processes in the microbial community while lake turnover occurred, and the water column was oxygenated. Interestingly, *sqr* genes maintained a relatively high coverage in December 2021 across metagenomes, suggesting that microbial polysulfide production continued as the lake overcome stratification. This was also observed in the MAGs found in the December 2021 metagenomes, where 6 of the 10 MAGs with sulfur cycling genes contained *sqr* genes. Previous work has shown that heterotrophic microorganisms containing *sqr* genes and genes that code for persulfide dioxygenase (PDO) can oxidize sulfide in aerobic environments without releasing hydrogen sulfide (Xia et al. 2017). This further supports that intermediate sulfur cycling is a useful metabolic strategy during lake mixing, when dissolved oxygen concentrations are high and hydrogen sulfide concentrations are low.

By April 2022, sulfate and %DO decreased from December and chemoclines reemerge, with higher concentrations in the epilimnion and lower concentrations in the hypolimnion. Hydrogen sulfide concentrations had marginally increased throughout the water column from an average of 2.7 μM in December 2021 to an average of 3.31 μM in April 2022. Relative coverage of genes coding for *fccB* and SOX enzymes increased and was evenly distributed across all metagenomes. Additionally, two MAGs assigned to the genus *HIMB30* that were isolated from April 2022 metagenomes contained almost complete SOX pathways with high relative coverage. Sulfide and thiosulfate oxidation are conserved metabolic pathways in the microbiome in April. Yet, sulfate concentration in the water column has decreased and hydrogen sulfide has marginally increased from December to April. Together, these findings demonstrate that the water column microbiome is utilizing incomplete sulfide and thiosulfate oxidation as the lake begins to stratify in spring, which is comparable to what we observed in August 2021.

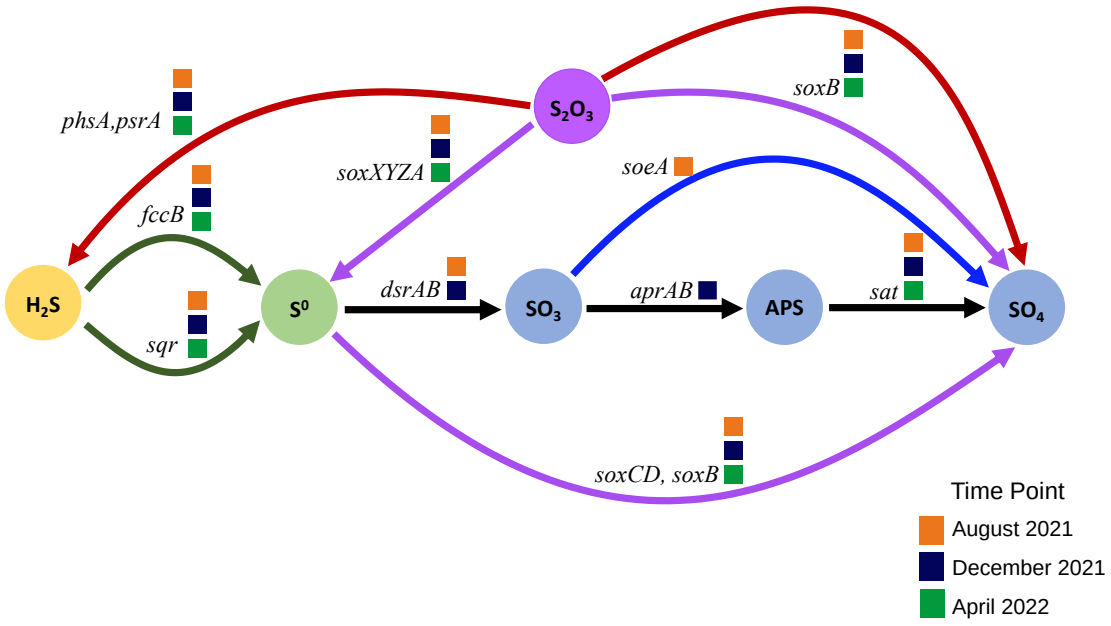

Figure 8. Diagram of Sulfur Oxidation Genes and Sulfur Cycling Pathways Found in the Salton Seawater Metagenomes. This is a diagram that shows the enzymes involved in hydrogen sulfide oxidation (i.e., dark green arrows), sulfur disproportionation (i.e., red arrows), reverse dissimilatory sulfate reduction (i.e., black arrows), thiosulfate oxidation (i.e., purple arrows), and sulfite oxidation (i.e., blue arrow). The squares next to a gene name indicate if that gene was present in August 2021 (orange), December 2021 (dark blue), and/or April 2022 (green).

Functional Flexibility and Redundancy is Required for Survival in the Salton Sea

Our results suggest that the Salton Seawater microbiome is resilient and well-adapted to this extreme ecosystem in flux. We see this in the functional redundancy in the sulfur cycling metabolisms in this microbiome, and in the set of species that dominate the water column over time. Recent research has revealed that *Litoricola*, which was previously thought to be a chemoheterotroph (Kim et al. 2007), contains sulfur oxidation genes (i.e., *soxAX* genes), genes involved in oyxgenic photosynthesis (i.e., RuBisCO, carbon monoxide dehydrogenase; *rbcL*, *coxL*), and genes involved in photoheterotrophy (i.e., rhodopsin genes) in their genomes (Pachiadaki et al. 2019, Auladell et al. 2023). A

close relative of *Litoricola*, *HIMB30* (Huggett and Rappé 2012), was assigned to eight of our 26 MAGs identified at the genus level. *HIMB30* has been shown to oxidize sulfide, fix CO2 via the Calvin-Benson-Bessham (CBB) cycle, and use proteorhodopsin as a means of photoheterotrophy (Savoie et al. 2021). Savoie et al. found that the clade within *Gammaproteobacteria* that houses *HIMB30*, OM252, are capable of alternating between chemoorganoheterotrophic or chemolithoautotrophic growth. The functional annotation of the *HIMB30* MAGs supports these results, showing that they contained genes that code for thiosulfate and hydrogen sulfide oxidation enzymes, enzymes in the CBB cycle, and genes involved in photoheterotrophy (i.e., *blh*, involved in proteorhodopsin function, and *sop* involved in the sensory rhodopsin complex). Other dominant genera we observed across seasons, *Synechococcus* and *Trupera*, are known to adapt to their surroundings. *Synechococcus* is a widely, globally distributed cyanobacteria that can adapt to both high light and low light conditions depending on its surroundings (Soulier et al. 2022). *Truepera* is facultatively halophilic thermophile that has been found in hypersaline lakes, marine environments, and hot springs (Albuquerque et al. 2005, Ivanova et al. 2011, Sirisena et al. 2018). Considering that these taxa maintained a stronghold in their microbiome throughout lake stratification and mixing, it is reasonable to surmise that the halophilic microorganisms have the functional flexibility and redundancy necessary to survive in this extreme, variable ecosystem.

Typically, functional convergence is observed with taxonomic variation within environmental microbiomes, particularly across redox gradients and depth (Louca et al. 2016, 2017, 2018). Larger ecosystems allow for the persistence of geochemical gradients,

creating a wide variety of habitats that promote niche partitioning, and thus, encourage greater microbial diversity (Nemergut et al. 2013). This has been observed in microbial communities inhabiting holomictic lakes, or lakes that occasionally mix, including both hypersaline (Phillips et al. 2021)and freshwater systems (Lee et al. 2017, Baricz et al. 2021), as well as in marine water bodies at pelagic and benthic depths (Guo et al. 2022, Broman et al. 2022). However, the Salton Sea offers a unique insight into how shared metabolic strategies are selected for, allowing for survival in rapidly changing environmental conditions within a confined space. Despite the Salton Sea being a shallow lake (only reaching a depth of 10.5m at the time of this study), lake stratification can continue for months each year until temperatures in the region finally cool down enough for lake turnover to occur (Tiffany et al. 2007, Ma et al. 2020). The shallow depths limit the spatial dispersal of the microorganisms in the water column, and yet, we observed both microbial taxonomic variation and functional redundancy. These findings speak to the strong selective pressures in this hypersaline, eutrophic, fluctuating ecosystem that foster the colonization, adaptation, and persistence of its halophilic microbiome.

The Lake Water and Dust Connection

Ongoing water diversion from the Salton Sea is causing the lake to rapidly shrink, exposing its playa sediment and increasing the playa's vulnerability to wind erosion (Kjelland and Swannack 2018). Research suggests that within the next five years, the volume of the Sea itself will be reduced by more than 60% and will expose 100 square miles of the Sea's playa (Cohen 2014). As the exposed playa's surface area increases, intensifying winds in the area will continue to introduce more particulate matter into the

atmosphere, in turn reducing air quality and threatening the pulmonary health of nearby residents and wildlife (Frie et al. 2017, 2019).

As we previously described, mineral signatures from the lake water such as SO_4 have been identified in playa dust collected in the region (Frie et al. 2019). Furthermore, Frie et al. found that $CaSO_4$ and $MgSO_4$ consistently dominated dust from the Salton Sea playa, suggesting that these minerals are indicative of wind erosion and dust production at the playa surface (Frie et al. 2019). Increases in atmospheric H_2S concentrations have also been found to correspond with increases in H_2S concentrations in the Salton Sea surface water (Reese et al. 2008). Collectively, these findings suggest that Salton Sea's sulfur cycle plays a role in the emissivity and composition of the dust in this region. Thus, considering that the Salton Seawater microbiome is involved in the ecosystem's sulfur cycle, it is plausible that these microorganisms are also involved in structuring the chemical and microbial composition of the Salton Sea dust. Microorganisms can traverse the atmosphere as free cells or attached to particulates (Maltz et al. 2022) and likely become entrained in the dust as sea spray and playa sediment become airborne. While the interface between the lake water and the atmosphere has been explored, more research is required to investigate the microbial composition of the Salton Sea dust and its relationship to the seasonal dynamics of the lake. This work is increasingly urgent due to the rapid shrinking of the Salton Sea which will disrupt the seasonal stratification and sulfur cycle in this ecosystem, thus changing the biogeochemistry of the playa sediment that is entrained into the atmosphere as dust. Additionally, understanding the drivers of the Salton Sea microbiome, and how the Salton Sea's microorganisms and their

metabolites are introduced into the atmosphere, can inform restoration and remediation strategies aimed at reducing harmful dust emissions in the region. Thorough investigation into the microbial interactions of the Salton Sea region across its substrates is required to holistically address and mitigate the unfolding public health crisis at the Salton Sea.

Conclusion

In this study, we have elucidated the assembly and functional diversity of the microbiome within the Salton Sea water column, which has not been previously explored. The taxonomic variation of the water column microbiome coincided with seasonal changes in the geochemistry because of lake stratification and mixing, particularly with the fluctuation of the temperature, dissolved oxygen, and dissolved organic matter. Despite the significant seasonal changes in microbiome composition, halophilic chemoorganotrophs, phototrophs, and mixotrophs (i.e., organisms that can alternate between chemorganotrophy and chemolithoautrophy) continued to dominate the microbial water column community. Metagenomes from the 0m, 5m, and 10m depths from the water column revealed that a variety of sulfur oxidation strategies are shared by the microorganisms in the lake, notably thiosulfate oxidation via the SOX pathway, sulfide oxidation via *sqr* and *fccB*, the reverse sulfate dissimilatory reduction pathway, and the sulfur disproportionation pathway. The prominence of the SOX pathway as well as sulfide oxidation genes (i.e., *sqr*, *fccB*) was also reflected in the isolated MAGs from the 0m, 5m, and 10m depths, with many of these MAGs being assigned to a known bacterial mixotroph capable of sulfur oxidation, *HIMB30*. Hydrogen sulfide was only present in the hypolimnion in summer, yet sulfur oxidation genes were prominent in the

water column microbiome across seasons. Our results highlight the functional versatility and redundancy in sulfur cycling strategies, namely sulfur oxidation, that are conserved in the Salton Seawater microbiome over time. Further work is needed to determine exactly how these microorganisms actively alternate between sulfur oxidation and reduction pathways throughout the Salton Sea water column, ideally using metatranscriptomics, to provide greater insight into the functional capabilities of the microbiome as the geochemical dynamics shift in this shrinking lake. Overall, our findings show that the water column microbiome within the Salton Sea is intimately involved with its seasonal nutrient cycling and redox structure and thus this ecosystem's function and stability.

References

Aanderud, Z. T., J. C. Vert, J. T. Lennon, T. W. Magnusson, D. P. Breakwell, and A. R. Harker. 2016. Bacterial dormancy is more prevalent in freshwater than hypersaline lakes. Frontiers in Microbiology 7.

Albuquerque, L., C. Simões, M. F. Nobre, N. M. Pino, J. R. Battista, M. T. Silva, F. A. Rainey, and M. S. Da Costa. 2005. Truepera radiovictrix gen. nov., sp. nov., a new radiation resistant species and the proposal of Trueperaceae fam. nov. FEMS Microbiology Letters 247:161–169.

Anantharaman, K., C. T. Brown, L. A. Hug, I. Sharon, C. J. Castelle, A. J. Probst, B. C. Thomas, A. Singh, M. J. Wilkins, U. Karaoz, E. L. Brodie, K. H. Williams, S. S. Hubbard, and J. F. Banfield. 2016. Thousands of microbial genomes shed light on interconnected biogeochemical processes in an aquifer system. Nature Communications 7.

Anderson, T. W., M. A. Tiffany, and S. H. Hurlbert. 2007. Stratification, sulfide, worms, and decline of the Eared Grebe (Podiceps nigricollis) at the Salton Sea, California. Lake and Reservoir Management 23:500–517.

Andrews, S. (n.d.). FastQC: A Quality Control Tool for High Throughput Sequence Data.

Aramaki, T., R. Blanc-Mathieu, H. Endo, K. Ohkubo, M. Kanehisa, S. Goto, H. Ogata, and A. Valencia. 2020. KofamKOALA: KEGG Ortholog assignment based on profile HMM and adaptive score threshold. Bioinformatics 36:2251–2252.

Auladell, A., I. Ferrera, L. Montiel Fontanet, C. D. Santos Júnior, M. Sebastián, R. Logares, and J. M. Gasol. 2023. Seasonality of biogeochemically relevant microbial genes in a coastal ocean microbiome. Environmental Microbiology 25:1465–1483.

Bankevich, A., S. Nurk, D. Antipov, A. A. Gurevich, M. Dvorkin, A. S. Kulikov, V. M. Lesin, S. I. Nikolenko, S. Pham, A. D. Prjibelski, A. V. Pyshkin, A. V. Sirotkin, N. Vyahhi, G. Tesler, M. A. Alekseyev, and P. A. Pevzner. 2012. SPAdes: A new genome assembly algorithm and its applications to single-cell sequencing. Journal of Computational Biology 19:455–477.

Baricz, A., C. M. Chiriac, A. Ștefan Andrei, P. A. Bulzu, E. A. Levei, O. Cadar, K. P. Battes, M. Cîmpean, M. Șenilă, A. Cristea, V. Muntean, M. Alexe, C. Coman, E. K. Szekeres, C. I. Sicora, A. Ionescu, D. Blain, W. K. O'Neill, J. Edwards, J. E. Hallsworth, and H. L. Banciu. 2021. Spatio-temporal insights into microbiology of the freshwater-to-hypersaline, oxic-hypoxic-euxinic waters of Ursu Lake. Environmental Microbiology 23:3523–3540.

Bowers, R. M., N. C. Kyrpides, R. Stepanauskas, M. Harmon-Smith, D. Doud, T. B. K. Reddy, F. Schulz, J. Jarett, A. R. Rivers, E. A. Eloe-Fadrosh, S. G. Tringe, N. N. Ivanova, A. Copeland, A. Clum, E. D. Becraft, R. R. Malmstrom, B. Birren, M. Podar, P. Bork, G. M. Weinstock, G. M. Garrity, J. A. Dodsworth, S. Yooseph, G. Sutton, F. O. Glöckner, J. A. Gilbert, W. C. Nelson, S. J. Hallam, S. P. Jungbluth, T. J. G. Ettema, S. Tighe, K. T. Konstantinidis, W. T. Liu, B. J. Baker, T. Rattei, J. A. Eisen, B. Hedlund, K. D. McMahon, N. Fierer, R. Knight, R. Finn, G. Cochrane, I. Karsch-Mizrachi, G. W. Tyson, C. Rinke, A. Lapidus, F. Meyer, P. Yilmaz, D. H. Parks, A. M. Eren, L. Schriml, J. F. Banfield, P. Hugenholtz, and T. Woyke. 2017, August 8. Minimum information about a single amplified genome (MISAG) and a metagenome-assembled genome (MIMAG) of bacteria and archaea. Nature Publishing Group.

Broman, E., D. Izabel-Shen, A. Rodríguez-Gijón, S. Bonaglia, S. L. Garcia, and F. J. A. Nascimento. 2022. Microbial functional genes are driven by gradients in sediment stoichiometry, oxygen, and salinity across the Baltic benthic ecosystem. Microbiome 10.

Buck, B. J., J. King, and V. Etyemezian. 2011. Effects of Salt Mineralogy on Dust Emissions, Salton Sea, California. Soil Science Society of America Journal 75:1971–1985.

Bushnell, B. (n.d.). BBMap.

Callahan, B. J., P. J. McMurdie, M. J. Rosen, A. W. Han, A. J. A. Johnson, and S. P. Holmes. 2016. DADA2: High-resolution sample inference from Illumina amplicon data. Nature Methods 13:581–583.

Carmichael, W. W., and R. H. Li. 2006. Cyanobacteria toxins in the Salton Sea. Saline systems 2:1–13.

Casamayor, E. O., X. Triadó-Margarit, and C. Castañeda. 2013. Microbial biodiversity in saline shallow lakes of the Monegros Desert, Spain. FEMS Microbiology Ecology 85:503–518.

Chaumeil, P. A., A. J. Mussig, P. Hugenholtz, and D. H. Parks. 2020. GTDB-Tk: A toolkit to classify genomes with the genome taxonomy database. Bioinformatics 36:1925–1927.

Cline, J. D. 1969. Spectrophotometric Determination of Hydrogen Sulfide in Natural Waters.

Cohen, M. J. 2014. Hazard's Toll The Costs of Inaction at the Salton Sea.

Davis, N. M., Di. M. Proctor, S. P. Holmes, D. A. Relman, and B. J. Callahan. 2018. Simple statistical identification and removal of contaminant sequences in marker-gene and metagenomics data. Microbiome 6.

Edgar, R. C., and H. Flyvbjerg. 2015. Error filtering, pair assembly and error correction for next-generation sequencing reads. Bioinformatics 31:3476–3482.

Fox, J., and S. Weisberg. 2019. An R Companion to Applied Regression. Sage, Thousand Oaks.

Freund, H., M. R. Maltz, M. P. Swenson, T. M. Topacio, V. A. Montellano, W. Porter, and E. L. Aronson. 2022. Microbiome interactions and their ecological implications at the Salton Sea. California Agriculture 76:16–26.

Frie, A. L., J. H. Dingle, S. C. Ying, and R. Bahreini. 2017. The Effect of a Receding Saline Lake (The Salton Sea) on Airborne Particulate Matter Composition. Environmental Science and Technology 51:8283–8292.

Frie, A. L., A. C. Garrison, M. V. Schaefer, S. M. Bates, J. Botthoff, M. Maltz, S. C. Ying, T. Lyons, M. F. Allen, E. Aronson, and R. Bahreini. 2019. Dust Sources in the Salton Sea Basin: A Clear Case of an Anthropogenically Impacted Dust Budget. Environmental Science & Technology 53:9378–9388.

Guo, R., X. Ma, J. Zhang, C. Liu, C. A. Thu, T. N. Win, N. L. Aung, H. S. Win, S. Naing, H. Li, F. Zhou, and P. Wang. 2022. Microbial community structures and important taxa across oxygen gradients in the Andaman Sea and eastern Bay of Bengal epipelagic waters. Frontiers in Microbiology 13.

Huang, F., L. Pan, M. Song, C. Tian, and S. Gao. 2018. Microbiota assemblages of water, sediment, and intestine and their associations with environmental factors and shrimp physiological health. Applied Microbiology and Biotechnology 102:8585–8598.

Huggett, M. J., and M. S. Rappé. 2012, February. Genome sequence of strain HIMB30, a novel member of the marine Gammaproteobacteria.

Hyatt, D., G. L. Chen, P. F. LoCascio, M. L. Land, F. W. Larimer, and L. J. Hauser. 2010a. Prodigal: Prokaryotic gene recognition and translation initiation site identification. BMC Bioinformatics 11.

Hyatt, D., G. L. Chen, P. F. LoCascio, M. L. Land, F. W. Larimer, and L. J. Hauser. 2010b. Prodigal: Prokaryotic gene recognition and translation initiation site identification. BMC Bioinformatics 11.

Illumina, Inc. 2017. Illumina Methods Guide.

Ivanova, N., C. Rohde, C. Munk, M. Nolan, S. Lucas, T. G. del Rio, H. Tice, S. Deshpande, J. F. Cheng, R. Tapia, C. Han, L. Goodwin, S. Pitluck, K. Liolios, K. Mavromatis, N. Mikhailova, A. Pati, A. Chen, K. Palaniappan, M. Land, L. Hauser, Y. J. Chang, C. D. Jeffries, E. Brambilla, M. Rohde, M. Göker, B. J. Tindall, T. Woyke, J. Bristow, J. A. Eisen, V. Markowitz, P. Hugenholtz, N. C. Kyrpides, H. P. Klenk, and A. Lapidus. 2011. Complete genome sequence of Truepera radiovictrix type strain (RQ-24 T). Standards in Genomic Sciences 4:91–96.

Kang, D. D., F. Li, E. Kirton, A. Thomas, R. Egan, H. An, and Z. Wang. 2019. MetaBAT 2: An adaptive binning algorithm for robust and efficient genome reconstruction from metagenome assemblies. PeerJ 2019:1–13.

Kim, H., Y. J. Choo, and J. C. Cho. 2007. Litoricolaceae fam. nov., to include Litoricola lipolytica gen. nov., sp. nov., a marine bacterium belonging to the order Oceanospirillales. International Journal of Systematic and Evolutionary Microbiology 57:1793–1798.

Kjelland, M. E., and T. M. Swannack. 2018. Salton Sea days of future past: Modeling impacts of alternative water transfer scenarios on fish and bird population dynamics. Ecological Informatics 43:124–145.

Klindworth, A., E. Pruesse, T. Schweer, J. Peplies, C. Quast, M. Horn, and F. O. Glöckner. 2013. Evaluation of general 16S ribosomal RNA gene PCR primers for classical and next-generation sequencing-based diversity studies. Nucleic Acids Research 41:1–11.

Laas, P., K. Ugarelli, R. Travieso, S. Stumpf, E. E. Gaiser, J. S. Kominoski, and U. Stingl. 2022. Water Column Microbial Communities Vary along Salinity Gradients in the Florida Coastal Everglades Wetlands. Microorganisms 10.

Lee, Z. M. P., A. T. Poret-Peterson, J. L. Siefert, D. Kaul, A. Moustafa, A. E. Allen, C. L. Dupont, L. E. Eguiarte, V. Souza, and J. J. Elser. 2017. Nutrient stoichiometry Shapes Microbial Community Structure in an Evaporitic Shallow Pond. Frontiers in Microbiology 8.

Liao, Y., G. K. Smyth, and W. Shi. 2014. FeatureCounts: An efficient general purpose program for assigning sequence reads to genomic features. Bioinformatics 30:923–930.

Louca, S., S. M. S. Jacques, A. P. F. Pires, J. S. Leal, D. S. Srivastava, L. W. Parfrey, V. F. Farjalla, and M. Doebeli. 2017. High taxonomic variability despite stable functional structure across microbial communities. Nature Ecology & Evolution 1:1–12.

Louca, S., M. F. Polz, F. Mazel, M. B. N. Albright, J. A. Huber, M. I. O'Connor, M. Ackermann, A. S. Hahn, D. S. Srivastava, S. A. Crowe, M. Doebeli, and L. W. Parfrey. 2018. Function and functional redundancy in microbial systems. Nature Ecology and Evolution 2:936–943.

Louca, S., L. Wegener Parfrey, and M. Deobeli. 2016. Decoupling function and taxonomy in the global ocean microbiome. Science 353:1272–1277.

Luther, G. W., A. J. Findlay, D. J. MacDonald, S. M. Owings, T. E. Hanson, R. A. Beinart, and P. R. Girguis. 2011. Thermodynamics and kinetics of sulfide oxidation by oxygen: A look at inorganically controlled reactions and biologically mediated processes in the environment. Frontiers in Microbiology 2.

Ma, J., H. Duan, L. He, M. Tiffany, Z. Cao, T. Qi, M. Shen, T. Biggs, and X. Xu. 2020. Spatiotemporal pattern of gypsum blooms in the Salton Sea, California, during 2000-2018. International Journal of Applied Earth Observation and Geoinformation 89:102090.

Maltz, M. R., C. J. Carey, H. L. Freund, J. K. Botthoff, S. C. Hart, J. E. Stajich, S. M. Aarons, S. M. Aciego, M. Blakowski, N. C. Dove, M. E. Barnes, N. Pombubpa, and E. L. Aronson. 2022. Landscape Topography and Regional Drought Alters Dust Microbiomes in the Sierra Nevada of California. Frontiers in Microbiology 13:1–19.

Martinez, A., A. S. Bradley, J. R. Waldbauer, R. E. Summons, and E. F. Delong. 2007. Proteorhodopsin photosystem gene expression enables photophosphorylation in a heterologous host.

Mikheenko, A., V. Saveliev, and A. Gurevich. 2016. MetaQUAST: evaluation of metagenome assemblies. Bioinformatics (Oxford, England) 32:1088–1090.

Nemergut, D. R., S. K. Schmidt, T. Fukami, S. P. O'Neill, T. M. Bilinski, L. F. Stanish, J. E. Knelman, J. L. Darcy, R. C. Lynch, P. Wickey, and S. Ferrenberg. 2013. Patterns and Processes of Microbial Community Assembly. Microbiology and Molecular Biology Reviews 77:342–356.

Nurk, S., D. Meleshko, A. Korobeynikov, and P. A. Pevzner. 2017. MetaSPAdes: A new versatile metagenomic assembler. Genome Research 27:824–834.

Oksanen, J., F. G. Blanchet, M. Friendly, R. Kindt, P. Legendre, D. McGlinn, P. R. Minchin, R. B. O'Hara, G. L. Simpson, P. Solymos, M. H. H. Stevens, E. Szoecs, and H. Wagner. 2020. vegan: Community Ecology Package. CRAN.

Pachiadaki, M. G., J. M. Brown, J. Brown, O. Bezuidt, P. M. Berube, S. J. Biller, N. J. Poulton, M. D. Burkart, J. J. La Clair, S. W. Chisholm, and R. Stepanauskas. 2019. Charting the Complexity of the Marine Microbiome through Single-Cell Genomics. Cell 179:1623-1635.e11.

Parks, D. H., M. Imelfort, C. T. Skennerton, P. Hugenholtz, and G. W. Tyson. 2015. CheckM: Assessing the quality of microbial genomes recovered from isolates, single cells, and metagenomes. Genome Research 25:1043–1055.

Pereira, M. B., M. Wallroth, V. Jonsson, and E. Kristiansson. 2018. Comparison of normalization methods for the analysis of metagenomic gene abundance data. BMC Genomics 19.

Phillips, A. A., D. R. Speth, L. G. Miller, X. T. Wang, F. Wu, P. M. Medeiros, D. R. Monteverde, M. R. Osburn, W. M. Berelson, H. L. Betts, R. S. Wijker, S. W. Mullin, H. A. Johnson, V. J. Orphan, W. W. Fischer, and A. L. Sessions. 2021. Microbial succession and dynamics in meromictic Mono Lake, California. Geobiology 19:376–393.

Quinn, T. P., I. Erb, G. Gloor, C. Notredame, M. F. Richardson, and T. M. Crowley. 2019. A field guide for the compositional analysis of any-omics data. GigaScience 8:1–14.

Quinn, T. P., I. Erb, M. F. Richardson, and T. M. Crowley. 2018. Understanding sequencing data as compositions: An outlook and review. Bioinformatics 34:2870–2878.

R Core Team. 2024. R: A Language and Environment for Statistical Computing. R Foundation for Statistical Computing, Vienna, Austria.

Reese, B. K., M. A. Anderson, and C. Amrhein. 2008. Hydrogen sulfide production and volatilization in a polymictic eutrophic saline lake, Salton Sea, California. Science of the Total Environment 406:205–218.

Salazar, R. N., C. Aguirre, J. Soto, P. Salinas, C. Salinas, H. Prieto, and M. Paneque. 2020. Physicochemical Parameters Affecting the Distribution and Diversity of the Water Column Microbial Community in the High-Altitude Andean Lake System of La Brava and La Punta. Microorganisms 8:1–24.

Savoie, E. R., V. Celeste Lanclos, M. W. Henson, C. Cheng, E. W. Getz, S. J. Barnes, D. E. LaRowe, M. S. Rappé, J. Cameron Thrash, and C. E. Savoie. 2021. Ecophysiology of the Cosmopolitan OM252 Bacterioplankton (Gammaproteobacteria).

Sirisena, K. A., S. Ramirez, A. Steele, and M. Glamoclija. 2018. Microbial Diversity of Hypersaline Sediments from Lake Lucero Playa in White Sands National Monument, New Mexico, USA. Microbial Ecology 76:404–418.

Soulier, N., K. Walters, T. N. Laremore, G. Shen, J. H. Golbeck, and D. A. Bryant. 2022. Acclimation of the photosynthetic apparatus to low light in a thermophilic Synechococcus sp. strain. Photosynthesis Research 153:21–42.

Taylor, M. 2018. The Salton Sea: A Status Update.

Tiffany, M. A., S. L. Ustin, and S. H. Hurlbert. 2007. Sulfide irruptions and gypsum blooms in the Salton Sea as detected by satellite imagery, 1979-2006. Lake and Reservoir Management 23:637–652.

Tompson, A. F. B. 2016. Born from a flood: The Salton Sea and its story of survival. Journal of Earth Science 27:89–97.

Wei, T., and V. Simko. 2021. R package "corrplot": Visualization of a Correlation Matrix.

Wood, A. M., S. R. Miller, W. K. W. Li, and R. W. Castenholz. 2002. Preliminary studies of cyanobacteria, picoplankton, and virioplankton in the Salton Sea with special attention to phylogenetic diversity among eight strains of filamentous cyanobacteria. Hydrobiologia 473:77–92.

Xia, Y. 2023. Statistical normalization methods in microbiome data with application to microbiome cancer research. Taylor and Francis Ltd.

Xia, Y., C. Lü, N. Hou, Y. Xin, J. Liu, H. Liu, and L. Xun. 2017. Sulfide production and oxidation by heterotrophic bacteria under aerobic conditions. ISME Journal 11:2754–2766.

Appendix B: Supplemental Information for Chapter II

Title: Diversity of Sulfur Cycling Halophiles within the Salton Sea, California's Largest Lake

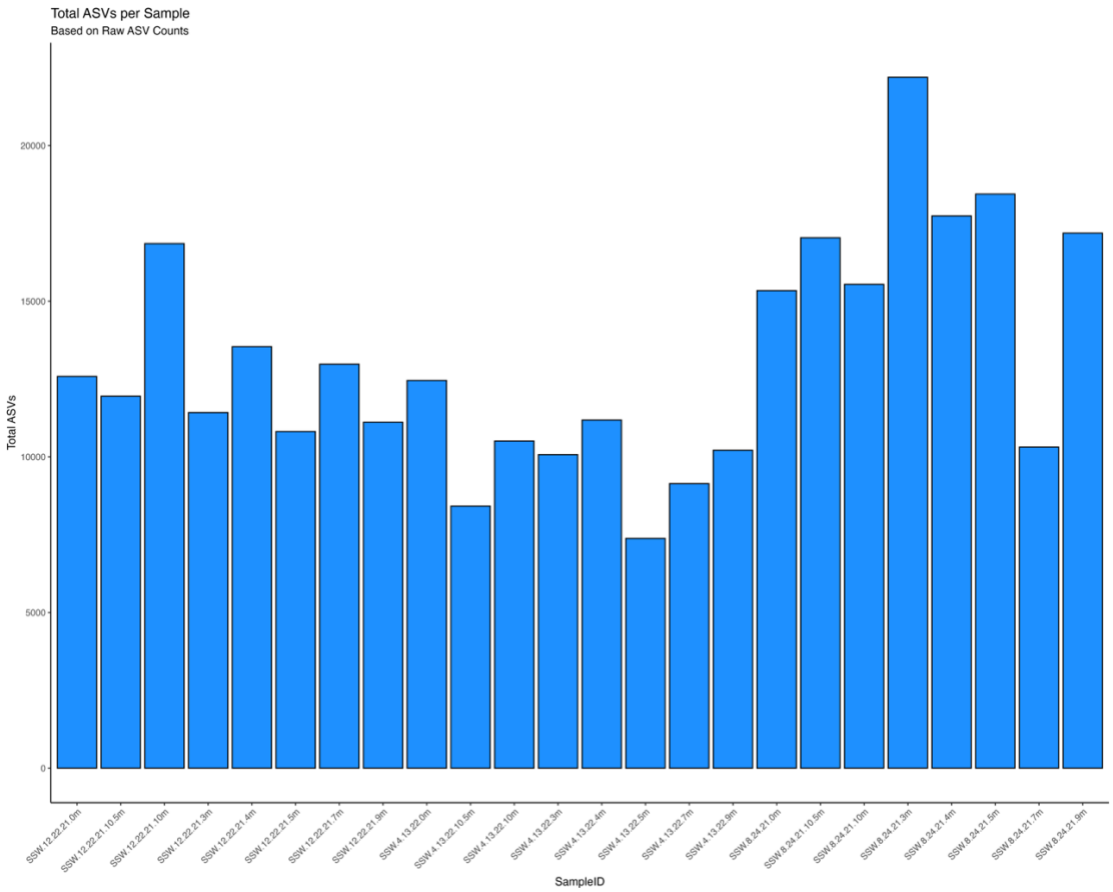

Figure B.1.1. Total Amplicon Sequence Variants (ASVs) by Sample. This bar plot shows the total number of unfiltered ASVs per sample by Sample ID.

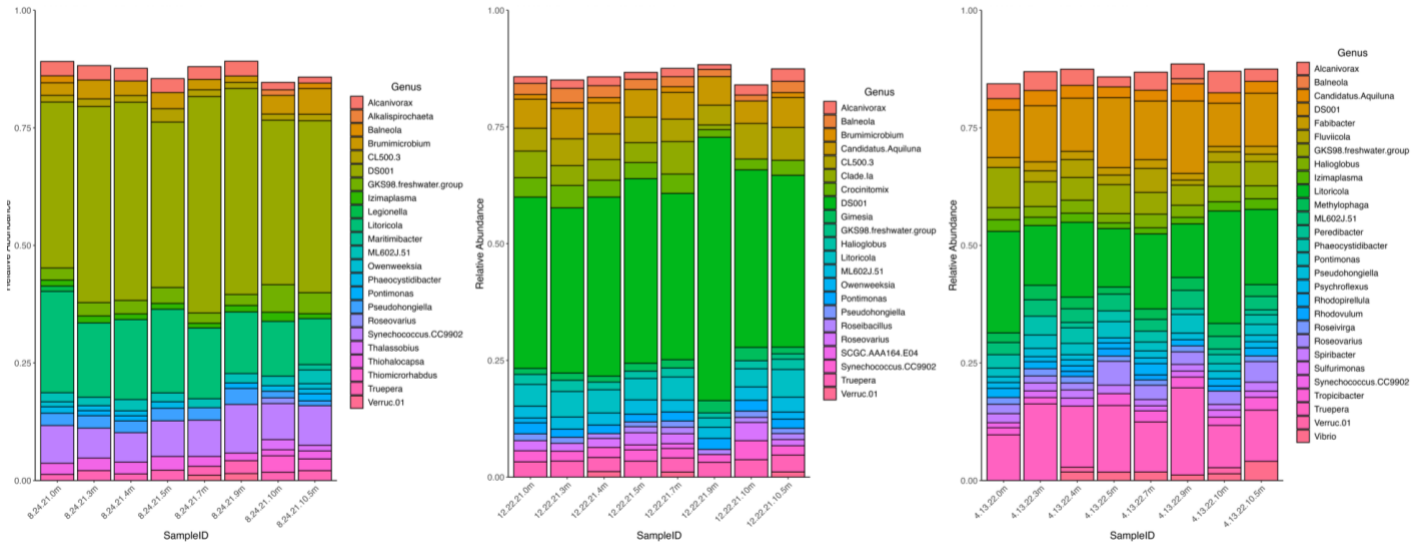

Figure B.1.2. Bacterial Genera by Sample Depth and Collection Date. These stacked barplots are ordered from left to right by their collection date (i.e., August 2021, December 2021, and April 2022) and depth. This plot only includes microbial genera with a relative abundance of at least 1%.

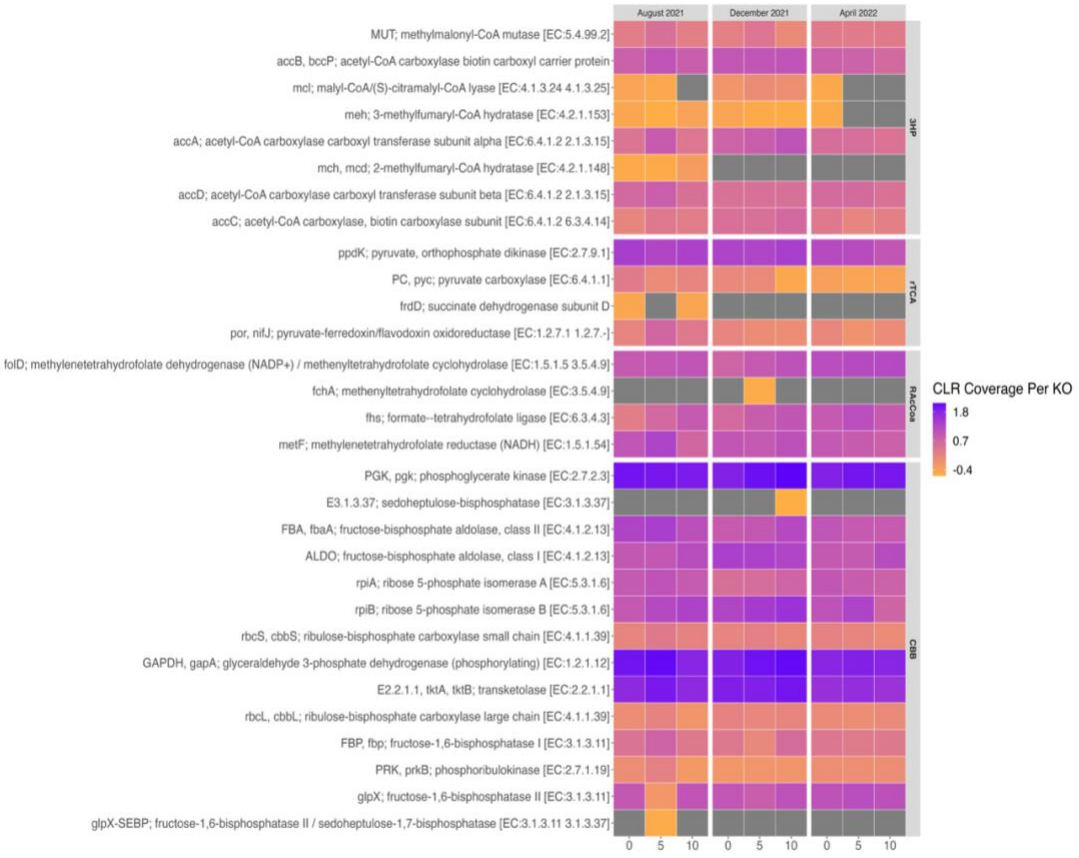

Figure B.1.3. Carbon Cycling in the Metagenomes by Depth and Collection Date. This heat map shows the relative coverage (i.e., center-log ratio transformed coverage) of genes assigned to KOs involved in carbon metabolism. Each column is a metagenome, organized from left to right by collection date and depth (0m, 5m, and 10m). The carbon cycling genes are broken up by their pathways: . Gray squares indicate that the gene is absent.

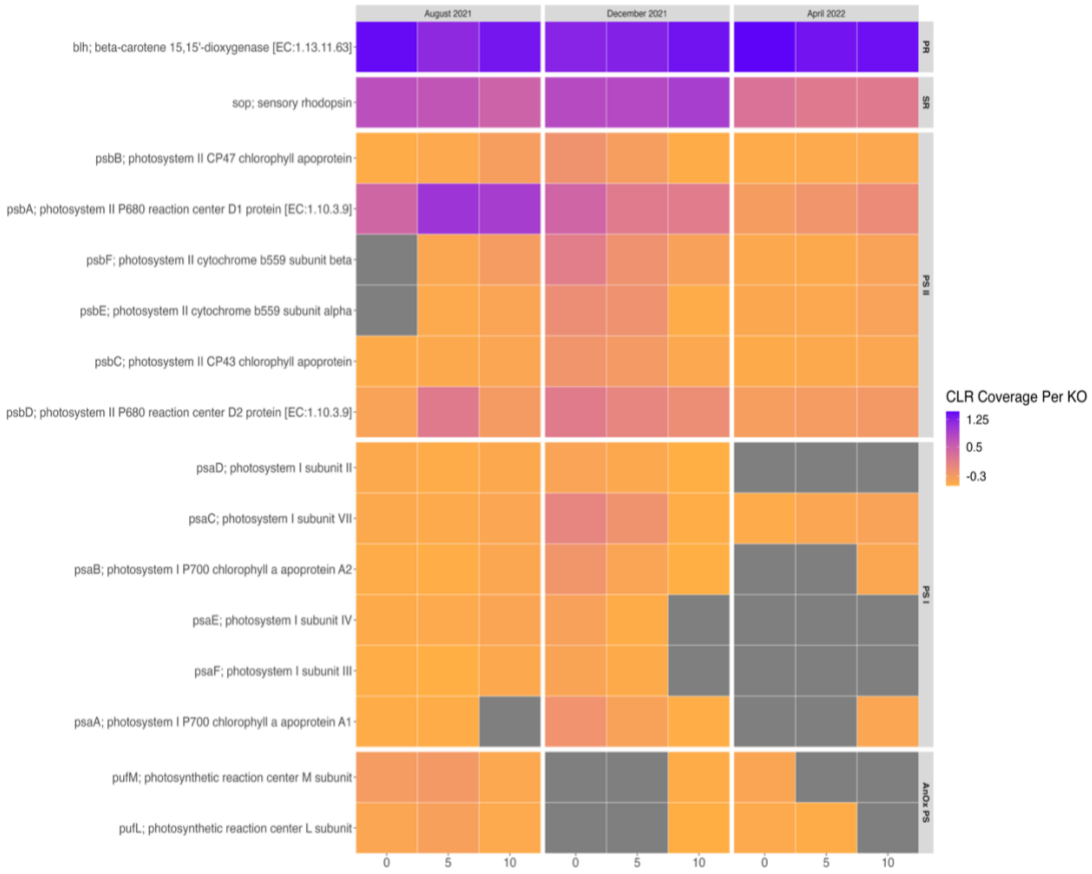

Figure B.1.4. Phototrophy in the Metagenomes by Depth and Collection Date. This heat map shows the relative coverage (i.e., center-log ratio transformed coverage) of genes assigned to KOs involved in various types of phototrophy. Each column is a metagenome, organized from left to right by collection date and depth (0m, 5m, and 10m). The phototrophy genes are broken up by their phototrophic systems/pigments: proteorhodopsin (i.e., PR), sensory rhodopsin (i.e., SR), oxygenic photosynthesis Photosystem II (i.e., PS II), oxygenic photosynthesis Photosystem I (i.e., PS I), and anoxygenic photosynthesis (i.e., AnOx PS). Gray squares indicate that the gene is absent.

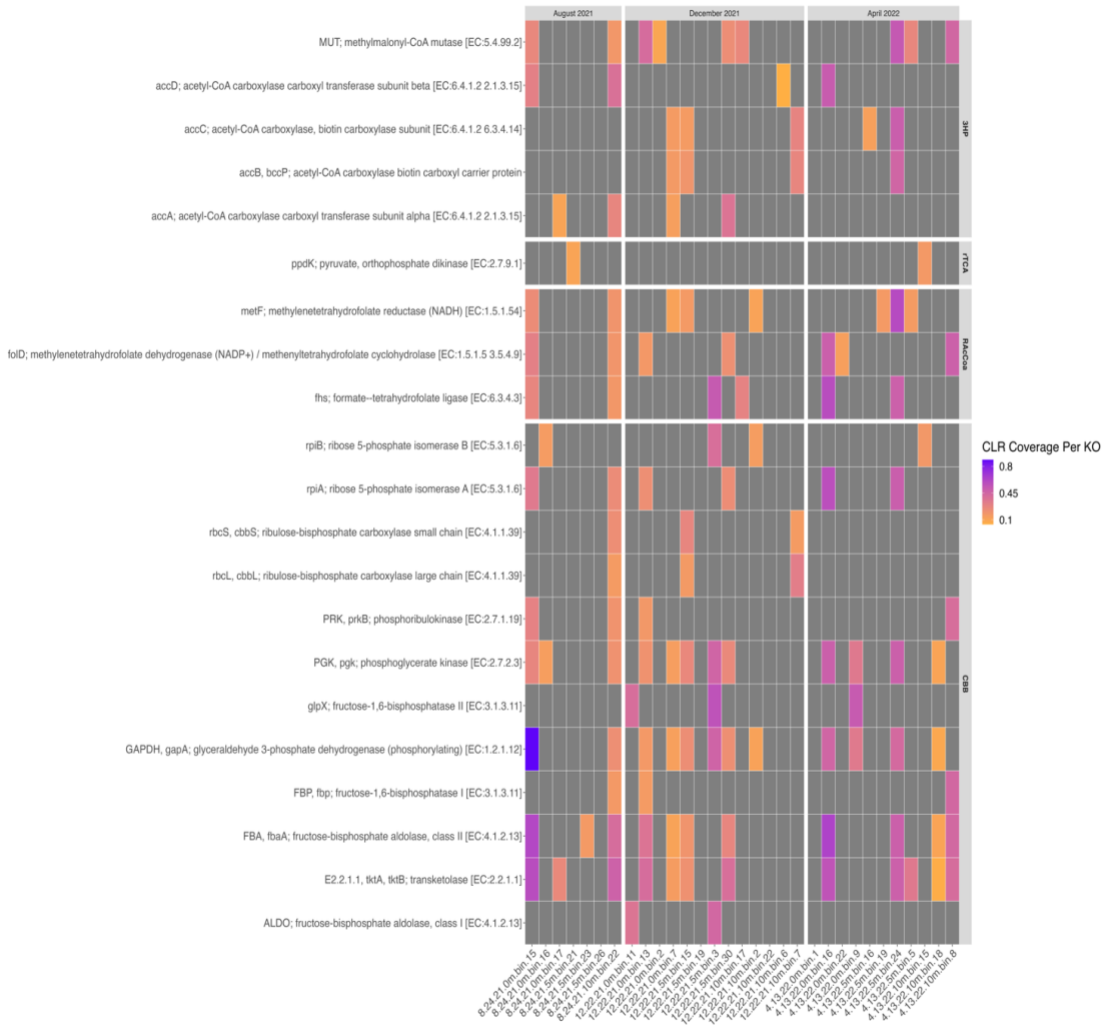

Figure B.1.5. Carbon Cycling in the Metagenome-Assembled Genomes (MAGs) by Depth and Collection Date. This heat map shows the relative coverage (i.e., center-log ratio transformed coverage) of genes assigned to KOs involved in carbon metabolism in the MAGs found. Each column is a MAG, organized from left to right by collection date and depth (0m, 5m, and 10m). The carbon cycling genes are broken up by their pathways: Gray squares indicate that the gene is absent. .

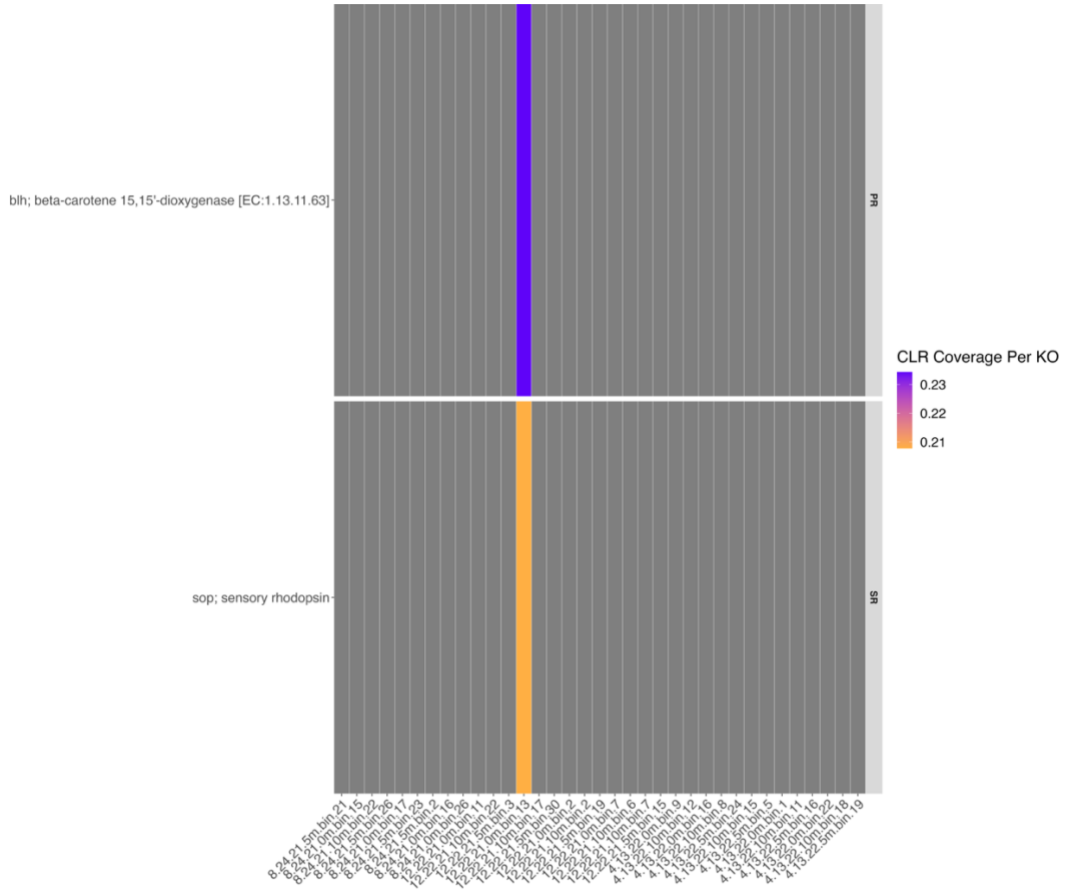

Figure B.1.6. Phototrophy in the Metagenome-Assembled Genomes (MAGs) by Depth and Collection Date. This heat map shows the relative coverage (i.e., center-log ratio transformed coverage) of genes assigned to KOs involved in various types of phototrophy. Each column is a MAG, organized from left to right by collection date and depth (0m, 5m, and 10m). The phototrophy genes are broken up by their phototrophic systems/pigments: proteorhodopsin (i.e., PR), sensory rhodopsin (i.e., SR), oxygenic photosynthesis Photosystem II (i.e., PS II), oxygenic photosynthesis Photosystem I (i.e., PS I), and anoxygenic photosynthesis (i.e., AnOx PS). Gray squares indicate that the gene is absent.

Sample ID	Sample Month	Sample Year	Depth (m)	Local %DO	Dissolved Oxygen (mgL)	Oxidative-Reduction Potential (mV)	Temperature (C)	Salinity (ppt)	Dissolved Organic Matter (RFU)	Sulfate (milliM)	Sulfide (microM)
SSW.8.24.21.0m	August	2021	0	74.6	3.88	0.8	31.15	57	29.46	180.561472	10.5070216
SSW.8.24.21.3m	August	2021	3	37.8	1.99	65.2	30.434	57.18	30.02	181.546976	3.14703062
SSW.8.24.21.4m	August	2021	4	23.9	1.26	65.3	30.369	57.23	30.08	181.118496	13.9811629
SSW.8.24.21.5m	August	2021	5	16	0.84	64.5	30.315	57.23	30.2	183.475136	2.5774068
SSW.8.24.21.7m	August	2021	7	11.8	0.62	61.9	30.268	57.31	30.28	178.14056	2.99475495
SSW.8.24.21.9m	August	2021	9	0.8	0.04	-30	30.377	57.42	30.8	184.717728	30.5566522
SSW.8.24.21.10m	August	2021	10	0.2	0.01	-240.9	30.448	57.54	31.19	184.589184	55.9528509
SSW.8.24.21.10.5m	August	2021	10.5	0.2	0.01	-240.9	30.448	57.54	31.19	183.003808	66.6854661
SSW.12.22.21.0m	December	2021	0	105.1	6.82	65.3	16.149	61.54	28.74	195.451152	2.71276296
SSW.12.22.21.3m	December	2021	3	88.4	5.76	66	15.926	61.51	28.89	193.758656	2.58868648
SSW.12.22.21.4m	December	2021	4	87.1	5.68	64.7	15.9	61.52	28.87	194.4228	2.59432632
SSW.12.22.21.5m	December	2021	5	87.2	5.69	66.1	15.899	61.52	28.86	195.618259	2.5492076
SSW.12.22.21.7m	December	2021	7	86.9	5.67	65.6	15.893	61.52	28.89	197.572128	2.81428007
SSW.12.22.21.9m	December	2021	9	84.9	5.6	66.4	15.359	61.49	28.75	196.522352	2.71276296
SSW.12.22.21.10m	December	2021	10	85.2	5.61	68.3	15.365	61.49	28.76	193.355885	2.87631831
SSW.12.22.21.10.5m	December	2021	10.5	85.2	5.61	68.3	15.365	61.49	28.76	196.89513	2.7748012
SSW.4.13.22.0m	April	2022	0	92.4	5.24	71.7	24.391	60.74	25.88	188.059872	3.09025068
SSW.4.13.22.3m	April	2022	3	69.8	4.23	70.8	20.304	60.95	28	187.46	2.65518433
SSW.4.13.22.4m	April	2022	4	59.7	3.63	70.8	20.122	60.61	28.11	184.974816	3.61488951
SSW.4.13.22.5m	April	2022	5	56	3.41	71	20.098	60.56	28.13	186.860128	3.64048164
SSW.4.13.22.7m	April	2022	7	52.4	3.19	70.7	20.075	60.56	28.22	169.506688	3.19901726
SSW.4.13.22.9m	April	2022	9	51.2	3.12	70.7	20.069	60.54	28.28	184.374944	3.0582605
SSW.4.13.22.10m	April	2022	10	51	3.11	70.9	20.066	60.56	28.29	179.147488	3.44214257
SSW.4.13.22.10.5m	April	2022	10.5	51	3.11	70.9	20.066	60.56	28.29	172.163264	3.81962661

Table B.2.1. Sample Metadata and Geochemistry Data. This table contains the sample metadata and geochemistry measurements (i.e., local % dissolved oxygen, dissolved oxygen (mg/L), oxidative-reduction potential (mV), temperature, salinity (ppt), dissolved organic matter (RFU), sulfate (milliM), and sulfide (microM) for each sample collected during August 2021, December 2021, And April 2022.

SampleID	Bin Num	Taxa Level	Marker Lineage	Lineage ID	Genome Num	Completeness	Contamination	Strain Heterogeneity	GC Content
SSW.8.24.21.0m	bin.15	c	Gammaproteobacteria	(UID4443)	356	94.51	0.74	33.33	53.4
SSW.8.24.21.0m	bin.16	p	Bacteroidetes	(UID2591)	364	86.73	1.24	0	42
SSW.8.24.21.0m	bin.17	s	algicola	(UID2846)	47	81.81	0.4	0	44
SSW.8.24.21.0m	bin.26	k	Bacteria	(UID2569)	434	83.52	1.42	14.29	43.6
SSW.8.24.21.5m	bin.2	k	Bacteria	(UID2569)	434	83.66	2.11	0	43.6
SSW.8.24.21.5m	bin.21	k	Bacteria	(UID1453)	901	92.31	4.7	88.89	64.2
SSW.8.24.21.5m	bin.23	s	algicola	(UID2846)	47	82.63	0.07	0	44
SSW.8.24.21.5m	bin.26	p	Cyanobacteria	(UID2143)	129	87.5	2.17	55.56	65.5
SSW.8.24.21.10m	bin.22	c	Gammaproteobacteria	(UID4443)	356	94.51	0.56	33.33	53.3
SSW.12.22.21.0m	bin.11	k	Bacteria	(UID1453)	901	92.31	1.92	66.67	66.7
SSW.12.22.21.0m	bin.13	c	Gammaproteobacteria	(UID4443)	356	94.14	1.11	25	53.3
SSW.12.22.21.0m	bin.2	k	Bacteria	(UID2569)	434	86.06	1.79	28.57	46.1
SSW.12.22.21.0m	bin.7	c	Gammaproteobacteria	(UID4274)	112	91.32	0.46	100	57
SSW.12.22.21.5m	bin.15	k	Bacteria	(UID203)	5449	82.76	0	0	57
SSW.12.22.21.5m	bin.19	k	Bacteria	(UID2569)	434	82.04	0.59	0	46.1
SSW.12.22.21.5m	bin.3	k	Bacteria	(UID1453)	901	93.16	0.85	0	66.7
SSW.12.22.21.5m	bin.30	c	Gammaproteobacteria	(UID4443)	356	94.51	0.37	0	53.3
SSW.12.22.21.10m	bin.17	c	Gammaproteobacteria	(UID4443)	356	94.14	0.37	0	53.4
SSW.12.22.21.10m	bin.2	k	Bacteria	(UID2569)	434	97.04	0.81	100	46
SSW.12.22.21.10m	bin.22	k	Bacteria	(UID1453)	901	88.58	1.99	66.67	66.8
SSW.12.22.21.10m	bin.6	k	Bacteria	(UID2569)	434	96.92	4.4	0	39.5
SSW.12.22.21.10m	bin.7	c	Gammaproteobacteria	(UID4274)	112	91.4	0.09	100	57
SSW.4.13.22.0m	bin.1	s	algicola	(UID2846)	47	83.15	1.2	25	44
SSW.4.13.22.0m	bin.16	c	Gammaproteobacteria	(UID4443)	356	93.28	0.74	33.33	53.3
SSW.4.13.22.0m	bin.22	c	Gammaproteobacteria	(UID4201)	1164	97.13	1.72	66.67	43.2
SSW.4.13.22.0m	bin.9	k	Bacteria	(UID1453)	901	80.16	2.99	100	74.1
SSW.4.13.22.5m	bin.16	s	algicola	(UID2846)	47	83.67	1	20	43.9
SSW.4.13.22.5m	bin.19	c	Gammaproteobacteria	(UID4201)	1164	92.43	1.05	66.67	43.3
SSW.4.13.22.5m	bin.24	c	Gammaproteobacteria	(UID4443)	356	94.69	0.37	0	53.3
SSW.4.13.22.5m	bin.5	o	Actinomycetales	(UID1663)	488	93.99	2.88	25	64.7
SSW.4.13.22.10m	bin.11	s	algicola	(UID2846)	47	80.71	0.59	28.57	43.9
SSW.4.13.22.10m	bin.12	k	Bacteria	(UID1453)	901	82.41	2.14	66.67	73.8
SSW.4.13.22.10m	bin.15	o	Actinomycetales	(UID1663)	488	88.67	3.55	14.29	64.6
SSW.4.13.22.10m	bin.18	c	Gammaproteobacteria	(UID4201)	1164	94.01	2.3	25	43.3
SSW.4.13.22.10m	bin.8	c	Gammaproteobacteria	(UID4443)	356	95.62	0.37	0	53.3

Table B.2.2. CheckM Results for Metagenome-Assembled Genomes (MAGs) Bin Assignments. This table contains the CheckM results for each putative, high-quality MAG bin assignment.

Sample ID	Shannon Wiener (Entropy)	Shannon Weiner Diversity	Species Richness
SSW.8.24.21.0m	4.30307865	73.9270391	1194
SSW.8.24.21.10.5m	4.55391783	95.0038891	1369
SSW.8.24.21.10m	4.51325818	91.2185412	1276
SSW.8.24.21.3m	4.21097987	67.4225727	1228
SSW.8.24.21.4m	4.26386379	71.0841076	1242
SSW.8.24.21.5m	4.41860564	82.9804998	1270
SSW.8.24.21.7m	4.20000386	66.6865887	1021
SSW.8.24.21.9m	3.7497824	42.5118302	507
SSW.12.22.21.0m	4.58879386	98.3757033	872
SSW.12.22.21.10.5m	4.65415079	105.019998	996
SSW.12.22.21.10m	4.57793663	97.313393	1070
SSW.12.22.21.3m	4.70919327	110.962607	954
SSW.12.22.21.4m	4.61605442	101.094368	1040
SSW.12.22.21.5m	4.63812073	103.349942	929
SSW.12.22.21.7m	4.70742802	110.766903	990
SSW.12.22.21.9m	4.12722217	62.0054428	796
SSW.4.13.22.0m	4.53543507	93.2640825	847
SSW.4.13.22.10.5m	4.83553778	125.906275	861
SSW.4.13.22.10m	4.64441814	104.002833	940
SSW.4.13.22.3m	4.29109902	73.046704	740
SSW.4.13.22.4m	4.48281071	88.4830236	829
SSW.4.13.22.5m	4.72598945	112.842095	788
SSW.4.13.22.7m	4.74851125	115.412336	906
SSW.4.13.22.9m	4.2845478	72.5697233	749

Table. B.2.3. Bacterial Alpha Diversity and Species Richness by Sample. This table shows the Shannon-Weiner entropy, Shannon-Weiner diversity, and species richness for each sample.

	Comparisons by Time Point	P_{adj} value
Shannon Diversity	December 2021 vs August 2021	0.027
	April 2022 vs August 2021	0.018
	April 2022 vs December 2021	0.983
Species Richness	December 2021 vs August 2021	0.312
	April 2022 vs August 2021	0.442
	April 2022 vs December 2021	1

Table. B.2.4. Pairwise Comparison of the Variance in Alpha Diversity and Species Richness. A Tukey test was used to compare the variance in Shannon diversity between collection dates, and a Dunn test was used to compare the variance in species richness between collection dates.

Comparisons by Time Point	DF	Sums of Squares	F Model	R^2	P value	P_{adj} value
December 2021 vs April 2022	1	7006.287	17.13323	0.5503196	0.001	0.003
December 2021 vs August 2021	1	7416.531	13.48028	0.4905437	0.001	0.003
April 2022 vs August 2021	1	7987.429	15.15788	0.5198554	0.002	0.006

Table. B.2.5. Pairwise PERMANOVA Results Comparing Beta Diversity by Collection Date. This is a pairwise permutational multivariate analysis of variance (PERMANOVA) comparing the variance in beta diversity between collection dates.

Site(s)	Model	Variance	F value	P value	P_{adj} value
All	Temperature °C + DOM + %DO	335.51	13.8841	0.001	0.004
		169.84	7.0285	0.001	0.004
		113.20	4.6845	0.001	0.004
August 2021	DOM	157.93	1.8571	0.001	0.002
December 2021	ORP	77.39	1.3089	0.002	0.012
April 2022	DOM	60.08	1.107	0.026	0.068

Table. B.2.6. Redundancy Analysis Results of Microbial Composition Across and Within Collection Dates. These results show which environmental variables were significant drivers of beta diversity across all three collection dates and within each collection date based on a redundancy analysis (RDA).

Sample ID	Domain	Phylum	Class	Order	Family	Genus	Species
SSW.8.24.21.0m.bin.15	Bacteria	Proteobacteria	Gammaproteobacteria	Pseudomonadales	Litoricolaceae	HIMB30	Unknown
SSW.8.24.21.0m.bin.16	Bacteria	Bacteroidota	Bacteroidia	Chitinophagales	Saprospiraceae	Unknown	Unknown
SSW.8.24.21.0m.bin.17	Bacteria	Bacteroidota	Bacteroidia	Flavobacteriales	Flavobacteriaceae	UBA3478	Unknown
SSW.8.24.21.0m.bin.26	Bacteria	Bacteroidota	Bacteroidia	Flavobacteriales	Salibacteraceae	Unknown	Unknown
SSW.8.24.21.5m.bin.2	Bacteria	Bacteroidota	Bacteroidia	Flavobacteriales	Salibacteraceae	UBA4419	Unknown
SSW.8.24.21.5m.bin.21	Bacteria	Actinobacteriota	Acidimicrobiia	Acidimicrobiales	Ilumatobacteraceae	Casp-actino5	Unknown
SSW.8.24.21.5m.bin.23	Bacteria	Bacteroidota	Bacteroidia	Flavobacteriales	Flavobacteriaceae	UBA3478	Unknown
SSW.8.24.21.5m.bin.26	Bacteria	Cyanobacteria	Cyanobacteriia	PCC-6307	Cyanobiaceae	Synechococcus_C	Synechococcus_C sp000153065
SSW.8.24.21.10m.bin.22	Bacteria	Proteobacteria	Gammaproteobacteria	Pseudomonadales	Litoricolaceae	HIMB30	Unknown
SSW.12.22.21.0m.bin.11	Bacteria	Actinobacteriota	Acidimicrobiia	Acidimicrobiales	Ilumatobacteraceae	Casp-actino5	Casp-actino5 sp017859785
SSW.12.22.21.0m.bin.13	Bacteria	Proteobacteria	Gammaproteobacteria	Pseudomonadales	Litoricolaceae	HIMB30	Unknown
SSW.12.22.21.0m.bin.2	Bacteria	Bacteroidota	Bacteroidia	Flavobacteriales	Cryomorphaceae	SKUL01	Unknown
SSW.12.22.21.0m.bin.7	Bacteria	Proteobacteria	Gammaproteobacteria	GCF-002020875	GCF-002020875	Unknown	Unknown
SSW.12.22.21.5m.bin.15	Bacteria	Proteobacteria	Gammaproteobacteria	GCF-002020875	GCF-002020875	Unknown	Unknown
SSW.12.22.21.5m.bin.19	Bacteria	Bacteroidota	Bacteroidia	Flavobacteriales	Cryomorphaceae	SKUL01	Unknown
SSW.12.22.21.5m.bin.3	Bacteria	Actinobacteriota	Acidimicrobiia	Acidimicrobiales	Ilumatobacteraceae	Casp-actino5	Casp-actino5 sp017859785
SSW.12.22.21.5m.bin.30	Bacteria	Proteobacteria	Gammaproteobacteria	Pseudomonadales	Litoricolaceae	HIMB30	Unknown
SSW.12.22.21.10m.bin.17	Bacteria	Proteobacteria	Gammaproteobacteria	Pseudomonadales	Litoricolaceae	HIMB30	Unknown
SSW.12.22.21.10m.bin.2	Bacteria	Bacteroidota	Bacteroidia	Flavobacteriales	Cryomorphaceae	SKUL01	Unknown
SSW.12.22.21.10m.bin.22	Bacteria	Actinobacteriota	Acidimicrobiia	Acidimicrobiales	Ilumatobacteraceae	Casp-actino5	Casp-actino5 sp017859785
SSW.12.22.21.10m.bin.6	Bacteria	Bacteroidota	Bacteroidia	Flavobacteriales	Crocinitomicaceae	Unknown	Unknown
SSW.12.22.21.10m.bin.7	Bacteria	Proteobacteria	Gammaproteobacteria	GCF-002020875	GCF-002020875	Unknown	Unknown
SSW.4.13.22.0m.bin.1	Bacteria	Bacteroidota	Bacteroidia	Flavobacteriales	Flavobacteriaceae	UBA3478	Unknown
SSW.4.13.22.0m.bin.16	Bacteria	Proteobacteria	Gammaproteobacteria	Pseudomonadales	Litoricolaceae	HIMB30	Unknown
SSW.4.13.22.0m.bin.22	Bacteria	Proteobacteria	Gammaproteobacteria	CACEW01	Unknown	Unknown	Unknown
SSW.4.13.22.0m.bin.9	Bacteria	Actinobacteriota	Actinomycetia	Nitriliruptorales	Nitriliruptoraceae	CSBr16-57R1	Unknown
SSW.4.13.22.5m.bin.16	Bacteria	Bacteroidota	Bacteroidia	Flavobacteriales	Flavobacteriaceae	UBA3478	Unknown
SSW.4.13.22.5m.bin.19	Bacteria	Proteobacteria	Gammaproteobacteria	CACEW01	Unknown	Unknown	Unknown
SSW.4.13.22.5m.bin.24	Bacteria	Proteobacteria	Gammaproteobacteria	Pseudomonadales	Litoricolaceae	HIMB30	Unknown
SSW.4.13.22.5m.bin.5	Bacteria	Actinobacteriota	Actinomycetia	Nanopelagicales	S36-B12	M55B157	Unknown
SSW.4.13.22.10m.bin.11	Bacteria	Bacteroidota	Bacteroidia	Flavobacteriales	Flavobacteriaceae	UBA3478	Unknown
SSW.4.13.22.10m.bin.12	Bacteria	Actinobacteriota	Actinomycetia	Nitriliruptorales	Nitriliruptoraceae	CSBr16-57R1	Unknown
SSW.4.13.22.10m.bin.15	Bacteria	Actinobacteriota	Actinomycetia	Nanopelagicales	S36-B12	M55B157	Unknown
SSW.4.13.22.10m.bin.18	Bacteria	Proteobacteria	Gammaproteobacteria	CACEW01	Unknown	Unknown	Unknown
SSW.4.13.22.10m.bin.8	Bacteria	Proteobacteria	Gammaproteobacteria	Pseudomonadales	Litoricolaceae	HIMB30	Unknown

Table B.2.7. Taxonomic Annotation of Metagenome Assembled Genomes (MAGs). This table contains the taxonomic annotation results from GTDB-tk of high-quality bins identified in this project.

CHAPTER III

Title: Climate Conditions Structure the Taxonomic and Functional Diversity of the Aeolian Dust Microbiome

Authors: Freund, L.[1], Topacio, Talyssa M.[2], Miao, Yaning[3], Porter, Will[3], Swenson, Mark[2], Maltz, Mia[4], Bothoff, Jon[2], Aronson, Emma L.[2]

1. Genetics, Genomics, and Bioinformatics Program, University of California, Riverside, CA
2. Department of Microbiology and Plant Pathology, University of California, Riverside, CA
3. Department of Environmental Sciences, University of California, Riverside, CA
4. Department of Plant Science and Landscape Architecture, University of Connecticut, CT

Abstract

The aeolian dust microbiome is composed of uniquely adapted microorganisms that can persist in the harsh conditions of the atmosphere. Specific microbial taxa and survival strategies have been observed in dust microbiomes from around the world, yet the environmental processes that select for both the composition and traits of the microbiome are poorly understood. Here we explore the taxonomic and functional diversity of the aeolian dust microbiome from sites around the Salton Sea in Southern California, and how dust sources and the local climate influenced the microbiome. Dust samples were collected from four locations around the Salton Sea in the summer and fall of 2020 and 2021, and 16S V3-V4 rRNA amplicon sequencing and shotgun metagenomic sequencing was used to characterize the aeolian dust microbiome. We observed significant differences in microbial composition between sites, and we were able to identify 13 microbial genera that were members of the core dust microbiome across samples. We also found that genes involved in sporulation, UV radiation resistance, thermal resistance, osmotic stress resistance, and quorum sensing were shared across the aeolian dust metagenomes. Lastly, local wind conditions and estimated dust source surface categories were significant predictors of the microbial adaptations we found in the aeolian dust metagenomes. Our results demonstrate the ability of airborne dust microorganisms to readily adapt to their harsh environment and highlight the survival strategies that allow them to disperse across broad distances, thus posing a potential health risk to exposed communities.

Introduction

Microorganisms are ubiquitous and can be found in every environment, even in the most arduous and extreme ecosystems. Aeolian (i.e., windblown) dust is an example of such a system and is garnering more attention by microbial ecologists as of late. This is because global dust load has increased upwards of 55% since the mid-1800's (Kok et al. 2018), impacting local and global climate, as well as public health. Dust is responsible for delivering abiotic and biotic particulates across thousands of kilometers as a constituent of aerosolized particulate matter (PM) in the atmosphere. Microorganisms become entrained in dust either as free-floating single cells or spores, or by attaching to existing particulates or aerosols to form aggregates, which can then serve as protection as they travel (Erkorkmaz et al. 2023). Some microorganisms can colonize the atmospheric environment, while others are readily dispersed and introduced to new ecosystems (Maltz et al. 2022). Like other forms of particulate matter, aeolian dust microorganisms impact the climate by acting as cloud or ice nucleating agents (Amato et al. 2015, Joly et al. 2015), contributing to the formation of clouds and affecting Earth's overall radiative budget (Kok et al. 2018, Shi and Liu 2019). They can also contribute to changes in the local ecology via dispersal and deposition, influencing the nutrient cycling dynamics in these new habitats. Furthermore, these microorganisms can also negatively impact public health as they can travel long distances and enter the respiratory tract via inhalation, leading to respiratory distress (Mayol et al. 2014, Biddle et al. 2021, Maltz et al. 2022). The assembly of the microbial communities associated with airborne dust is of crucial importance due to its implications for both ecological and public health, demonstrating

the strong connections between this ubiquitous microbiome, our own health, and the health of our environment.

For microorganisms to survive in aeolian dust, they must overcome environmental stressors that are not commonly experienced in terrestrial or aquatic ecosystems. First, microorganisms can be introduced into the atmosphere via emission and suspension and are subjected to wind shear stress in the process. Once in the atmosphere, these microorganisms are exposed to UV radiation from unobstructed sun exposure and will experience rapid changes in temperature and pressure as the wind travels both horizontally and vertically through atmospheric advection (Schepanski 2018). Additionally, moisture and nutrient availability is unpredictable in aeolian dust, which can lead to osmotic stress, desiccation stress, and starvation (Tang et al. 2018). Thus, the aeolian dust microbiome must have the adaptations required to survive inhabiting the atmosphere. Airborne microbial communities sampled around the world have been found to contain genes involved in UV-radiation resistance, osmotic stress resistance, and thermal resistance (Aalismail et al. 2019). Some Gram-positive dust microorganisms have been found to form endospores to endure the fluctuating conditions of the atmosphere. Lastly, both Gram-positive and Gram-negative bacteria can form biofilms, which may assist them in adhering to dust particulates in the air (Hu et al. 2024). This allows the bacteria to form aggregates which can shield them against wind shear stress and provide nutrition when nutrients are scarce. These traits have been observed in other ecosystems, however, the combined environmental stressors

experienced by aeolian dust consistently selects for these adaptations in dust microbiomes.

The Salton Sea ecosystem in Southern California presents a unique and urgent opportunity to explore the mechanisms that structure the taxonomic and functional composition of its aeolian dust microbiome. The Salton Sea is a hypersaline lake that is rapidly shrinking, exposing its playa sediment to wind erosion and thus increasing the dust load in the atmosphere. Emissions from increasingly dried lakebed surfaces have been associated with increases in PM in the area (Parajuli and Zender 2018, Jones and Fleck 2020) as well as increases in respiratory illnesses (Farzan et al. 2019, Jones and Fleck 2020), and have been shown in lab studies to induce lung inflammation upon exposure (Biddle et al. 2021, 2023). Furthermore, those experiencing the highest incidence of respiratory distress are primarily vulnerable populations that lack access to healthcare and are systemically barred from informing local policy, such as the Latinx and Indigenous Latin American (i.e., P'urhépecha) residents living around the Salton Sea (Doede and DeGuzman 2020, Rodriguez 2021, Knoerr 2022, Cheney et al. 2023). The rise in dust emissions coupled with the ongoing respiratory distress that predominantly affects local marginalized communities highlights the connection between local climate and public health, yet the influence of aeolian dust microorganisms on this relationship has yet to be explored.

While the major elemental composition of this dust has been investigated and not found to be toxic (Frie et al. 2017), there is concern about dust toxicity in the region, and the microbial community of the dust has not been characterized. Here, we investigate the

taxonomic and functional diversity of the aeolian dust microbiome sampled from the Salton Sea. We utilize 16S (V3-V4) rRNA amplicon sequencing to determine the microbial composition of the dust and shotgun metagenomics to assess the functional capacity and redundancy of the aeolian dust microbiome. We explore how dust sources and wind conditions in this region select for the assembly and survival strategies of the aeolian dust microbiome, and how its diversity may influence the health of nearby residents.

Methods

Dust Collection & Processing

Passive dust collectors were used to capture aeolian dust from around the Salton Sea at four different sites during the Summer and Fall months in 2020 and 2021 (Supplemental Table 1). Five replicate collectors were deployed at each of the following sites: the UC Riverside Palm Desert campus (PD; coordinates here), the Boyd Deep Canyon Reserve (BDC; coordinates), the Dos Palmas Preserve (DP; coordinates), and the Wister Recreation Area (WI; coordinates). Dust collector deployment dates varied based on access to our collection sites, which was variable, for example due to rain events. The sites were selected such that 2 sites, DP and WI, are located adjacent to the Salton Sea, and would be more likely to be impacted by dust and aerosols from the Sea, while the other 2 sites are locates within the same region but more geographically separated from the Sea, PD and BDC. The passive collectors consisted of Teflon-lined bundt pans (Nordic Ware, St. Louis Park, MN, United States) holding a Kevlar mesh (Industrial Netting Inc., Maple Grove, MN, United States) and filled with sterile glass marbles (12.7

mm diameter, Brooklyn, NY, United States). All materials used to assemble the passive dust collectors were first acid washed in 2M HCl followed by two subsequent rinses in pure MilliQ water, and were always treated as such prior to re-deployment.

Upon retrieval from the field, passive dust collectors were placed in Whirlpak bags and stored in 4C refrigerator for no longer than 24 hours before they were processed in the lab. Each passive collector was rinsed with 1L of 18.2 M water and used to create a dust suspension that was poured into acid-washed 1L Nalgene bottles (low density polyethylene), passing through a 2mm filter to remove insects or large particulates. Dust suspensions were immediately filtered via vacuum filtration through an acid-wash sterilized glass funnel using sterile 0.2 μm filters (47-mm diameter; Pall Supor 200 Sterile Grid filters, Pall Corporation, Port Washington, NY, United States) into an acid-washed collecting flask, as described in Maltz et al. (2022). Four to five filters were used per filtration of 1 L of dust suspension. Filters were then stored in sterile Whirlpak bags at –20°C until they could be used for DNA extraction.

DNA Extraction and Library Preparation

DNA extraction from the 0.2 μm filters were performed in duplicate with the Qiagen DNeasy PowerWater kit (Qiagen, Germantown, MD, USA), and the extracts were quantified with a NanoDrop 2000 (Thermo Fisher Scientific, Wilmington, DE, USA). Two negative controls were included during the DNA extraction process to confirm that contamination did not occur. Raw DNA extracts and the negative DNA extraction controls were quantified with a NanoDrop 2000. Half of the duplicate extracts were select for purification based on their higher raw DNA concentrations, then purified

via a bead clean-up using AMPure XP Beads and quantified with a NanoDrop 2000. Raw and purified DNA extracts were stored at −20 °C. The purified DNA extracts were then amplified via through a 2-step PCR using dual indices and sequencing adapters in the Nextera XT Index Kit (Illumina, San Diego, CA, USA) targeting the V3-V4 region of the 16S rRNA gene. Nextera-adapted Klindworth primers targeting the 16S rRNA V3-V4 region (S-D-Bact-0341-b-S-17 and S-D-Bact-0785-a-A-21; Klindworth et al. 2013) were used. Samples were prepared with the Nextera XT Index Kit and each amplification reaction contained the following: 2.5uL of DNA template, 5uL each of the 1uM forward and reverse index primers, and 12.5 uL of PCR KAPA HiFi HotStart Ready Mix to create a 25uL reaction. Positive and negative controls were included in each step of the 2-step PCR and included in the sequencing libraries.

DNA Sequencing

The amplified DNA extracts for 28 samples were pooled and sequenced via the Illumina, Inc. MiSeq platform (2 x 300bp; Illumina 2017) by the UC Riverside Genomics Core. 24 raw DNA extracts were sent on dry ice to the SeqCenter for shotgun metagenome sequencing. The SeqCenter prepared these libraries using the Illumina DNA Prep kit and IDT 10bp UDI indices and sequenced the libraries on an Illumina NovaSeq 6000 (2 x 151bp). Adapters were trimmed by the SeqCenter using the bcl-convert v4.0.3. DNA extracts from samples that were collected in October 2020 were not submitted for shotgun metagenome sequencing due to extremely low DNA concentrations across samples and were thus used only for 16S rRNA amplicon sequencing.

Bioinformatics – Amplicon Sequence Data

Amplicon sequences were demultiplexed by the UC Riverside Genomics Core, and the FASTQ sequences were assessed for sequencing quality via FastQC (Andrews n.d.). In addition to FastQC, the eestats2 program (Edgar and Flyvbjerg 2015) was used to determine the percentage of reads of specific lengths that will pass through the expect error threshold for a specific sample. The results supplied by FastQC and eestats2 were used to determine where the reads should be trimmed across the samples. Before trimming, there was a total of 11,646,700 reads (including forward and reverse reads) with a length of 301 base pairs across all 28 samples. The reads were then trimmed and filtered with BBDuk, a k-mer-based trimming and decontamination program from the BBTools suite created by the Joint Genome Institute (Bushnell n.d.), resulting in a total of 11,616,898 trimmed reads, ranging from 250 – 271 base pairs in length, across the samples. After trimming, the Divisive Amplicon Denoising Algorithm 2 (DADA2) pipeline (Callahan et al. 2016) was used via the RStudio environment (version 2023.03.0+386) to assign reads to amplicon sequence variants (ASVs). Contaminant ASVs identified by the "decontam" package for R (Davis et al. 2018), as well as ASVs identified in the 2-step PCR positive and negative controls, were removed from the ASV count data. A total of 2,156 contaminant ASVs. Singletons and ASVs that were assigned to "Chloroplast" or "Mitochondria" taxonomic classifications were also removed from the ASV count data set. Before statistical analyses took place, the counts for each ASV were divided by the number of deployment days for that specific sample; this was performed to account for the variation in deployment duration across samples. The scaled

counts were then multiplied by 100 and rounded to ensure that scaling by deployment did not skew the statistical analyses.

Bioinformatics – Metagenome Sequence Data

The sequence quality of the shotgun metagenomic data was assessed using FastQC (Andrews n.d.), and adapter and primer sequences were trimmed using BBDuk (Bushnell n.d.). After trimming, BBNorm (BBTools suite, (Bushnell n.d.) was used to normalize the depth of read coverage in each metagenome. This normalization step ensures that there is an equal distribution of reads across all the sequenced regions, which is a necessary consideration with shotgun metagenomes due to their unequal sequence coverage (Bushnell n.d.). The normalized reads were then merged using BBMerge. The normalized reads are also error-corrected with SPades (Bankevich et al. 2012) and subsequently used for contig co-assembly with MEGAHIT (Li et al. 2015). Co-assembling contigs ensures that predicted genes identified by the functional annotation process are consistent across the metagenomes. The merged reads were also used to assist in the co-assembly of the contigs. The quality of the co-assembled contigs was determined using MetaQuast (Mikheenko et al. 2016). Trimmed, non-normalized metagenomic reads were then aligned to the co-assembled contigs using BWA-MEM. After read mapping, contigs and scaffolds were binned into genomes (i.e., metagenome-assembled genomes; MAGs) with metaBAT (Kang et al. 2019), using the read mapping results from BWA-MEM to guide the binning. The quality and completeness of the MAGs was determined using CheckM (Parks et al. 2015). A custom bash script was then used to read the output from CheckM and parse out bins based on their completeness and

contamination, identifying high-quality (i.e., >80% complete, <5% contamination) bins for downstream analyses (Bowers et al. 2017; Supplemental Table 4). Gene prediction was performed on the contigs and high-quality MAGs respectively using Prodigal (Hyatt et al. 2010a). KOFamScan was then used to assign functions and KEGG orthologies (i.e., KO identifiers) to the predicted genes (Hyatt et al. 2010b, Aramaki et al. 2020) in the contigs and high-quality MAGs. Gene assignments from KOFamScan were filtered so that each gene was assigned to a single KO identifier based on the lowest e-value for that gene assignment using the "bit-filter-KOFamScan-results" script from the "bit" package (Lee 2022). Genes assigned the same KO ID are functional orthologs of one another, and thus code for the same function across organisms. High-quality MAGs were also taxonomically annotated using GTDB-tk (Chaumeil et al. 2020).

The number of metagenome reads that mapped to each gene in both the contigs and the high-quality MAGs was determined using featureCounts (Liao et al. 2014), which compares the alignment of the reads against the assembly (i.e., the co-assembled contigs or the MAGs) by BWA-MEM and the predicted genes found by Prodigal. The number of reads mapped to each gene calculated by featureCounts was combined with the functional annotations from KOFamScan via a custom bash script. The featureCounts results were then used to calculate depth of coverage for each gene in R by dividing the number of reads mapped to a gene from a sample by the gene's length. This was done because different genes may be assigned the same KO, and thus their gene length must be taken into consideration. These gene coverages were then divided by the number of days deployed for each sample to account for the variation in dust collector deployment. After

scaling the gene coverages by deployment, these coverages were multiplied by 100 to ensure that the small gene coverages did not skew or interfere with the median of ratios normalization calculation (see below). Because multiple genes were assigned the same KO identifier(s), the scaled coverages for each gene assigned to the same KO were summed together to determine the summed, summed coverage per KO assignment within the contigs and high-quality MAGs respectively. The summed, scaled coverages per KO, per sample were subsequently normalized using the median of ratios normalization with the DESeq2 package in R to account for differences in sequencing depth across libraries (Love et al. 2014, Pereira et al. 2018, Xia 2023). The normalized, summed coverages for the KOs will be referred to as normalized coverage throughout this manuscript.

The median of ratios normalization process calculates the geometric mean by each gene across the samples to create a reference that each raw gene count is divided by, generating a size factor for each sample. Each raw gene count (or coverage in our case) is then divided by this size factor to normalize the data. Because we are working with gene coverages that have been scaled by deployment days rather than raw counts, we decided to scale up the gene coverages by 100. Without this step, the normalization process is less effective due to the size factor value being equal to or larger than the coverage of most of the KOs in the metagenomes.

Surface Type Frequencies & Wind Conditions

Estimates of likely source surfaces associated with PM during each collection period was calculated using hourly back-trajectories from the HYSPLIT dispersion and trajectory model, in combination with observed hourly PM data from nearby EPA surface

stations (Environmental Protection Agency 2024)and the gridded National Land Cover Database (NLCD) data product. For each hour of each collection period, HYSPLIT back trajectory simulations were run originating at multiple heights over each collector site. The resulting back trajectory points near the surface were then categorized based on a simplified set of NLCD surface types, including categories for barren land (i.e., Barren Land STF), crops (i.e., Crop Land STF), developed (i.e., urban; Developed STF), forest (i.e., Forest STF), herbaceous (i.e., Herbaceous STF), ocean (i.e., Ocean Water STF), and shrubs (i.e., Shrubs STF). The Salton Sea itself was also included as a distinct surface type (i.e., Salton Sea STF), representing possible emissions from the surrounding dried lakebed, as well as lake spray aerosol emitted directly from the water surface. Lastly, the "Others STF" category consists of land use types within NLCD that have extremely low frequencies for this region, including: "Hay/Pasture", "Emergent Herbaceous Wetlands", "Woody Wetlands", and "Perennial Snow/Ice". These surface categories were then weighted to account for factors influencing emissions and suspension, including wind speed, surface emissivity, and gravitational settling, as well as by actual hourly PM observed at the nearest long term measurement site. This final data product, including a percent contribution from each surface type for every collection site and period, represents an estimate of likely source surfaces for collected PM, based on atmospheric dynamics and surface properties.

To retrieve publicly available weather data for the areas around our dust collector sites, weather stations were selected based on their proximity to the dust collector sites and the climate data available. Wind climate data from MesoWest/Synoptic weather

stations was retrieved using the "mw" function from the "mesowest" package (Fick 2018). Wind speed, wind direction, air temp, and relative humidity data was collected from the following weather stations: CI200 (nearest to our PD site), UCDE (nearest to our BDC) site, DPMC1 (nearest to our DP site), and CQ125 (nearest to our WI site). Accumulated precipitation data for a 24-hour period was collected from the following weather stations: C2285 (nearest to our PD site), COOPDEEC1 (nearest to our BDC site), COOPMCAC1 (nearest to our DP site), and D3583 (nearest to our WI site). Each variable was measured every hour between our dates of interest. After these data were retrieved for our dates of interest, all variables excluding wind direction were averaged by our dates and times of interest, with each date corresponding to our dust collector deployment dates (with the deployment starting at 12:00pm and collection ending at 5:00pm; Supplemental Table 2). Wind direction was converted into its mathematical direction, then the meridional (north-south, v) and zonal components of the wind vector (east-west, u) were calculated for each site during our dates and times of interest. These wind components were then averaged with the other climate variables included here. Before surface type frequencies and climate data were used for statistical analyses, they were centered (i.e., each value was subtracted by its column mean) and scaled (i.e., dividing the centered values by their standard deviation) using the "scale" function from the "base" R package.

Statistical Analyses and Data Visualization

The 16S rRNA amplicon data, the annotated contigs and MAGs, the surface type frequencies, and the wind conditions (i.e., average 24-hour accumulated precipitation,

average wind speed, average relative humidity, average wind direction) were analyzed in the RStudio environment using R software version 4.2.2. All climate variables considered were centered and scaled via the "scale" function from "base" package in R before statistical analyses were performed. Correlations between the climate variables were compared using the "cor.test" function from the "stats" package and visualized using the "corrplot.mixed" function from the "corrplot" package (Wei and Simko 2021, R Core Team 2024). To determine if dust collector sites significantly varied by their climate conditions, the scaled surface type frequencies and wind condition data were log transformed, and the homogeneity of variance across sites were compared respectively using the "betadisper" function from the "vegan" package (Oksanen et al. 2020). Permutational multivariate analyses of variance (PERMANOVA) were performed with the "adonis2" function from the "vegan" package. All p-values for the PERMANOVAs were adjusted using the Bonferroni correction via the "p.adjust" function from the "stats" package. Additionally, specific site differences were explored using the "pairwise.adonis" function with 999 permutations from the "pairwiseAdonis" package (Martinez Arbizu 2017).

Scaled, decontaminated 16S V3-V4 rRNA amplicon counts were rarefied to a sequencing depth of 295 via rarefaction using the "rrarefy" function from the "vegan" package. The sequencing depth used for rarefaction was the minimum number of total ASV counts observed across the samples, which was identified using the "min" and "rowSums" functions from the "base" package in R. Shannon-Wiener diversity (i.e., alpha diversity) and species richness of the rarefied 16S V3-V4 rRNA amplicon count

data (i.e., microbial composition data) were calculated using repeated rarefaction and averaging. To do this, the ASV counts were rarefied, then the Shannon-Wiener diversity or species richness was calculated using the "diversity" and "specnumber" functions from the "vegan" package, and this result was saved. This process was then repeated 100 times. Then the average of the Shannon-Wiener diversity and species richness measurements were calculated for each sample. Alpha diversity and species richness were checked for normality via Shapiro-Wilks tests using the "shapiro.test" function from the "stats" package. The Shapiro-Wilks test determined that alpha diversity (P = 0.000151) and species richness (P = 0.0002459) were not normally distributed, and thus, analyzing alpha diversity and species richness would require non-parametric statistical tests for this work.

The compositional relative abundance across samples was calculated using the scaled, decontaminated 16S V3-V4 rRNA amplicon counts and the "decostand" function (with "method = `total`") argument from the "vegan" package. The core aeolian dust microbiome was determined using the "core_members" and "plot_core" functions from the "microbiome" package (Shetty S 2019), with a low detection (i.e., relative abundance in a sample) of 0.1% and a high detection threshold of 3%. Only microbial genera that had a minimum detection of 0.1% in at least 50% of the samples were considered members of the core microbiome. The justification for this detection threshold is two-fold: because dust is an extremely low biomass substrate, and because we did not want to exclude potentially rarer, yet widely distributed taxa from this analysis.

A Wilcoxon test was used to compare the mean of alpha diversity and species richness between sites respectively using the “wilcox.test” function from the “stats” package, and p-values were adjusted using the Bonferroni correction via the “p.adjust” function from the “stats” package. Additionally, a Kruskal-Wallis test was used to compare variance of alpha diversity and species richness between sites using the “kruskal.test” function from the “stats” package. After the Kruskal-Wallis, a Dunn test was used via the “dunn_test” function from the “rstatix” package to determine which sites’ variances were significantly different from one another (Kassambara 2021). To then compare the homogeneity of variances across sites, a Fligner-Killeen test using the “fligner.test” function from the “stats” package was performed.

Beta diversity of the microbial composition data was performed by first transforming the data via a center-log ratio (i.e., CLR) transformation using the “decostand” function (with “method = `clr`”) from the “vegan” package. This function adds a pseudocount of 1 to all function counts, including those functions that have a count of zero, before performing the transformation. Then a Euclidean distance matrix of the CLR-transformed 16S V3-V4 amplicon count data was created using the “dist” function from the “vegan” package to calculate Aitchison distance, which was used as input to create a Principal Coordinates Analysis (i.e., PCoA) with the “pcoa” function from the “vegan” package. To determine how these samples cluster together, K-means clustering was performed using the “eclust” function from the “factoextra” package (Kassambara and Mundt 2020). The gap statistic was calculated using the “fviz_gap_stat” and “fviz_nbclust” functions from the “factoextra” package to determine the ideal

number of clusters (i.e., value for k). SSU-Align (Nawrocki 2009)was used to create a multiple sequence alignment of the 16S V3-V4 rRNA sequences assigned to each ASV, and FastTree (Price et al. 2010)was used to build a phylogenetic tree for this specific locus. This phylogenetic tree and the CLR-transformed ASV counts were used to calculate the weighted and unweighted Unifrac distances of these samples using the "beta.div" function from the "rbiom" package.

Homogeneity of variance in the microbial composition data across sites were compared using the "betadisper" function from the "vegan" package. This was done using the Aitchison distance as input. Permutational multivariate analyses of variance (PERMANOVA) were performed with the "adonis2" function from the "vegan" package (with 10,000 permutations) to determine if there were significant differences in microbial composition across sites and depths. All p-values for the PERMANOVAs were adjusted using the Bonferroni correction via the "p.adjust" function from the "stats" package. Significant differences in microbial composition between specific sites was explored using the "pairwise.adonis" function from the "pairwiseAdonis" package using 9,999 permutations.

A Detrended Correspondence Analysis (i.e., DCA) was performed using the "decorana" function from the "vegan" package to determine if there was an arch effect present within the microbial composition data across sites and within sites. Due to the length of the first DCA axes, Redundancy Analysis (i.e., RDA) was chosen to determine if and how the microbial composition data are constrained by the climate data. RDAs were calculated using the "rda" function from the "vegan" package. The variation

explained by the RDAs was obtained using the "RsquareAdj" function from the "vegan" package, and the significance of the RDAs was determined using the "anova" function from the "stats" package. The variance inflation factors for each predictor variable (i.e., the climate data) in the RDAs was determined using the "vif.cca" function from the "vegan" package. To find the best fitting model, the "ordistep" and "ordiR2step" functions from the "vegan" package were used. The "ordistep" function builds the RDA stepwise to determine which variables lead to significant changes in variance and a lower AIC value for the model. The "ordiR2step" function builds the RDA stepwise based on which variables maximize the adjusted variation explained by each predictor variable considered (i.e., their adjusted R^2) and are statistically significant. To determine the contributed variation for each variable in the RDAs, variance partitioning was performed using the "varpart" function from the "vegan" package.

Generalized linear models (i.e., GLMs) were used to determine which climate variables (i.e., wind data and surface type frequencies) were significant predictors of specific functions of interest (i.e., KOs) found in the contigs from the metagenomes. Functions of interest were first chosen based on their involvement in dust microbial survival according to previous literature. Of these functions, KOs were selected for these models based on their scaled coverage (i.e., after median of ratios normalization) across the metagenomes, specifically choosing KOs that exhibited higher mean scaled coverage across the metagenomes. A Shapiro-Wilks test was used to see if these KOs were normally distributed across the metagenomes. For functions that were normally distributed, a linear regression was run using the "lm" function from the "stats" package,

where the y variable was the scaled coverage for a specific KO and the x variable was a specific climate variable. For functions that were not normally distributed, generalized linear models were run using the "glm" function from the "stats" package using the Poisson distribution or a negative binomial distribution, where the y variable was the scaled coverage for a specific KO and the x variable was a specific climate variable. To determine the appropriate distribution for the non-normal dependent variables, a likelihood ratio test was performed using the lrtest() function from the lmtest package (Zeileis and Hothorn 2002) and the Aikaike's 'An Information Criterion' (i.e., AIC) was calculated using the AIC() function from the stats package. Models with higher log likelihoods and smaller AIC values were then chosen as the best fit model for a particular formula. Significant predictors were identified by first iterating these GLMs in a stepwise fashion to identify which climate variables could be significant predictors of the distribution of these KO scaled coverages using the "step" function from the "stats" package. The "step" function runs these GLMs repeatedly, removing insignificant variables with every iteration, to determine which model has the lowest AIC. Based on the output of the stepwise GLM, the final GLMs were adjusted to only include significant climate predictors. After the final model for each function of interest was constructed, a Quantile-Quantile (i.e., Q-Q) plot of the models' residuals was generated with the qqnorm() and qqline() functions from the stats package to assess their distribution. Additionally, the McFadden's Pseudo R^2 value for the negative binomial GLMs, as well as the GLMs using the Poisson distribution, was calculated to determine the variation explained by these models.

Results

Surface Type Frequencies and Wind Conditions by Site

A PERMANVOA of the surface type frequencies and wind conditions showed that these conditions significantly varied by site, respectively (P = 0.003, P = 0.0003), while the dispersion of these data did not significantly vary (P = 0.704, P = 0.963). This indicates that these climate conditions were significantly different, and this difference cannot be attributed to the dispersion of these data by site alone. Further investigation into the differences in STFs between specific sites found that BDC and DP (P = 0.006), BDC and WI (P = 0.006), PD and DP (P = 0.006), and PD and WI (P = 0.006) varied significantly in their STFs. BDC and PD (P = 1) and DP and WI (P = 0.939) did not significantly vary from each other based on their STFs. All the sites significantly differed from each other based on their respective wind conditions. BDC and DP (P = 0.005), BDC and PD (P = 0.006), BDC and WI (P = 0.022), DP and PD (P = 0.002), DP and WI (P = 0.004), and PD and WI (P = 0.018) also varied significantly by their wind conditions.

Microbial Composition

Of the 54,118 ASVs identified, 3,306 bacterial and archaea genera were classified in our 28 samples. The fraction of Archaea identified in the samples were extremely low, with Archaea only being found in 10 of the 28 samples. The highest relative abundance of Archaea was found in the WI.D.11.5.20 sample, with a relative abundance of 0.175%. The bacterial phylum Proteobacteria was the most relatively abundant across all the samples, followed by Firmicutes, Bacteroidota, and Actinobacteriota (Supplemental

Figure 1). The bacterial order Burkholderiales was a major order (i.e., had a relative abundance of at least 5%) in all 28 samples. Bacterial genera and species that had a relative abundance of at least 10% in at least one sample include the following: *Acinetobacter baumannii, Rhizobium unknown, Azohydromonas unknown, Bacillus funiculus, Brevundimonas unknown, Burkholderia unknown, Candidatus Soleaferrea unknown, Desulfovibrio cuneatus, Dyadobacter unknown, Hymenobacter unknown, Massilia unknown, Nibribacter unknown, Paenibacillus alvei, Panibacillus borealis, Pseudomonas lutea, Pseudomonas unknown, Ramibacter unknown, Ramlibacter unknown, Roboutsia ilealis, Rosenbergiella unknown, Spirosoma rigui, Variovorax paradoxus,* and *Zymobacter palmae.*

A core aeolian dust microbiome was identified by examining which bacterial genera were detected across all samples (i.e., prevalence) at various relative abundances. These analyses revealed 13 bacterial genera that had a relative abundance of at least 0.1% across over 50% of the samples. From most to least abundant, these genera include: *Massilia, Sphingomonas, Planomicrobium, Hymenobacter, Planococcus, Nibribacter, Devosia*, *Rhizobium*, *Pseudomonas, Novosphingobium, Roseomonas*, *Kocuria,* and *Paracoccus,* which we have determined to be members of the core microbiome (Figure 1). Only two taxa, *Kocuria rosea* and *Paracoccus marcusii,* were identified in this analysis at the species level. These 13 genera were found in 61% of the samples at a minimum of 0.1% the samples' relative abundances. Major genera (i.e., genera with a relative abundance of at least 10% in one or more samples) that were identified in the core aeolian microbiome include *Massilia, Hymenobacter, Nibribacter, Rhizobium,* and

Pseudomonas. *Massilia* species were the most abundant bacteria at the genus level, and this genus represents one or more species that are member(s) of the core microbiome, with 64% of the samples containing *Massilia* taxa with a relative abundance of at least 3%. *Sphingomonas* was the only other genus to be observed at a relative abundance of at least 3% in 32% of the samples. The remaining 11 genera that were members of the core microbiome had a relative abundance of at least 1% in 4 – 29% of the samples.

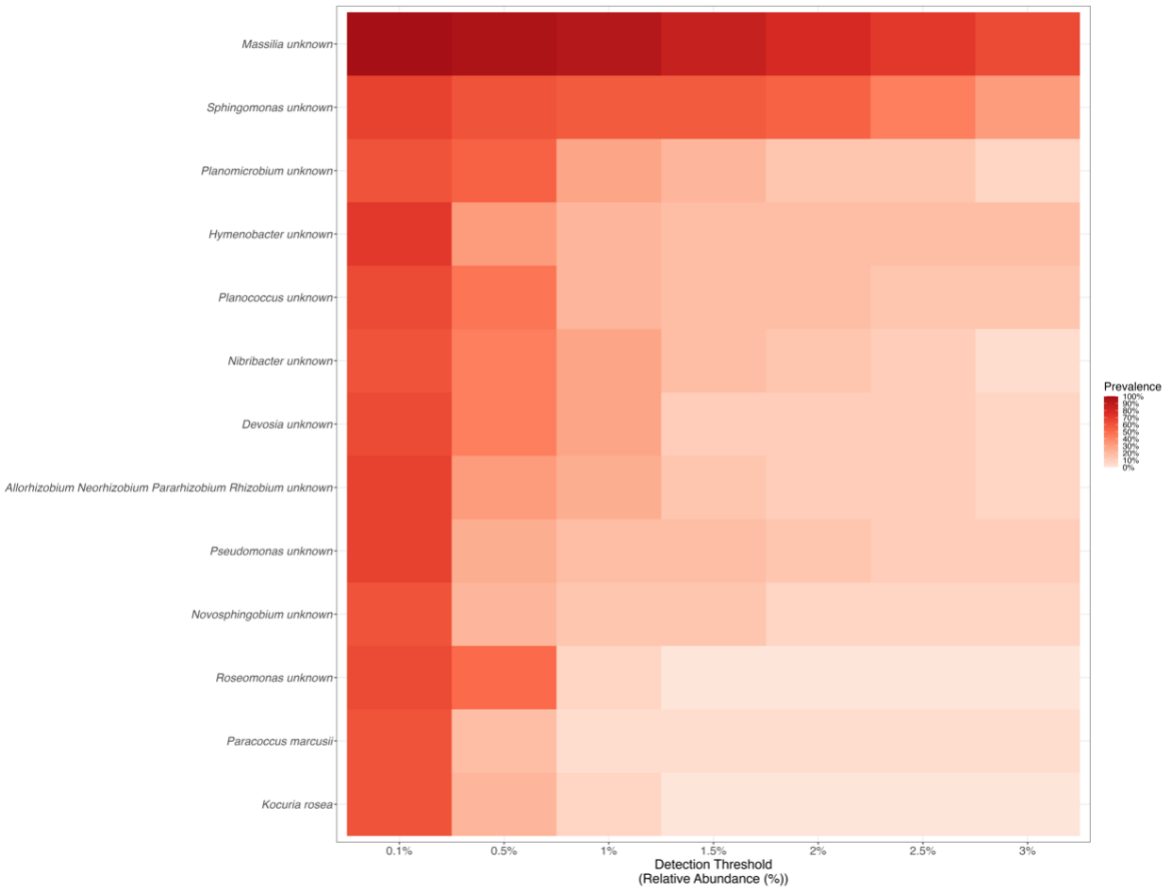

Figure 1. The Core Aeolian Dust Microbiome. This heatmap contains the 13 bacteria genera that compose the core aeolian dust microbiome in Salton Sea dust. The x-axis shows the detection threshold, which represents the relative abundance across all samples. The shade of red corresponds to the prevalence which describes how many samples contain each taxa.

Alpha Diversity and Species Richness

Shannon-Wiener diversity and species richness did not significantly vary by site ($P = 0.749$, $P = 0.658$). This appears to be because of the within-sample variance exhibited in both alpha diversity and species richness across the sites (Supplemental Figures 2 and 3). Alpha diversity and species richness did not significantly correlate with any of the surface type frequencies and wind condition data collected.

Microbial Beta Diversity and its Environmental Drivers

Microbial composition significantly varied between the four sites ($R^2 = 0.144$, $P = 0.0463$) and the dispersion across sites was homogenous ($P = 0.342$). A principal coordinates analysis (PCoA; Figure 2) and K-means clustering revealed that the microbial composition forms three distinct clusters in these data. The first axis of variation in the PCoA (i.e., PC1) had a relative eigenvalue of 24.47%, indicating that this axis explained 24.47% of the total variation in microbial composition across the samples. The second axis of variation (i.e., PC2) had a relative eigenvalue of 8.31%, indicating that this axis explained 8.31% of the total variation in microbial composition. While a PERMANOVA found that these four sites were significantly different in their microbial composition, a pairwise PERMANOVA found that the sites were not significantly different from one another (Supplemental Table 7). PD and WI ($R^2 = 0.121$, $P = 0.068$) and PD and DP ($R^2 = 0.113$, $P = 0.0904$) exhibited differences in microbial composition that were near significant. A PERMANOVA also revealed that beta diversity did not significantly differ between samples collected after rain events compared to samples collected during dry periods ($P = 0.844$).

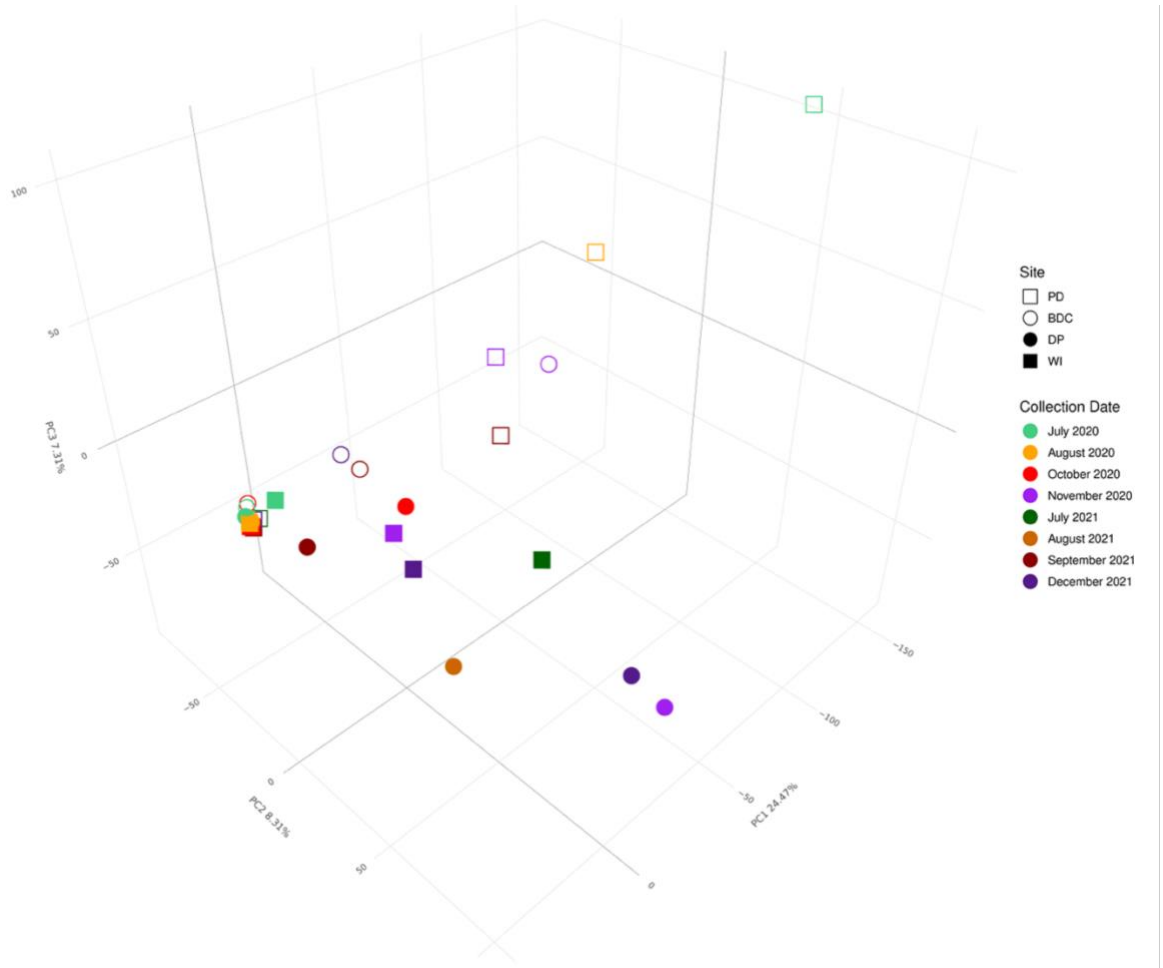

Figure 2. Principal Coordinates Analysis of Microbial Composition. This is a Principal Coordinates Analysis (i.e., PCoA) of microbial composition from the 16S V3-V4 rRNA amplicon sequence data. Each sample is represented by a point, where the shape corresponds to the collection site and the color is the collection date of that sample.

A redundancy analysis (i.e., RDA) of our samples found that the Developed STF (Adj $R^2 = 0.058$, $P = 0.0012$), the average wind speed (Adj $R^2 = 0.02$, $P = 0.01$), and the average 24-hour accumulated precipitation (Adj $R^2 = 0.043$, $P = 0.033$; Figure 3) were significant drivers of microbial composition across sites (Adj $R^2 = 0.121$, $P = 0.0002$; Supplemental Table 8). Yet, these environmental variables were not necessarily

significant drivers of microbial composition within each site. Microbial composition within the WI samples across time points was driven by average relative humidity (Adj $R^2 = 0.211$, $P = 0.02$) and u, the zonal (east-west) component of local winds (Adj $R^2 = 0.17$, $P = 0.02$). The microbial composition within DP samples were significantly driven by both average 24-hour accumulated precipitation (Adj $R^2 = 0.179$, $P = 0.013$) and the Barren Land STF (Adj $R^2 = 0.094$, $P = 0.034$). Across the PD samples, average 24-hour accumulated precipitation (Adj $R^2 = 0.29$, $P = 0.002$) and average wind speed (Adj $R^2 = 0.22$, $P = 0.012$) were significant environmental drivers of microbial composition. Lastly, average 24-hr accumulated precipitation (Adj $R^2 = 0.102$, $P = 0.045$) and v, the meridional (north-south) component of local winds (Adj $R^2 = 0.038$, $P = 0.3$), were significant environmental drivers of microbial composition in the BDC site across time points. While an ANOVA found the north-south wind component to be insignificant, the ordistep() function identified this variable as significant ($P = 0.022$).

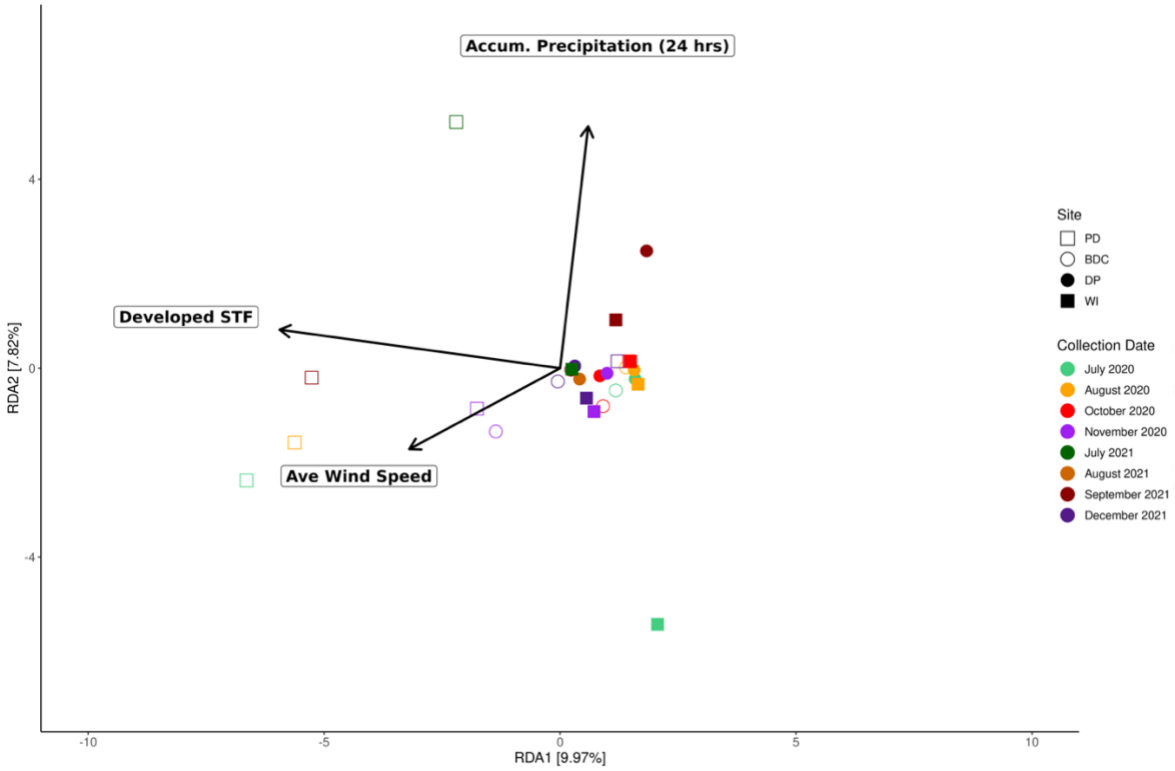

Figure 3. Environmental Drivers of Beta Diversity. This redundancy analysis displays the significant environmental drivers of microbial composition across sites: the Developed STF (Adj R^2 = 0.058, P = 0.0012), average wind speed (Adj R^2 = 0.02, P = 0.01), and the average 24-hour accumulated precipitation (Adj R^2 = 0.043, P = 0.033).

Metagenome Sequence Processing

2,130,808,324 reads were produced from the 24 shotgun metagenomes sequenced. After trimming with BBduk, 2,130,495,120 reads were used for contig assembly and genome binning. MEGAHIT yielded 4,947,761 co-assembled contigs. After mapping the trimmed reads to the co-assembled contigs, genome binning produced a total of 730 bins across the 24 metagenomes. A total of 1,059,642,227 reads from the 24 metagenomes were mapped to predicted genes identified in the co-assembled contigs. Of the 730 bins, 101 bins were considered high quality and used for taxonomic and

functional annotation. The average genome completeness across the 101 bins was 93.81%, and the average contamination in the bins was 1.29%.

Functions of Interest and their Depth of Coverage in the Co-Assembled Contigs

A total of 3,569,088 genes were identified by Prodigal, but not all genes were assigned corresponding KO IDs. After dropping genes that did not receive KO assignments, there was a total of 1,249,948 genes used to calculate the scaled gene coverages. The average number of reads mapped to all the genes was 20. The mean coverage (i.e., after dividing the number of reads per gene by the gene's length) was 0.0254 per gene, and the mean coverage scaled by deployment (i.e., after dividing the gene coverage by the number of deployment days) was 0.00057. After scaling up the coverage by deployment (i.e., multiplying the coverages-by-deployment by 100), the mean scaled coverage was 0.057.

12,012 KO ID assignments were given to the 1,249,948 genes found across the contigs. After dropping KOs with low scaled, summed coverage (i.e., KOs with a scaled coverage of <= 3), 8,777 KOs from genes in the contigs were normalized via median of ratios normalization and used for statistical analyses. Before normalization, the mean normalized, summed coverage per KO was 5.94. Normalized, summed gene coverages of KOs previously identified in aeolian dust microbiomes were used to determine if there is a core, aeolian dust microbiome at the functional level (DasSarma and DasSarma 2018, Aalismail et al. 2019). For simplicity, the normalized, summed coverages per KO ID will be referred to as "normalized coverage" for the remainder of this manuscript.

Genes assigned to KOs involved in endospore formation, UV-damaged DNA repair, the temperature shock response, osmoprotectant transport and accumulation, lipopolysaccharide (LPS) synthesis and modification, and quorum sensing were found in all 24 metagenomes. As for genes involved in forming endospores, four of the 38 sporulation genes (i., the spore maturation protein A - *spmA*; site-specific DNA recombinase - *spoIVCA*, stage V sporulation protein K - *spoVK*, and stage V sporulation protein R - *spoVR*) were found in all 24 metagenomes while the remaining sporulation genes included in this work were absent. Only three of the metagenomes contained 35 of the 38 endospore formation genes examined in this study: PD.D.7.27.21, BDC.D.7.27.21, and WI.D.9.18.21.

UV-damaged DNA repair genes were also found in all 24 metagenomes, though their normalized coverages were not evenly distributed. Excinuclease subunits ABC (i.e, *uvrA*, *uvrB*, *uvrC*) were at found at higher coverages than the repressor LexA (i.e., *lexA*) and DNA polymerase V (i.e., *umuC*, *umuD*) across the metagenomes. Only one metagenome (PD.D.12.8.21) did not contain *umuC* and *umuD* but did contain the other UV-damaged DNA repair genes of interest. Due to the presence and distribution of these genes in the metagenomes, a PERMANOVA was calculated to determine if these genes significantly varied in their normalized coverages by site and collection date. The PERMANOVA found that the normalized coverages of the UV-damaged DNA repair genes in the metagenomes did not significantly vary by site ($P = 0.646$) or collection date ($P = 0.350$).

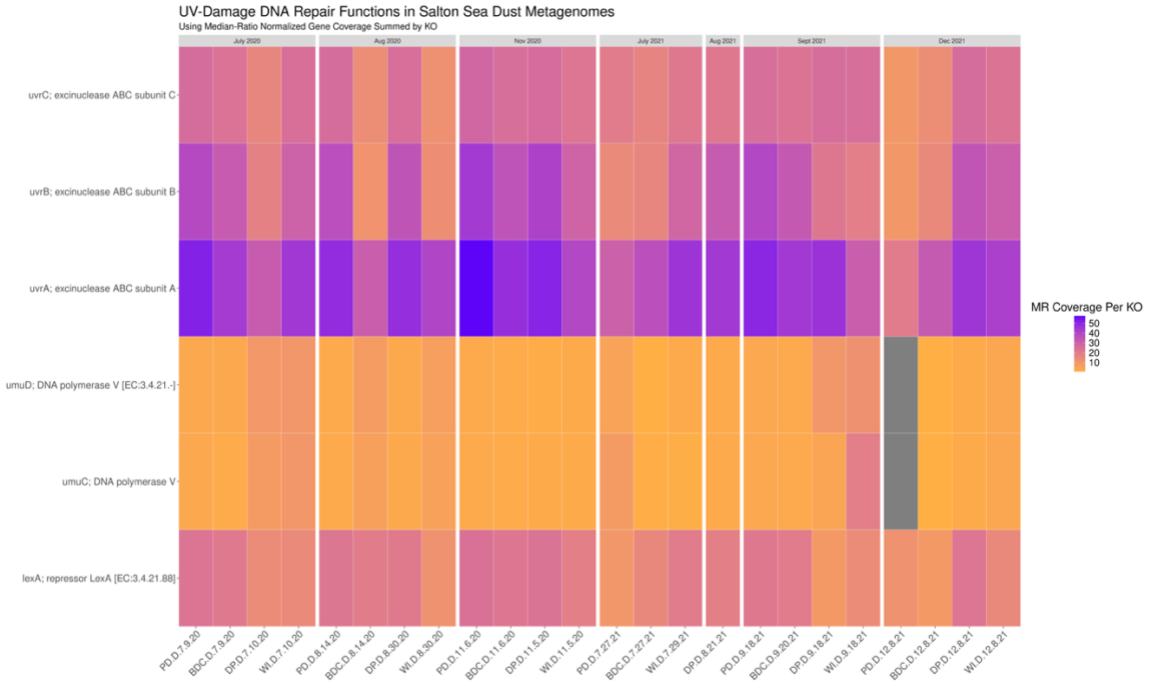

Figure 4. Heatmap of UV Radiation Resistance in Aeolian Dust Metagenomes. This heatmap shows the normalized coverage of KO IDs involved in repairing UV-damaged DNA across the metagenomes. Each column is a metagenome (i.e., one sample), and the metagenomes are organized by their collection dates from July 2020 to December 2021.

Genes involved in regulating heat and cold shock responses were found in all 24 metagenomes. Heat shock proteins HtpX (i.e., *htpX*), 12.6 (i.e., *HSP12.6*), and ribosome-associated Hsp15 (i.e., *hsIR*) were found across the metagenomes. Additionally, the cold shock protein (i.e., *cspA*) was found in every metagenome at twice the normalized coverage of the other temperature shock-related proteins examined in this work. The mean normalized coverage of *cspA* was 83.37. Other temperature shock-related genes found in the metagenomes include heat shock protein HspR (i.e., *hspR*), heat shock protein HsQ (i.e., *hspQ*), and a transcriptional regulator of stress and heat shock response known as *ctsR*. The heat shock 70kDa protein known as *HSPA1s* was only found in one metagenome (WI.D.11.5.20). To determine if these genes significantly varied in their

normalized coverages by site and collection date, a PERMANOVA was calculated. The PERMANOVA revealed that the normalized coverages of the temperature shock response genes did not significantly differ by site (P = 0.840) or by collection date (P = 0.637).

Osmoprotectant transport and accumulation genes were also shared across the 24 metagenomes. The hyperosmotically inducible periplasmic protein (i.e., *osmY*), osmotically inducible lipoprotein OsmB (i.e., *osmB*), osmoprotectant transport system substrate-binding protein (i.e., *opuC*), osmoprotectant transport system permease protein (i.e., opuBD), osmoprotectant transport system ATP-binding protein (i.e., *opuA*), and the osmolarity sensor histidine kinase of the OmpR family EnvZ (i.e., *envZ*) were found in all the metagenomes. The osmotically inducible lipoprotein OsmE (i.e., *osmE*) was found in only two of the 24 metagenomes (WI.D.9.18.21, BDC.D.12.8.21) and the SHO1 osmosensor (i.e., *SHO1*) gene was found in four of the 24 metagenomes (BDC.D.7.9.20, DP.D.11.5.20, WI.D.11.5.20, and DP.D.8.21.21). Due to the distribution of most of the osmoprotectant transport/accumulation genes in the metagenomes, a PERMANOVA was calculated to determine if these genes were significantly different in their normalized coverages by site and collection date. This PERMANOVA revealed that the normalized coverages of the osmoprotectant transport/accumulation genes found did not significantly differ by site (P = 0.831) or by collection date (P = 0.296).

LPS synthesis and modification genes were widely distributed across the metagenomes. All genes that are involved in constructing or modifying various segments of LPS considered here were found in at least one of the 24 metagenomes. Most of the

genes that contribute to building or modifying the core region and the lipid A portion of LPS were found in at least 12 of the 24 metagenomes. However, one gene involved in the LPS core region synthesis/modification (i.e., UDP-glucose:(glucosyl)LPS beta-1,3-glucosyltransferase (i.e., *waaV*) was found only in the PD.D.7.27.21 metagenome, and the heptosyltransferase (i.e., *opsX*) was found in three metagenomes (BDC.D.7.9.20, BDC.D.9.20.21, and DP.D.12.8.21). Additionally, two genes involved in lipid A synthesis and modification were also only found in 2-3 metagenomes. Genes involved in constructing or modifying the O-antigen repeat unit within the LPS were widely distributed across the metagenomes, with two genes exhibiting the highest normalized coverages of the LPS genes considered: the UDP-GalNac:undecaprenyl-phosphate GalNac-1-phsophate transferase (i.e., *wecP*) and the O55-antigen biosynthesis glycosyltransferase (i.e., *wbgP*). Conversely, a few O-antigen repeat unit synthesis/modification genes were found in only 2-3 metagenomes: undecaprenyl-phosphate galacotse phosphotransferase (i.e., *rfbP*; in DP.D.7.10.20 and WI.D.8.30.20), O-antigen biosynthesis alpha-1,3-rhamnosyltransferase (i.e., rfbN/wbaV; in BDC.D.7.9.20, DP.D.7.10.20, and BDC.D.8.14.20), and rhamnosyltransferase (i.e., rfbG; in DP.D.7.10.20, BDC.D.8.14.20, and BDC.D.12.8.21).

Genes involved in various types of quorum sensing were also found in the metagenomes, though only one gene was shared across all 24 metagenomes: the LuxR family transcriptional regulator/ quorum-sensing system regulator BisR (i.e., *bisR*). Other genes in the LuxI/LuxR acyl-homoserine lactone (i.e., AHL) quorum sensing system that were identified in the metagenomes include the LuxR family transcriptional

regulator/quorum-sensing system regulators BjaR1 (i.e., *bjaR1*, 12 of 24 metagenomes), LasR (i.e., *lasR*, 20 of 24 metagenomes), and SolR (i.e., *solR*, 16 of 24 metagenomes). The HTH-type transcriptional regulator/major conjugation operon repressor known as *prgX*, which is involved in the Rap/NprR/PlcR/PrgX (i.e., RNPP) pathway, was found in 20 of the 24 metagenomes. Of the quorum sensing genes considered, *bisR* had the highest normalized coverage, exhibiting a mean normalized coverage of 68.24.

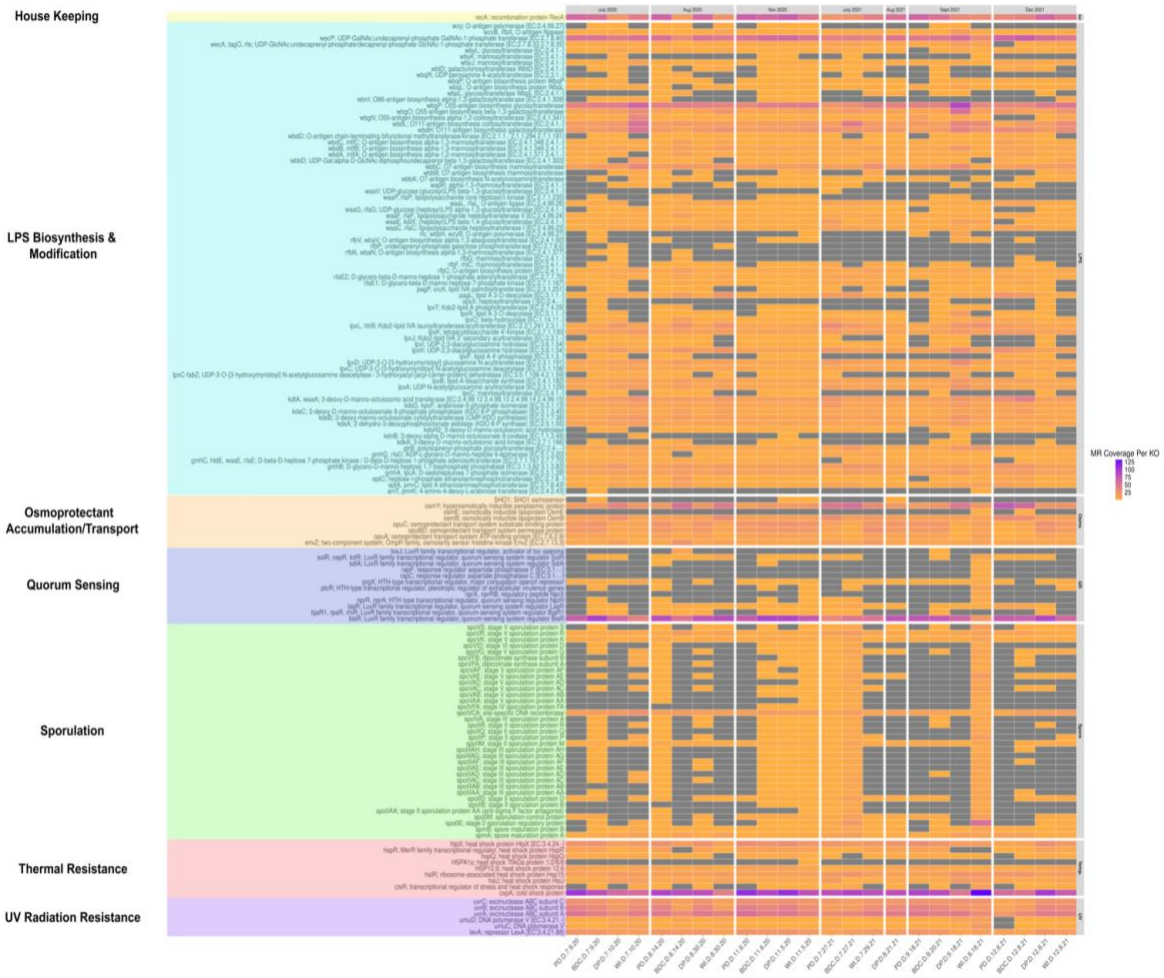

Figure 5. Heatmap of Functions of Interest in Aeolian Dust Metagenomes. This heatmap shows the normalized coverage of KO IDs of interest identified in the metagenomes. The genes are grouped by functions in this order: housekeeping gene (i.e., HK), LPS biosynthesis/modification genes (i.e., LPS), osmoprotectant transport/accumulation (i.e., Osmo), quorum sensing genes (i.e., QS), sporulation genes (i.e., Spore), temperature shock response genes (i.e., TS), and UV-damaged DNA repair genes (i.e., UV).

Surface Type Frequencies and Wind Conditions as Predictors of Dust Microbiome Function

After identifying the core aeolian microbiome functions of interest in the metagenomes, certain KOs were selected for generalized linear models based on their normalized coverages compared to other KOs in their adaptation category (Supplemental

Table 9). The KOs chosen had the highest mean normalized coverage within their respective categories across the metagenomes. *spoIVCA* and *spmA* represented sporulation genes, *lexA, uvrA, uvrB,* and *uvrC* represented the genes responsible for UV-damaged DNA repair, *cspA* and *htpX* represented the temperature shock response genes, *osmY* and *opuC* represented genes involved in osmoprotectant transport and accumulation, *wecP* and *wbgP* represented genes involved in LPS modification and synthesis (of the O-antigen repeat unit), and *bisR* and *prgX* represented genes involved in quorum sensing pathways.

spoIVCA was significantly predicted by average 24-hour accumulated precipitation ($P = 0.013$), average relative humidity ($P = 0.016$), and an interaction between these two predictors was near significant (Adj $R^2 = 0.375$, $P = 0.068$). *spmA* was also significantly predicted by average 24-hour accumulated precipitation ($P = 0.0009$), near significantly predicted by the meridional (north-south) component of local winds, v ($P = 0.089$), and significantly predicted by the interaction between these variables (McFadden's pseudo $R^2 = 0.333$, $P = 0.023$).

lexA was significantly, solely predicted by the meridional (north-south) component (v; McFadden's pseudo $R^2 = 0.179$, $P = 0.016$). *uvrA*, *uvrB*, and *uvrC* shared the same environmental predictors, though their relationships with these predictors were not identical. *uvrA* was significantly predicted by the meridional (north-south) component (v; $P = 0.038$) and the OpenWater STF ($P = 0.019$), and the overall model was also significant (Adj $R^2 = 0.239$, $P = 0.022$). *uvrB* was also significantly predicted by both the meridional (north-south) component (v; $P = 0.01$) and the OpenWater STF ($P = 0.032$),

and the model was significant (Adj R^2 = 0.278, P = 0.013). Lastly, *uvrC* was also significantly predicted by the meridional (north-south) component (v; P = 0.022) and the OpenWater STF (P = 0.006; McFadden's Pseudo R^2 = 0.327).

cspA was significantly predicted by the meridional (north-south) component alone (v; Adj R^2 = 0.145, P = 0.038; Figure 5). *htpX* was significantly predicted by the Barren Land (P = 0.0008) and the Open Water STFs (P = 0.001), and the overall model was significant (Adj R^2 = 0.402, P = 0.002).

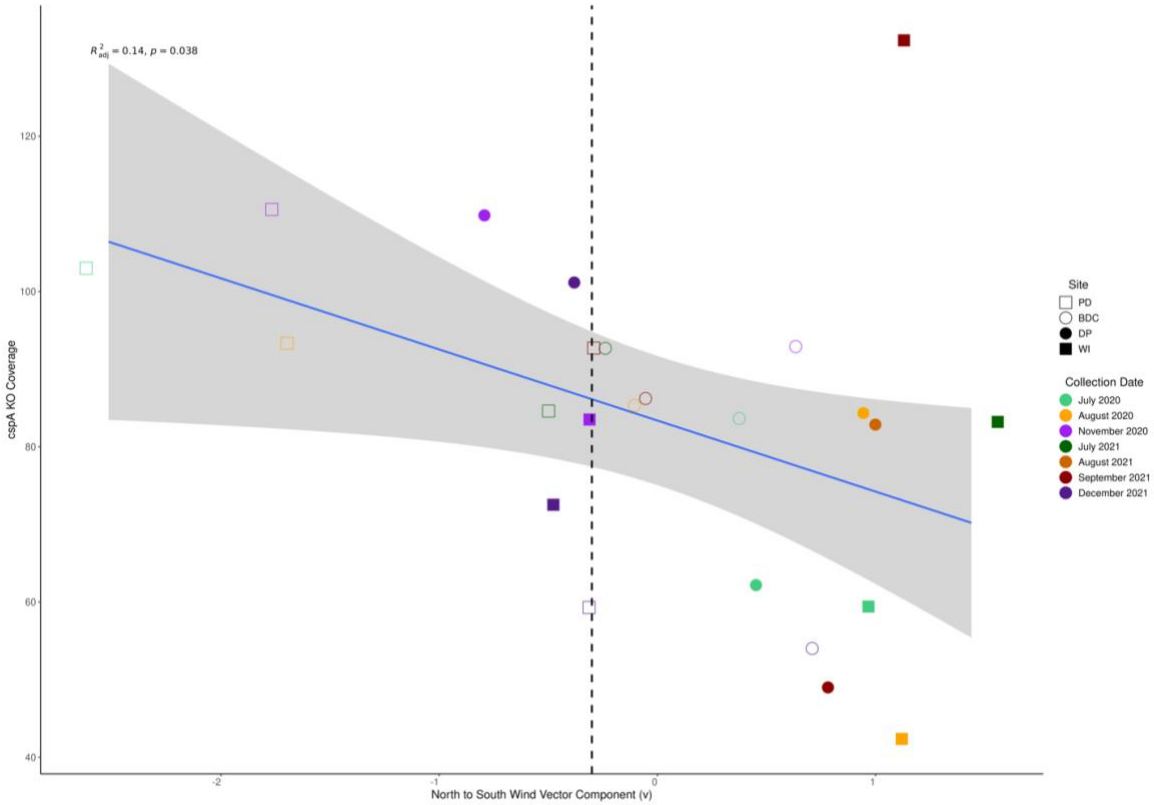

Figure 6. Meridional Wind Component (v) Predicts *cspA* in Dust Metagenomes. This scatterplot shows how the meridional component (v) of local winds significantly predicts the normalized coverage of the cold shock protein *cspA*. Most points to the left of the dashed line include samples that received northerly winds, and points to the right of the dashed line include samples that received southerly winds.

osmY was significantly predicted by average 24-hour accumulated precipitation (P = 5.49e-7), average wind speed (P = 0.0005), and the meridional (north-south) component (v; P = 0.012; McFadden's Pseudo R^2 = 0.21). *opuC* was significantly predicted by average 24-hour accumulated precipitation (P = 0.001), and an interaction between average 24-hour accumulated precipitation and average wind speed (P = 0.017, McFadden's Pseudo R^2 = 0.336). However, average wind speed alone was not a significant predictor of *opuC* (P = 0.133).

wecP was significantly predicted by average air temperature (P = 0.016) and the zonal (east-west) component of local winds (u) (P = 0.016), and the overall model was significant (Adj R^2 = 0.442, P = 0.00084). *wbgP* was significantly predicted by the Salton Sea (P = 1.29e-8) and Shrub STFs (P = 0.00018), as well as the interaction between these two predictors (McFadden's Pseudo R^2 = 0.327, P = 6.41e-5).

bisR was significantly predicted by average 24-hour accumulated precipitation (P = 0.013) and the Crop Land STF (P = 0.024), and the overall model was significant (Adj R^2 = 0.441, P = 0.0009). *prgX* is significantly predicted by the average wind speed (P = 0.0002) and the Developed STF (P = 0.039; McFadden's Pseudo R^2 = 0.334).

Taxonomic Annotation of the Metagenome-Assembled Genomes (MAGs)

The 101 high-quality MAGs were assigned to the Bacteria domain and to the following phyla: Proteobacteria (n = 44), Firmicutes (n = 27), Actinobacteriota (n = 19), Bacteroidota (n = 7), Spirochaetota (n = 3), and Desulfobacterota (n = 1). The Proteobacteria MAGs were assigned to the Gammaproteobacteria (n = 30) and Alphaproteobacteria (n = 14) classes. Firmicutes MAGs were assigned to the Bacilli (n =

25) and Clostridia (n = 2) classes. All 19 Actinobacteriota MAGs were assigned to the Actinomycetia class, and all 7 Bacteroidota MAGs were assigned to the Bacteroidia class. The 3 Spirochaeota MAGs were all assigned the same identity (i.e., Spirochaetia class, Borreliales order, and Borreliaceae family), but were not classified beyond the family level. Lastly, the MAG within the Desulfobacterota was assigned to the genus Frigididesulfovibrio (i.e., Desulfovibrionia class, Desulfovibrionales order, Desulfovibrionaceae family).

88 of the 101 MAGs were identified at the genus level, and 37 MAGs were identified at the species level (Supplemental Table 5). The 37 MAGs identified at the species level include the following taxa: *Corynebacterium sp012838715* (n = 12), *Salinicoccus roseus* (n = 11), *Acinetobacter baumannii* (n = 2), *Bartonella sp016102265* (n = 2), *Priestia megaterium* (n = 2), *Brevundimonas vesicularis* (n = 1), *Cereibacter changlensis* (n = 1),*Curtobacterium sp001705035* (n = 1), *Cutibacterium acnes* (n = 1), *Enterobacter kobei* (n = 1), *Exiguobacterium acetylicum* (n = 1), *Gilliamella apicola* (n = 1), and *Pseudarthrobacter phenanthrenivorans* (n = 1).

Functions of Interest and their Depth of Coverage in the Metagenome-Assembled Genomes (MAGs)

As was done with the co-assembled contigs, genes assigned to KOs previously identified in aeolian dust microbiomes were also identified in the MAGs. Genes assigned to KOs involved in UV-damaged DNA repair, the temperature shock response, osmoprotectant transport and accumulation, lipopolysaccharide (LPS) synthesis and modification, and quorum sensing were found in 95 of the 101 MAGs (Supplemental

Figure 4). Certain functions of interest were more widely distributed than others across the MAGs. 88 of the 95 MAGs contained the *cspA* gene, and 25 of the 95 MAGs had a normalized coverage greater than or equal to three for *cspA.* These bins were assigned to both Gram-negative and Gram-positive bacteria and were isolated from all four sites. In addition to *cspA*, other temperature shock genes shared across the MAGS included *hsIR* (i.e., a gene that codes for the ribosome-associated heat shock protein Hsp15) in 67 MAGs and *htpX* in 39 of the MAGs. As for genes involved in UV-damaged DNA repair, 87 of the 95 MAGs contained the *uvrC* gene, 85 of the 95 MAGs contained the *uvrB* gene, and 83 of the 95 MAGs contained the *uvrA* gene (Supplemental Figures 4, 5). Genes involved in osmoprotectant transport and accumulation were shared across the metagenomes as well, with 35 MAGs containing *opuC* and 28 MAGs containing *osmY*. 12 of the 95 MAGs contained at least 18 of the 35 sporulation genes examined in this study. LPS development genes included *wbgP* in 51 MAGs, *gtrB* (i.e., polyisoprenyl-phosphate glycosyltransferase; involved in O-antigen modification) in 43 MAGs, *wecP* in 41 MAGs, and *lpxD* (i.e., UDP-3-O-[3-hydroxymyristoyl] glucosamine N-acyltransferase; involved in Lipid A synthesis) in 41 MAGs. Lastly, while most of the quorum sensing genes and sporulation genes considered here were not widely distributed across the MAGs as other functions of interest, *bisR* was found in 53 of the MAGs, *spoVR* (i.e., codes for the stage V sporulation protein R) was found in 25 MAGs, and *spmA* was found in 24 MAGs.

It should be noted that not all the functions of interest investigated here were identified in these 95 MAGs (Supplemental Figure 4). Only 82 of the 161 genes involved

in LPS biosynthesis and modification were found across the 95 MAGs. 35 of the 38 sporulation genes considered here were shared across the MAGs, and 11 of the 37 genes considered that are involved in various quorum sensing pathways were found in our MAGs. Eight of the 29 genes considered that are involved in the bacterial temperate shock response and seven of the 11 genes involved in osmoprotectant transport/accumulation were found in our high-quality MAGs. Conversely, all six genes examined here that are involved in repairing UV-damaged DNA were found across the 95 MAGs.

A few MAGs contained many of these functions with a normalized coverage of greater than or equal to three. 25 MAGs contained *cspA* at a normalized coverage of at least three or higher, with its highest normalized coverage of 27.33 observed in the MAG WI.D.9.18.21.bin.6, which was assigned to *Priestia megaterium*. DP.D.7.10.20.bin.68, assigned to the genus *Spirosoma*, contained the following genes at a normalized coverage of greater than or equal to three: *uvrA*, the gene coding for the heat shock protein HsIJ (i.e., *hsij*), and 17 genes involved in LPS biosynthesis and modification. Specifically, this MAG contained LPS-related genes involved in various types of O-antigen synthesis at relatively high normalized coverages, with *wbgP* at a normalized coverage of 28.43, *wecP* at a normalized coverage of 19.29, and *wbbC* (i.e., O7-antigen biosynthesis mannosyltransferase) at a normalized coverage of 15.24. PD.D.7.27.21.bin.6 and WI.D.9.18.21.bin.11, both of which were assigned to *Acinetobacter baumannii*, contained the same set of genes at a normalized coverage greater than or equal to three. These genes included five genes involved in UV-damaged DNA repair (i.e., *uvrA, uvrB,*

uvrC, umuC, umuD), four genes the temperature shock response (i.e., *cspA, htpX, hsIJ,* and the *hsIR* gene that codes for the ribosome-associated heat shock protein Hsp15), two genes involved in quorum sensing (i.e., *bisR* and LuxR family transcriptional regulator *solR*), 1 gene involved in osmoprotectant transport (i.e., osmolarity sensor histidine kinase EnvZ, *envZ*), 16 genes involved in LPS biosynthesis, and the *recA* gene (i.e., a bacterial housekeeping gene).

Discussion

Here we investigate the microbial composition and functional diversity of the previously uncharacterized dust microbiome from the Salton Sea region. Despite significant differences in the dust sources and the wind conditions of our four sites (i.e., PD, BDC, DP, and WI) across several months in 2020 and 2021, we observed a core aeolian microbiome in both compositional and functional assembly. Additionally, the dust sources and wind conditions in this region contributed to the overall composition of the dust microbiome as well as specific adaptations required for aeolian microbial survival. Collectively, our results suggest that the influence of the local climate as well as the resilience of the microorganisms entrained in the dust work in tandem to structure the taxonomic and functional diversity of the core, aeolian dust microbiome.

Dust Sources and Local Wind Conditions Drive Dust Microbiome Assembly

We observed that aeolian dust microbial composition from around the Salton Sea significantly varied between our sites: PD, BDC, DP, and WI. A PERMANOVA found that microbial beta diversity significantly differed between sites, and K-means clustering of these data revealed three clusters, with one cluster containing four PD samples and one

BDC sample (i.e., PD.D.7.9.20, PD.D.8.14.20, BDC.D.11.6.20, PD.D.11.6.20, and PD.9.18.21) and another cluster containing three DP and two WI samples (DP.D.11.5.20, WI.D.7.29.21, DP.D.8.21.21, DP.D.12.8.21, and WI.D.12.8.21). Furthermore, while alpha diversity and species richness did not significantly differ between sites, we did observe that most of the samples in each site with a Shannon diversity of at least 117 and a species richness of at least 200 were grouped into these two respective clusters (i.e., PD/BDC and DP/WI). Upon deeper investigation, we found that the PD/BDC cluster shared microbial genera with a relative abundance of at least 2% or more, namely *Adhaeribacteri, Segetibacter,* and *Bombilactobacillus*. The DP/WI cluster also share major microbial genera including *Adhaeribacter*, *Flavisolibacter,* and *Massilia* (Supplemental Figure 6). The third cluster identified by K-means clustering groups the remaining samples from across the four sites together, with 17 of the 18 samples in this third cluster contain *Massilia* as a major taxon with a relative abundance of at least 2. The one sample in this cluster that does not have *Massilia* as a major genus, DP.D.10.10.20, has *Spirosoma* at a relative abundance of at least 2%, which is also observed in other samples in this cluster including BDC.D.9.20.21 and WI.D.11.5.20. These results demonstrate that samples from sites further from the Salton Sea (i.e., PD and BDC) share a specific set of bacteria, whereas sites closer to the Salton Sea (i.e., DP and WI) share a different set of taxa. Additionally, the third cluster containing samples dominated by *Massilia* represents the strength and resistance of specific taxa that have the ability to withstand a wide variety of environmental conditions. Collectively these findings suggest that while there are generalist, aeolian microorganisms driving compositional similarity

between our samples (i.e., like *Massilia*), there appears to be a location-specific signal regarding which taxa are dominant and shared between samples collected closer to verses further from the Salton Sea.

Our findings are further supported by the significant differences we observed between the four sites based on their respective dust sources and contributors (i.e., surface type frequencies, STFs) and their wind conditions. We also found that dust sources and local wind conditions differentially structured the dust microbiomes within each site. For example, microbial composition within samples collected from the southernmost site, WI, were significantly driven by average relative humidity and the average zonal (east-west) component of local winds (u), whereas the microbial composition within samples from DP were significantly driven by both average 24-hour accumulated precipitation and the Barren Land STF, which represents desert land. These results suggest that the chemical composition of the dust and the source of the dust are stringent selective filters that differentially determine which microorganisms become entrained, persist, and disperse in aeolian dust around the Salton Sea and beyond. Previous research into the chemical composition and sources of dust collected around the Salton Sea has shown that dust composition and source vary depending on where the dust was collected. Frie et al. (2019) collected aeolian dust at our four sites (PD, BDC, DP, and WI) as well as a fifth site (Sonny Bono; SB) and found that evaporite-associated elements (i.e., Na, Ca, K, Mg, Sr) were most enriched in sites nearest to the Salton Sea (i.e., WI, DP) and decreased in concentration as the dust traveled north (Frie et al. 2019). Conversely, elements associated with soil crusts (i.e., Ti, Fe, Co, Ba, Sn) exhibited the

opposite trend, with the highest enrichment at PD and BDC, and decreasing as the dust moved south (Frie et al. 2019). The Frie et al. (2019) findings parallel our K-means clustering results described above (Supplemental Figure 6), where bacterial composition was distinct between several PD/BDC samples (i.e., collected further from the lake) and DP/WI samples (i.e., collected closer to the lake). Considering that nutrient availability and space are important factors in microbial dispersal and assembly, our results demonstrate that local wind conditions and sources select for the variation in taxonomic assembly of dust microbiomes in the Salton Sea region.

Aeolian Dust has a Core Microbiome Based on Composition

Despite the differences in aeolian dust microbial composition across our four sites, we observed a core aeolian dust microbiome composed of thirteen bacterial genera. Our results demonstrate that aeolian dust from around the Salton Sea shares a set of unique microorganisms that can withstand the harsh conditions of the atmosphere. Twelve of the thirteen bacterial genera identified in the Salton Sea core dust microbiome have been previously identified in dusts and aerosols from around the world (Figure 1). Of these thirteen taxa, *Massilia* dominated our samples and appeared to be the most abundant member of the core dust microbiome, appearing in all 28 samples with a minimum relative abundance of 0.33% (WI.D.7.10.20) and a high of 70.33% (i.e., PD.D.12.8.21). This Gram-negative genus was previously identified in the core microbiome of airborne dust in Kuwait (Al Salameen et al. 2020), dust samples from the Eastern Mediterranean (Erkorkmaz et al. 2023), and air samples collected in the Suwon region of South Korea (Weon et al. 2008). *Massilia* is of particular interest due to its

presence in all our samples and due to its known resiliency against both hot and cold temperatures as well as UV-radiation stress. *Massilia* species are known to be pyrophilous and heat resistant, dominating forest soils immediately after a fire (Pulido-Chavez et al. 2023), and have been isolated from desert soil crusts in Moab, Utah, photovoltaic cells in southeast Brazil (Moura et al. 2021), and microbial mats in Antarctica (Shaffer et al. 2023). *Massilia* was found to dominate dust rains collected in Beirut, Lebanon and Granada, Spain (Itani and Smith 2016, Navarro et al. 2023). Our results are consistent with these studies' findings, and comprehensively these results speak not only to *Massilia*'s ubiquity in atmospheric samples globally, but also to this genus' ability to readily adapt to its harsh, dynamic conditions. Recent research discovered that *Massilia frigida* isolated from a microbial mat in the Don Juan Pond basin in Antarctica were capable of producing the red pigment prodigiosin, which assists with UV protection; yet non-psychrotolerant *Massilia* did not contain the necessary biosynthetic gene clusters to produce this pigment (Shaffer et al. 2023). Given the presence and abundance of *Massilia* species across our samples and collection periods, in both dry and wet months, it is evident that *Massilia* is has the necessary attributes to dominate the aeolian dust microbiome.

In addition to *Massilia*, other members of the core dust microbiome have been isolated in a variety of environmental dust and soil surface samples. Air samples collected at Peking University in Beijing, China contained nine of our 13 core dust microbial taxa: *Sphingomonas, Hymenobacter, Planomicrobium, Pseudomonas, Novosphingobium, Roseomonas, Paracoccus, Kocuria,* and *Massilia* (Zhang et al.

2019b). Bacterial cultures isolated from dust collected in Ilam city, Iran, contained *Pseudomonas, Planococcus, Paracoccus,* and *Rhizobium* colonies (Amarloei et al. 2020). Additionally, a global study of settled dust (i.e., including samples from 33 countries and six continents) found that not only did *Sphingomonas* and *Hymenobacter* dominate their dust samples, but they also identified the presence of *Devosia*, *Paracoccus*, and *Pseudomonas* in their dust microbiomes (Chen et al. 2021). Lastly, while *Nibribacter* has not been explicitly identified in dust, this genus was abundant in emissive surface sand from the Kyzyl-Kum desert in Uzbekistan along with other known dust-inhabiting microorganisms such as *Roseomonas, Hymenobacter, Novosphinogobium, Planococcus, Planomicrobium, Sphingomonas,* and *Massilia* (Osman et al. 2023). Our results, in addition to prior research exploring the composition of the dust microbiome, confirm that these bacteria are capable of persisting in the harsh and volatile conditions of aeolian dust.

Aeolian Dust has a Core Microbiome Based on Function

Functional annotation of the aeolian dust metagenomes sampled from the Salton Sea revealed that the aeolian dust microbiome in this region is equipped to survive atmospheric conditions. Genes that code for proteins involved in endospore formation, UV-damaged DNA repair, the temperature shock response, osmoprotectant transport and accumulation, lipopolysaccharide (LPS) synthesis and modification, and quorum sensing were widely distributed across genes our metagenomes (Figure 5) as well as MAGs. The presence and distribution of these traits throughout the metagenomes from all four sites indicates that the aeolian dust microbiome contains the set of features required to

withstand entrainment and colonization of the atmospheric ecosystem. Furthermore, we observed that the normalized coverages of temperature shock response genes, genes involved in UV-damaged DNA repair, and genes involved in osmoprotectant transport did not significantly differ between metagenomes from different sites and collection periods. Previous studies into the functional diversity of atmospheric microbiomes have found similar traits that are necessary for windblown survival and dispersal. Metagenomes from air samples collected over the Red Sea contained genes that code for proteins involved in UV radiation resistance (i.e., *uvrA*), quorum sensing and biofilm formation genes (i.e., *vpsT*), heat shock resistance (i.e., *HSP70*, *HSP90*), and sporulation (i.e., *spoVK*, *spoIVFB*; Aalismail et al. 2019). Bacteria sampled from clouds (Joly et al. 2015), rainwater (Ling et al. 2021) and air (Daussin et al. 2023) have been shown to resist a variety of stressors associated with the atmosphere and wind including UV radiation, osmotic stress, and the freeze-thaw cycle. Thus, we can conclude that the dust microbiome in the Salton Sea region has the functional capacity and redundancy to withstand the atmospheric stressors associated with aeolian entrainment, colonization, and dispersal.

Sporulation genes were not as widely distributed throughout the metagenomes as the other aeolian-survival functions we considered, yet at least four of the 38 genes considered here found in each metagenome: *spmA*, *spoIVCA*, *spoVK*, and *spoVR* (Figure 5). It is possible that the low representation of sporulation genes throughout the metagenomes and the MAGs is due to the presence of endospore formers traveling as endospores in the dust rather than as bacterial cells. Extracting DNA from endospores is

more challenging than extracting DNA from bacteria cells due to their resilience against both mechanical and temperature stress (Wunderlin et al. 2016). Future work into the functional diversity of aeolian dust microbiomes should take this into consideration when extracting DNA from atmospheric samples.

Wind Direction and Seasonality Select for Microbial Adaptations

We find that while the aeolian dust microbiome has a core set of required adaptations for survival, a single abiotic factor cannot explain the prevalence and distribution of these functions. Furthermore, these results highlight the complexity of the aeolian environment and its multiple selective pressures that synergistically structure the functional diversity of dust microbiomes. The average meridional (north-south) components (v) and zonal (east-west) components (u) of local winds were significant or near significant predictors for several core dust microbiome traits. Notably, the meridional (north-south) component (v) was a significant predictor for functions involved in sporulation (i.e., *spmA*), UV radiation resistance (i.e., *lexA, uvrA, uvrB,* and *uvrC*), thermal resistance (i.e., *cspA*), and osmotic stress resistance (i.e., *osmY*). When plotting the normalized coverage of these functions against the meridional (north-south) component (v; Figure 6, Supplemental Figure 7), a seasonal trend emerged: the UV radiation resistance genes and *cspA* appeared to have higher normalized coverage with northerly winds in the winter months compared to the lower coverage with southerly winds summer and fall months; whereas *spmA* and *osmY* exhibited a slight increase in normalized coverages with southerly winds during the summer months. These trends observed in the shared adaptations across sites highlight the functional plasticity,

redundancy, and resiliency of the aeolian dust microbiome throughout changing climate conditions over time.

The wind conditions we observed here were like those described in Frie et al (2019), with predominantly northerly winds during the winter months. They found that dust flux in the region was highest during spring and summer, coinciding with high wind speeds and an increase in playa emissions from the Salton Sea (Frie et al. 2019). Similarly, we observed higher average temperatures during the summer months across our sites compared to the fall and winter months (Supplemental Table 2), and we found a positive correlation between the meridional (north-south) component (v) and the Salton Sea STF, where the Salton Sea contribution was greater with southerly winds and decreased with northerly winds ($r = 0.67$, $P = 9.74e\text{-}05$; Supplemental Tables 10, 11). The functional annotation results as well as the relationship between the Salton Sea STF and wind direction suggest that the aeolian microbiome is functionally resilient in the face of ecological disturbance. During the spring and summer months, temperatures are high, wind directions shift, wind speeds increase, and the contribution of Salton Sea playa dust and sea spray also increase. Together, these conditions disturb the aeolian microbiome. As summer turns to fall and winter, dust flux, wind speeds, and air temperatures decrease, and the generalist aeolian dust microbiome can thrive unhindered by the local climate. This could explain why there was an apparent recovery in the normalized coverages of the UV radiation resistance genes and *cspA* during the fall months. Moreover, this conclusion also supports the increase in the normalized coverage of *spmA* and *osmY* we observed during the summer months when UV radiation resistance

genes and *cspA* decreased; microorganisms that colonize the Salton Sea water and playa must be halophiles, and thus are uniquely adapted to survive severe osmotic stress (Freund et al. 2022). We did identify microbial genera that were shared between Salton Sea dust and seawater samples (Freund et al, in progress; Supplemental Figure 8), yet more comparisons of the taxonomic and functional diversity of these interacting microbiomes across seasons would further clarify this disturbance-recovery hypothesis.

Despite observing this seasonal and directional shift in the distribution in dust microbial adaptations, the relative abundance of the genera found dust core microbiome did not follow this pattern (Supplemental Figure 9). This could be due to horizontal gene transfer (i.e., HGT) within the aeolian dust microbiome, contributing to the functional convergence and survival of microorganisms beyond those in the core dust microbiome. Evidence of HGT events using specific marker genes such as the Class I integron-integrase gene (i.e., *intI1*) and commonly shared antibiotic resistance genes (i.e., ARGs) have been observed in dust microbial communities (Li et al. 2018, Zhang et al. 2019a, Maamar et al. 2020). Additionally, *Massilia* and *Sphingomonas* isolated from rain and snow samples showed evidence of previous HGT events via the ARGs they contained (Cáliz et al. 2022). We did identify the presence of several ARGs in all 24 aeolian dust metagenomes and in 12 MAGs, specifically macrolide phosphotransferase, beta-lactamase class D OXA-9, dihydrofolate reductase DfrA, aminoglycoside 6'-N-acetyltransferase I, and the ribosomal protection tetracycline resistance protein (Supplemental Figures 10, 11). Three of the 12 MAGs contained two ARGs that target different antibiotics, revealing that some of these microorganisms have multi-drug

resistance. Of note is beta-lactamase class D OXA-9 which exhibited the highest normalized coverage across the metagenomes; beta-lactamases have been found to be associated with plasmid mobilization and HGT, and they have been found in environmental microbiomes (Marathe et al. 2018). The identification of multi-drug ARGs in the aeolian dust microbiome from the Salton Sea region is alarming because these genes can be shared via HGT from the aeolian microbiome to the airway and lung microbiomes (Aogáin et al. 2020, Bai et al. 2024). The transfer of these ARGs to host microbiomes can reduce the efficacy of antibiotics used to treat infections, and thus increase the vulnerability of the exposed individual to a wide variety of illnesses, including respiratory illness. The distribution and dispersal of ARGs because of HGT has been well studied due to their pathogenic impact, yet the sharing of niche-specific adaptations via HGT within environmental microbiomes and between the environment and the host microbiomes requires further investigation (Fuchsman et al. 2017). Future work exploring HGT events in the Salton Sea dust microbiome is required to better understand the selective mechanisms behind the functional convergence and taxonomic divergence we observed in this microbial community, and how these selective processes give rise to the pathogenicity of the aeolian microbiome.

Precipitation and Moisture Availability Impacts Dust Microbial Survival Strategies

Average accumulated precipitation was a significant predictor of several microbial functions of interest that are involved in surviving osmotic stress (i.e., *spoIVCA*, *spmA*, *osmY*, *opuC*, and *bisR*). Average relative humidity was a driver of microbial composition within the WI samples and, with average precipitation, was a

significant driver of *spoIVCA* normalized coverage across the dust metagenomes. Our results highlight the importance of moisture availability and osmotic stress resistance within the aeolian dust microbiome. We found that the normalized coverage of *spoIVCA*, *opuC*, and *bisR* decreased as precipitation increased. This could be because precipitation provides readily available water for the dust microbiome, and thus the microbial responses to deal with this stress (i.e., sporulation, osmoprotectant accumulation, and biofilm formation) are not necessary. This relationship between *spoIVCA*, *opuC*, *bisR*, and precipitation is supported by the fact that moisture availability and osmotic pressure are triggers for the expansion of biofilms in both Gram-positive and Gram-negative bacteria, and are involved in initiating sporulation particularly within biofilm formation (Bremer and Krämer 2019). Conversely, *spmA* and *osmY* normalized coverages slightly increase with both precipitation and southerly winds. The opposing trends seen here with *spoIVCA* verses *spmA* and *opuC* verses *osmY* respectively suggests that aeolian dust microorganisms utilize a variety of survival strategies depending on their climate conditions. Furthermore, as described above, the increase in normalized coverages of *spmA* and *osmY* with southerly winds during the summer months may denote that playa and seawater microorganisms from the Salton Sea could be entrained in the aeolian dust when regional dust emissions are high. The functional redundancy, versatility, and flexibility we observed speak to the ability of the aeolian microbiome to employ multiple survival mechanisms as conditions change, allowing this community to travel long distances and withstand periods of ecological stress.

Conclusion

We characterized the taxonomic and functional diversity of the aeolian dust microbiome from the Salton Sea ecosystem. The microbiome of the aeolian dust revealed that although there were location-specific differences in microbial composition between our four sites, there was a core microbiome of bacterial genera that are shared in the dust. These genera have been previously identified in other dust and atmospheric samples and are known to withstand the environmental stressors indicative of the aeolian dust ecosystem. The aeolian dust microbiome also contained a set of shared genes that contribute to its survival in the atmospheric environment, specifically genes involved in UV radiation resistance, thermal resistance, and osmotic stress. Moreover, the conservation and redundancy of these functions in the aeolian dust microbiome are selected for by climate characteristics such as relative humidity and precipitation and contributing dust sources.

Our results help to establish a direct connection between microbial ecology in the environment and public health. There is a bias in the field of microbiology that focuses on studying human pathogens, which is reflected by the lack of environmentally sourced and/or non-culturable microorganisms in our reference databases (Steen et al. 2019, Dias et al. 2020). This perspective does us a disservice because as climate change worsens, our environment will continue to select for resilient and resistant microorganisms that may be pathogenic or can readily become pathogenic upon receiving ARGs and other harmful traits via HGT. While the dust microorganisms we observed were not necessarily pathogenic, their adaptations allow them to remain viable across long distances,

increasing the likelihood that they are inhaled upon exposure and induce inflammation. Furthermore, the Salton Sea aeolian microbiome contains multi-drug ARGs that can be transmitted via HGT to the host during inhalation and colonization of the airway and lungs, increasing the susceptibility of the exposed populations to respiratory illness. Individuals with respiratory illnesses such as chronic obstructive pulmonary disease (i.e., COPD) and bronchiectasis exhibited an increased abundance of certain ARGs compared to healthy individuals (Aogáin et al. 2020); considering the high rate of respiratory distress and asthma experienced by the community in the Salton Sea region, the variety of ARGs and other potentially dangerous adaptations we found in the Salton Sea aeolian microbiome could pose a serious threat to the local population. Thus, understanding the accumulation and exchange of ARGs and other harmful traits in the dust microbiome, and their transmission to the host microbiomes via exposure and HGT, warrants further study. As saline lakes like the Salton Sea are shrinking globally and increasing the global dust load, it seems plausible that this dust will drive the structure and function of global atmospheric dust microbiomes as we observed in the Salton Sea dust, and have unforeseen, detrimental health impacts. We use this work to urge healthcare professionals, policy makers, and community members alike to consider the importance of environmental microbiomes, especially dust microbiomes, as they work to combat the harm caused by industrialization and climate change.

References

Aalismail, N. A., D. K. Ngugi, R. Díaz-Rúa, I. Alam, M. Cusack, and C. M. Duarte. 2019. Functional metagenomic analysis of dust-associated microbiomes above the Red Sea. Scientific Reports 9:1–12.

Amarloei, A., M. Fazlzadeh, A. J. Jafari, A. Zarei, and S. Mazloomi. 2020. Particulate matters and bioaerosols during Middle East dust storms events in Ilam, Iran. Microchemical Journal 152.

Amato, P., M. Joly, C. Schaupp, E. Attard, O. Möhler, C. E. Morris, Y. Brunet, and A. M. Delort. 2015. Survival and ice nucleation activity of bacteria as aerosols in a cloud simulation chamber. Atmospheric Chemistry and Physics 15:6455–6465.

Andrews, S. (n.d.). FastQC: A Quality Control Tool for High Throughput Sequence Data.

Aogáin, M. Mac, K. J. X. Lau, Z. Cai, J. K. Narayana, R. W. Purbojati, D. I. Drautz-Moses, N. E. Gaultier, T. K. Jaggi, P. Y. Tiew, T. H. Ong, M. S. Koh, A. L. Y. Hou, J. A. Abisheganaden, K. Tsaneva-Atanasova, S. C. Schuster, and S. H. Chotirmall. 2020. Metagenomics reveals a core macrolide resistome related to microbiota in chronic respiratory disease. American Journal of Respiratory and Critical Care Medicine 202:433–447.

Aramaki, T., R. Blanc-Mathieu, H. Endo, K. Ohkubo, M. Kanehisa, S. Goto, H. Ogata, and A. Valencia. 2020. KofamKOALA: KEGG Ortholog assignment based on profile HMM and adaptive score threshold. Bioinformatics 36:2251–2252.

Bai, H., L. Y. He, F. Z. Gao, K. S. Yao, M. Zhang, L. K. Qiao, Z. Y. Chen, L. X. He, Y. S. Liu, J. L. Zhao, and G. G. Ying. 2024. Airborne antibiotic resistome and microbiome in pharmaceutical factories. Environment International 186.

Bankevich, A., S. Nurk, D. Antipov, A. A. Gurevich, M. Dvorkin, A. S. Kulikov, V. M. Lesin, S. I. Nikolenko, S. Pham, A. D. Prjibelski, A. V. Pyshkin, A. V. Sirotkin, N. Vyahhi, G. Tesler, M. A. Alekseyev, and P. A. Pevzner. 2012. SPAdes: A new genome assembly algorithm and its applications to single-cell sequencing. Journal of Computational Biology 19:455–477.

Biddle, T. A., Q. Li, M. R. Maltz, P. N. Tandel, R. Chakraborty, K. Yisrael, R. Drover, D. R. Cocker, and D. D. Lo. 2021. Salton Sea aerosol exposure in mice induces a pulmonary response distinct from allergic inflammation. Science of the Total Environment 792.

Biddle, T. A., K. Yisrael, R. Drover, Q. Li, M. R. Maltz, T. M. Topacio, J. Yu, D. Del Castillo, D. Gonzales, H. L. Freund, M. P. Swenson, M. L. Shapiro, J. K. Botthoff, E. Aronson, D. R. Cocker, and D. D. Lo. 2023. Aerosolized aqueous dust extracts collected

near a drying lake trigger acute neutrophilic pulmonary inflammation reminiscent of microbial innate immune ligands. Science of the Total Environment 858.

Bowers, R. M., N. C. Kyrpides, R. Stepanauskas, M. Harmon-Smith, D. Doud, T. B. K. Reddy, F. Schulz, J. Jarett, A. R. Rivers, E. A. Eloe-Fadrosh, S. G. Tringe, N. N. Ivanova, A. Copeland, A. Clum, E. D. Becraft, R. R. Malmstrom, B. Birren, M. Podar, P. Bork, G. M. Weinstock, G. M. Garrity, J. A. Dodsworth, S. Yooseph, G. Sutton, F. O. Glöckner, J. A. Gilbert, W. C. Nelson, S. J. Hallam, S. P. Jungbluth, T. J. G. Ettema, S. Tighe, K. T. Konstantinidis, W. T. Liu, B. J. Baker, T. Rattei, J. A. Eisen, B. Hedlund, K. D. McMahon, N. Fierer, R. Knight, R. Finn, G. Cochrane, I. Karsch-Mizrachi, G. W. Tyson, C. Rinke, A. Lapidus, F. Meyer, P. Yilmaz, D. H. Parks, A. M. Eren, L. Schriml, J. F. Banfield, P. Hugenholtz, and T. Woyke. 2017, August 8. Minimum information about a single amplified genome (MISAG) and a metagenome-assembled genome (MIMAG) of bacteria and archaea. Nature Publishing Group.

Bremer, E., and R. Krämer. 2019. Responses of Microorganisms to Osmotic Stress. Annu. Rev. Microbiol 73:313–334.

Bushnell, B. (n.d.). BBMap.

Cáliz, J., J. Subirats, X. Triadó-Margarit, C. M. Borrego, and E. O. Casamayor. 2022. Global dispersal and potential sources of antibiotic resistance genes in atmospheric remote depositions. Environment International 160.

Callahan, B. J., P. J. McMurdie, M. J. Rosen, A. W. Han, A. J. A. Johnson, and S. P. Holmes. 2016. DADA2: High-resolution sample inference from Illumina amplicon data. Nature Methods 13:581–583.

Chaumeil, P. A., A. J. Mussig, P. Hugenholtz, and D. H. Parks. 2020. GTDB-Tk: A toolkit to classify genomes with the genome taxonomy database. Bioinformatics 36:1925–1927.

Chen, Y., M. J. Gebert, S. A. Faith, R. R. Dunn, N. Fierer, and A. Barberán. 2021. Global Patterns and Climatic Controls of Dust-Associated Microbial Communities. Microbiology Spectrum 9.

Cheney, A. M., G. Ortiz, A. Trinidad, S. Rodriguez, A. Moran, A. Gonzalez, J. Chavez, and M. Pozar. 2023. Latinx and Indigenous Mexican Caregivers' Perspectives of the Salton Sea Environment on Children's Asthma, Respiratory Health, and Co-Presenting Health Conditions. International Journal of Environmental Research and Public Health 20.

DasSarma, P., and S. DasSarma. 2018, June 1. Survival of microbes in Earth's stratosphere. Elsevier Ltd.

Daussin, A., P. Vannier, É. Mater, T. Šantl-Temkiv, C. Cockell, and V. Þ. Marteinsson. 2023. Survival of Icelandic airborne microbes towards simulated atmospheric stress factors. Extremophiles 27.

Davis, N. M., Di. M. Proctor, S. P. Holmes, D. A. Relman, and B. J. Callahan. 2018. Simple statistical identification and removal of contaminant sequences in marker-gene and metagenomics data. Microbiome 6.

Dias, C. K., R. Starke, V. S. Pylro, and D. K. Morais. 2020. Database limitations for studying the human gut microbiome. PeerJ Computer Science 6.

Doede, A. L., and P. B. DeGuzman. 2020. The Disappearing Lake: A Historical Analysis of Drought and the Salton Sea in the Context of the GeoHealth Framework. GeoHealth 4.

Edgar, R. C., and H. Flyvbjerg. 2015. Error filtering, pair assembly and error correction for next-generation sequencing reads. Bioinformatics 31:3476–3482.

Environmental Protection Agency. 2024, July 10. Air Quality System. https://www.epa.gov/aqs.

Erkorkmaz, B. A., D. Gat, and Y. Rudich. 2023. Aerial transport of bacteria by dust plumes in the Eastern Mediterranean revealed by complementary rRNA/rRNA-gene sequencing. Communications Earth and Environment 4.

Farzan, S. F., M. Razafy, S. P. Eckel, L. Olmedo, E. Bejarano, and J. E. Johnston. 2019. Assessment of respiratory health symptoms and asthma in children near a drying saline lake. International Journal of Environmental Research and Public Health 16.

Fick, S. 2018. mesowest.

Freund, H., M. R. Maltz, M. P. Swenson, T. M. Topacio, V. A. Montellano, W. Porter, and E. L. Aronson. 2022. Microbiome interactions and their ecological implications at the Salton Sea. California Agriculture 76:16–26.

Frie, A. L., J. H. Dingle, S. C. Ying, and R. Bahreini. 2017. The Effect of a Receding Saline Lake (The Salton Sea) on Airborne Particulate Matter Composition. Environmental

Frie, A. L., A. C. Garrison, M. V. Schaefer, S. M. Bates, J. Botthoff, M. Maltz, S. C. Ying, T. Lyons, M. F. Allen, E. Aronson, and R. Bahreini. 2019. Dust Sources in the Salton Sea Basin: A Clear Case of an Anthropogenically Impacted Dust Budget. Environmental Science & Technology 53:9378–9388.

Fuchsman, C. A., R. E. Collins, G. Rocap, and W. J. Brazelton. 2017. Effect of the environment on horizontal gene transfer between bacteria and archaea. PeerJ 2017:1–26.

Hu, P., Y. Sharaby, J. D. Gu, A. Radian, and N. Lang-Yona. 2024. Environmental processes and health implications potentially mediated by dust-borne bacteria. Environmental Microbiology Reports 16.

Hyatt, D., G. L. Chen, P. F. LoCascio, M. L. Land, F. W. Larimer, and L. J. Hauser. 2010a. Prodigal: Prokaryotic gene recognition and translation initiation site identification. BMC Bioinformatics 11.

Hyatt, D., G. L. Chen, P. F. LoCascio, M. L. Land, F. W. Larimer, and L. J. Hauser. 2010b. Prodigal: Prokaryotic gene recognition and translation initiation site identification. BMC Bioinformatics 11.

Illumina, Inc. 2017. Illumina Methods Guide.

Itani, G. N., and C. A. Smith. 2016. Dust Rains Deliver Diverse Assemblages of Microorganisms to the Eastern Mediterranean. Scientific Reports 6.

Joly, M., P. Amato, M. Sancelme, V. Vinatier, M. Abrantes, L. Deguillaume, and A. M. Delort. 2015. Survival of microbial isolates from clouds toward simulated atmospheric stress factors. Atmospheric Environment 117:92–98.

Jones, B. A., and J. Fleck. 2020. Shrinking lakes, air pollution, and human health: Evidence from California's Salton Sea. Science of the Total Environment 7127:136490.

Kang, D. D., F. Li, E. Kirton, A. Thomas, R. Egan, H. An, and Z. Wang. 2019. MetaBAT 2: An adaptive binning algorithm for robust and efficient genome reconstruction from metagenome assemblies. PeerJ 2019:1–13.

Kassambara, A. 2021. Rstatix: Pipe-Friendly Framework for Basic Statistical Tests.

Kassambara, A., and F. Mundt. 2020. Factoextra: Extract and Visualize the Results of Multivariate Data Analyses.

Klindworth, A., E. Pruesse, T. Schweer, J. Peplies, C. Quast, M. Horn, and F. O. Glöckner. 2013. Evaluation of general 16S ribosomal RNA gene PCR primers for classical and next-generation sequencing-based diversity studies. Nucleic Acids Research 41:1–11.

Knoerr, J. 2022, August 12. Salton Sea Policy-Making Excludes Vulnerable Purepecha Community Members. https://www.pbssocal.org/news-community/salton-sea-policy-making-excludes-vulnerable-purepecha-community-members.

Kok, J. F., D. S. Ward, N. M. Mahowald, and A. T. Evan. 2018. Global and regional importance of the direct dust-climate feedback. Nature Communications 9.

Lee, M. 2022. bit: a multipurpose collection of bioinformatics tools. F1000Research 11:122.

Li, D., C. M. Liu, R. Luo, K. Sadakane, and T. W. Lam. 2015. MEGAHIT: An ultra-fast single-node solution for large and complex metagenomics assembly via succinct de Bruijn graph. Bioinformatics 31:1674–1676.

Li, J., J. Cao, Y. G. Zhu, Q. L. Chen, F. Shen, Y. Wu, S. Xu, H. Fan, G. Da, R. J. Huang, J. Wang, A. L. De Jesus, L. Morawska, C. K. Chan, J. Peccia, and M. Yao. 2018. Global Survey of Antibiotic Resistance Genes in Air. Environmental Science and Technology 52:10975–10984.

Liao, Y., G. K. Smyth, and W. Shi. 2014. FeatureCounts: An efficient general purpose program for assigning sequence reads to genomic features. Bioinformatics 30:923–930.

Ling, M. L., I. P. G. Marshall, B. Rosati, L. Schreiber, T. Boesen, K. Finster, and T. Šantl-Temkiv. 2021. Properties relevant to atmospheric dispersal of the ice-nucleation active Pseudomonas syringae strain R10.79 isolated from rain water. Aerobiologia 4.

Love, M. I., W. Huber, and S. Anders. 2014. Moderated estimation of fold change and dispersion for RNA-seq data with DESeq2. Genome Biology 15:1–21.

Maamar, S. Ben, A. J. Glawe, T. K. Brown, N. Hellgeth, J. Hu, J. P. Wang, C. Huttenhower, and E. M. Hartmann. 2020. Mobilizable antibiotic resistance genes are present in dust microbial communities. PLoS Pathogens 16.

Maltz, M. R., C. J. Carey, H. L. Freund, J. K. Botthoff, S. C. Hart, J. E. Stajich, S. M. Aarons, S. M. Aciego, M. Blakowski, N. C. Dove, M. E. Barnes, N. Pombubpa, and E. L. Aronson. 2022. Landscape Topography and Regional Drought Alters Dust Microbiomes in the Sierra Nevada of California. Frontiers in Microbiology 13:1–19.

Marathe, N. P., A. Janzon, S. D. Kotsakis, C. F. Flach, M. Razavi, F. Berglund, E. Kristiansson, and D. G. J. Larsson. 2018. Functional metagenomics reveals a novel carbapenem-hydrolyzing mobile beta-lactamase from Indian river sediments contaminated with antibiotic production waste. Environment International 112:279–286.

Martinez Arbizu, P. 2017. pairwiseAdonis: Pairwise Multilevel Comparison using Adonis.

Mayol, E., M. A. Jiménez, G. J. Herndl, C. M. Duarte, and J. M. Arrieta. 2014. Resolving the abundance and air- sea fluxes of airborne microorganisms in the North Atlantic Ocean. Frontiers in Microbiology 5.

Mikheenko, A., V. Saveliev, and A. Gurevich. 2016. MetaQUAST: evaluation of metagenome assemblies. Bioinformatics (Oxford, England) 32:1088–1090.

Moura, J. B., T. P. Delforno, P. F. Do Prado, and I. C. Duarte. 2021. Extremophilic taxa predominate in a microbial community of photovoltaic panels in a tropical region. FEMS Microbiology Letters 368.

Navarro, A., A. del Moral, B. Weber, J. Weber, A. Molinero, R. Delgado, J. Párraga, and F. Martínez-Checa. 2023. Microbial composition of Saharan dust plumes deposited as red rain in Granada (Southern Spain). Science of The Total Environment:169745.

Nawrocki, P. 2009. Structural RNA Homology Search and Alignment using Covariance Models. Washington University in Saint Louis.

Oksanen, J., F. G. Blanchet, M. Friendly, R. Kindt, P. Legendre, D. McGlinn, P. R. Minchin, R. B. O'Hara, G. L. Simpson, P. Solymos, M. H. H. Stevens, E. Szoecs, and H. Wagner. 2020. vegan: Community Ecology Package. CRAN.

Osman, J. R., G. R. Fernandes, E. Kamilova, and M. S. DuBow. 2023. Genomic microbiome analyses of surface sand samples from the Kyzyl-Kum Desert (Uzbekistan): characterization and comparative study. Archives of Microbiology 205.

Parajuli, S. P., and C. S. Zender. 2018. Projected changes in dust emissions and regional air quality due to the shrinking Salton Sea. Aeolian Research 33:82–92.

Parks, D. H., M. Imelfort, C. T. Skennerton, P. Hugenholtz, and G. W. Tyson. 2015. CheckM: Assessing the quality of microbial genomes recovered from isolates, single cells, and metagenomes. Genome Research 25:1043–1055.

Pereira, M. B., M. Wallroth, V. Jonsson, and E. Kristiansson. 2018. Comparison of normalization methods for the analysis of metagenomic gene abundance data. BMC Genomics 19.

Price, M. N., P. S. Dehal, and A. P. Arkin. 2010. FastTree 2 - Approximately maximum-likelihood trees for large alignments. PLoS ONE 5.

Pulido-Chavez, M. F., J. W. J. Randolph, C. Zalman, L. Larios, P. M. Homyak, and S. I. Glassman. 2023. Rapid bacterial and fungal successional dynamics in first year after chaparral wildfire. Molecular Ecology 32:1685–1707.

R Core Team. 2024. R: A Language and Environment for Statistical Computing. R Foundation for Statistical Computing, Vienna, Austria.

Rodriguez, S. S. 2021. Environmental Racism in the Eastern Coachella Valley: P'urhépecha Parents' Testimonios on Childhood Asthma-Related Symptoms and Its Relationship to the Salton Sea. San Diego State University.

Al Salameen, F., N. Habibi, S. Uddin, K. Al Mataqi, V. Kumar, B. Al Doaij, S. Al Amad, E. Al Ali, and F. Shirshikhar. 2020. Spatio-temporal variations in bacterial and fungal community associated with dust aerosol in Kuwait. PLoS ONE 15:1–23.

Schepanski, K. 2018. Transport of mineral dust and its impact on climate. Geosciences (Switzerland) 8.

Shaffer, J. M. C., L. A. Giddings, R. M. Samples, and J. A. Mikucki. 2023. Genomic and phenotypic characterization of a red-pigmented strain of Massilia frigida isolated from an Antarctic microbial mat. Frontiers in Microbiology 14.

Shetty S, L. L. 2019. microbiome R package.

Shi, Y., and X. Liu. 2019. Dust Radiative Effects on Climate by Glaciating Mixed-Phase Clouds. Geophysical Research Letters 46:6128–6137.

Steen, A. D., A. Crits-Christoph, P. Carini, K. M. DeAngelis, N. Fierer, K. G. Lloyd, and J. Cameron Thrash. 2019. High proportions of bacteria and archaea across most biomes remain uncultured. ISME Journal 13:3126–3130.

Tang, K., Z. Huang, J. Huang, T. Maki, S. Zhang, X. Ma, J. Shi, J. Bi, T. Zhou, G. Wang, and L. Zhang. 2018. Characterization of atmospheric bioaerosols along the transport pathway of Asian dust during the Dust-Bioaerosol 2016 Campaign. Atmospheric Chemistry and Physics 18:7131–7148.

Wei, T., and V. Simko. 2021. R package "corrplot": Visualization of a Correlation Matrix.

Weon, H. Y., B. Y. Kim, J. A. Son, H. B. Jang, S. K. Hong, S. J. Go, and S. W. Kwon. 2008. Massilia aerilata sp. nov., isolated from an air sample. International Journal of Systematic and Evolutionary Microbiology 58:1422–1425.

Wunderlin, T., T. Junier, C. Paul, N. Jeanneret, and P. Junier. 2016. Physical isolation of endospores from environmental samples by targeted lysis of vegetative cells. Journal of Visualized Experiments 2016.

Xia, Y. 2023. Statistical normalization methods in microbiome data with application to microbiome cancer research. Taylor and Francis Ltd.

Zeileis, A., and T. Hothorn. 2002. Diagnostic Checking in Regression Relationships. R News 2:7–10.

Zhang, T., X. Li, M. Wang, H. Chen, Y. Yang, Q. lin Chen, and M. Yao. 2019a. Time-resolved spread of antibiotic resistance genes in highly polluted air. Environment International 127:333–339.

Zhang, T., X. Li, M. Wang, H. Chen, and M. Yao. 2019b. Microbial aerosol chemistry characteristics in highly polluted air. Science China Chemistry 62:1051–1063.

Appendix C: Supplemental Information for Chapter III

Title: Climate Conditions Structure the Taxonomic and Functional Diversity of the Aeolian Dust Microbiome

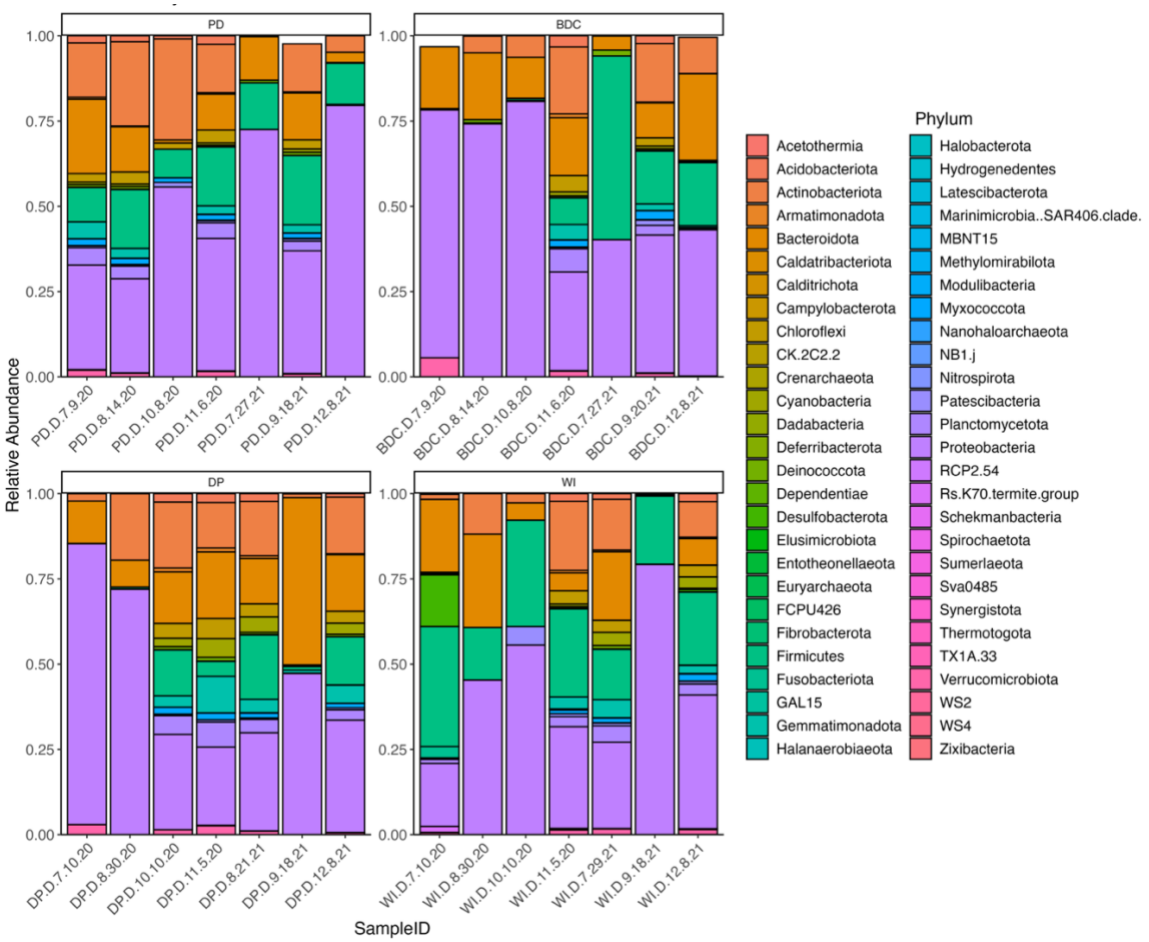

Figure C.1.1. Bacterial Phyla Relative Abundance by Sample and Site. These stacked barplots show the relative abundance of bacterial phyla found in each sample and are separated by site: Palm Desert (PD), Boyd Deep Canyon (BDC), Dos Palmas (DP), and Wister (WI).

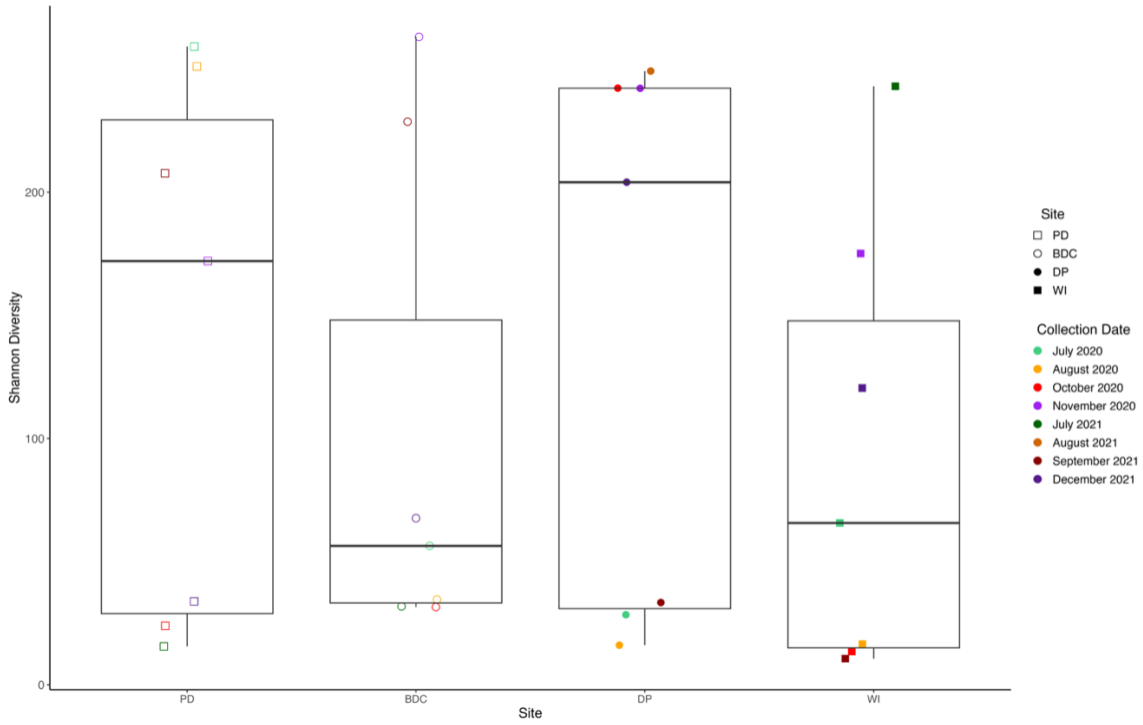

Figure C.1.2. Alpha Diversity by Site and Collection Date. These box-and-whisker plots show the alpha (Shannon-Weiner) diversity calculated from rarefied ASV counts from each sample within each site. The shape of the points indicate the site, whereas the color indicates the collection date.

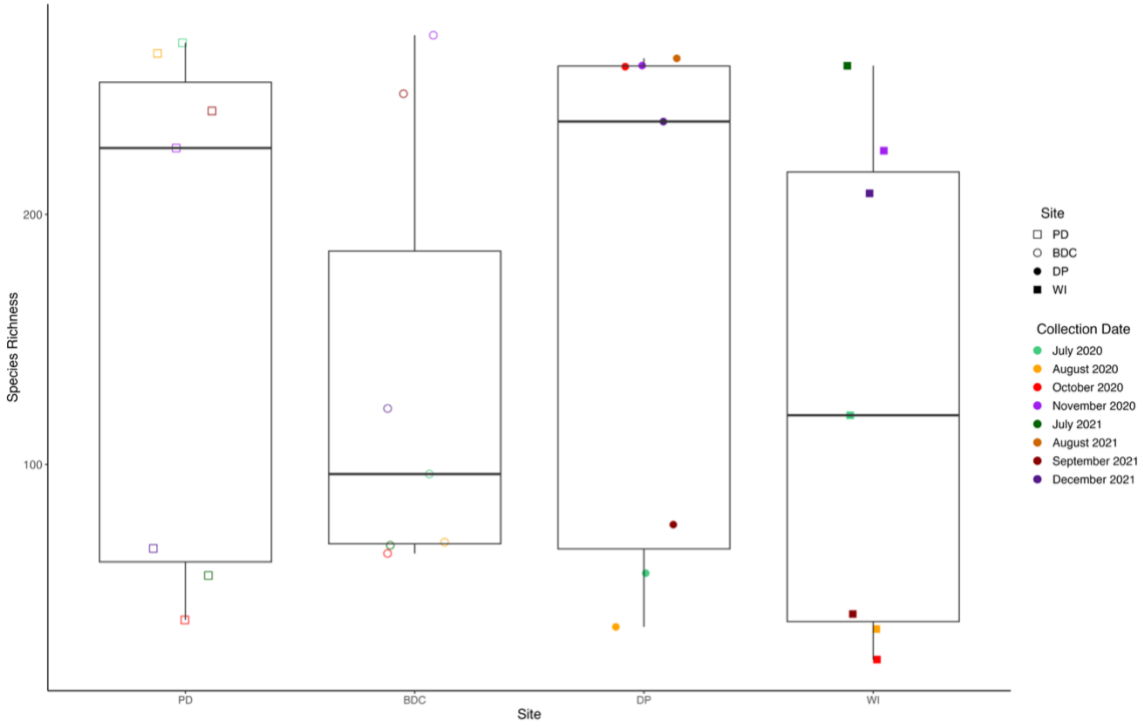

Figure C.1.3. Species Richness by Site and Collection Date. These box-and-whisker plots show the species richness calculated from rarefied ASV counts from each sample within each site. The shape of the points indicate the site, whereas the color indicates the collection date.

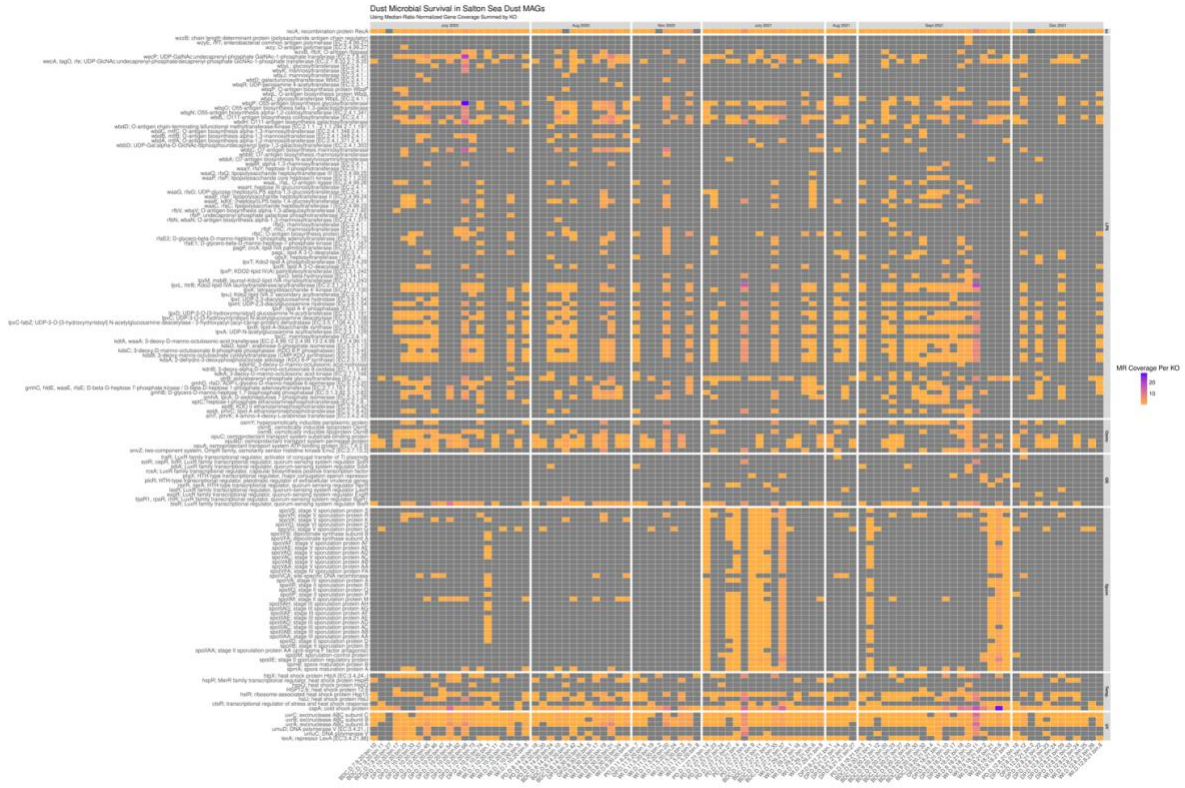

Figure C.1.4. Genes of Interest and their Normalized Coverage in the Metagenome-Assembled Genomes (MAGs). This heatmap shows the normalized coverage (median-ratio normalized, scaled coverages) of specific genes in the MAGs. Each column represents a MAG and the MAGs are organized by collection month from left to right. The genes are separated into functional categories: LPS modification genes (LPS), osmoprotectant transport/accumulation genes (Osmo), quorum sensing genes (QS), sporulation genes (Spore), temperature resistance genes (Temp), and UV radiation resistance genes (UV). Gray squares indicate that the gene is absent.

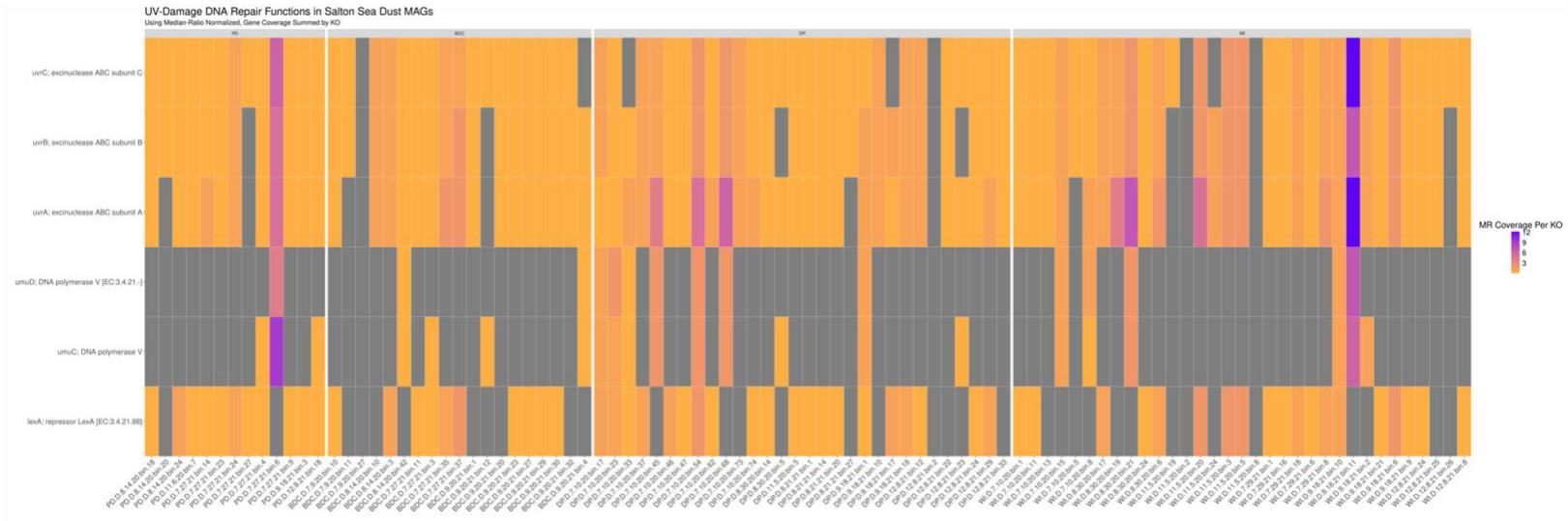

Figure C.1.5. Heatmap of UV Radiation Resistance Genes in the Metagenome Assembled Genomes (MAGs). This heatmap shows the normalized coverage (median-ratio normalized, scaled coverages) of UV radiation resistance genes in the MAGs. Each column represents a MAG and the MAGs are organized by site from left to right: PD, BDC, DP, and WI. Gray squares indicate that the gene is absent.

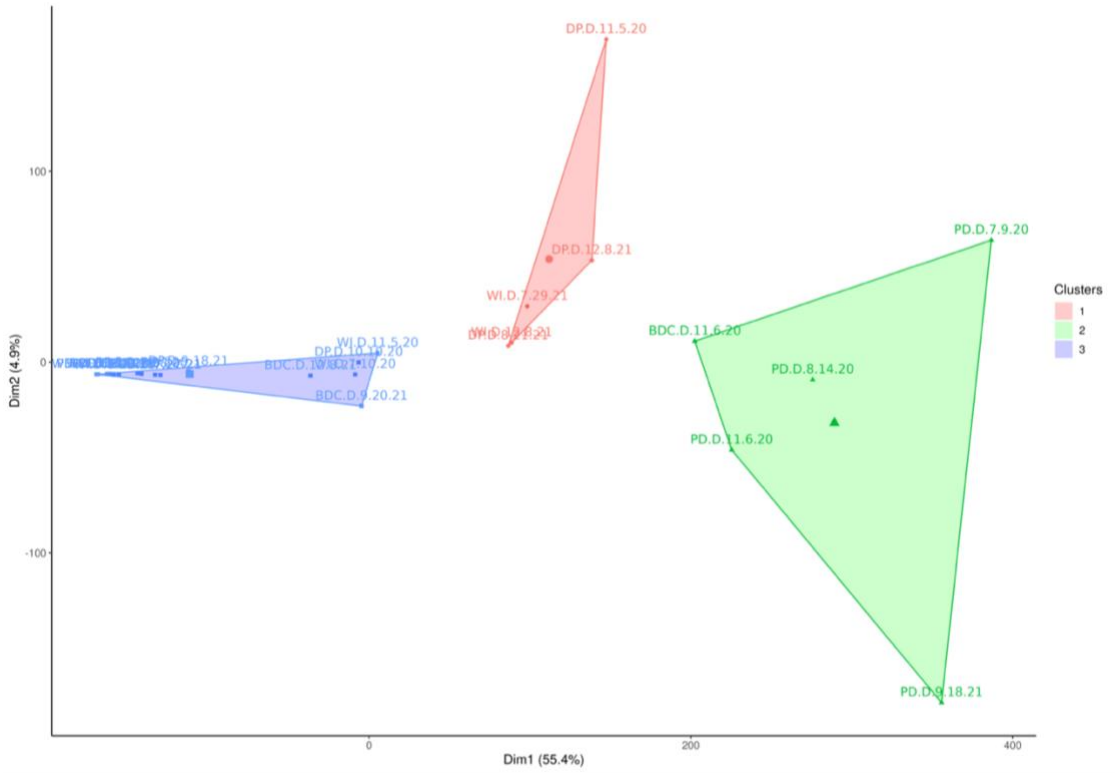

Figure C.1.6. K-Means Clustering of Microbial Composition Data. This is a principle coordiantes analysis (PCoA) showing the K-means clustering of the samples. Each point represents an individual samples, and all points within a cluster only belong to that cluster. The clusters have been assigned the colors blue, red, and green.

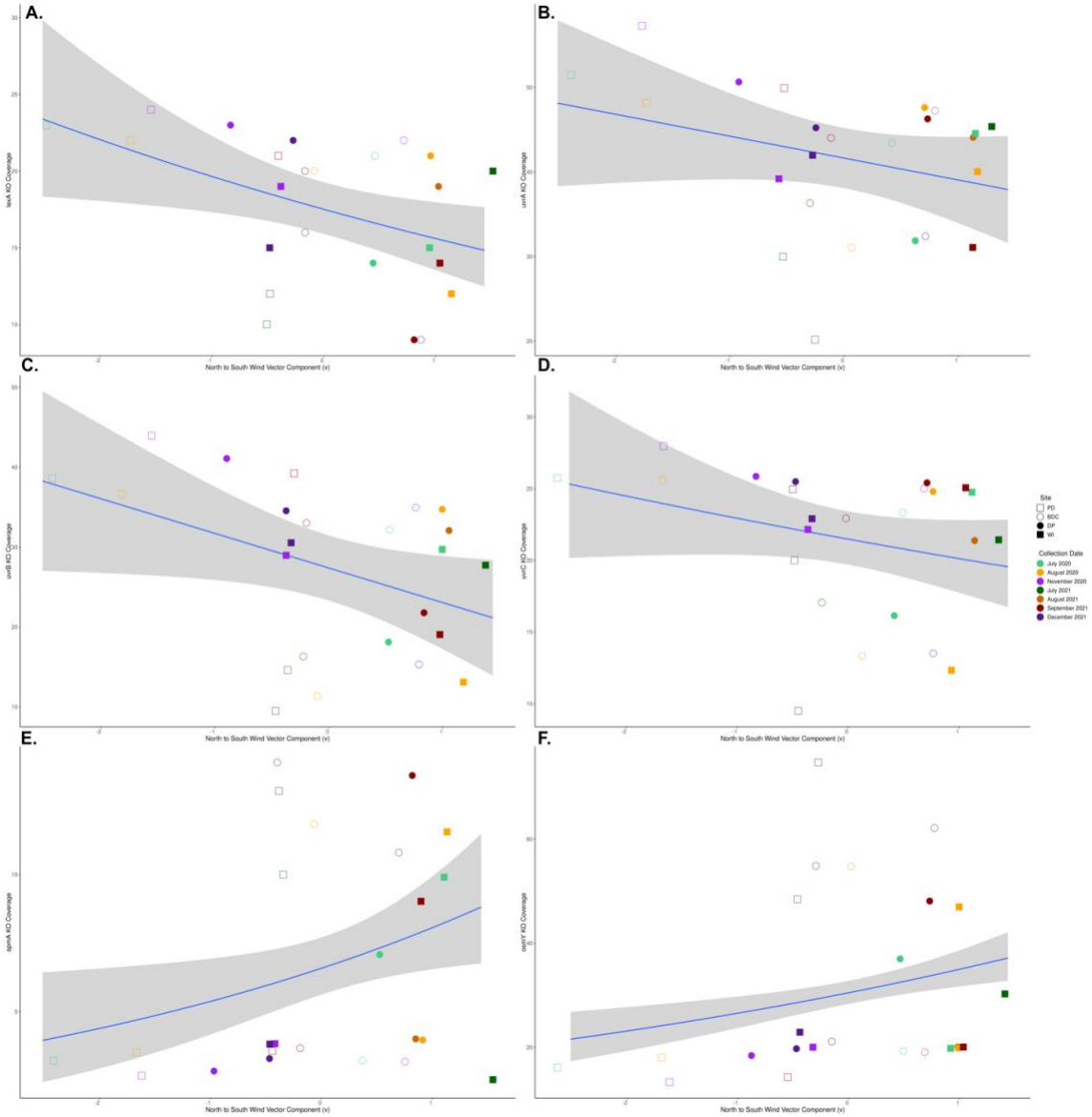

Figure C.1.7. UV Radiation Resistance Genes *lexA* (A), *uvrA* (B), *uvrB* (C), *uvrC* (D), *spmA* (E), and *osmY* (F) plotted against the Meridional Wind Component (north-south, v). These scatterplots show how the normalized coverages of these genes decreases (*lexA*, *uvrA*, *uvrB*, *uvrC*) or increases (*spmA*, *osmY*) with the meridional wind component. Most points to the left of the center of the x-axis are northerly winds, whereas points to the right of the center are southerly winds.

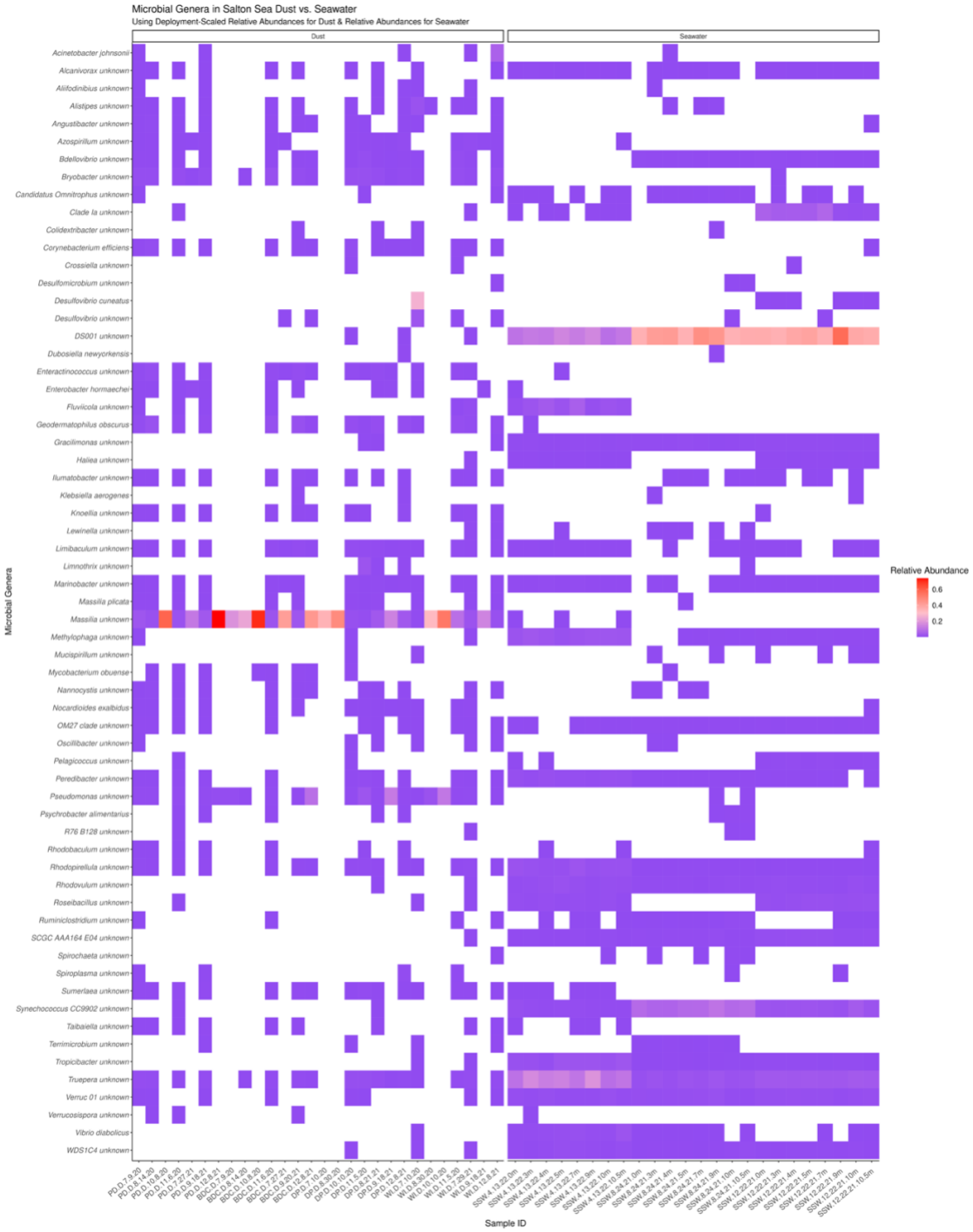

Figure C.1.8. Bacterial Genera Shared between Salton Sea Dust and Lake Water. This heatmap shows the relative abundance of bacterial genera that were found in both Salton Sea dust (Ch III) and lake water (Ch II). Each column is a sample, with dust samples on the left and seawater samples on the right. The values displayed for the dust samples were first scaled based on dust collector deployment duration by days before

calculating relative abundance, whereas the relative abundance for seawater samples was not scaled before calculating.

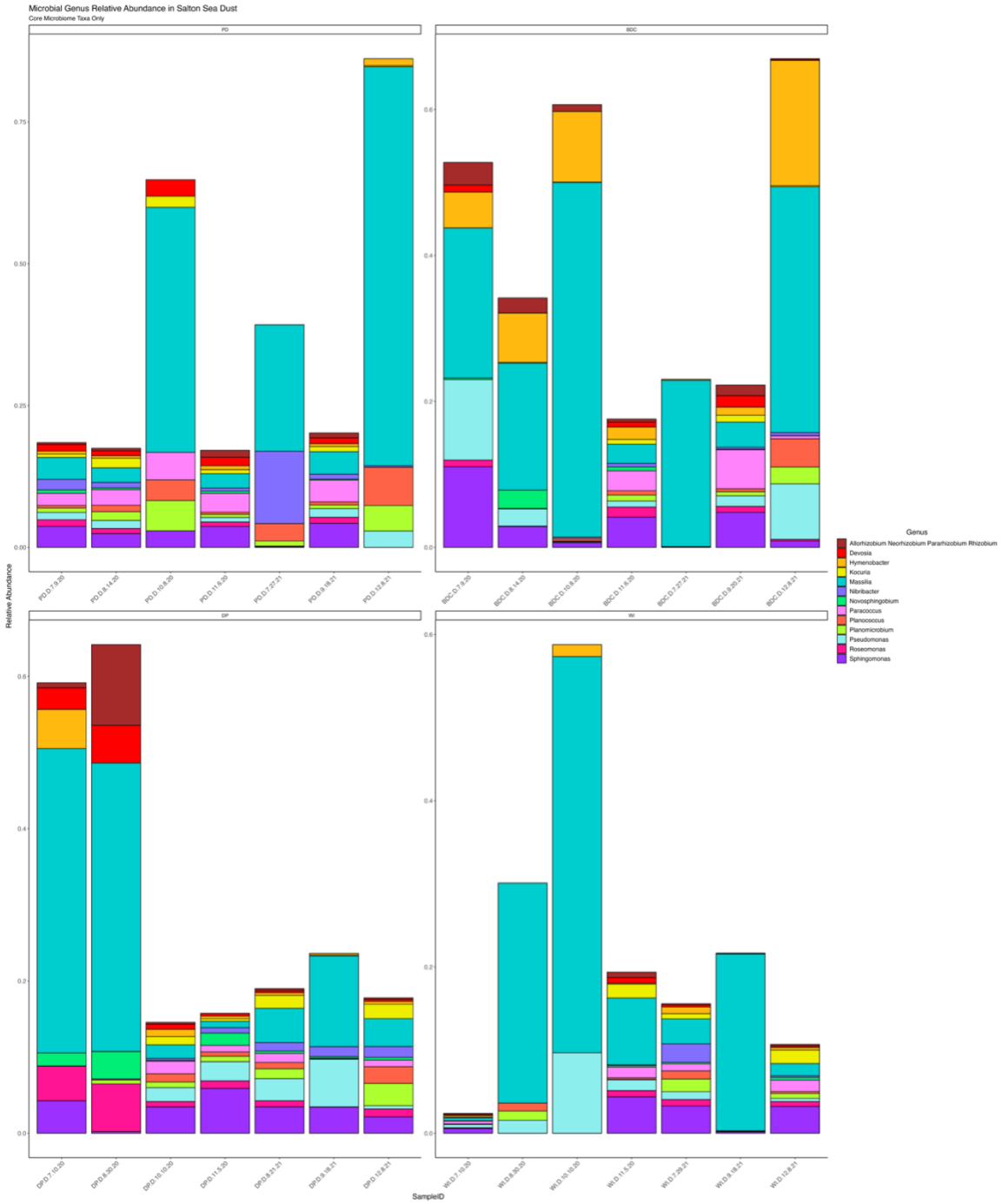

Figure C.1.9. Core Microbiome Bacterial Genera by Sample and Site. These stacked bar plots show the relative abundance of bacterial genera that were found in the core dust microbiome from the Salton Sea. Each column represents a sample, and samples are organized from left to right by collection date, then site (PD, BDC, DP, and WI).

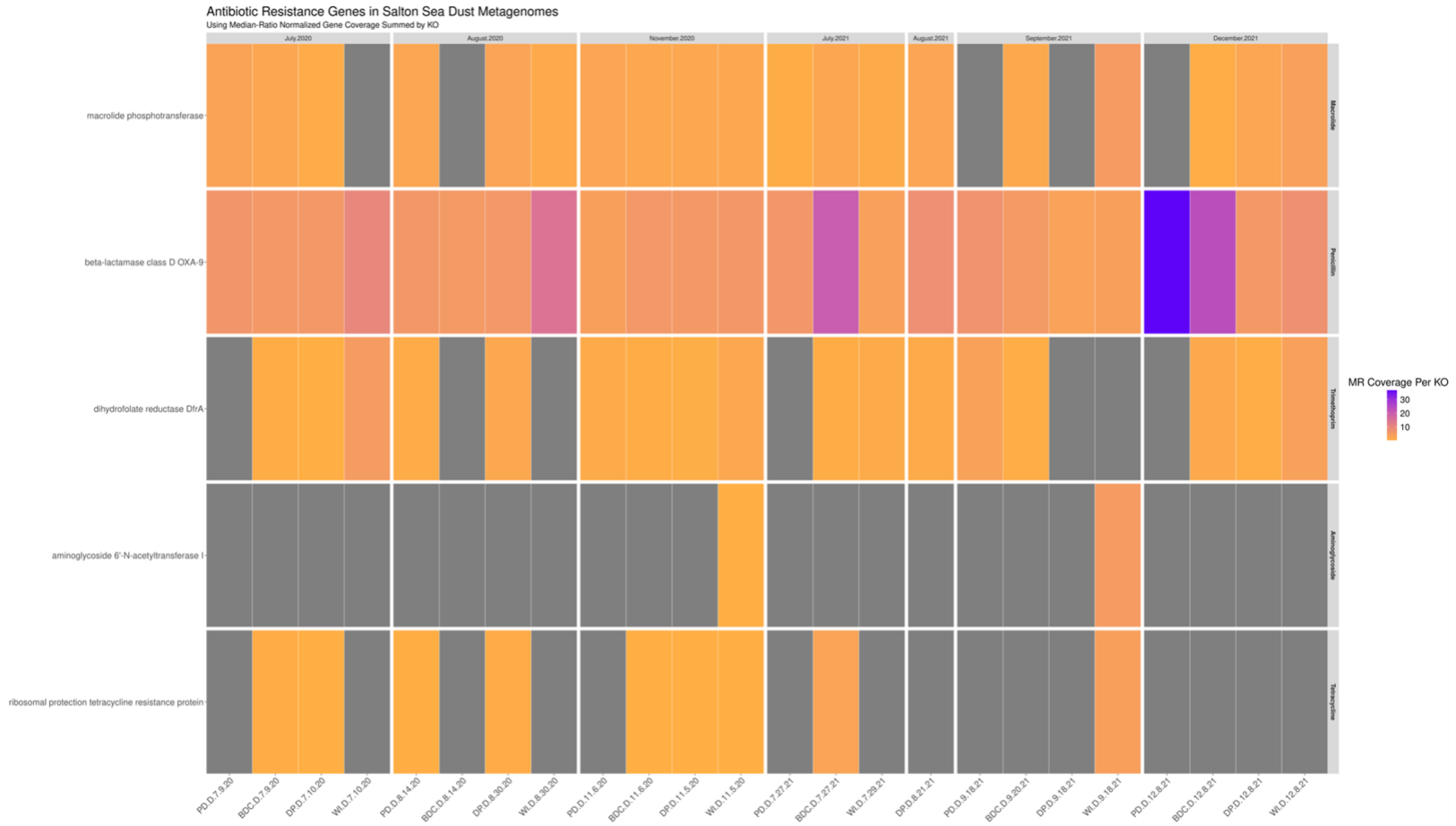

Figure C.1.10. Heatmap of Antibiotic Resistance Genes in the Dust Metagenomes. This heatmap shows the normalized coverage (median-ratio normalized, scaled coverages) of antibiotic resistance genes (ARGs) in the metagenomes. Each column represents a metagenome and the metagenomes are organized by collection date from left to right. Gray squares indicate that the gene is absent.

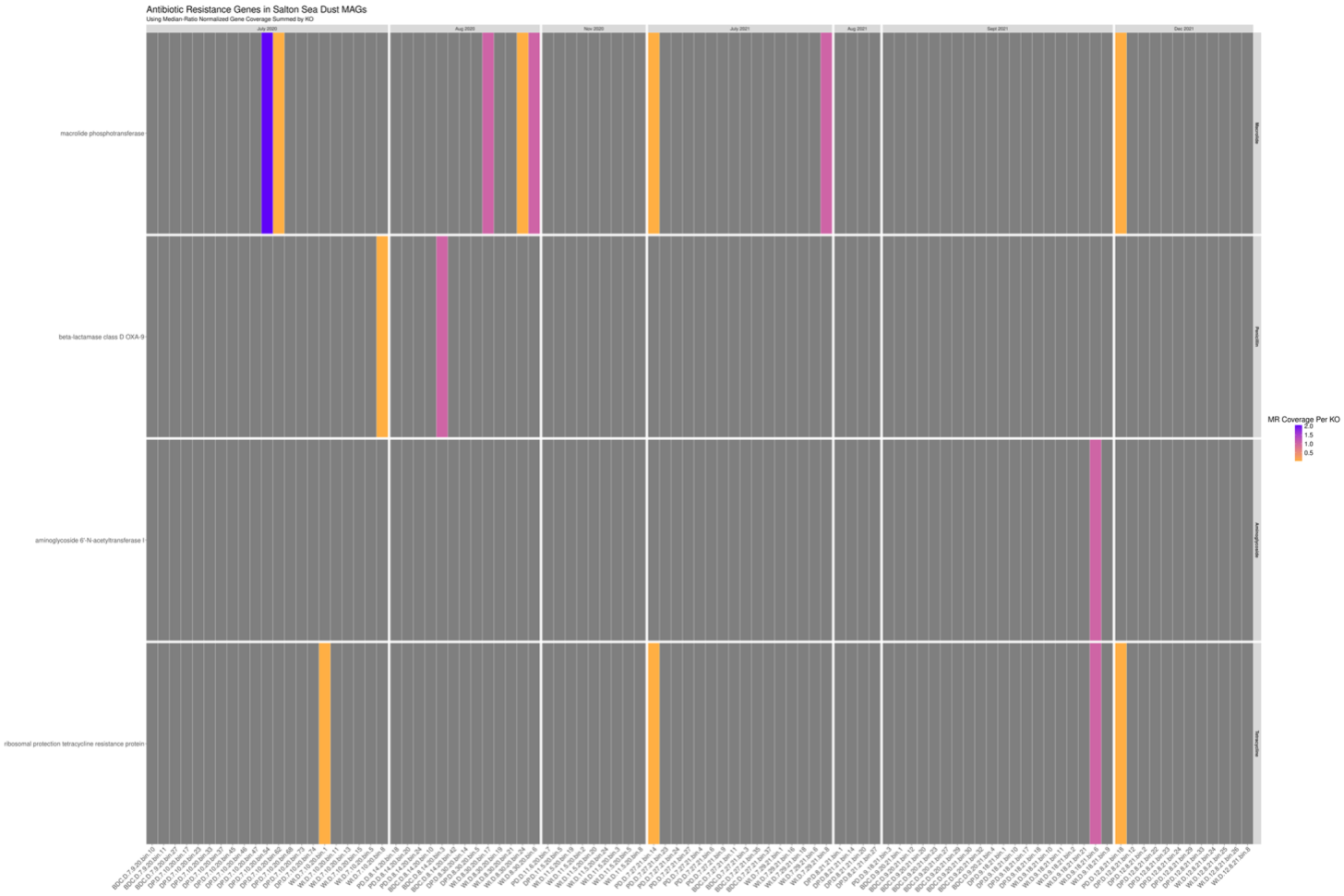

Figure C.1.11. Heatmap of Antibiotic Resistance Genes in the Metagenome Assembled Genomes (MAGs). This heatmap shows the normalized coverage (median-ratio normalized, scaled coverages) of antibiotic resistance genes (ARGs) in the MAGs. Each column represents a MAG, and the MAGs are organized by collection date from left to right. Gray squares indicate that the gene is absent.

Sample ID	Site	Collection Year	Sample Month	Deployment Date	Collection Date	Deployment Duration	Latitude	Longitude
PD.D.7.9.20	PD	2020	July	5/13/20	7/9/20	57	33.773808	-116.35286
PD.D.8.14.20	PD	2020	August	7/9/20	8/14/20	36	33.773808	-116.35286
PD.D.10.8.20	PD	2020	October	8/14/20	10/8/20	55	33.773808	-116.35286
PD.D.11.6.20	PD	2020	November	10/8/20	11/6/20	29	33.773808	-116.35286
PD.D.7.27.21	PD	2021	July	6/5/21	7/27/21	52	33.773808	-116.35286
PD.D.9.18.21	PD	2021	September	7/27/21	9/18/21	53	33.773808	-116.35286
PD.D.12.8.21	PD	2021	December	9/18/21	12/8/21	81	33.773808	-116.35286
BDC.D.7.9.20	BDC	2020	July	5/13/20	7/9/20	57	33.6516667	-116.37264
BDC.D.8.14.20	BDC	2020	August	7/9/20	8/14/20	36	33.6516667	-116.37264
BDC.D.10.8.20	BDC	2020	October	8/14/20	10/8/20	55	33.6516667	-116.37264
BDC.D.11.6.20	BDC	2020	November	10/8/20	11/6/20	29	33.6516667	-116.37264
BDC.D.7.27.21	BDC	2021	July	6/5/21	7/27/21	52	33.6516667	-116.37264
BDC.D.9.20.21	BDC	2021	September	7/27/21	9/20/21	55	33.6516667	-116.37264
BDC.D.12.8.21	BDC	2021	December	9/29/21	12/8/21	70	33.6516667	-116.37264
DP.D.7.10.20	DP	2020	July	6/1/20	7/10/20	39	33.48859	-115.83517
DP.D.8.30.20	DP	2020	August	7/10/20	8/30/20	51	33.48859	-115.83517
DP.D.10.10.20	DP	2020	October	8/30/20	10/10/20	41	33.48859	-115.83517
DP.D.11.5.20	DP	2020	November	10/10/20	11/5/20	26	33.48859	-115.83517
DP.D.8.21.21	DP	2021	August	6/8/21	8/19/21	72	33.48859	-115.83517
DP.D.9.18.21	DP	2021	September	8/19/21	9/18/21	30	33.48859	-115.83517
DP.D.12.8.21	DP	2021	December	9/18/21	12/8/21	81	33.48859	-115.83517
WI.D.7.10.20	WI	2020	July	6/1/20	7/10/20	39	33.283861	-115.60008
WI.D.8.30.20	WI	2020	August	7/10/20	8/30/20	51	33.283861	-115.60008
WI.D.10.10.20	WI	2020	October	8/30/20	10/10/20	41	33.283861	-115.60008
WI.D.11.5.20	WI	2020	November	10/10/20	11/5/20	26	33.283861	-115.60008
WI.D.7.29.21	WI	2021	July	6/8/21	7/29/21	51	33.283861	-115.60008
WI.D.9.18.21	WI	2021	September	7/29/21	9/18/21	51	33.283861	-115.60008
WI.D.12.8.21	WI	2021	December	9/18/21	12/8/21	81	33.283861	-115.60008

Table C.2.1. Sample Metadata. This table details the metadata for each sample. PD represents Palm Desert, BDC represents Boyd Deep Canyon, DP represents Dos Palmas, and WI represents Wister.

SampleID	STID	Precip.STID	Deploy Date	Collect Date	Ave. Accum. Precip (24hr)	Ave. Air Temp	Ave. Wind Speed	Ave. Relative Humidity	Ave. Wind Component u (E-W)	Ave. Wind Component v (N-S)
PD.D.7.9.20	CI200	C2285	5/13/20	7/9/20	0	31.6192405	3.17936125	30.5940233	1.44284857	-1.7500013
WI.D.7.10.20	CQ125	D3583	6/1/20	7/10/20	0	31.4917673	3.20078266	27.5925357	0.21191109	1.1614761
DP.D.7.10.20	DPMC1	COOPMCAC1	6/1/20	7/10/20	0	32.363759	2.11469002	24.6093418	0.33744625	0.72253833
BDC.D.7.9.20	UCDE	COOPDEEC1	5/13/20	7/9/20	0	29.800629	2.89061972	22.0888646	0.10022889	0.65080543
PD.D.8.14.20	CI200	C2285	7/9/20	8/14/20	0	36.6467379	2.87533448	26.9252874	1.08484132	-1.0977327
WI.D.8.30.20	CQ125	D3583	7/10/20	8/30/20	0	35.6510586	2.69738355	31.4058632	-0.5215483	1.21374693
DP.D.8.30.20	DPMC1	COOPMCAC1	7/10/20	8/30/20	0	36.3095279	1.88516995	28.3029557	0.15674952	1.03202101
BDC.D.8.14.20	UCDE	COOPDEEC1	7/9/20	8/14/20	0	34.584064	2.40315613	17.6465517	-0.3452522	0.35372597
PD.D.10.8.20	CI200	C2285	8/14/20	10/8/20	0	32.7084236	2.19324196	33.6508058	0.62860594	-0.3656956
WI.D.10.10.20	CQ125	D3583	8/30/20	10/10/20	0	30.9193939	2.23787677	31.9631313	-0.8053231	0.41322402
DP.D.10.10.20	DPMC1	COOPMCAC1	8/30/20	10/10/20	0	31.9323771	1.49573407	24.5995956	0.11249049	0.45022024
BDC.D.10.8.20	UCDE	COOPDEEC1	8/14/20	10/8/20	0	34.3467205	2.48082334	17.7515083	0.11591291	0.65468414
PD.D.11.6.20	CI200	C2285	10/8/20	11/6/20	0	24.3785977	2.27683595	37.6091298	1.07231029	-1.062306
WI.D.11.5.20	CQ125	D3583	10/10/20	11/5/20	0	23.5542265	2.4398756	36.100319	-0.1189558	-0.0414189
DP.D.11.5.20	DPMC1	COOPMCAC1	10/10/20	11/5/20	0	25.0017599	1.63676312	25.0063593	0.58507038	-0.3522882
BDC.D.11.6.20	UCDE	COOPDEEC1	10/8/20	11/6/20	0	29.8421252	2.58693316	19.1742809	0.77225557	0.86968527
PD.D.7.27.21	CI200	C2285	6/5/21	7/27/21	0.22632446	35.177882	2.92311164	29.6523126	0.97276723	-0.0770987
WI.D.7.29.21	CQ125	D3583	6/8/21	7/29/21	0.29323005	34.6982114	2.92981626	32.5853659	-1.0305128	1.51636973
DP.D.8.21.21	DPMC1	COOPMCAC1	6/8/21	8/19/21	0	36.2092131	2.07629194	32.0076516	0.04857882	1.15186789
BDC.D.7.27.21	UCDE	COOPDEEC1	6/5/21	7/27/21	0.48768	34.7081867	2.32900484	20.4458576	-0.5772526	0.12069683
PD.D.9.18.21	CI200	C2285	7/27/21	9/18/21	0.0395233	34.0172514	2.59678712	34.6449332	0.76791974	-0.0186239
WI.D.9.18.21	CQ125	D3583	7/29/21	9/18/21	0.2486511	34.0477588	2.61034694	38.7784026	-0.8598018	1.16034868
DP.D.9.18.21	DPMC1	COOPMCAC1	8/19/21	9/18/21	0.21166667	34.5156171	1.72249174	36.3112948	0.06495099	0.9728898
BDC.D.9.20.21	UCDE	COOPDEEC1	7/27/21	9/20/21	0.13854545	32.9690504	2.19504593	26.7910129	-0.4308111	0.28229088
PD.D.12.8.21	CI200	C2285	9/18/21	12/8/21	0.02522125	22.0988492	2.25398153	37.7321703	1.07625653	-0.6142271
WI.D.12.8.21	CQ125	D3583	9/18/21	12/8/21	0.00717957	21.413641	2.33039897	40.4497436	0.10867062	0.03284329
DP.D.12.8.21	DPMC1	COOPMCAC1	9/18/21	12/8/21	0	23.3848234	1.64802729	30.438208	0.60341188	0.00521018
BDC.D.12.8.21	UCDE	COOPDEEC1	9/29/21	12/8/21	0.09012903	23.7779629	2.55024971	19.9816397	0.94124775	1.00408106

Table C.2.2. Sample Climate and Precipitation Data. This table contains the wind condition data and precipitation data from Synoptic. The precipitation data includes the average, accumulated precipitation (in a 24-hour period). The wind data includes average air temperature, average wind speed, average relative humidity, the average zonal wind component (east-west, u), and meridional wind component (north-south, v).

SampleID	Date Start	Date End	Barren Land	Crop Land	Developed	Forest	Herbaceous	Mexico	Open Water	Others	Salton Sea	Shrub
BDC.D.7.9.20	5/13/20	7/10/20	0.07322056	0.01297334	0.14651081	0.02503976	0.06772567	0.00604489	0.016034	0.01004535	2.69e-06	0.64240294
BDC.D.8.14.20	7/10/20	8/30/20	0.02367024	0.0146429	0.12042544	0.032043	0.07802577	0.00198004	0.01920307	0.014634	0.00019225	0.6951833
BDC.D.10.8.20	8/30/20	10/10/20	0.13443645	0.01089365	0.13340866	0.01440556	0.04611422	5.8e-05	0.00294073	0.00475144	0.00052367	0.65246762
BDC.D.11.6.20	10/10/20	11/6/20	0.18093467	0.00680144	0.10053623	0.00868282	0.04070882	0	0.00103723	0.00198321	6.65e-05	0.65924912
BDC.D.7.27.21	6/5/21	8/19/21	0.0681913	0.01551662	0.11158094	0.03471532	0.07214976	0.00440204	0.00669423	0.01092161	0.00048259	0.6753456
BDC.D.9.20.21	8/19/21	10/1/21	0.16206552	0.02308375	0.09404165	0.02603989	0.05451374	0.01118828	0.00791524	0.00963109	0.00106754	0.61045329
BDC.D.12.8.21	10/1/21	12/8/21	0.12686537	0.0135476	0.13669878	0.01164132	0.04738955	0	0.01735052	0.00527006	4.74e-05	0.64118935
DP.D.7.10.20	5/13/20	7/10/20	0.3425539	0.03768778	0.05103636	0.0052857	0.02849791	0.01015245	0.00231048	0.00759165	0.08074333	0.43414044
DP.D.8.30.20	7/10/20	8/30/20	0.35894683	0.04741788	0.05094149	0.00539539	0.02106017	0.00365814	0.00221514	0.00818428	0.08859748	0.4135832
DP.D.10.10.20	8/30/20	10/10/20	0.30053338	0.02469771	0.03382912	0.00265595	0.04263803	0.00132635	0.0003168	0.00746317	0.01244322	0.57409628
DP.D.11.5.20	10/10/20	11/6/20	0.18618336	0.00928874	0.02733272	0.00324026	0.06784859	4.4e-06	0.00052345	0.00358963	0.00123141	0.70075744
DP.D.8.21.21	6/5/21	8/19/21	0.38694083	0.05133939	0.05987361	0.00382841	0.02037435	0.00892055	0.00069019	0.00823634	0.0924024	0.36739392
DP.D.9.18.21	8/19/21	10/1/21	0.34635375	0.06346146	0.03868698	0.00385657	0.02248277	0.01872453	0.00038984	0.01222721	0.14363171	0.35018519
DP.D.12.8.21	10/1/21	12/8/21	0.19903967	0.02407875	0.04713999	0.00413071	0.05948762	0.00133103	0.00736264	0.00678254	0.00963938	0.64100769
PD.D.7.9.20	5/13/20	7/10/20	0.10861349	0.01199928	0.30194873	0.01816956	0.05927331	0.00299202	0.00974925	0.00803661	1.82e-06	0.47921594
PD.D.8.14.20	7/10/20	8/30/20	0.05853381	0.01623364	0.36434508	0.02079035	0.07135971	0.00070631	0.0107935	0.00828889	6.45e-05	0.44888419
PD.D.10.8.20	8/30/20	10/10/20	0.17780306	0.00940879	0.18829575	0.00962776	0.04294059	0	0.0013125	0.00345215	0.00036642	0.56679299
PD.D.11.6.20	10/10/20	11/6/20	0.20801019	0.00330571	0.09345096	0.00801725	0.04145163	0	0.00081306	0.00132809	5.42e-06	0.64361768
PD.D.7.27.21	6/5/21	8/19/21	0.09970635	0.01665161	0.34421231	0.0193936	0.05673494	0.00167123	0.00455538	0.00706927	0.0009234	0.44908191
PD.D.9.18.21	8/19/21	10/1/21	0.13978181	0.02860087	0.3145067	0.017189	0.05098705	0.00471429	0.00417088	0.00765748	0.00837097	0.42402096
PD.D.12.8.21	10/1/21	12/8/21	0.18101446	0.00704376	0.16126502	0.00887213	0.04736612	0	0.01273217	0.00346016	1.47e-05	0.57823151
WI.D.7.10.20	5/13/20	7/10/20	0.45672618	0.05665537	0.03012024	0.0022247	0.02777861	0.02719231	0.00126884	0.01274943	0.14920259	0.23608173
WI.D.8.30.20	7/10/20	8/30/20	0.50702475	0.05586727	0.02779496	0.002216	0.01756764	0.01832024	0.00085284	0.01389667	0.18704336	0.16941627
WI.D.10.10.20	8/30/20	10/10/20	0.37051278	0.06611746	0.02867629	0.00135519	0.05782299	0.00933686	0.00023521	0.01407066	0.03993598	0.41193659
WI.D.11.5.20	10/10/20	11/6/20	0.22655944	0.02693476	0.01637446	0.00065457	0.09026512	0.00052604	0.00184687	0.00462337	0.00323696	0.62897841
WI.D.7.29.21	6/5/21	8/19/21	0.42048804	0.09138852	0.03429356	0.00201323	0.02025885	0.04146066	0.00041462	0.01784795	0.19155439	0.18028019
WI.D.9.18.21	8/19/21	10/1/21	0.39852806	0.1301901	0.02982851	0.00137064	0.02558595	0.0519148	0.0005992	0.02287856	0.15902737	0.1800768
WI.D.12.8.21	10/1/21	12/8/21	0.29890757	0.04348993	0.03635549	0.00276938	0.06039352	0.00550029	0.00628978	0.00802298	0.0310373	0.50723375

Table C.2.3. Surface Type Frequencies. This table contains the surface type frequencies for each sample. The categories for the surface types are Barren Land, Crop Land, Developed, Forest, Herbaceous, Mexico, Open Water, Others (i.e., not within surfaces listed), Salton Sea, and Shrub. The surface type frequencies for each sample total to one.

Sample ID	Bin Num	Taxa Level	Marker Lineage	Lineage ID	Genome Num	Completeness	Contamination	Strain Heterogeneity	GC_Content
DP_D_8_21_21_A	bin.1	o	Actinomycetales	(UID1590)	562	98.46	0.11	50	70.3
DP_D_8_21_21_A	bin.14	c	Alphaproteobacteria	(UID3305)	564	98.69	4.41	7.14	67.5
DP_D_8_21_21_A	bin.20	c	Gammaproteobacteria	(UID4267)	119	98.89	2.46	6.25	67.4
DP_D_8_21_21_A	bin.27	c	Bacilli	(UID285)	586	92.53	0.72	50	50.7
BDC_D_9_20_21_B	bin.1	o	Bacillales	(UID828)	139	89.66	0	0	38.6
BDC_D_9_20_21_B	bin.12	c	Bacilli	(UID285)	586	83.48	0.72	50	51.2
BDC_D_9_20_21_B	bin.20	p	Bacteroidetes	(UID2605)	350	86.27	1.32	100	40.7
BDC_D_9_20_21_B	bin.23	k	Bacteria	(UID203)	5449	81.93	0.88	100	61.4
BDC_D_9_20_21_B	bin.27	o	Actinomycetales	(UID1590)	562	97.27	0.06	0	70.3
BDC_D_9_20_21_B	bin.29	c	Gammaproteobacteria	(UID4202)	67	98.55	0	0	61.9
BDC_D_9_20_21_B	bin.30	c	Gammaproteobacteria	(UID4267)	119	98.54	2.29	7.69	67.6
BDC_D_9_20_21_B	bin.32	o	Burkholderiales	(UID4002)	107	80.8	3.29	36.84	65.5
BDC_D_9_20_21_B	bin.4	c	Gammaproteobacteria	(UID4387)	965	83.18	2.07	54.55	33.9
WI_D_7_29_21_A	bin.1	c	Bacilli	(UID285)	586	93.1	0.72	50	50.7
WI_D_7_29_21_A	bin.16	o	Actinomycetales	(UID1590)	562	99.06	0.7	25	70.3
WI_D_7_29_21_A	bin.18	o	Rhodospirillales	(UID3754)	63	98.91	0	0	57.1
WI_D_7_29_21_A	bin.6	c	Gammaproteobacteria	(UID4201)	1164	99.43	1.15	0	47.5
WI_D_7_29_21_A	bin.8	o	Actinomycetales	(UID1593)	69	96.36	1.3	16.67	72.7
PD_D_11_6_20_B	bin.7	c	Gammaproteobacteria	(UID4202)	67	98.55	0	0	61.9
BDC_D_12_8_21_A	bins.30	c	Bacilli	(UID259)	750	96.52	0.99	50	43.3
BDC_D_12_8_21_A	bins.6	o	Clostridiales	(UID1212)	172	87.25	0	0	48.8
BDC_D_11_6_20_A	bins.11	c	Alphaproteobacteria	(UID3305)	564	85.92	3.86	87.5	45.2
BDC_D_11_6_20_A	bins.15	c	Bacilli	(UID285)	586	89.94	0.72	50	50.7
BDC_D_11_6_20_A	bins.20	c	Gammaproteobacteria	(UID4202)	67	98.55	0	0	61.9
BDC_D_11_6_20_A	bins.25	o	Actinomycetales	(UID1590)	562	98.46	0.26	33.33	70.3
BDC_D_8_14_20_A	bin.10	p	Bacteroidetes	(UID2605)	350	96.16	4.35	53.85	40.8
BDC_D_8_14_20_A	bin.3	o	Rhizobiales	(UID3447)	356	98.39	1.21	0	66.2
BDC_D_8_14_20_A	bin.42	o	Cytophagales	(UID2936)	47	98.21	0.6	0	52.5
DP_D_8_30_20_A	bin.14	o	Actinomycetales	(UID1590)	562	98.46	0.82	16.67	70.3
DP_D_8_30_20_A	bin.5	c	Bacilli	(UID285)	586	90.09	0.72	50	51.1

DP_D_12_8_21_B	bin.12	c	Alphaproteobacteria	(UID3305)	564	98.69	4.41	7.14	67.5
DP_D_12_8_21_B	bin.2	k	Bacteria	(UID2495)	2993	98.77	0.62	100	25
DP_D_12_8_21_B	bin.22	c	Gammaproteobacteria	(UID4444)	263	90.84	2.92	12.5	54.5
DP_D_12_8_21_B	bin.23	c	Bacilli	(UID285)	586	91.38	0.72	50	50.7
DP_D_12_8_21_B	bin.24	o	Actinomycetales	(UID1590)	562	98.46	0.11	50	70.3
DP_D_12_8_21_B	bin.29	c	Gammaproteobacteria	(UID4267)	119	98.54	2.64	7.14	67.5
DP_D_12_8_21_B	bin.33	o	Actinomycetales	(UID1530)	622	95.86	2.96	83.33	60.2
BDC_D_7_9_20_A	bin.10	o	Actinomycetales	(UID1590)	562	99.06	0.11	50	70.3
BDC_D_7_9_20_A	bin.11	c	Bacilli	(UID285)	586	92.53	0.72	50	50.7
BDC_D_7_9_20_A	bin.27	k	Bacteria	(UID2495)	2993	97.18	0	0	23.2
DP_D_7_10_20_C	bin.17	o	Rhizobiales	(UID3447)	356	96.43	1.02	0	61
DP_D_7_10_20_C	bin.23	o	Burkholderiales	(UID4000)	193	92.4	4.19	15.38	68
DP_D_7_10_20_C	bin.33	o	Burkholderiales	(UID4000)	193	89.68	4.63	56.25	65.4
DP_D_7_10_20_C	bin.37	o	Rhodospirillales	(UID3754)	63	90.69	3.61	7.69	69.5
DP_D_7_10_20_C	bin.45	o	Cytophagales	(UID2936)	47	95.89	1.34	20	61.3
DP_D_7_10_20_C	bin.46	k	Bacteria	(UID203)	5449	80.34	0	0	68.4
DP_D_7_10_20_C	bin.47	o	Sphingomonadales	(UID3310)	26	97.78	0.46	75	65.9
DP_D_7_10_20_C	bin.54	f	Micrococcaceae	(UID1631)	31	95.03	0.55	25	65.9
DP_D_7_10_20_C	bin.62	o	Actinomycetales	(UID1593)	69	93.98	2.53	0	67.8
DP_D_7_10_20_C	bin.68	o	Cytophagales	(UID2936)	47	99.7	0.6	0	52.5
DP_D_7_10_20_C	bin.73	c	Alphaproteobacteria	(UID3422)	26	83.32	3.29	82.35	66.1
DP_D_7_10_20_C	bin.74	p	Proteobacteria	(UID3887)	1487	97.56	1.98	25	64.6
WI_D_8_30_20_B	bin.17	o	Actinomycetales	(UID1593)	69	97.38	2.95	18.18	67.2
WI_D_8_30_20_B	bin.19	g	Burkholderia	(UID4006)	64	92.68	2.98	42.86	59.3
WI_D_8_30_20_B	bin.21	o	Cytophagales	(UID2936)	47	90.18	0.3	100	45.9
WI_D_8_30_20_B	bin.24	o	Actinomycetales	(UID1593)	69	94.9	2.98	36.36	68.5
WI_D_8_30_20_B	bin.6	o	Actinomycetales	(UID1593)	69	99.49	4.25	31.25	64.1
PD_D_9_18_21_C	bin.3	c	Gammaproteobacteria	(UID4202)	67	98.55	0	0	61.9
DP_D_11_5_20_A	bin.5	o	Actinomycetales	(UID1590)	562	97.87	1.4	0	70.3
BDC_D_7_27_21_A	bin.11	k	Bacteria	(UID203)	5449	82.14	0.89	0	45.3
BDC_D_7_27_21_A	bin.3	f	Bacillaceae	(UID829)	128	80.59	3.28	51.72	42.2
BDC_D_7_27_21_A	bin.35	o	Burkholderiales	(UID4000)	193	92.12	2.44	33.33	65.7

BDC_D_7_27_21_A	bin.37	o	Bacillales	(UID828)	139	89.63	1.6	0	49.1
PD_D_12_8_21_A	bin.18	c	Bacilli	(UID259)	750	96.52	0.99	50	43.3
DP_D_9_8_21_B	bin.1	c	Gammaproteobacteria	(UID4387)	965	96.74	0.14	100	34.3
DP_D_9_8_21_B	bin.10	c	Gammaproteobacteria	(UID4444)	263	95.98	0.52	0	35.7
DP_D_9_8_21_B	bin.17	c	Alphaproteobacteria	(UID3305)	564	82.35	2.53	81.82	45.2
DP_D_9_8_21_B	bin.18	o	Burkholderiales	(UID4002)	107	94.74	2.5	13.64	62.6
WI_D_9_18_21_A	bin.10	f	Enterobacteriaceae	(UID5124)	134	96.68	2.16	55.17	55.3
WI_D_9_18_21_A	bin.11	f	Moraxellaceae	(UID4680)	86	95.39	0.27	0	39
WI_D_9_18_21_A	bin.2	c	Bacilli	(UID259)	750	96.05	1.32	100	47.4
WI_D_9_18_21_A	bin.21	o	Bacillales	(UID828)	139	91.11	1.99	12.5	49.6
WI_D_9_18_21_A	bin.6	o	Bacillales	(UID828)	139	98.28	0.03	0	38.4
WI_D_9_18_21_A	bin.9	o	Bacillales	(UID828)	139	96.52	1.73	0	48.8
WI_D_12_8_21_A	bin.24	o	Actinomycetales	(UID1590)	562	98.46	0.11	50	70.3
WI_D_12_8_21_A	bin.25	c	Spirochaetia	(UID2496)	72	98.13	0	0	27.3
WI_D_12_8_21_A	bin.26	c	Bacilli	(UID285)	586	92.53	0.72	50	50.7
WI_D_12_8_21_A	bin.8	o	Rhodospirillales	(UID3754)	63	98.91	0	0	57.1
PD_D_8_14_20_B	bin.18	o	Actinomycetales	(UID1590)	562	98.46	0.11	50	70.3
PD_D_8_14_20_B	bin.20	c	Bacilli	(UID285)	586	92.53	0.72	50	50.7
PD_D_8_14_20_B	bin.24	c	Gammaproteobacteria	(UID4202)	67	98.55	0	0	61.9
WI_D_7_10_20_A	bin.1	o	Clostridiales	(UID1212)	172	90.94	0	0	43.3
WI_D_7_10_20_A	bin.11	o	Actinomycetales	(UID1590)	562	98.46	0.11	50	70.3
WI_D_7_10_20_A	bin.13	c	Spirochaetia	(UID2496)	72	98.13	0	0	27.5
WI_D_7_10_20_A	bin.15	c	Deltaproteobacteria	(UID3218)	61	97.04	0.59	100	45.5
WI_D_7_10_20_A	bin.5	c	Bacilli	(UID285)	586	92.53	0.72	50	50.7
WI_D_7_10_20_A	bin.8	o	Bacteroidales	(UID2621)	198	94.04	0.96	0	37.1
WI_D_11_5_20_A	bin.19	c	Bacilli	(UID285)	586	91.38	0.72	50	50.7
WI_D_11_5_20_A	bin.2	k	Bacteria	(UID2495)	2993	98.77	0.62	100	25
WI_D_11_5_20_A	bin.20	o	Burkholderiales	(UID4001)	108	96.88	4.07	10	66.3
WI_D_11_5_20_A	bin.24	c	Spirochaetia	(UID2496)	72	88	0	0	27.3
WI_D_11_5_20_A	bin.3	o	Actinomycetales	(UID1590)	562	98.46	0.11	50	70.3
WI_D_11_5_20_A	bin.5	o	Rhodospirillales	(UID3754)	63	98.91	0	0	57.1
WI_D_11_5_20_A	bin.8	k	Bacteria	(UID2495)	2993	97.18	0	0	23.2

PD_D_7_27_21_A	bin.14	k	Bacteria	(UID203)	5449	81.03	1.72	0	52.3
PD_D_7_27_21_A	bin.23	p	Proteobacteria	(UID3887)	1487	82.61	0.62	0	71.6
PD_D_7_27_21_A	bin.24	c	Alphaproteobacteria	(UID3305)	564	99.57	0.04	0	63.9
PD_D_7_27_21_A	bin.27	o	Bacillales	(UID828)	139	81.34	1.99	12.5	49.8
PD_D_7_27_21_A	bin.4	f	Bacillaceae	(UID829)	128	82.49	2.73	53.57	42.2
PD_D_7_27_21_A	bin.6	f	Moraxellaceae	(UID4680)	86	93.74	0	0	38.8
PD_D_7_27_21_A	bin.9	o	Bacillales	(UID828)	139	94.23	1.64	0	49

Table C.2.4. CheckM Results for Metagenome-Assembled Genomes (MAGs) Bin Assignments. This table contains the CheckM results for each putative, high-quality MAG bin assignment.

Bin.ID	Domain	Phylum	Class	Order	Family	Genus	Species
WI.D.7.29.21.A.bin.8	Bacteria	Actinobacteriota	Actinomycetia	Actinomycetales	Microbacteriaceae	Curtobacterium	Curtobacterium sp001705035
WI.D.8.30.20.B.bin.17	Bacteria	Actinobacteriota	Actinomycetia	Actinomycetales	Microbacteriaceae	Frondihabitans	Unknown
WI.D.8.30.20.B.bin.24	Bacteria	Actinobacteriota	Actinomycetia	Actinomycetales	Microbacteriaceae	Frondihabitans	Unknown
WI.D.8.30.20.B.bin.6	Bacteria	Actinobacteriota	Actinomycetia	Actinomycetales	Microbacteriaceae	Mycetocola_A	Unknown
DP.D.7.10.20.C.bin.62	Bacteria	Actinobacteriota	Actinomycetia	Actinomycetales	Microbacteriaceae	Okibacterium	Unknown
DP.D.7.10.20.C.bin.54	Bacteria	Actinobacteriota	Actinomycetia	Actinomycetales	Micrococcaceae	Pseudarthrobacter	Pseudarthrobacter phenanthrenivorans
BDC.D.11.6.20.A.bins.25	Bacteria	Actinobacteriota	Actinomycetia	Mycobacteriales	Mycobacteriaceae	Corynebacterium	Corynebacterium sp012838715
BDC.D.7.9.20.A.bin.10	Bacteria	Actinobacteriota	Actinomycetia	Mycobacteriales	Mycobacteriaceae	Corynebacterium	Corynebacterium sp012838715
BDC.D.9.20.21.B.bin.27	Bacteria	Actinobacteriota	Actinomycetia	Mycobacteriales	Mycobacteriaceae	Corynebacterium	Corynebacterium sp012838715
DP.D.11.5.20.A.bin.5	Bacteria	Actinobacteriota	Actinomycetia	Mycobacteriales	Mycobacteriaceae	Corynebacterium	Corynebacterium sp012838715
DP.D.12.8.21.B.bin.24	Bacteria	Actinobacteriota	Actinomycetia	Mycobacteriales	Mycobacteriaceae	Corynebacterium	Corynebacterium sp012838715
DP.D.8.21.21.A.bin.1	Bacteria	Actinobacteriota	Actinomycetia	Mycobacteriales	Mycobacteriaceae	Corynebacterium	Corynebacterium sp012838715
DP.D.8.30.20.A.bin.14	Bacteria	Actinobacteriota	Actinomycetia	Mycobacteriales	Mycobacteriaceae	Corynebacterium	Corynebacterium sp012838715
PD.D.8.14.20.B.bin.18	Bacteria	Actinobacteriota	Actinomycetia	Mycobacteriales	Mycobacteriaceae	Corynebacterium	Corynebacterium sp012838715
WI.D.11.5.20.A.bin.3	Bacteria	Actinobacteriota	Actinomycetia	Mycobacteriales	Mycobacteriaceae	Corynebacterium	Corynebacterium sp012838715
WI.D.12.8.21.A.bin.24	Bacteria	Actinobacteriota	Actinomycetia	Mycobacteriales	Mycobacteriaceae	Corynebacterium	Corynebacterium sp012838715
WI.D.7.10.20.A.bin.11	Bacteria	Actinobacteriota	Actinomycetia	Mycobacteriales	Mycobacteriaceae	Corynebacterium	Corynebacterium sp012838715
WI.D.7.29.21.A.bin.16	Bacteria	Actinobacteriota	Actinomycetia	Mycobacteriales	Mycobacteriaceae	Corynebacterium	Corynebacterium sp012838715
DP.D.12.8.21.B.bin.33	Bacteria	Actinobacteriota	Actinomycetia	Propionibacteriales	Propionibacteriaceae	Cutibacterium	Cutibacterium acnes
WI.D.7.10.20.A.bin.8	Bacteria	Bacteroidota	Bacteroidia	Bacteroidales	Tannerellaceae	Tannerella	Unknown
DP.D.7.10.20.C.bin.45	Bacteria	Bacteroidota	Bacteroidia	Cytophagales	Hymenobacteraceae	Hymenobacter	Unknown
WI.D.8.30.20.B.bin.21	Bacteria	Bacteroidota	Bacteroidia	Cytophagales	Spirosomaceae	Dyadobacter	Unknown
BDC.D.8.14.20.A.bin.42	Bacteria	Bacteroidota	Bacteroidia	Cytophagales	Spirosomaceae	Spirosoma	Unknown
DP.D.7.10.20.C.bin.68	Bacteria	Bacteroidota	Bacteroidia	Cytophagales	Spirosomaceae	Spirosoma	Unknown

BDC.D.8.14.20.A.bin.10	Bacteria	Bacteroidota	Bacteroidia	Sphingobacteriales	Sphingobacteriaceae	Pedobacter	Unknown
BDC.D.9.20.21.B.bin.20	Bacteria	Bacteroidota	Bacteroidia	Sphingobacteriales	Sphingobacteriaceae	Pedobacter	Unknown
WI.D.7.10.20.A.bin.15	Bacteria	Desulfobacterota_I	Desulfovibrionia	Desulfovibrionales	Desulfovibrionaceae	Frigididesulfovibrio	Unknown
WI.D.9.18.21.A.bin.9	Bacteria	Firmicutes	Bacilli	Bacillales	Bacillaceae_G	Ectobacillus	Unknown
BDC.D.7.27.21.A.bin.11	Bacteria	Firmicutes	Bacilli	Bacillales	Bacillaceae_G	Ectobacillus	Unknown
BDC.D.7.27.21.A.bin.37	Bacteria	Firmicutes	Bacilli	Bacillales	Bacillaceae_G	Ectobacillus	Unknown
PD.D.7.27.21.A.bin.27	Bacteria	Firmicutes	Bacilli	Bacillales	Bacillaceae_G	Ectobacillus	Unknown
PD.D.7.27.21.A.bin.9	Bacteria	Firmicutes	Bacilli	Bacillales	Bacillaceae_G	Ectobacillus	Unknown
WI.D.9.18.21.A.bin.21	Bacteria	Firmicutes	Bacilli	Bacillales	Bacillaceae_G	Ectobacillus	Unknown
BDC.D.9.20.21.B.bin.1	Bacteria	Firmicutes	Bacilli	Bacillales	Bacillaceae_H	Priestia	Priestia megaterium
WI.D.9.18.21.A.bin.6	Bacteria	Firmicutes	Bacilli	Bacillales	Bacillaceae_H	Priestia	Priestia megaterium
BDC.D.12.8.21.A.bins.30	Bacteria	Firmicutes	Bacilli	Bacillales_A	Planococcaceae	Planococcus	Unknown
PD.D.12.8.21.A.bin.18	Bacteria	Firmicutes	Bacilli	Bacillales_A	Planococcaceae	Planococcus	Unknown
BDC.D.7.27.21.A.bin.3	Bacteria	Firmicutes	Bacilli	Bacillales_B	DSM-18226	Robertmurraya	Unknown
PD.D.7.27.21.A.bin.4	Bacteria	Firmicutes	Bacilli	Bacillales_B	DSM-18226	Robertmurraya	Unknown
WI.D.9.18.21.A.bin.2	Bacteria	Firmicutes	Bacilli	Exiguobacterales	Exiguobacteraceae	Exiguobacterium_A	Exiguobacterium_A acetylicum
PD.D.7.27.21.A.bin.14	Bacteria	Firmicutes	Bacilli	Paenibacillales	NBRC-103111	Unknown	Unknown
BDC.D.11.6.20.A.bins.15	Bacteria	Firmicutes	Bacilli	Staphylococcales	Salinicoccaceae	Salinicoccus	Salinicoccus roseus
BDC.D.7.9.20.A.bin.11	Bacteria	Firmicutes	Bacilli	Staphylococcales	Salinicoccaceae	Salinicoccus	Salinicoccus roseus
BDC.D.9.20.21.B.bin.12	Bacteria	Firmicutes	Bacilli	Staphylococcales	Salinicoccaceae	Salinicoccus	Salinicoccus roseus
DP.D.12.8.21.B.bin.23	Bacteria	Firmicutes	Bacilli	Staphylococcales	Salinicoccaceae	Salinicoccus	Salinicoccus roseus
DP.D.8.21.21.A.bin.27	Bacteria	Firmicutes	Bacilli	Staphylococcales	Salinicoccaceae	Salinicoccus	Salinicoccus roseus
DP.D.8.30.20.A.bin.5	Bacteria	Firmicutes	Bacilli	Staphylococcales	Salinicoccaceae	Salinicoccus	Salinicoccus roseus
PD.D.8.14.20.B.bin.20	Bacteria	Firmicutes	Bacilli	Staphylococcales	Salinicoccaceae	Salinicoccus	Salinicoccus roseus
WI.D.11.5.20.A.bin.19	Bacteria	Firmicutes	Bacilli	Staphylococcales	Salinicoccaceae	Salinicoccus	Salinicoccus roseus
WI.D.12.8.21.A.bin.26	Bacteria	Firmicutes	Bacilli	Staphylococcales	Salinicoccaceae	Salinicoccus	Salinicoccus roseus
WI.D.7.10.20.A.bin.5	Bacteria	Firmicutes	Bacilli	Staphylococcales	Salinicoccaceae	Salinicoccus	Salinicoccus roseus
WI.D.7.29.21.A.bin.1	Bacteria	Firmicutes	Bacilli	Staphylococcales	Salinicoccaceae	Salinicoccus	Salinicoccus roseus
WI.D.7.10.20.A.bin.1	Bacteria	Firmicutes_A	Clostridia	Oscillospirales	Acutalibacteraceae	UBA945	Unknown
BDC.D.12.8.21.A.bins.6	Bacteria	Firmicutes_A	Clostridia	Oscillospirales	Ruminococcaceae	Unknown	Unknown
WI.D.11.5.20.A.bin.5	Bacteria	Proteobacteria	Alphaproteobacteria	Acetobacterales	Acetobacteraceae	Unknown	Unknown

WI.D.12.8.21.A.bin.8	Bacteria	Proteobacteria	Alphaproteobacteria	Acetobacterales	Acetobacteraceae	Unknown	Unknown
WI.D.7.29.21.A.bin.18	Bacteria	Proteobacteria	Alphaproteobacteria	Acetobacterales	Acetobacteraceae	Unknown	Unknown
DP.D.7.10.20.C.bin.37	Bacteria	Proteobacteria	Alphaproteobacteria	Acetobacterales	Acetobacteraceae	Belnapia	Unknown
DP.D.7.10.20.C.bin.73	Bacteria	Proteobacteria	Alphaproteobacteria	Caulobacterales	Caulobacteraceae	Brevundimonas	Brevundimonas vesicularis
DP.D.12.8.21.B.bin.12	Bacteria	Proteobacteria	Alphaproteobacteria	DSM-16000	Inquilinaceae	Unknown	Unknown
DP.D.8.21.21.A.bin.14	Bacteria	Proteobacteria	Alphaproteobacteria	DSM-16000	Inquilinaceae	Unknown	Unknown
DP.D.7.10.20.C.bin.17	Bacteria	Proteobacteria	Alphaproteobacteria	Rhizobiales	Devosiaceae	Devosia	Unknown
BDC.D.8.14.20.A.bin.3	Bacteria	Proteobacteria	Alphaproteobacteria	Rhizobiales	Rhizobiaceae	Aureimonas_A	Unknown
BDC.D.11.6.20.A.bins.11	Bacteria	Proteobacteria	Alphaproteobacteria	Rhizobiales_A	Rhizobiaceae_A	Bartonella	Bartonella sp016102285
DP.D.9.8.21.B.bin.17	Bacteria	Proteobacteria	Alphaproteobacteria	Rhizobiales_A	Rhizobiaceae_A	Bartonella	Bartonella sp016102285
DP.D.7.10.20.C.bin.46	Bacteria	Proteobacteria	Alphaproteobacteria	Rhodobacterales	Rhodobacteraceae	Cereibacter	Cereibacter changlensis
PD.D.7.27.21.A.bin.24	Bacteria	Proteobacteria	Alphaproteobacteria	Sphingomonadales	Sphingomonadaceae	Unknown	Unknown
DP.D.7.10.20.C.bin.47	Bacteria	Proteobacteria	Alphaproteobacteria	Sphingomonadales	Sphingomonadaceae	Novosphingobium	Unknown
PD.D.7.27.21.A.bin.23	Bacteria	Proteobacteria	Gammaproteobacteria	Burkholderiales	Burkholderiaceae	Unknown	Unknown
WI.D.8.30.20.B.bin.19	Bacteria	Proteobacteria	Gammaproteobacteria	Burkholderiales	Burkholderiaceae	Caballeronia	Unknown
BDC.D.7.27.21.A.bin.35	Bacteria	Proteobacteria	Gammaproteobacteria	Burkholderiales	Burkholderiaceae	Noviherbaspirillum	Unknown
DP.D.9.8.21.B.bin.18	Bacteria	Proteobacteria	Gammaproteobacteria	Burkholderiales	Burkholderiaceae	Noviherbaspirillum	Unknown
DP.D.7.10.20.C.bin.74	Bacteria	Proteobacteria	Gammaproteobacteria	Burkholderiales	Burkholderiaceae	Pigmentiphaga	Unknown
BDC.D.9.20.21.B.bin.32	Bacteria	Proteobacteria	Gammaproteobacteria	Burkholderiales	Burkholderiaceae	Pseudoduganella	Unknown
DP.D.7.10.20.C.bin.23	Bacteria	Proteobacteria	Gammaproteobacteria	Burkholderiales	Burkholderiaceae	Pseudorhodoferax	Unknown
DP.D.7.10.20.C.bin.33	Bacteria	Proteobacteria	Gammaproteobacteria	Burkholderiales	Burkholderiaceae	Pseudorhodoferax	Unknown
WI.D.11.5.20.A.bin.20	Bacteria	Proteobacteria	Gammaproteobacteria	Burkholderiales	Burkholderiaceae	Robbsia	Unknown
WI.D.7.29.21.A.bin.6	Bacteria	Proteobacteria	Gammaproteobacteria	CAIQBE01	CAIQBE01	Unknown	Unknown
WI.D.9.18.21.A.bin.10	Bacteria	Proteobacteria	Gammaproteobacteria	Enterobacterales	Enterobacteriaceae	Enterobacter	Enterobacter kobei
DP.D.9.8.21.B.bin.1	Bacteria	Proteobacteria	Gammaproteobacteria	Enterobacterales	Enterobacteriaceae	Gilliamella	Unknown
BDC.D.9.20.21.B.bin.4	Bacteria	Proteobacteria	Gammaproteobacteria	Enterobacterales	Enterobacteriaceae	Gilliamella	Gilliamella apicola
BDC.D.7.9.20.A.bin.27	Bacteria	Proteobacteria	Gammaproteobacteria	Enterobacterales_A	Enterobacteriaceae_A	Buchnera	Unknown
DP.D.12.8.21.B.bin.2	Bacteria	Proteobacteria	Gammaproteobacteria	Enterobacterales_A	Enterobacteriaceae_A	Buchnera	Unknown
WI.D.11.5.20.A.bin.2	Bacteria	Proteobacteria	Gammaproteobacteria	Enterobacterales_A	Enterobacteriaceae_A	Buchnera	Unknown
WI.D.11.5.20.A.bin.8	Bacteria	Proteobacteria	Gammaproteobacteria	Enterobacterales_A	Enterobacteriaceae_A	Buchnera	Unknown
BDC.D.9.20.21.B.bin.30	Bacteria	Proteobacteria	Gammaproteobacteria	Nitrococcales	Nitrococcaceae	Arhodomonas	Unknown

DP.D.12.8.21.B.bin.29	Bacteria	Proteobacteria	Gammaproteobacteria	Nitrococcales	Nitrococcaceae	Arhodomonas	Unknown
DP.D.8.21.21.A.bin.20	Bacteria	Proteobacteria	Gammaproteobacteria	Nitrococcales	Nitrococcaceae	Arhodomonas	Unknown
DP.D.12.8.21.B.bin.22	Bacteria	Proteobacteria	Gammaproteobacteria	Pseudomonadales	Halomonadaceae	Zymobacter	Unknown
PD.D.7.27.21.A.bin.6	Bacteria	Proteobacteria	Gammaproteobacteria	Pseudomonadales	Moraxellaceae	Acinetobacter	Acinetobacter baumannii
WI.D.9.18.21.A.bin.11	Bacteria	Proteobacteria	Gammaproteobacteria	Pseudomonadales	Moraxellaceae	Acinetobacter	Acinetobacter baumannii
DP.D.9.8.21.B.bin.10	Bacteria	Proteobacteria	Gammaproteobacteria	Pseudomonadales	Pseudomonadaceae	Entomomonas	Unknown
BDC.D.9.20.21.B.bin.23	Bacteria	Proteobacteria	Gammaproteobacteria	Pseudomonadales	Pseudomonadaceae	Pseudomonas_E	Unknown
BDC.D.11.6.20.A.bins.20	Bacteria	Proteobacteria	Gammaproteobacteria	Xanthomonadales	Xanthomonadaceae	Xanthomonas	Unknown
BDC.D.9.20.21.B.bin.29	Bacteria	Proteobacteria	Gammaproteobacteria	Xanthomonadales	Xanthomonadaceae	Xanthomonas	Unknown
PD.D.11.6.20.B.bin.7	Bacteria	Proteobacteria	Gammaproteobacteria	Xanthomonadales	Xanthomonadaceae	Xanthomonas	Unknown
PD.D.8.14.20.B.bin.24	Bacteria	Proteobacteria	Gammaproteobacteria	Xanthomonadales	Xanthomonadaceae	Xanthomonas	Unknown
PD.D.9.18.21.C.bin.3	Bacteria	Proteobacteria	Gammaproteobacteria	Xanthomonadales	Xanthomonadaceae	Xanthomonas	Unknown
WI.D.11.5.20.A.bin.24	Bacteria	Spirochaetota	Spirochaetia	Borreliales	Borreliaceae	Unknown	Unknown
WI.D.12.8.21.A.bin.25	Bacteria	Spirochaetota	Spirochaetia	Borreliales	Borreliaceae	Unknown	Unknown
WI.D.7.10.20.A.bin.13	Bacteria	Spirochaetota	Spirochaetia	Borreliales	Borreliaceae	Unknown	Unknown

Table C.2.5. Taxonomic Annotation of Metagenome Assembled Genomes (MAGs). This table contains the taxonomic annotation results from GTDB-tk of the high-quality MAGs found in this work.

Sample ID	Average Shannon Entropy	Average Shannon Weiner Diversity	Average Species Richness
PD.D.7.9.20	5.58651627	257.587506	268.39
PD.D.8.14.20	5.49306021	251.884917	263.9
PD.D.10.8.20	3.17969277	24.0374646	37.88
PD.D.11.6.20	5.10144386	176.817695	226.54
PD.D.7.27.21	2.85625398	15.1319115	54.76
PD.D.9.18.21	5.16974897	203.481405	241.72
PD.D.12.8.21	3.56770734	34.1414489	66.82
BDC.D.7.9.20	4.04827087	56.8750242	97.25
BDC.D.8.14.20	3.49191003	34.9647012	68.31
BDC.D.10.8.20	3.35610049	31.71798	63.66
BDC.D.11.6.20	5.55184743	262.400544	271.74
BDC.D.7.27.21	3.50690192	31.019953	68.06
BDC.D.9.20.21	5.43019555	229.814552	249.08
BDC.D.12.8.21	4.18342686	67.095712	122.63
DP.D.7.10.20	3.29487321	28.2201776	56.52
DP.D.8.30.20	2.75125404	16.4169953	35.31
DP.D.10.10.20	5.50130696	240.433636	259.06
DP.D.11.5.20	5.45460927	242.601314	260.04
DP.D.8.21.21	5.50859887	247.205155	262.46
DP.D.9.18.21	3.43817222	34.1079388	74.6
DP.D.12.8.21	5.29072436	204.054367	236
WI.D.7.10.20	4.21581267	66.344652	118.37
WI.D.8.30.20	2.61146746	16.5978292	33.71
WI.D.10.10.20	2.60362997	13.5126999	22
WI.D.11.5.20	5.06746513	173.0724	224.8
WI.D.7.29.21	5.50692347	242.420872	259.22
WI.D.9.18.21	2.21999821	10.4367424	39.95
WI.D.12.8.21	4.81033473	118.698956	208.29

Table C.2.6. Average Alpha Diversity and Species Richness per Sample. This table contains the average Shannon Weiner entropy, average Shannon Weiner diversity, and average species richness per sample.

Pairs	Sums of Squares	F value	R^2	P value	P_{adj} value
BDC vs DP	15216.07	1.225157	0.09263834	0.1374	0.8244
BDC vs PD	24238.00	1.420882	0.10587098	0.1497	0.8982
BDC vs WI	12253.51	1.025153	0.07870566	0.3050	1.0000
DP vs PD	28382.01	1.523036	0.11262533	0.0902	0.5412
DP vs WI	13648.12	0.008762	0.07754479	0.3503	1.0000
PD vs WI	30062.35	1.654658	0.12117904	0.0717	0.4302

Table C.2.7. Pairwise PERMANOVA Results Comparing Beta Diversity by Site. This is a pairwise permutational multivariate analysis of variance (PERMANOVA) comparing the variance in beta diversity between sites.

Site(s)	Model	Variance	F value	P value
All	average accumulated precipitation (24 hrs) + average wind speed + Developed STF	22.500	2.1097	0.0317
		20.914	1.9609	0.0121
		28.238	2.6477	0.0015
PD	average accumulated precipitation (24 hrs) + average wind speed	128.78	2.7279	0.001984
		129.75	2.7485	0.011706
BDC	average accumulated precipitation (24 hrs) + average meridional (north-south) component (v)	93.661	2.2868	0.04484
		50.596	1.2354	0.29524
DP	average accumulated precipitation (24 hrs) + Barren Land STF	65.890	2.3012	0.0131
		46.379	1.6198	0.03413
WI	average relative humidity + zonal (east-west) component (u)	80.367	2.5942	0.01964
		69.044	2.2287	0.01984

Table C.2.8. Redundancy Analysis Results of Microbial Composition Across and Within Sites. These results show which environmental variables were significant drivers of beta diversity across all four sites and within each site based on a redundancy analysis (RDA).

Category	Gene	Model	GLM Family	Adj R^2 or McFadden's R^2	P value
Sporulation	*spoIVCA*	average accumulated precipitation (24 hrs) * average relative humidity	Gaussian	0.375	0.013
					0.016
					0.068
	spmA	average accumulated precipitation (24 hrs) * average meridional (north-south) component (v)	Poisson	0.333	0.0009
					0.089
					0.023
UV Radiation Resistance	*lexA*	average meridional (north-south) component (v)	Poisson	0.179	0.016
	uvrA	average meridional (north-south) component (v) + Open Water STF	Gaussian	0.239	0.038
					0.019
					0.022
	uvrB	average meridional (north-south) component (v) + Open Water STF	Gaussian	0.278	0.01
					0.032
					0.013
	uvrC	average meridional (north-south) component (v) + Open Water STF	Poisson	0.327	0.022
					0.006
Thermal Resistance	*cspA*	average meridional (north-south) component (v)	Gaussian	0.145	0.038
	htpX	Barren Land STF + Open Water STF	Gaussian	0.402	0.0008
					0.001
					0.002
Osmotic Stress Resistance	*osmY*	average accumulated precipitation (24 hrs) + average wind speed + average meridional (north-south) component (v)	Poisson	0.21	5.49e-7
					0.0005
					0.012
	opuC	average accumulated precipitation (24 hrs) * average wind speed	Negative Binomial	0.336	0.001
					0.133
					0.017
LPS Synthesis/Modification	*wecP*	average air temperature + zonal (east-west) component (u)	Gaussian	0.442	0.016
					0.016
					0.00084
	wbgP	Salton Sea STF * Shrub STF	Poisson	0.327	1.29e-8
					0.00018
					6.41e-5
Quorum Sensing	*bisR*	average accumulated precipitation (24 hrs) + Crop Land STF	Gaussian	0.441	0.013
					0.024
					0.0009
	prgX	average wind speed + Developed STF	Poisson	0.334	0.0002
					0.039

Table C.2.9. Generalized Linear Models Results of Functions of Interest in the Metagenomes and Climate Variables. This table displays the generalized linear models of genes of interest by category, the model for each gene and the GLM family used, and the associated statistics for each model.

	Ave. Accum. Precip (24 hrs)	Ave. Air Temp	Ave. Wind Speed	Ave. Relative Humidity	Ave. E-W Wind Component (u)	Ave. N-S Wind Component (v)	Barren Land STF	Crop Land STF	Developed STF	Forest STF	Herbaceous STF	Mexico STF	Open Water STF	Others STF	SaltonSea STF	Shrub STF
Ave. Accum. Precip (24 hrs)	1	0.29921918	0.11066017	0.01068755	-0.41089 29	0.21612202	-0.03506 85	0.33155999	0.00839417	0.30660347	-0.06151 66	0.44269571	-0.05596 44	0.44986576	0.24061157	-0.18697 9
Ave. Air Temp	0.29921918	1	0.20982958	-0.24738 39	-0.33407 88	0.31903069	0.13778214	0.31940739	0.24096124	0.28872878	-0.36820 9	0.32836614	-0.20281 67	0.48553789	0.39125858	-0.47914 6
Ave. Wind Speed	0.11066017	0.20982958	1	-0.04708 68	0.07717019	-0.05407 52	-0.11382 6	0.08384029	0.47394588	0.28365181	0.05524157	0.28138318	0.25293225	0.26174712	0.13468076	-0.33301 27
Ave. Relative Humidity	0.01068755	-0.24738 39	-0.04708 68	1	-0.00781 68	-0.19156 38	0.43753982	0.43589243	-0.09148 92	-0.52206 97	-0.22254 87	0.32470969	-0.37378 02	0.12819069	0.32159823	-0.46056 3
Ave. E-W Wind Component (u)	-0.41089 29	-0.33407 88	0.07717019	-0.00781 68	1	-0.65176 72	-0.48571 3	-0.67443 92	0.62553728	0.10590411	0.17940314	-0.62281 7	0.26167709	-0.74678 11	-0.55117 7	0.37435786
Ave. N-S Wind Component (v)	0.21612202	0.31903069	-0.05407 52	-0.19156 38	-0.65176 72	1	0.60051 86	0.59948345	-0.58884 22	-0.31261 51	-0.58772 78	0.55775089	-0.25480 54	0.49938 08	0.66958395	-0.45052 69
Barren Land STF	-0.03506 85	0.13778214	-0.11382 6	0.43753982	-0.48571 3	0.60051 86	1	0.76268517	-0.66545 42	-0.79570 81	-0.75326 58	0.64438132	-0.67330 38	0.44460292	0.86267453	-0.77426 41
Crop Land STF	0.33155999	0.31940739	0.08384029	0.43589243	-0.67443 92	0.59948345	0.76268517	1	-0.45585 79	-0.49954 11	-0.55751 96	0.91239182	-0.43753 93	0.83378609	0.84915 36	-0.83054 82
Developed STF	0.00839417	0.24096124	0.47394588	-0.09148 92	0.62553728	-0.58884 22	-0.66545 42	-0.45585 79	1	0.58244546	0.32302307	-0.36770 65	0.41170579	-0.25542 78	-0.47932 86	0.13445761
Forest STF	0.30660347	0.28872878	0.28365181	-0.52206 97	0.10590411	-0.31261 51	-0.79570 81	-0.49954 11	0.58244546	1	0.52023819	-0.33060 32	0.66384254	-0.02380 46	-0.52225 06	0.45860846
Herbaceous STF	-0.06151 66	-0.36820 9	0.05524157	-0.22254 87	0.17940314	-0.58772 78	-0.75326 58	-0.55751 96	0.32302307	0.52023819	1	-0.55119 09	0.51237141	-0.27998 53	-0.76523 78	0.69324885

Mexico STF	0.44269571	0.32836614	0.28138318	0.32470969	-0.622817	0.55775089	0.64438132	0.91239182	-0.3677065	-0.3306032	-0.5511909	1	-0.33515	0.84182208	0.84336356	-0.7930494
Open Water STF	-0.0559644	-0.2028167	0.25293225	-0.3737802	0.26167709	-0.2548054	-0.6733038	-0.4375393	0.41170579	0.66384254	0.51237141	-0.33515	1	-0.0489063	-0.4700787	0.44489007
Others STF	0.44986576	0.48553789	0.26174712	0.12819069	-0.7467811	0.49938808	0.44460292	0.83378609	-0.2554278	-0.0238046	-0.2799853	0.84182208	-0.0489063	1	0.69684631	-0.6822025
Salton Sea STF	0.24061157	0.39125858	0.13468076	0.32159823	-0.551177	0.66958395	0.86267453	0.84915536	-0.4793286	-0.5222506	-0.7652378	0.84336356	-0.4700787	0.69684631	1	-0.8930179
Shrub STF	-0.186979	-0.479146	-0.3330127	-0.460563	0.37435786	-0.4505269	-0.7742641	-0.8305482	0.13445761	0.45860846	0.69324885	-0.7930494	0.44489007	-0.6822025	-0.8930179	1

Table C.2.10. Correlations between Climate Variables and Surface Type Frequencies. This table shows the correlation coefficients (r values) for correlations between the climate variables of interest and the surface type frequencies.

	Ave. Accum. Precip (24 hrs)	Ave. Air Temp	Ave. Wind Speed	Ave. Relative Humidity	Ave. E-W Wind Comp. (u)	Ave. N-S Wind Comp. (v)	Barren Land STF	Crop Land STF	Developed STF	Forest STF	Herbaceous STF	Mexico STF	Open Water STF	Others STF	SaltonSea STF	Shrub STF
Ave. Accum. Precip. (24hrs)	0	0.12190757	0.57507835	0.95695412	0.0298501 2	0.2693377 8	0.8593835 8	0.0847799 3	0.9661851 6	0.1125313 7	0.7558240 9	0.0183190 8	0.7772874 4	0.0163081 1	0.2174388 9	0.3407270 5
Ave Air Temp.	0.12190757	0	0.28386407	0.20437382	0.0822988 9	0.0979751 7	0.4844394	0.0975572 1	0.2167508 1	0.1361983 4	0.0538677	0.0880072	0.3006304 1	0.0088138 5	0.0395086 5	0.0098876 3
Ave. Wind Speed	0.57507835	0.28386407	0	0.81193374	0.6963059 9	0.7846279 9	0.5641220 2	0.6714471 3	0.0108400 9	0.1435353 8	0.7800936 9	0.1469044 7	0.1940785 7	0.1784686 1	0.4944204 1	0.0833422
Ave. Relative Humidity	0.95695412	0.20437382	0.81193374	0	0.96851	0.3288025 4	0.0198878 3	0.0204117 1	0.6435258	0.0043770 8	0.2550062 5	0.0918153 7	0.0500699 6	0.5156368 2	0.0951529 1	0.0136495 1
Ave. E-W Wind Comp. (u)	0.02985012	0.02982989	0.69630599	0.96851	0	0.0001717 1	0.0087858 8	8.2952202 7770288e-05	0.0003712 7	0.5917134 5	0.3609938 3	0.0004006 1	0.1785890 4	5.0124661 0036283e-06	0.0023664 3	0.0496886
Ave. N-S Wind Comp. (v)	0.26933778	0.00979751 7	0.78462799	0.32880254	0.0001717 1	0	0.0007282 9	0.0007479 8	0.0009790 3	0.1053019 3	0.0010064 8	0.0020436 8	0.1906851 7	0.0068203 2	9.7438390 5314209e-05	0.0161322 6
Barren La	0.85938	0.48443 94	0.56412	0.01988	0.0087858 8	0.0007282 9	0	2.3816084 9841	0.00011	4.1616160 5863	3.7254020 3742	0.0002149	8.6156513 9273	0.0177652 4	3.5627765 8407	1.3353362 1697

nd STF	358		202	783				633e-06	148	535e-07	451e-06		335e-05		583e-09	196e-06
Crop Land STF	0.084 77993	0.097 55721	0.671 44713	0.020 41171	8.295 22027 770288e-05	0.000 74798	2.381 60849 841633e-06	0	0.014 77072	0.006 79968	0.002 05435	1.382 31033 602821e-11	0.019 888	3.588 07933 118589e-08	1.114 48871 624248e-08	4.522 06071 980 89e-08
Developed STF	0.966 18516	0.216 75081	0.010 840009	0.643 35258	0.000 37127	0.000 97903	0.000 11148	0.014 77072	0	0.001 14592	0.093 61337	0.054 22101	0.029 49575	0.189 56688	0.009 85549	0.495 14252
Forest STF	0.112 53137	0.136 19834	0.143 53538	0.004 37708	0.591 71345	0.105 30193	4.161 61605 863535e-07	0.006 79968	0.001 14592	0	0.004 54171	0.085 73711	0.000 11743	0.904 29637	0.004 3611	0.014 10637
Herbaceous STF	0.755 82409	0.053 8677	0.780 09369	0.255 00625	0.360 99383	0.001 00648	3.725 40203 742451e-06	0.002 05435	0.093 61337	0.004 54171	0	0.002 36571	0.005 31014	0.149 00853	2.102 28953 324871e-06	4.320 20520 580769e-05
Mexico STF	0.018 31908	0.088 00072	0.146 90447	0.009 18153 7	0.000 40061	0.002 04368	0.000 2149	1.382 31033 602821e-11	0.054 22101	0.085 73711	0.002 36571	0	0.081 26072	1.976 97317 884581e-08	1.756 76911 002876e-08	4.843 96510 371169e-07
Open Water STF	0.777 28744	0.300 06304 1	0.194 07857	0.005 00699 6	0.178 58904	0.190 68517	8.615 65139 273335e-05	0.019 888	0.029 49575	0.000 11743	0.005 31014	0.081 26072	0	0.804 8025	0.011 59712	0.017 68306
Others STF	0.016 30811	0.008 81385	0.178 46861	0.515 63682	5.012 46610 036283e-06	0.006 82032	0.017 76524	3.588 07933 118589e-08	0.189 56688	0.904 29637	0.149 00853	1.976 97317 884581e-08	0.804 8025	0	3.792 45447 600046e-05	6.373 30550 105223e-05
Salton Sea STF	0.217 43889	0.039 50865	0.494 42041	0.009 51529 1	0.002 36643	9.743 83905 314209e-05	3.562 77658 407583e-09	1.114 48871 624248e-08	0.009 85549	0.004 3611	2.102 28953 324871e-06	1.756 76911 002876e-08	0.011 59712	3.792 45447 600046e-05	0	1.658 11125 790532e-10
Shrub STF	0.340 72705	0.009 88763	0.083 3422	0.013 64951	0.049 6886	0.016 13226	1.335 33621 697196e-06	4.522 06071 980 89e-08	0.495 14252	0.014 10637	4.320 20520 580769e-05	4.843 96510 371169e-07	0.017 68306	6.373 30550 105223e-05	1.658 11125 790532e-10	0

Table C.2.11. Correlations between Climate Variables and Surface Type Frequencies. This table shows the significance (p values) for correlations between the climate variables of interest and the surface type frequencies (see Table C.2.10).

General Conclusions

My dissertation research focused on understanding how extreme environments select for the taxonomic and functional diversity of their microbiomes. I explored how these microbial communities use multiple trophic and resistance strategies to influence the geochemistry of these environments. Here, I studied the microbial communities of dust and seawater from the Salton Sea, a hypersaline ecosystem that is rapidly shrinking due to environmental policy failures and ongoing water diversion (Tompson 2016). Though the microbial ecology from substrates within the Salton Sea have been investigated (Freund et al. 2022), this is the first time that amplicon and shotgun metagenome sequencing have been used in tandem to clarify the composition and functional attributes of these microbiomes. My research explores the geochemical dynamics of the Salton Sea that select for specific microbial metabolic and survival strategies, and how these adaptations allow these microbiomes to regulate nutrient cycling and dispersal within and across ecosystems.

The first chapter is a literature review describing the current conditions of the Salton Sea environment, and how these conditions predispose the Salton Sea to a unique set of microbial taxa. Water diversion and rising regional temperatures are causing the Salton Sea to rapidly shrink, increasing the lake's salinity and exposing its playa sediment (Frie et al. 2017, California Natural Resources Agency 2020). Evaporation and mineral precipitation leave the playa vulnerable to wind erosion, contributing to worsening dust emissions in the region (Frie et al. 2017). Moreover, the inflow that the Salton Sea receives is from nearby rivers carrying agricultural runoff, increasing the lake's nutrient load (Vogl and Henry 2002). Thus, we proposed that the conditions of the

Salton Sea as well as the interactions between the lake's sub-ecosystems (i.e., playa, seawater, and aeolian) select for extremophilic microbial taxa that can survive the volatile Salton Sea. We described the previous research that has explored the microbial composition of Salton Sea surface water and lake sediment (Table A.1.1), and we hypothesized that halophilic microorganisms dominant the sub-ecosystem microbiomes. We also posited that microorganisms commonly found in dust samples around the global such as *Bacillus* (Tignat-Perrier et al. 2019) would also be found in the dust from the Salton Sea playa due to the adaptations required to survive stressors unique to the atmosphere such as UV radiation, thermal stress, and desiccation stress. We then described a variety of sampling methods, DNA sequencing technologies (i.e., metagenomics, metatranscriptomics, and metaproteomics), and dust modeling tools like wind backward trajectories that can be used to further investigate the sub-ecosystem microbiomes of the Salton Sea. We also suggested that due to the high incidence of respiratory distress in the region (Farzan et al. 2019), further study of the Salton Sea's microbiomes is warranted to understand how this ecosystem is contributing to the local public health crisis.

In the second chapter, we explored the microbial composition of a water column within the Salton Sea across seasons and characterized the sulfur metabolic pathways conserved within this microbial community. Microbial composition significantly varied between time points, however, several bacterial genera including *DS001*, *Litoricola*, *Truepera*, and *Synechococcus* were found to dominate the water column and differentially fluctuate with the seasons. These taxa can be mixotrophic, facultative

anaerobes, and/or facultative halophiles depending on their surroundings (Ivanova et al. 2011, Casamayor et al. 2013, Auladell et al. 2023). The functional flexibility we observed was further supported by the diverse set of sulfur oxidation genes identified in the Salton Seawater metagenomes. Genes involved in thiosulfate oxidation (i.e., the SOX pathway), hydrogen sulfide oxidation (i.e., *sqr, fccB*), and reverse dissimilatory sulfate reduction were found in all the metagenomes, yet their relative coverages appeared to shift with seasonal changes in sulfide, sulfate, and oxygen concentrations. Our findings suggest that multiple sulfur oxidation pathways are a conserved within the Salton Seawater microbiome, and thus, this community is deeply involved in regulating the seasonal sulfur cycle and redox conditions within the lake.

In the third chapter, we characterized the microbial composition of the aeolian dust microbiome as well as the survival strategies these microorganisms use to colonize the harsh atmospheric environment. Wind geospatial data from weather stations near our four study sites around the Salton Sea was used to determine if wind conditions were driving the distribution of microbial taxa and their niche-specific adaptations. We found that the local wind conditions significantly influenced aeolian microbial assembly across sites; however, we also observed a core microbiome consisting of 13 bacterial genera that have been previously identified in dust sampled from around the world (Zhang et al. 2019b, Amarloei et al. 2020, Chen et al. 2021, Osman et al. 2023). Furthermore, we identified genes involved in various forms of stress-resistance that are required to persist in the atmosphere. Of the genes of interest, genes involved in repairing UV damaged DNA (i.e., *lexA*, *uvrA*, *uvrB*, *uvrC*), thermal resistance (i.e., *cspA*, *htpX*),

and osmoprotectant transport (i.e., *osmY*, *opuC*) were widely distributed in metagenomes sampled from our four sites. Additionally, wind direction components, specifically the meridional wind component (north-south, v), significantly predicted the normalized coverage of the UV radiation resistance genes (i.e., *lexA*, *uvrA*, *uvrB*, *uvrC*) and *cspA* across the samples, with the highest normalized coverages found with northerly winds and decreasing coverages with southerly winds. Northerly winds reaching our dust collectors were predominantly occurring in the fall months, whereas southerly winds were occurring during the summer months. Prior research into the seasonal wind patterns at the Salton Sea have found that dust emissions are greatest during the summer months, corresponding with heightened dust and aerosol contributions from the Salton Sea playa and water (Frie et al. 2019). Based on these results, we propose that high winds coupled with southerly dust emissions from the Salton Sea playa and water during summer may disturb the aeolian microbiome, negatively impacting the overall survival of its native constituents. As wind speeds and dust emissions from the Salton Sea decline in the fall, the resilient aeolian microbiome can return to its undisturbed state. This hypothesis is further supported by our observation that *spmA* and *osmY* normalized coverages increase with southerly winds, suggesting that Salton Seawater microorganisms with the ability to withstand extreme osmotic stress can be introduced to the aeolian microbiome and persist. Collectively, our findings demonstrate that wind conditions and dust sources select for the various survival strategies that are conserved within the aeolian dust microbiome.

Holistically, the results from the second and third chapters in this work contextualize the mechanisms that allow microorganisms to traverse the sub-ecosystem microbiomes and become entrained in Salton Sea dust and sea spray. Bacterial genera found in Salton Sea dust and seawater samples appear to be shared (Supplemental Figure 2.7), which is not surprising considering $CaSO_4$ and $MgSO_4$ have been found in dust from the Salton Sea playa and sulfide has been found in higher concentrations in the air above the lake (Reese et al. 2008, Frie et al. 2019). We also identified antibiotic resistance genes (i.e., ARGs) involved in multidrug resistance within the aeolian dust microbiome (Supplemental Figures 9, 10), which are often exchanged between microorganisms via horizontal gene transfer (i.e., HGT; Fuchsman et al. 2017). The presence of ARGs in the aeolian dust microbiome suggests that these microorganisms have the potential to be pathogenic upon exposure and can share this pathogenicity with other taxa within the host. Thus, the results of this dissertation have important implications for understanding the sources responsible for the respiratory distress experienced by the local community. Deeper investigation into the distribution and frequency of pathogenic traits like ARGs in the Salton Sea's sub-ecosystem microbiomes is necessary to address and remediate the worsening public health crisis in this region.

References

Amarloei, A., M. Fazlzadeh, A. J. Jafari, A. Zarei, and S. Mazloomi. 2020. Particulate matters and bioaerosols during Middle East dust storms events in Ilam, Iran. Microchemical Journal 152.

Auladell, A., I. Ferrera, L. Montiel Fontanet, C. D. Santos Júnior, M. Sebastián, R. Logares, and J. M. Gasol. 2023. Seasonality of biogeochemically relevant microbial genes in a coastal ocean microbiome. Environmental Microbiology 25:1465–1483.

California Natural Resources Agency. 2020. 2020 Annual Report on the Salton Sea Management Program.

Casamayor, E. O., X. Triadó-Margarit, and C. Castañeda. 2013. Microbial biodiversity in saline shallow lakes of the Monegros Desert, Spain. FEMS Microbiology Ecology 85:503–518.

Chen, Y., M. J. Gebert, S. A. Faith, R. R. Dunn, N. Fierer, and A. Barberán. 2021. Global Patterns and Climatic Controls of Dust-Associated Microbial Communities. Microbiology Spectrum 9.

Farzan, S. F., M. Razafy, S. P. Eckel, L. Olmedo, E. Bejarano, and J. E. Johnston. 2019. Assessment of respiratory health symptoms and asthma in children near a drying saline lake. International Journal of Environmental Research and Public Health 16.

Freund, H., M. R. Maltz, M. P. Swenson, T. M. Topacio, V. A. Montellano, W. Porter, and E. L. Aronson. 2022. Microbiome interactions and their ecological implications at the Salton Sea. California Agriculture 76:16–26.

Frie, A. L., J. H. Dingle, S. C. Ying, and R. Bahreini. 2017. The Effect of a Receding Saline Lake (The Salton Sea) on Airborne Particulate Matter Composition. Environmental Science and Technology 51:8283–8292.

Frie, A. L., A. C. Garrison, M. V. Schaefer, S. M. Bates, J. Botthoff, M. Maltz, S. C. Ying, T. Lyons, M. F. Allen, E. Aronson, and R. Bahreini. 2019. Dust Sources in the Salton Sea Basin: A Clear Case of an Anthropogenically Impacted Dust Budget. Environmental Science & Technology 53:9378–9388.

Fuchsman, C. A., R. E. Collins, G. Rocap, and W. J. Brazelton. 2017. Effect of the environment on horizontal gene transfer between bacteria and archaea. PeerJ 2017:1–26.

Ivanova, N., C. Rohde, C. Munk, M. Nolan, S. Lucas, T. G. del Rio, H. Tice, S. Deshpande, J. F. Cheng, R. Tapia, C. Han, L. Goodwin, S. Pitluck, K. Liolios, K. Mavromatis, N. Mikhailova, A. Pati, A. Chen, K. Palaniappan, M. Land, L. Hauser, Y. J. Chang, C. D.

Jeffries, E. Brambilla, M. Rohde, M. Göker, B. J. Tindall, T. Woyke, J. Bristow, J. A. Eisen, V. Markowitz, P. Hugenholtz, N. C. Kyrpides, H. P. Klenk, and A. Lapidus. 2011. Complete genome sequence of Truepera radiovictrix type strain (RQ-24 T). Standards in Genomic Sciences 4:91–96.

Osman, J. R., G. R. Fernandes, E. Kamilova, and M. S. DuBow. 2023. Genomic microbiome analyses of surface sand samples from the Kyzyl-Kum Desert (Uzbekistan): characterization and comparative study. Archives of Microbiology 205.

Reese, B. K., M. A. Anderson, and C. Amrhein. 2008. Hydrogen sulfide production and volatilization in a polymictic eutrophic saline lake, Salton Sea, California. Science of the Total Environment 406:205–218.

Tignat-Perrier, R., A. Dommergue, A. Thollot, C. Keuschnig, O. Magand, T. M. Vogel, and C. Larose. 2019. Global airborne microbial communities controlled by surrounding landscapes and wind conditions. Scientific Reports 9:1–11.

Tompson, A. F. B. 2016. Born from a flood: The Salton Sea and its story of survival. Journal of Earth Science 27:89–97.

Vogl, R. A., and R. N. Henry. 2002. Characteristics and contaminants of the Salton Sea sediments. Hydrobiologia 473:47–54.

Zhang, T., X. Li, M. Wang, H. Chen, and M. Yao. 2019. Microbial aerosol chemistry characteristics in highly polluted air. Science China Chemistry 62:1051–1063.